OPTIMAL ENERGY MANAGEMENT MODELLING OF A GRID-CONNECTED MICRO-HYDROKINETIC WITH PUMPED HYDRO STORAGE

By

SANDILE PHILLIP KOKO

Submitted in fulfilment of the requirements for the degree:

DOCTOR OF ENGINEERING

IN ELECTRICAL ENGINEERING

In the

Faculty of Engineering and Information Technology:

Department of Electrical, Electronic and Computer Engineering

Central University of Technology, Free State

Supervisor: **Prof. K. Kusakana** (D.Tech)

Co-supervisor: **Prof. H.J. Vermaak** (PhD)

Bloemfontein

2018

Declaration

I, Sandile Phillip Koko hereby declare that this research project which has been submitted to the Central University of Technology, Free State for the degree of DOCTOR OF ENGINEERING: ELECTRICAL ENGINEERING, is my own independent work; complies with the Code of Academic Integrity, as well as other relevant policies, procedures, rules and regulations of the Central University of Technology, Free State, and has not been submitted before by any person in fulfilment (or partial fulfilment) of the requirements for the attainment of any qualification.

 Student Signature:

Date: 2018-08-01

Dedication

I dedicate this thesis to the memory of my dad, NTOZAKHE KOKO and my mom, KETSELETSO KOKO. Mom and dad, you have instilled perseverance and hard-work ethics in me. You taught me how to hold firmly, whenever I want to achieve great rewards and no matter how complicated it may become. I am eternally grateful with honour and appreciation to you.

I dedicate this thesis to my lovely, gentle and caring partner, THANDI. Your continuous love, support, care and prayers have enriched my soul and inspired me to pursue and complete this research. Your consistent endless love towards me, always reveals a holy blessing that will last forever in my life. God gave me you by purpose, since you are the definition to everything that I asked from our Saviour, Jesus Christ. I am very grateful and forever is our final destination in our relationship.

Acknowledgements

First and foremost, I would like to thank our Almighty Heavenly Father for making everything possible for me, by strengthening me throughout this study. Eternal Glory to our Almighty Father, His Son Jesus Christ and the Holy Spirit! Amen!

I would like to express my sincere appreciation to my supervisors, Prof. Kanzumba Kusakana and Prof. Herman Jacobus Vermaak, who were very supportive in this study. Their continuous guidance, support and knowledge were indeed instrumental. Their guidance made it possible for me to make such a contribution in a renewable energy research science.

In the same breath, I acknowledge Dr. TN Mathaba, for his valuable guidance during the study. Furthermore, thanks to my colleagues from the department of electrical, electronic and computer engineering. Your inspirations renewed my hope in pursuing this study. I would further like to thank the CUT and RGEMS for granting me the opportunity and financial assistance in undertaking this study.

In a special way, I would like to take this opportunity to thank my siblings, Mlungisi and Qhathiwe Koko, my guardians, Vuyisile and Mateboho Koko, as well as my nieces, Moleboheng and Unathi Koko. Your love, care and extensive support was indeed valuable and ever-present in this important study time of my life. I am very grateful to have you. Also thanks to Dr. CS Masoabi, for encouraging me to complete my studies. Finally, a big thank to my friends for being there for me. Phumelele Nomtshongwana, you showed lot of support and created laughter when needed most.

Abstract

The pressure on greenhouse gases (GHGs) emission reduction and energy deficit crisis are of global concern. The ever increasing energy demand due to population growth as well as industrial and commercial business developments, leads to energy deficit crisis for electric utility operators around the globe. This generates an increased probability of grid instability and blackout challenges. Hence, this promotes the requirement for the additional fossil fuel power plants, leading to electricity price increase for consumers, due to high investment cost and the rising fossil fuels prices. The exploitation of an onsite grid-connected renewable energy (RE) system may mitigate all of the above-mentioned challenges.

However, the intermittent nature of RE resources (such as solar, wind, hydro, geothermal and marine) leads to a challenge of high uncertainty output power. Hence, power demand cannot be reliably met, due to daily or seasonal weather changes. Therefore, a stand-alone RE system should comprise of an energy storage system (ESS), to store surplus energy for later use when the power demand is more than the generated output power. Additionally, a grid-interactive RE system should also comprise of the ESS, due to the variable tariff rates imposed by utility companies around the globe. The aim is to store excess energy during low-priced off-peak periods, for later use during high-priced peak periods. Hence, minimal electricity bill may be achieved by the consumers. The utility grid operator may also reap a benefit of a reduced blackout probability, especially during peak demanding periods.

Among various RE technologies, hydrokinetic is a promising RE solution to be exploited in areas with flowing water resources, such as rivers, tidal current or artificial water channels. It is easily predictable and has proved to generate electricity at flowing water speeds, ranging from 0.5 m/s and above. It has proved to generate electricity markedly better and affordable than solar and wind energy systems. Furthermore, it has proved to operate cost-effectively, if

v

it comprises of a pumped-hydro storage (PHS) system instead of a battery-based storage system.

Rural consumers, such a farms, industries and mines situated in close proximity to flowing water resources, may make use of a grid-connected micro-hydrokinetic-pumped-hydro-storage (MHK-PHS) system to reduce electricity bills and sell the excess energy to the grid. However, a grid-connected MHK-PHS system requires a complex optimal energy management system, instead of expecting a consumer to respond to a change in real-time electricity price. The system should allow for optimal energy storage and sales, while ensuring that the consumer load demand is met at all times, by considering variable time-of-use (TOU) tariffs and load demand uncertainties that might take place in real-time context.

This work deals with optimal energy management of a grid-connected MHK-PHS system, under different demand seasons for different load demand sectors, through the consideration of variable TOU tariffs. The aim is to minimize the customer electricity bills if the proposed system is approved to be non-interactive or interactive with the utility grid. Additionally, the alternative aim is to maximize the energy sales into the grid, if the system is grid-interactive.

The results have proved that the developed optimization-based model is capable of minimizing the grid-cost, particularly during expensive peak-periods. Furthermore, the energy sales revenue has been maximized during peak-periods. Sundays have proved to lead to the largest amount of grid-power storage into the storage system, as compared to other days of the week. The industrial load profile led to the low net income, since most energy sales take place during the evening peak hours, instead of morning peak hours.

However, if the load demand uncertainty constraint is considered, the above-mentioned open-loop optimization-based model has been unable to optimize the power flow. This led to the unmet load demand difficulty, as well as the excessive supply of power. Hence, an

additional control model has been developed to assist the open-loop optimization-based model, to handle the load demand uncertainty disturbance in real-time context. The control model proved to mitigate the issue of both unmet load demand and excessive supply of power through the application of a rule-based algorithm. Additionally, a higher energy savings was achieved through the successful reduction of the excessively supplied power.

Table of Contents

ix

List of Figures

xiv

xvi

List of Tables

Nomenclature

A	Swept area of a turbine [m^2]
C_o	Off-peak tariff rates [ZAR/kWh]
C_p	Peak tariff rates [ZAR/kWh]
C_s	Standard tariff rates [ZAR/kWh]
C_t	TOU tariff price at time t [ZAR/kWh]
C_p	Power coefficient of a hydrokinetic turbine
Cap^{min}	Minimum allowable capacity of the upper reservoir [%]
Cap^{max}	Maximum allowable capacity of the upper reservoir [%]
$Cap_{(j)}$	Upper reservoir state of charge at j^{th} sampling interval [%]
$Cap_{(t)}$	Upper reservoir state of charge at time t [%]
$Cap_{(t-1)}$	Upper reservoir state of charge at the end of the next time period [%]
D	Turbine diameter [m]
Δt	Sampling time [30 minutes]
E_{HK}	Energy generated by a hydrokinetic system [Wh]
E_p	Output energy of a PHS's turbine-generator unit [Wh]
E_{pot}	Nominal potential energy of the upper reservoir [kWh]
F	Discrete cost objective function
g	Gravitational acceleration [9.81 m/s^2]
h	Head between lower and upper reservoirs [m]
H	Turbine height [m]
j	Sampling interval during optimization-based approach
N	Number of sampling intervals
ρ	Water density [1000 kg/m^3]

xix

P_{ch}	Power supplied for pumping process [W]
$P_{i(j)}$	Electrical power flow at j^{th} sampling interval [kW]
$P_{i(r)}$	Actual power flow during rule-based control at r^{th} sampling interval [kW]
$P_{i(t)}$	Electrical power flow at time t [kW]
P_i^{max}	Maximum power of a system component [kW]
P_i^{rated}	Rated power of a system component [kW]
$P_{Load(j)}$	Primary load power demand at j^{th} sampling interval [kW]
$P_{Load(r)}$	Actual load power demand during rule-based method at r^{th} sampling interval [kW]
$P_{Load(t)}$	Primary load power demand at time t [kW]
P_{MHK}^{max}	Maximum power generated by the MHK system [kW]
$P_{Pi(r)}$	Predicted power flow during rule-based control at r^{th} sampling interval [kW]
$P_{PLoad(r)}$	Predicted load power demand during rule-based method at r^{th} sampling interval [kW]
$P_{T\,G}^{rated}$	Rated output power of a turbine-generator unit of a PHS system [kW]
ρ_w	Water density [1000 kg/m^3]
Q_P	Volumetric water flow rate during pumping process [m^3/s]
Q_t	Volumetric water flow rate during generation process [m^3/s]
r	Sampling interval during rule-based control approach
R	Turbine radius [m]
R_a	Contracted percentage ratio during FIT [0.65]
t	Time [h]
v	Wind/Water speed [m/s]
V	Water volume stored in the upper reservoir [m^3]
$\eta_{HKT\text{-}G}$	Overall efficiency of a hydrokinetic turbine-generator unit

η_g Overall efficiency of a turbine-generator unit

η_p Overall efficiency of a motor-pump unit

Abbreviations

COE	Cost of Energy
CPP	Critical-Peak-Pricing
DG	Diesel Generator
DR	Demand Response
Eskom	South African Electric Utility Company
ESS	Energy Storage System
FFPPs	Fossil Fuel Power Plants
FIT	Feed-in-tariff
GHGs	Concentration of Greenhouse Gases
HEM	Home Energy Management
HOMER	Hybrid Optimization Model for Electric Renewable
HPWH	Heat Pump Water Heater
MHK	Micro-Hydrokinetic River System
MPC	Model Predictive Control
NPC	Net Present Cost
PHS	Pumped-Hydro Storage
PTR	Peak-Time-Rebates
PV	Photovoltaic
RCGA	Real-Coded Generic Algorithm
RE	Renewable Energy
RTP	Real-Time-Pricing
SCIP	Solving Constraint Integer Programming
SOC	State of Charge

TOU   Time-of-use

WT   Wind Turbine

CHAPTER 1: INTRODUCTION

1.1   Background

Provision of a reliable and affordable electric power service to the community is key to ensure efficient economic growth. The ever increasing energy demand around the world is expected to continue, particularly in developing countries, due to factors such as population growth and economic developments (Asif & Muneer, 2007; Mollahosseinia et al., 2017). The aforementioned demand increase crisis may result in a long-term capacity expansion challenge of constructing additional fossil fuel power plants (FFPPs) (Hemmati, 2017). However, the installation of additional FFPPs is not an economical idea, due to high investment costs leading to electricity price increase for end-users (Hemmati, 2017; Soudmand et al., 2017). Moreover, this leads to an increased emission level of Greenhouse gases (GHGs), resulting in climatic changes. Climatic changes result in significant threats to an annual death rate of 160, 000 people, according to the World Health Organization (Asif & Muneer, 2007). Irrespective of the emission of GHGs, the construction of additional FFPPs is not a long-term sustainable solution to cope with the future energy needs. The reason is due to the depletion of global fossil fuel reserves (Capellán-Pérez et al., 2014; Hil Baky et al., 2017). Therefore, the future supply security is then compromised. Additionally, it has been estimated that the global fossil fuel prices will continue to rise, as the demand for energy increases (Foley et al., 2015).

In addition to long-term capacity expansion challenges, a temporal energy challenge, such as the fluctuation of daily energy demand further exists. The grid power system might operate far from the base load. This is a considerable challenge to electric grid operators, due to the resultant financial implications (P. Yang et al., 2013). Moreover, an unexpected growth

1

of short-term peak demand may result in temporal supply-demand imbalance (P. Yang et al., 2013; Cheng et al., 2017). Nevertheless, the end-users are expecting a reliable power supply system to meet their daily needs. To ensure that the national load demand is continuously met, it is a challenging and costly process for electric grid operators. To instantaneously address such a challenge, electric grid operators demand backup facilities to prevent power outage situations that may impair the economic and social functions. The backup facilities that are brought online to supply electricity during peak demand period, usually operate on fossil fuels and are costly (Cosmo & O'Hora, 2017). This leads to an additional GHGs emission level per unit of the generated electricity. Additionally, the cost of building new backup power plants needs to be transferred into the electricity price, since there is no economic incentive offered to the grid operators for building new backup plants (Azofra et al., 2015). This leads to an increased electricity price for consumers.

Reduction of peak energy consumption by end-users may mitigate the challenge of grid instability and thus reduces the investment cost of the additional FFPPs and standby facilities. This further increases energy efficiency, by ensuring the complete usage of current energy sources. Demand response (DR) programmes are usually implemented in many countries to address the issue of peak energy consumption. They are employed to regulate an imbalance between the supply and demand, through the use of variable electricity pricing strategy. DR programmes include strategies, such as real-time-pricing (RTP), time-of-use (TOU), critical-peak-pricing (CPP) and peak-time-rebates (PTR) (Alasseri et al., 2017; Wang et al., 2017).

The TOU pricing strategy has been the most widely adopted DR approach or pricing mechanism imposed by electric grid operators around the world (Babu & Ashok, 2009; P. Yang et al., 2013; Li et al., 2016; Cheng et al., 2017; Meyabadi & Deihimi, 2017). The objective is to flatten the load demand curve during peak periods. The electricity price is permitted to vary over two or three various price levels, such as off-peak, mid-peak and peak

periods (Geem & Yoon, 2017). The electricity rate is designed to be costly during peak periods, average during mid-peak periods and inexpensive during off-peak periods. Consumers are therefore encouraged to shift a part of their electricity usage from peak to mid-peak and/or off-peak, in order to earn the benefit of reduced energy bills [Cheng et al., 2017; L. Yang et al. 2013]. However, in contrast to the high income households, the low income households proved not react to a change in electricity costs (Cosmo & O'Hora, 2017). They are unable to recognize the benefit of reduced peak consumption, due to lower level of education or insufficient knowledge.

Investing in renewable energy (RE) systems is a feasible solution to reduce GHGs emission level, through reduced reliance on fossil fuels (Banshwar et al., 2017). They may further assist with the minimization of grid instability problem (Al-falahi et al., 2017; Obi & Bass, 2016). The RE sources are abundant, inexhaustible and environmentally friendly sources of electrical energy (Asif et al., 2007). However, the main challenge with RE system is the requirement for a high initial capital cost. It is worth noting that the aforementioned capital cost implication may be minimized, by integrating a RE system with the utility grid (Badwawi et al., 2015).

If consumers are encouraged to have their own grid-tied RE system, both the consumers and the grid operator will reap the benefits. This will lower the electricity costs of the consumers by generating their own onsite energy and further lowers the probability of approaching the grid instability problem. However, RE sources such as solar, wind, hydro, geothermal and marine are intermittent in nature (Cai et al., 2014). The main challenge is the high uncertainty with their generated output power (Ngoko et al., 2018). A continuous power generation is not guaranteed due to daily or seasonal weather changes. Hence, a need exists to integrate a RE system with the energy storage system (ESS) for storing excess energy during inexpensive off-peak periods, since the energy deficit crisis takes place during expensive

3

peak periods (Cai et al., 2014). Moreover, the stored excess energy may further be sold into the grid during the expensive peak-period to generate utmost revenue. Therefore, this will further increase the probability of improved grid-network reliability, due to energy sales and reduced peak demand.

However, the adoption of a grid-connected RE system is a challenge, due to the requirement of designing an optimal home energy management (HEM) system, instead of expecting consumers to monitor and respond to price fluctuation in real-time. The optimal HEM system should be able to satisfy the owner's load demand, while considering the intermittent nature of RE sources and variation, in both the electricity price and load demand.

The South African electric utility company (Eskom) utilizes the TOU tariff scheme to encourage consumers to reduce the peak energy demand. Eskom TOU tariff costs involve peak, standard and off-peak periods for low and high demand seasons, as shown in Fig. 1.1 (Eskom, 2017/2018). Depending on the consumer types, TOU tariff consists of various schemes, such as Nightsave, Homeflex, Megaflex, Miniflex, Genflex, Ruraflex, Business-rate, Public-lighting, Land-rate, etc. In this study, the Ruraflex TOU tariff rates will be considered. It is applied to rural customers who consume energy (from Eskom) and further generate energy for sales (to Eskom).
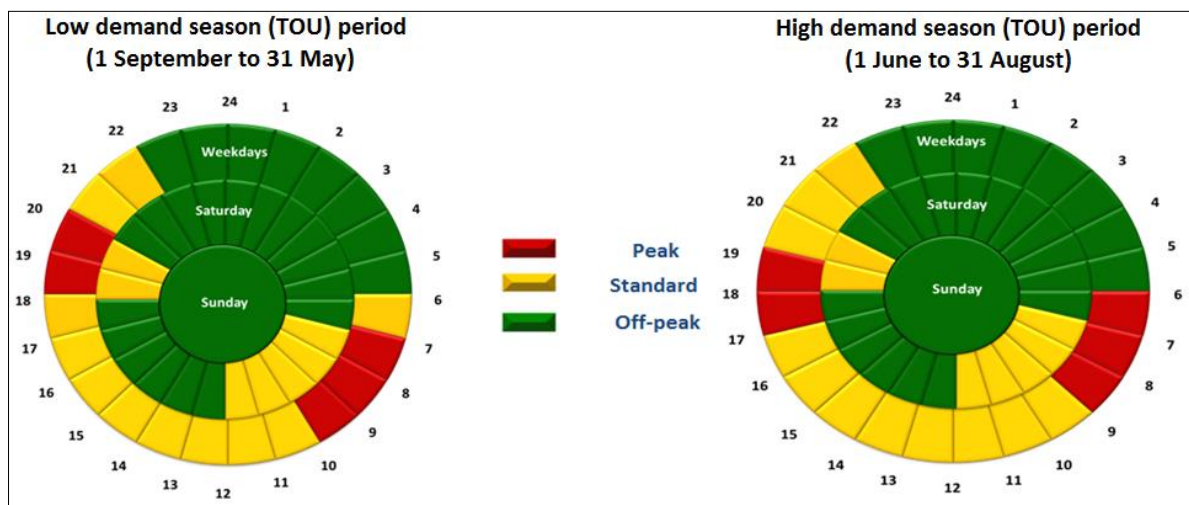
Figure 1.1: Eskom Time-of-Use seasonal periods (Eskom, 2017/2018)

4

River-based hydrokinetic technology is a promising RE technology that may off-set the stochastic nature of solar and wind turbine technologies. Few studies have proved that it generates electricity markedly improved and affordable than wind and solar systems (Koko et al., 2014; Kusakana, 2014; Koko et al., 2015). It generates electricity without requiring a water head and further generates electricity within the flowing water resources such as river streams, tidal current or other artificial water ways/channels, having a speed of 0.5 m/s or more (Vermaak et al., 2014; Kumar & Saini, 2016). It is easily predictable, since the speed of the flowing water resources proved to vary seasonally, instead of hourly. A river-based hydrokinetic system may be incorporated with a pumped hydro storage (PHS) system, instead of the battery-based storage system, to offer a supplementary cost-effective, reliable and environmentally friendly solution (Kusakana, 2015). PHS technology has proved to be the preferred commercially viable storage technology, since it offers the lowest cost of energy (COE) per cycle (Zhao et al., 2015; Ma et al., 2014). Therefore, further research is needed to develop an effective optimization approach for the grid-connected micro-hydrokinetic-Pumped-hydro storage (MHK-PHS) system.

Lastly, the most prevailing potential disturbance of load demand uncertainties is possible in real life context. It is impossible to expect the predicted load demand to match the actual load demand for hours throughout the day. Most optimal control studies are based on the predicted and constant load demand during modelling. Load demand uncertainty might negatively affect the system power flow if not well managed. Hence, an optimal energy management approach must therefore be designed to compute corrective control actions in real-time. This study aims to develop an optimal control model that will be able to address such challenges for a grid-connected MHK-PHS system.

5

1.2 Problem Statement

Most optimization studies for the RE systems have concentrated mainly on solar-wind battery-based hybrid system. However, none of the studies have considered proving the effectiveness of the model under variety of factors such a variable daily load demand, load demand uncertainty/disturbance and variable TOU tariff rates during weekdays and weekends. Load demand uncertainties are caused by the predicted-modelled load demand being either more or less than the actual load demand. Mismanagement of the above-mentioned factors may negatively impact the operation of an optimization model.

Additionally, decidedly limited studies have concentrated on the optimization of hydrokinetic-based systems, since this technology is immature and still in the development stage. There is a lack of optimization studies that have concurrently considered the above-mentioned factors. The implementation of a robust optimal energy management system for a grid-connected MHK-PHS system, which considers the above-mentioned factors is critical, due to the following sub-problems:

- Sub-Problem 1: Determining the optimal schedule for each energy source (utility grid, ESS and hydrokinetic system) to meet the daily variable on-site load demand economically and reliably.

- Sub-Problem 2: Determining the optimal schedule for storing energy from the utility grid and/or MHK system, depending on the state of charge and variable tariff rates.

- Sub-Problem 3: Determining the optimal schedule for permitting the stored power within the PHS system to discharge, as a means of supplementing the unmet load demand and/or selling energy to the grid.

- Sub-Problem 4: Implementing a control strategy for assisting the developed model to handle the load demand uncertainty constraint/disturbance.

6

1.3   Objectives of the Study

As mentioned previously, due to variable daily and/or seasonal weather conditions, the intermittent RE sources cannot guarantee a continuous electric power supply in response to the actual load demand (Ishigaki et al., 2014). Incorporating an ESS can improve the reliability of the systems (Chauhan & Saini, 2014; Canales et al., 2015). Hence, power flow management is correspondingly vital to ensure the efficient use of energy. For a grid-interactive RE system, both the energy sales and consumption into and from the grid need to be appropriately managed, to maximize the sales revenue and to minimize the customer's electricity costs. Additionally, an onsite load demand should be economically met at all times, irrespective of the load demand forecasting error.

This study focuses on developing an optimal energy management model for the proposed grid-connected MHK-PHS system. The model should ensure the economic, reliable and optimal power flow between the grid and the proposed system. Hence, an innovative model will be developed to attend to time-varying electricity price throughout the week, feed-in tariffs, variable load demand and disturbance, due to load demand uncertainty.

The objectives of this study are as follows:

- To develop an optimal energy management model for the proposed MHK-PHS system if it is non-interactive with grid under TOU tariff scheme.

- To develop an optimal energy management model for the proposed MHK-PHS system if it is grid-interactive under TOU tariff scheme.

- To study the behaviour of the above-mentioned model when supplying the variable residential, commercial and industrial load demands, respectively.

- To develop a rule-based control strategy, as to benchmark and assist with the inability of an open loop approach in handling a disturbance due to load demand uncertainty.

7

- To apply the developed models in the MATLAB simulation tool in order to study and compare the behaviour of the developed models.

1.4   Research Methodology

To achieve the above-mentioned objectives, the methodology is as follows:

1.4.1   Literature Review: A thorough survey of literatures related to the hydrokinetic and PHS systems will be carried to analyse the operation of the system's components. Optimization studies based on grid-connected hydrokinetic and alternative RE systems that consider TOU tariff strategy, will be reviewed. TOU tariff rates as applied by Eskom for real-time pricing of Ruraflex customers will be determined.

1.4.2   Optimal Sizing: The optimal size of the proposed MHK-PHS system will be determined through the use of the HOMER (hybrid optimization model for electric renewable) software, on the basis of supplying the residential, commercial and industrial load types, respectively. The results obtained using the HOMER Legacy Version will be compared to the HOMER Pro Version results.

1.4.3   System Modelling: After studying the operation of various components of the proposed system, a mathematical model for the optimal energy management controller will be developed, using the open-loop optimization-based approach and rule-based control strategy, so as to close the gap offered by the traditional open loop approach. Hence, various constraints and variables of the system's operation will be identified and used to develop multiple-objective functions.

1.4.4   Simulations: After developing the mathematical model for both open-loop and rule-based control approaches, the real input data such as TOU tariffs, river-based hydrokinetic resources data for the selected site, and a variable load demand data

8

(residential, commercial, and industrial) extracted from the HOMER software, will be used and applied in MATLAB software.

1.5   Hypothesis

1.5.1   For the same daily energy consumption, various load profile types affect the sizing of the MHK-PHS system, differently.

1.5.2   The consideration of the time-varying electricity prices, the open-loop optimization-based approach may maximize the energy sales revenue and minimize the grid electricity costs for residential, commercial and industrial consumers possessing the proposed MHK-PHS system, respectively.

1.5.3   Sundays lead to the large number of grid-to-load operational hours and charge-discharge cycles, when compared to other days.

1.5.4   A disturbance due to load demand uncertainties negatively affects the open-loop optimization-based approach, by initiating unmet load demand and excessive energy supply challenges.

1.5.5   Rule-based control algorithm evades the issue of the unmet load demand and excessive energy supply, without compromising the power flow boundaries.

1.6   Limitation of the Study

The study has been conducted with the following limitations:

- This study focuses solely on Genflex rural tariff scheme since it is used for customers that consume energy (from Eskom) and further generates energy for sales (to Eskom).

- This study does not focus on performing the life cycles cost and payback period analysis.

- The study focuses primarily on the grid-connected systems since the TOU tariffs are applied.

- Parameters, such as fixed transmission and distribution network charges, have not been considered.

1.7   Contribution to Knowledge

In this study, contributions are as follows:

- Analysed the potential impact of various load types on the optimal sizing of the proposed MHK-PHS system.

- The development of an innovative optimal energy management model for grid-interactive and non-interactive MHK-PHS systems. The model considers time-varying electricity price, for both weekdays and weekends, as well as the variability of the load demand. The main objective is to adequately meet the variable load demand of the consumer, while minimizing the grid-cost and maximizing the energy sales revenue.

- The development of an additional control model that will assist the developed optimization-based model to be able to deal with load demand uncertainty problem, as a result of forecasting error. Hence, the load demand forecasting errors are unavoidable in real-time operation and need not to be neglected.

- To create awareness, based on the potential benefits of utilizing MHK-PHS for the purpose of minimizing the electricity bills and maximizing the energy sales revenue. This will encourage consumers to invest further on hydrokinetic renewable resources,

10

since this technology is gaining more interest. As a result, this may bring a significant social impact, by minimizing the chances of load shedding through the reduction of reliance on fossil fuel.

1.8 Research Output

Book Chapter:

S.P. Koko, K. Kusakana, H.J. Vermaak, "*Optimal Sizing of a Micro-Hydrokinetic Pumped-Hydro-Storage Hybrid System for Different Demand Sectors*". Sustainable Cloud and Energy Services. Springer, Cham, pp. 219-242, 2018.

Journal Publications:

S.P. Koko, K. Kusakana, H.J. Vermaak, "*Optimal energy management of a grid-connected micro-hydrokinetic with pumped hydro storage system*". Journal of Energy Storage, Volume 14, pp. 8-15, 2017.

S.P. Koko, K. Kusakana, H.J. Vermaak, "*Optimal power dispatch of a grid-interactive micro-hydrokinetic-pumped hydro storage hybrid system*". Journal of Energy Storage, Volume 17, pp. 8-15, 2018.

S.P. Koko, K. Kusakana, H.J. Vermaak, "*Optimal power flow control of a grid-connected hydrokinetic-pumped hydro storage system for residential load profile*". Advanced Science Letters, Volume 24, pp. 8190-8195, 2018.

S.P. Koko, K. Kusakana, H.J. Vermaak, "*A Review on recent optimal energy control studies of grid-connected renewable energy systems applying time-of-use tariff strategy*", (accepted on 19 March 2018 and to be published in SCOPUS Journal).

11

Conference Papers:

S.P. Koko, K. Kusakana, H.J. Vermaak, "*Impact of different load profiles on sizing and performance of a micro-hydrokinetic system*", Proceedings of the South African Universities Power Engineering Conference (SAUPEC), pp. 410-421, January 2017.

S.P. Koko, K. Kusakana, H.J. Vermaak, "*Grid-interactive micro-hydrokinetic with pumped-hydro storage: The case study of three South African demand sectors*", Domestic Use of Energy (DUE), 2017 International Conference, pp. 83-88, *IEEE*, 4 April 2017.

S.P. Koko, K. Kusakana, H.J. Vermaak, "*Energy flow modelling between grid and micro-hydrokinetic-pumped hydro storage hybrid system*", Proceedings of the Industrial and Commercial Use of Energy (ICUE 2017) conference, pp. 19-25, *IEEE*, 14-16 August 2017.

S.P. Koko, K. Kusakana, H.J. Vermaak, "*Rule-based control strategy for a river-based grid-connected hydrokinetic system*", International Conference on Intelligent and Innovative Computing Applications (ICONIC 2018), *IEEE*, 06-07 December 2018, Mauritius.

S.P. Koko, K. Kusakana, T. Mathaba, "*Managing residential demand uncertainty in a smart grid-interactive hydrokinetic river system*", 2nd International Conference on New Energy and Environment Engineering (ICNEE 2019), 03-05 May 2019, Singapore.

1.9   Outline of the Thesis

The layout of the thesis is as follows:

Chapter 1 is an introduction to the thesis, which presents background, problem statement, objectives, methodology, hypothesis, delimitation of the study and the research outputs.

Chapter 2 provides a thorough survey on the operation principle of the hydrokinetic and PHS as the system's components, as well as a comprehensive review on the optimization

studies, based on grid-connected system (hydrokinetic and other RE systems), applying the TOU tariff strategy.

Chapter 3 determines the optimal size of the proposed system through the use of various HOMER simulation versions when supplying residential, commercial and industrial load profiles, respectively. The impact brought by each load type on the optimal size of the proposed system is further analysed.

Chapter 4 discusses the development of an open-loop optimization-based model for a non-interactive grid-connected MHK-PHS system on the basis of supplying the residential, commercial and industrial loads, respectively.

Chapter 5 discusses the development of an open-loop optimization-based model for a grid-interactive MHK-PHS system, on the basis of supplying the residential, commercial and industrial loads, respectively.

Chapter 6 discusses the development of the rule-based control model used to mitigate the negative effect caused by the load demand uncertainty on the open-loop optimization-based model.

Chapter 7 concludes all the work that has been done in the preceding chapters and also suggests future studies to be carried out.

CHAPTER 2: LITERATURE REVIEW

2.1 Introduction

This Chapter presents a brief overview on operating principle of all components of the proposed MHK-PHS system. Various optimal energy management studies have been undertaken to develop energy optimization models. The main aim of the developed models is to minimize the grid electricity consumption costs. Few studies are based on off-grid systems, while others are based on grid-connected systems. For grid-connected systems, a TOU pricing strategy has been the most widely adopted DR approach (Babu & Ashok, 2009; Yang et al., 2013; Li et al., 2016; Cheng et al., 2017; Meyabadi & Deihimi, 2017). The energy optimization studies are based on RE systems, while others are combined with non-RE systems. To minimize the high initial capital cost of RE systems, grid integration is a solution (Badwawi et al., 2015). Therefore, this Chapter further focuses on the review of recent optimal energy management studies of grid-connected RE systems, applying the TOU tariff scheme.

2.2 Operational Principle of the System Components

The proposed MHK-PHS system consists of the main component such as hydrokinetic river turbines to drive the generators as well as the PHS system for storing excess energy for later use. Fig. 2.1 shows the general layout of the proposed grid-connected MHK-PHS system. A hydrokinetic turbines-generator system is inserted into the river consisting of the flowing water resource. The main function is to convert the kinetic energy of the flowing

water into electrical energy. The operational principles of the system main components are to be described below.
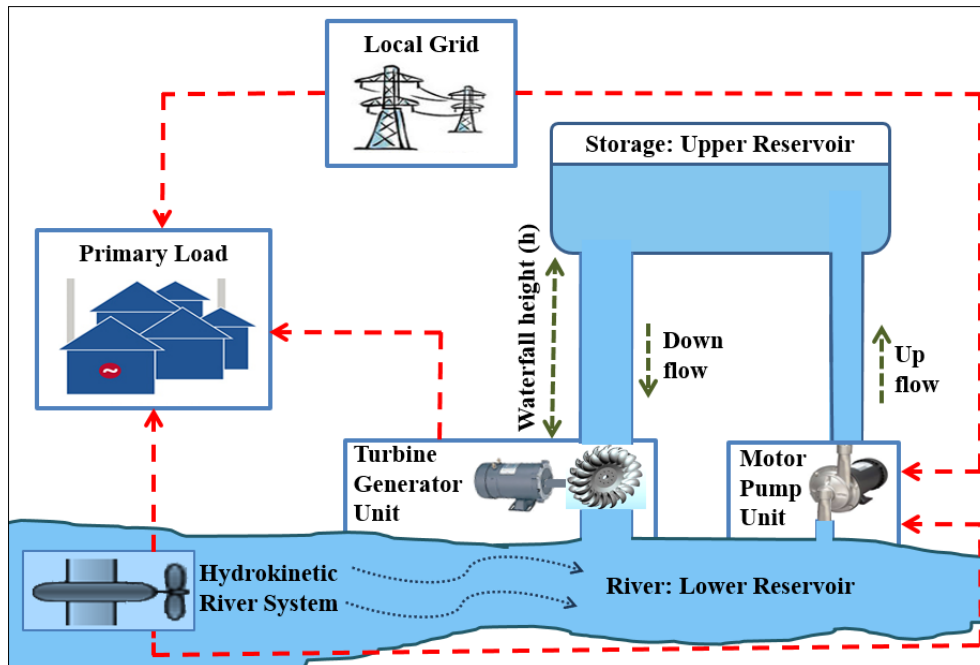
Figure 2.1: General layout of a river based MHK-PHS system

2.2.1 Hydrokinetic river turbines

Hydrokinetic turbines are available in different configurations, such as horizontal and vertical axis turbines (Vermaak et al., 2014). Hydrokinetic river turbines extract the kinetic energy of the flowing water using the swept areas of the blades. Its output power depends on the speed of the flowing water instead of the falling water. Its operation principle is similar to the one of a wind turbine system (Zhou, 2012; Güney and Kaygusuz, 2010; Vermaak et al., 2014; Koko et al., 2015). Since the water density is 800 times greater than the air density, hydrokinetic turbines extract enough power albeit at a low speed (Grabbe et al. 2009; Yuen et al., 2009; Kuschke & Strunz, 2011). This simply implies that the amount of energy generated by a hydrokinetic turbine is much greater than that produced by a wind turbine of equal

15

diameter and performance, under equal wind and water speed (Vermaak et al., 2014). Moreover, several studies proved that the hydrokinetic-based systems generate electricity markedly better and affordable than wind system (Koko et al., 2014; Kusakana, 2014; Koko et al., 2015). The results revealed that the wind speed should approximately be at nine times the flowing water speed, in order for a wind system to generate the same amount of power as a hydrokinetic system, using the same turbine-generator size. The energy generated by the hydrokinetic system (E_{HK}) is expressed as follows (Kusakana, 2015):

$$E_{HK} = 0.5 \times \rho_W \times A \times v^3 \times C_p \times \eta_{HKT-G} \times t \tag{3.1}$$

Where, ρ_W = water density (1000 Kg/m^3);

A = hydrokinetic turbine swept area (m^2);

v = water speed (m/s);

C_p = power coefficient of a hydrokinetic turbine;

$\eta_{HKT\text{-}G}$ = overall efficiency of a hydrokinetic turbine-generator unit;
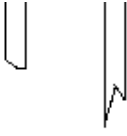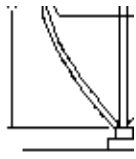
t = time (s).

Various hydrokinetic turbine configurations are available to convert kinetic energy of the flowing water into mechanical power, which rotates a generator to produce electricity. These are avialable as either vertical or horizontal turbines, similar to the wind turbines. The selection of the turbine depends on the flow type, water speed and desired output power (Vermaak et al., 2014). In this study, a conventional horizontal hydrokinetic turbine will be considered, since its operational characteristics have been investigated for many years. Moreover, the horizontal turbines proved to be more efficient than the vertical turbines (Saad

16

& Asmuin, 2014; Zhou, 2012). Hence, it influences the elimination of a gearbox unit through the use of a water speed increaser. The inclusion of a gearbox unit in a system reduces the efficiency of the overall hydrokinetic river system (Koko et al. 2015).

Determining the swept area (A) of the hydrokinetic turbine blades is critical for determining the total power of the system. The swept area is determined based on the rotor blade configuration, as shown in Table 3.1 below.

Table 2.1: Swept area for various rotor blade configurations (Bekker, 2012)

Rotor blade arrangement	Conventional rotor	H-Darrieus rotor	Darrieus rotor
Swept Area	$A=\pi.R^2$	$A= DH$	$A=0.65DH$

Where, D= turbine diameter (m);

H = turbine height (m);

R= turbine radius (m).

Similar to the wind turbines, hydrokinetic turbines may solely extract a portion of the total kinetic power of the flowing water. The rotor power coefficient (C_p) is limited to 16/27=0.593, as revealed by the well-known Betz law (Bryans, 2006).

2.2.2 Pumped-hydro storage system

PHS technology is a means of storing the off-peak electrical energy for later use during the peak demand period. A conventional PHS system relies on the gravitational energy of the stored water to generate electricity. In this study, the selected PHS system consists of two water reservoirs; namely upper and lower reservoirs linked, using two separate penstocks as shown in Fig. 2.2 below. Hence, both charging and discharging processes may occur concurrently. These reservoirs are maintained at various heights. The technology used in a PHS system consists of an electric generator, hydraulic turbines and a motor-pump unit. During the low demand period, it is economical to pump the water from the lower reservoir back into the upper reservoir, to allow storage for later use. In this study, the pumping motor will use the power from the grid and/or excess power from the hydrokinetic system. During the high demand period, the stored water is allowed to flow back into the lower reservoir, in order to enable the generation of electricity using a turbine-generator unit.

2.2.2.1 Upper reservoir

Based on this study, the volume of the stored water should be sufficient to support the unmet load demand, as the power generated by the hydrokinetic system is insufficient to meet the demand. The water level within the upper reservoir (storage tank) may be regarded as the current state of charge (SOC). The amount of stored energy is proportional to the volume of the stored water, as well as the height of the waterfall. Hence, the stored potential energy (*Es*) of the water in the upper reservoir (in joules) is expressed as follows (Goswami & Kreith, 2008; Díaz-González et al., 2016; Akinyele & Rayudu, 2014):

$$E_S = V \times \rho \times g \times h \qquad (3.2)$$

Where: V = volume of stored water (m^3);

g = gravitational acceleration (9.81 m/s^2);

h = head between lower and upper reservoirs (m).
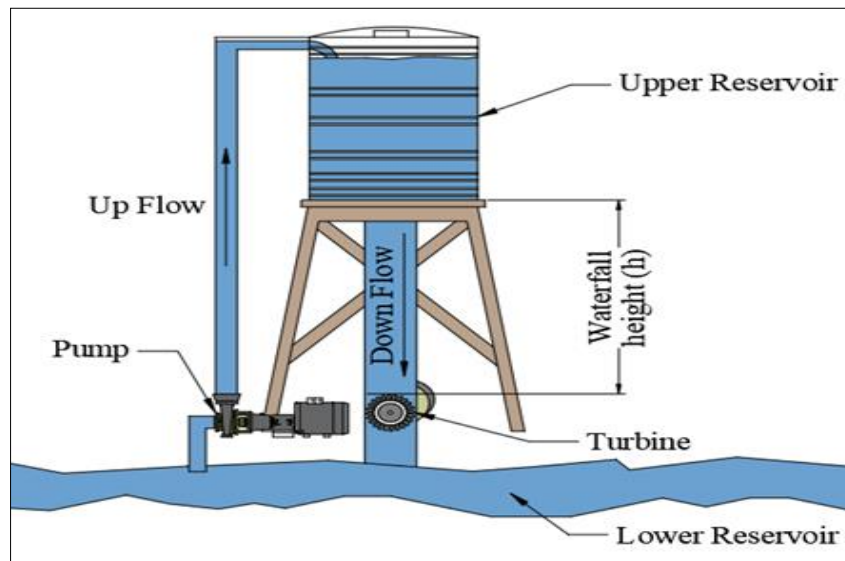
Figure 2.2: The operating principle of a PHS system

2.2.2.2   Motor-pump unit

During pumping mode, a certain volume of water should be delivered from the lower reservoir into the upper reservoir. The energy required by the motor-pump unit to recharge the upper reservoir, situated at a certain height, is determined using Equation (3.3) (Ter-Gazarian, 1994; Al Zohbi et al., 2016). This energy will be supplied by the hydrokinetic system and/or lower-cost utility grid power.

$$E_p = \frac{V \times \rho \times g \times h}{\eta_p}$$

(3.3)

Where: η_p = overall pumping efficiency.

Hence, during the charging process, the volumetric water flow rate, Q_p (m³/s) from the lower reservoir to the upper reservoir is extracted by the motor-pump unit and is expressed as follows (Al Zohbi et al., 2016; Ma et al., 2014):

$$Q_p = \frac{P_{ch} \times \eta_p}{\rho \times g \times h}$$

(3.4)

Where: P_{ch} = power supplied for pumping process (W).

2.2.2.3   Turbine-generator unit

During the generation process, the water flows downwards through the penstock to enable the turbine-generator units to convert the gravitational potential energy into electrical energy. The discharged water is thereafter collected in the lower reservoir. The most efficient turbine-generator unit should be selected, to minimize a need for the larger upper reservoir. Hence, the electrical energy generated by the turbine-generator unit is determined as follows (Ter-Gazarian, 1994; Ma et al., 2014):

$$E_p = V \times \rho \times g \times h \times \eta_{t:g}$$

(3.5)

20

Where: $\eta_{t:g}$ = overall efficiency of the turbine-generator unit.

During generation mode, the water is drawn from the upper reservoir in order to drive the hydro-turbines coupled to the generators. Hence, during the discharge process, the volumetric water flow rate, Q_t (m³/s) from the upper reservoir into the turbine, is expressed as follows (Ma et al., 2014):

$$Q_t = \frac{P_{t:g}}{\rho \times g \times h \times \eta_{t:g}}$$
(3.6)

Where: $P_{t:g}$ = power generated by a turbine-generator unit (W).

2.3 Recent Studies on Optimal Energy Management of Grid-integrated RE Systems

Below is a review of recent optimal energy management studies of a grid-integrated RE system, applying the TOU tariffs. These optimal energy management studies determine the optimal solution, without controlling or shifting the household appliances demand. In a few of the studies, the grid-connected RE systems are integrated with a non-RE system such as DG, in order to improve the reliability. However, the common goal of these studies is to minimize the grid energy expenditures and/or operation costs, by allowing/disallowing the energy sales into the grid.

A few of the reviewed optimal energy management studies are grid-interactive, meaning they allow the energy to be sold into the utility grid and to be purchased from the utility grid,

whenever it is economical to do so based on the TOU rates. Energy purchasing may further take place if there is an insufficient energy from the RE system. Other studies considered in this review, are said to be solely grid-connected and not grid-interactive. This simply implies that they solely allow the purchasing of energy from the utility grid when charges are inexpensive or there is insufficient energy from the RE system. Hence, the energy sales into the utility grid are not permitted.

2.3.1 Grid-interactive renewable energy systems

The section below covers the review of the recent grid-interactive RE systems, applying the TOU tariffs. These studies allow the energy to be purchased from the utility grid and to be sold into the utility grid.

Sichilalu and Xia (2015a) developed an optimal scheduling strategy for a grid-tied PV (photovoltaic)-battery system, to power the heat pump water heater (HPWH) system and the domestic load. The aim of the model is to reduce the energy costs, while meeting the technical and operational constraints, by considering the TOU tariff scheme. The optimization problem was addressed using a mixed-integer nonlinear programming solver in MATLAB for a 24 hour interval, using the demand of 4 seasonal dates. The TOU tariff rates were assumed to be constant for all seasons. The results have revealed that the optimal strategy uses the cheaper stored energy and the PV system to power HPWH, whenever it is sufficient. The battery is recharged by the grid power during inexpensive off-peak hours, in order to minimize the grid consumption costs. In another study (Sichilalu & Xia, 2015b), a DG was to the same grid-tied PV-battery system and the optimal scheduling strategy was determined. The results concluded that the model has the potential to save energy by up to 114.06 kWh per day, with a maximum cost saving of 68.09%.

Wanjiru et al., (2016) developed an open-loop model for an optimal control strategy of a hybrid heat water pump and instantaneous water heaters, powered using grid-connected PV and wind turbine (WT) system, consisting of a diesel generator (DG) grid. The aim of the model is to save both energy and water consumption. TOU tariff prices, applied by the South African electric utility company, were considered. The simulations were carried out for a 24 hour horizon, with a sampling period of 30 minutes. The optimization problem was solved in MATLAB, using OPTI toolbox. This optimal model proved to lower the operational cost of a DG grid system. It saved 5.5% of power-not-delivered from the DG grid system in 24 hours. Furthermore, about 5.05 kWh of energy was sold back into the DG grid in 24 hours. Additionally, the instant shower, used to heat the water inside the pipe, led to approximately 24% of water savings than the regular shower heads. In another study (Wanjiru et al., 2017a), they advanced the abovementioned open-loop control model by making use of the closed-loop model predictive control (MPC) approach to optimize the same system, while dealing with disturbances. The MPC model proved to save 32.24% of energy and 19 litres of water. The system proved to have a 9 year and 4 months payback period.

Sichilalu et al., (2016a) developed an optimal energy management strategy for a grid-tied PV-fuel cell hybrid system to power the domestic load and HPWH system supplying the thermal load. The main objective of the developed model is to minimize the energy cost, by considering the TOU tariffs. The optimization problem has been solved through the use of a mixed binary and real linear programming method for a 24 hour control horizon. The proposed model proved to reduce the power consumption of a HPWH system from 84 kWh to 45.50 kWh. In another study (Sichilalu et al., 2016b), they incorporated a WT to the same grid-tied-PV-fuel cell hybrid system and determined the optimal energy management strategy. The main objective was to minimize the energy cost and maximize fuel cell output,

23

taking the TOU tariffs into account. The proposed model proved to minimize the energy losses by effectively improving the operational and system efficiency.

Kusakana (2016) developed an optimal operation control model for a grid-connected PV-battery hybrid system by considering the TOU tariffs. The model aimed to minimize the grid energy costs. The simulations have been carried out for a 24 hour period, through the use of a linear programming method in MATLAB. The results revealed that the model reduced the operation cost and generated substantial income by selling power to the grid. In another study (Phiri & Kusakana, 2016), the WT was incorporated to the same system and the optimal energy management model was developed. The operation cost of the system was minimized and more income was generated by selling power to the grid.

Siti et al. (2016) developed a closed loop optimal control strategy for a grid-connected solar-wind-PHS system, using TOU tariff as a control variable. The simulations were carried for a 24 hour period. The results concluded that the model was able to handle external disturbances as compared to the open-loop approach. Additionally the energy sales to the grid were maximized.

Wanjiru et al. (2017b) developed a model for an optimal operation control strategy of the grid-connected solar PV system, integrated with a HPWH powered system. TOU tariff prices applied by the South African electric utility company were considered. The simulations were carried for a 24 hour horizon with a sampling interval of 30 minutes. The optimization problem was solved in MATLAB using OPTI toolbox. This strategy proved to lower the energy cost by about 19% and saved up to 35% of power-not-delivered from the grid in 24 hours. About 7.7 kWh of energy was sold back into the grid, to generate some cash through feed-in-tariff (FIT). Hence, both energy and water bills of the consumer are lowered. Since, there was no ESS involved, excess RE was continuously sold into the grid to generate some revenue for the consumer.

Wanjiru et al. (2017c) developed a model for an optimal control strategy of a hybrid heat water pump heater and an instantaneous shower, powered using grid-connected solar and WT system. TOU tariff prices applied by the South African electric utility company were considered. The simulations were carried out for a 24 hour horizon, with a sampling period of 15 minutes. The objective function was solved using Solving Constraint Integer Programming (SCIP) solver available in the MATLAB toolbox. This strategy proved to save 23.4% of energy and 19 litres of water per day. Hence, both energy and water costs of the consumer are lowered. Since, there was no ESS involved, excess RE was continuously sold into the grid to generate some revenue for the consumer.

Kusakana (2017a) developed an optimal scheduling for a grid-connected hydrokinetic battery-based system, under the TOU tariff scheme and involved energy sales into the grid. The aim of the model is to minimize the electricity cost subject to power balance, hydrokinetic and battery storage outputs. The optimal schedule was developed for a typical household and base transceiver station load profiles, respectively. The optimization problem was solved through the use of the linprog function in MATLAB. The simulations were carried out for a 24 hour horizon with a sampling period of 30 minutes. The model proved to maximize the hydrokinetic energy power and battery storage system during peak hours. The grid power was used during inexpensive off-peak periods to store energy in the battery storage system. The operational cost has been reduced and a considerable income is generated by trading power to the utility grid.

Lu et al. (2017) proposed a multi-objective optimal dispatch model for a grid-connected microgrid comprising of solar PV, WT, diesel engine, micro-turbine and an electric vehicle, used as a storage system. The aim of the model is to reduce the system operation cost by considering the TOU tariff scheme, through the use of an improved particle swarm optimization algorithm. The simulations were carried out for an interval of a 24 hour period.

25

The simulation results revealed the effectiveness and superiority of the proposed model in reducing the user's electricity costs and environmental pollution. It proved to promote the optimal operation of microgrid and the economic management of the battery was achieved. The model did not allow the power to be sold into the grid, since the solar PV and WT capacities cannot meet the load demand at all times.

Sichilalu et al. (2017) developed an optimal control model of a grid-tied WT-PV hybrid system, supplying the HPWH system and the domestic load. The aim of the study is to minimize the energy costs by taking the TOU tariffs into account. A mixed integer linear program has been used to solve the problem for a 24 hour control horizon. The optimization model proved to bring 70.7% energy cost reduction.

Kusakana (2017b) developed an optimal power scheduling for a grid-connected PV-wind-battery based hybrid system. The aim of the developed model is to minimize the electricity purchased from the grid, while maximizing the energy sales into the grid under the weekday's TOU tariff scheme. Load demand is assumed to be constant for each weekday. The simulations were carried out for a 24 hour horizon and the model proved to lead to the reduction of the operation cost and generation of substantial income revenue through energy sales into the grid.

Kusakana (2018) developed an optimal power scheduling for a grid-connected PV-battery based system supplying residential, commercial and industrial loads, respectively. The model was developed to investigate the difference in energy savings, resulting from each load profile, under the low demand season TOU tariff for weekdays. The variability of the load profile for each weekday was ignored. The simulations were carried out for a 24 hour horizon, through the use of linear programing solver in MATLAB. The model proved to lead to the energy savings potential for each load profile. The commercial and industrial load profiles proved to generate higher savings when compared to the domestic load profile.

Numbi and Malinga (2017) developed an optimal energy management model for a grid-interactive battery-based solar PV system, under FIT for energy sales and TOU tariffs for grid-consumption cost. The simulations were carried for a 24 hour horizon through the use of *fmincon* optimization solver in the MATLAB toolbox. The results prove that 69.41% of potential cost savings is possible at the current FIT of US$0.046/kWh. If the FIT's are increased to US$0.16/kWh, an attractive payback period of 8.6 years is achieved at an energy cost saving potential of 144.4%.

2.3.2 Non-interactive grid-connected renewable energy system

Below is a review of the grid-connected RE system, applying the TOU tariffs. These studies allow the purchasing energy from grid and disallow the energy sales into the grid.

Yoon and Kim (2014) developed a charge scheduling of an ESS under both TOU and demand charge, using real-coded generic algorithm (RCGA). The aim of the model is to address the scheduling problem experienced by consumers having their own onsite grid-connected PV-battery based generation facility. Optimal battery scheduling reduces the customers' electricity costs. Simulations where carried out for a 24 hour horizon, applying both summer and winter TOU tariff rates in the Intel Xeon CPU E5530. The daily variability of the load profile was not considered in the study. The simulation results showed that the RCGA enabled the storage schedule to reduce electricity costs by approximately 17%, as compared to the system without an ESS.

Wu and Xia (2015) proposed an optimal switching control model for a grid connected solar PV system. The aim of the model is to sufficiently utilize the solar energy and to minimize electricity costs under the TOU tariff program. The optimization problem has been solved using bintprog function in MATLAB. The simulations were carried out for the

27

evaluation period of 24 hours. Weekends and weekdays load profiles were used during simulations. The electricity tariffs for both summer and winter were further assumed to be constant. The results revealed that the electricity costs have been largely reduced by approximately 50%, through the use of the optimal switching control method.

Pallonetto et al. (2016) developed a rule-based demand response algorithm for a smart-grid residential building. The residential building is equipped with a heat pump, water storage tank, PV array, solar thermal collectors for domestic hot water heating and an electric vehicle. The algorithm is developed with the purpose of minimizing the electricity expenditure under the TOU tariff scheme. The control algorithm was injected in an energy management system of the EnergyPlus model, through the use of the native programming language. The algorithm proved to guarantee monetary savings, by reducing the generation cost, electricity expenditure, and carbon emission by 22.5%, 4.9 % and 7.6%, respectively, while maintaining thermal comfort. This was made possible through the use of the TOU tariff scheme, in conjunction with Zone thermal control.

Wang et al. (2017) proposed an optimal scheduling demand model to optimally schedule and manage the interaction between an electricity provider and users. The onsite grid-connected RE system consists of the PV thermal, WT and hydrogen powered fuel cells. The main objective is to meet production requirements, while minimizing the overall operating and environmental costs, through producing, purchasing and selling of electricity. The optimization challenge has been solved using SDPT3 solver in MATLAB. The simulations were carried out for the evaluation period of 24 hours for a series of DR schemes. The results suggested that the electricity contract and incentive based scheme with industrial customers is an effective method for both the grid operator and user.

Geem and Yoon (2017) proposed the efficient harmony search algorithm for RE charging with ESS. The aim is to discover the optimized scheduling of the ESS under the

28

TOU pricing for a grid-connected PV-battery based system supplying the residential consumers. The simulations were carried out for 24 hours in both winter and summer seasons. The results proved that optimization using a harmony search algorithm, improved the results when compared to genetic algorithm. The optimal schedules determined by the presented harmony search algorithm, proved to reduce both the peak power and purchase of electricity during peak period, as compared to the genetic algorithm. Hence, it proved to be more useful in reducing the electricity bills of the customer.

Zang et al. (2017) proposed the methodology to minimize the electricity cost of a grid connected factory having an onsite PV-battery based system. The aim of the model is to determine the optimal manufacturing and onsite energy flow schedules at a minimal electricity cost, under TOU tariff rates. Both winter and summer TOU price schemes were simulated. Time-indexed mixed integer-programming model has been used to solve the optimization problem. The simulations have been carried out for a 24 hour horizon and the economic performances associated with various PV capacity and battery bank sizes were investigated. The results showed that the factory's electricity costs may be reduced 54% and 0.7% under the summer TOU rates and winter TOU rates, respectively. This was achievable with the selection a 557.4 m^2 PV panel and a 100 kWh battery bank.

Di Santo et al. (2018) developed a methodology for managing the active demand side for household consisting of the grid-tied battery-based solar PV system, using optimization and artificial intelligence. The main aim of the methodology is to optimally manage the battery state of charge, in order to reduce the consumer electricity cost under TOU tariff. The simulations have been carried out for a 24 hour horizon. Load profiles of three various solar generation profiles for three various consumer profiles were used during the simulation. The results revealed that the Manager's decision-making system could perform the battery management, to reduce the consumer's electricity cost efficiently.

29

The summary of these recent grid-interactive and grid-connected RE based studies is as highlighted in Table 2.2 and 2.3, respectively.

Table 2.2: Summary of recent grid-interactive RE studies

Author(s)	System Type	Load Type	Solver/Algorithm & Horizon	Results
Sichilalu et al. (2015)[a]	PV-Battery	HPWH & Domestic	MATLAB (mixed-integer nonlinear solver) : 24h	52.54% cost savings
Sichilalu et al. (2015)[b]	PV-Battery-DG	HPWH & Domestic	MATLAB (mixed-integer nonlinear solver) : 24h	68.09% cost savings
Wanjiru et al. (2016) Row Name Here	PV-WT-DG	HPWH	MATLAB (OPTI toolbox): 24h	24% water savings & 5.5% power savings
Siti et al. (2016)	PV-WT-PHS	Domestic	MATLAB (close-loop approach): 24h	Maximized grid energy sales
Sichilalu et al. (2016)[a]	PV-fuel cell	HPWH & Domestic	MATLAB (mixed-binary & real linear): 24h	45.8% power savings
Sichilalu et al. (2016)[b]	PV-WT-fuel cell	HPWH & Domestic	MATLAB (mixed-binary & real linear): 24h	Maximized energy losses & better efficiency
Kusakana (2016)	PV-Battery	Domestic	MATLAB (*linprog*): 24h	Minimized operation cost & higher income
Kusakana & Phiri (2016)	PV-WT-Battery	Domestic	MATLAB (*linprog*): 24h	Minimized operation cost & higher income
Wanjiru et al. (2017)[a]	PV	HPWH	MATLAB (OPTI toolbox): 24h	35% power savings & 7.7 kWh energy sales
Wanjiru et al. (2017)[b]	PV-WT	HPWH & Shower	MATLAB (SCIP toolbox): 24h	19 litres of water savings & 23.4% energy savings

30

Wanjiru et al. (2017)[c)]	PV-WT-DG	HPWH	MATLAB (close-loop approach)	19 litres of water savings & 32.2% energy savings
Kusakana et al. (2017)[a)]	Hydrokinetic-Battery	Domestic & Base Transceiver	MATLAB (*linprog*): 24h	Maximized RE & storage usage
Kusakana et al. (2017)[a]	PV-WT-Battery	Domestic	MATLAB (*linprog*): 24h	Maximized energy sales & minimized operation cost.
Sichilalu et al. (2017)	PV-WT	HPWH & domestic	MATLAB (mixed-integer *linprog*): 24h	70.7% energy cost savings.
Numbi & Malinga (2017)	PV-Battery	HPWH	MATLAB (Fmincon) : 24h	69.41% of energy cost savings.
Kusakana (2018)	PV-Battery	Domestic, Commercial & Industrial	MATLAB (*linprog*): 24h	Commercial and industrial yield higher savings

Table 2.3: Summary of recent grid-connected RE studies

Author(s)	System Type	Load Type	Solver/Algorithm & Horizon	Results
Yoon & Kim (2015)	PV-Battery	Domestic (winter & summer)	Intel Neon (RCGA): 24h	17% cost savings
Wu & Xia (2015)	PV-Battery	Community clinic (weekend & weekday)	MATLAB (bintprog): 24h	50% cost savings
Pallonetto et al. (2016)	PV-Solar thermal collector	Domestic	EnergyPlus (native programmable language):24h	22.5% cost savings
Wang et al. (2017)	PV-WT-fuel cell	Industrial	MATLAB (SDPT3 solver): 24h	Electricity contract and incentive proved to be sufficient

31

Geem & Yoon (2017)	PV-Battery	Domestic	Harmony search & generic algorithm: 24h	Harmony search proved to reduce the electricity bills.
Zang et al. (2017)	PV-Battery	Factory	MATLAB (time-indexed mixed integer): 24h	Cost savings of 54% (summer) & 0.7% (winter).
Di Santo et al. (2018)	PV-Battery	Household	Optimization & artificial intelligence: 24h	Battery management proved to reduce electricity cost.

2.4 Conclusion

Various studies based on the recent developments of optimal energy management models of the grid-connected RE systems, applying the TOU tariff scheme, were investigated. Various approaches or solvers have been used, depending on the nature of the objective function and constraints. However, it has been observed that the common goal intended by these studies is to minimize the grid energy expenditures and system operation costs. Most of the studies have allowed energy sales into the grid, in order to acquire the energy sales revenue leading to the increased energy savings. It has been noticed that MATLAB toolbox solvers have been the widely used tool to address the optimization problems.

The most dominating RE sources have been solar PV and WT technologies. Hydrokinetic technology proved to generate electricity markedly better and cheaper than solar and wind (Koko et al., 2014; Kusakana, 2014; Koko et al., 2015). However, very few studies have concentrated on developing an optimal model for alternative sources such as biomass and hydrokinetic. It has been noted that among the studies that have considered the use of ESS, the battery has been the widely used ESS. Very few studies have considered alternative ESS's.

The impracticality being that the daily load demand profiles were assumed to be constant in most studies, since simulations were carried out for a 24 hour horizon. Some studies used the seasonal load profiles in order to consider the seasonal variability of the load demand. However, the TOU tariff rates were assumed to be the same for all seasons (winter and summer) and for the entire week schedule (weekdays and weekend). Contrary to these studies, a few studies considered the seasonal variability of the TOU tariff. However, the variability of the load demand was not considered.

Based on the review findings, the study has led to the following recommendations for further optimization research:

- Further optimization studies need to be done on alternative renewable sources, such as hydrokinetic, biomass, etc.

- Further studies need to be done in analysing the behaviour of the optimization models, by considering seasonal variability of the load demand and RE resources. The performance of the model should be investigated under both weekdays and weekend days TOU tariffs, in order to analyse their effect on the behaviour of the model.

CHAPTER 3: OPTIMAL SIZING OF THE PROPOSED MHK-PHS SYSTEM

3.1 Introduction

Due to the high investment cost of RE systems, an optimal sizing is critical to adequately meet the load demand at a low investment cost. Hence, an optimal size of a proposed river-based MHK-PHS system should be determined before developing an optimal energy management model in Chapter 4. The HOMER software will be used in this study to determine the optimal system architecture. HOMER has been the most widely used tool to carry out the prefeasibility, optimization, sensitivity analysis, as well as sizing of off-grid or grid-connected RE systems (Sinha & Chandel, 2014; Bahramara et al., 2016).

Many hydrokinetic studies have used the HOMER Legacy Version to determine the optimal size of hydrokinetic-based systems (Kusakana & Vermaak, 2013; Yakub, 2014; Koko, 2014; Kusakana & Vermaak, 2014; Kusakana, 2014; Kusakana, 2015). However, the Legacy Version does not have a built-in hydrokinetic module in its library. As a result, the authors had to use the wind turbine module to represent a hydrokinetic turbine, since the two technologies share many of the similarities, in terms of physical operation (Güney & Kaygusuz, 2010; Vermaak et al., 2014; Koko et al., 2015). An assumption stating that both the anemometer height and turbine hub height are equal, was to be considered when modelling the hydrokinetic turbine, using a wind turbine module (HOMER Energy Support, 2016).

In this study, an optimal size of the proposed MHK-PHS system is determined through the use of the HOMER Pro Version 3.6.1. The HOMER Pro Version 3.6.1 is equipped with a

hydrokinetic module in its library. The sizing results obtained using HOMER Pro Version 3.6.1 are compared to the ones obtained using the Legacy Version. The aim is to validate the best economical approach for sizing the proposed system. The optimal system size will be determined for supplying various load classes, such as residential, commercial and industrial load respectively. The aim is to investigate the effect of each load type or profile on sizing and operation of the proposed river-based MHK-PHS system, when operated as a stand-alone and when connected to the grid under TOU tariff scheme.

3.2 Load Demand Profiles

As mentioned in the introduction, the optimal size of the proposed river-based MHK-PHS system will be determined for supplying the residential, commercial and industrial load profiles respectively. The aim is to investigate the effect of each load profile on sizing and operation of the proposed system. It has been proven that various demand sectors, such as residential, commercial and industrial, have load profiles with dissimilar curves. Meaning, the electric usage pattern for each customer class varies. For each load profile, the peak demand takes place at various times of the day, as compared to others. However, irrespective of various load profile shapes, the TOU tariff schedule applied by the electric utility company remains the same and the load demand should be satisfied at all times.

However, it is practically impossible to expect the demand of each load class/type to remain constant throughout the day and in both winter and summer seasons. The demand of each load class/type is controlled by factors, such as the change in weather, type of activities, as well as the economic situation (Bokhari et al., 2014).

For appropriate sensitivity analysis of the effect brought on by each load type, the three load classes are standardized to have the same daily energy consumption of 60 kWh, in this

35

study. An hourly and daily random variability of 10% was used to create a variable yearly load profile.

3.2.1 Residential load profile

A recent residential load profile/curve of typical South African consumers, situated in Matshana area of Kwazulu Natal Province, was used to estimate daily power curve (Setlhogo et al., 2017). The load profile was entered into the HOMER software and standardised to obtain a daily average energy consumption of 60 kWh, as shown in Fig. 3.1. To yield the daily energy consumption of 60 kWh, the residential load profile resulted in a peak power consumption of 5.34 kW, at a small base load of 1.3 kW.

After entering 10% hourly and daily random variability, a more sensible variable load profile was created, as shown in Fig. 3.2 and Fig. 3.3. It is observed that HOMER allowed the load to peak more during June to August. This is regarded as a high demand season.
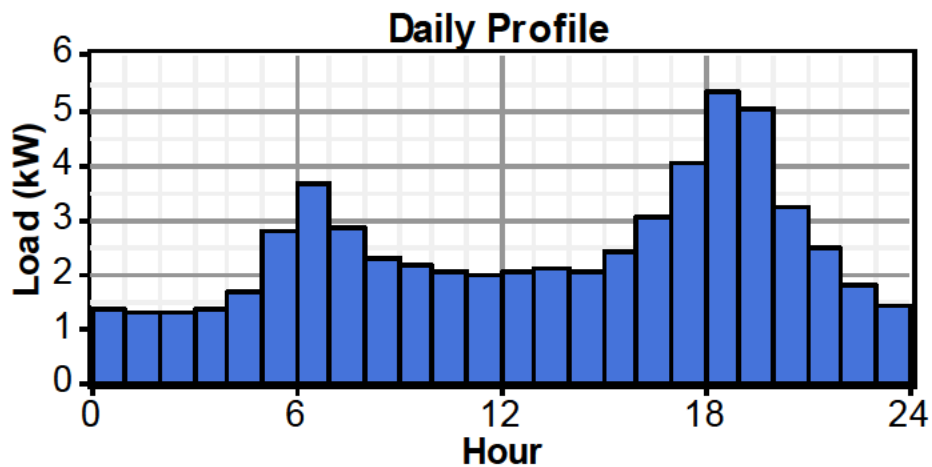
Figure 3.1: 60kWh average daily load profile (residential)

36
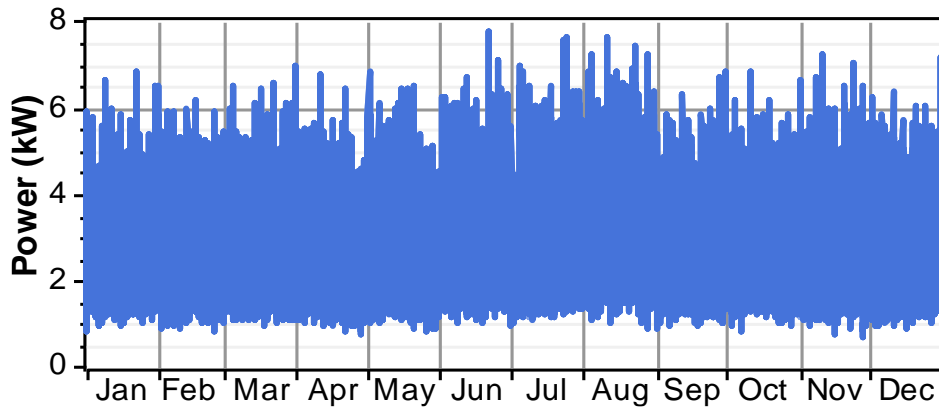
Figure 3.2: Annual load profile with random variability (residential)
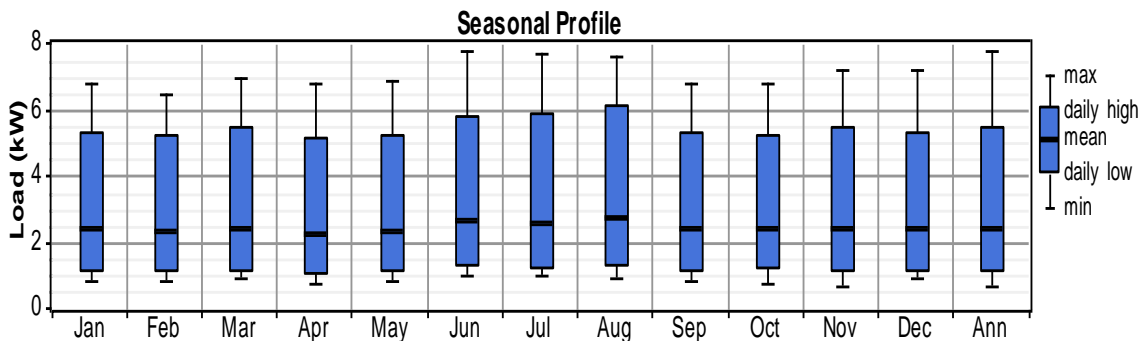
Figure 3.3: Monthly average scaled data (residential)

3.2.2   Commercial load profile

A typical commercial load curve for low voltage consumers is used in this study to estimate the commercial load behaviour (Jardini et al., 2000). It can be seen that the commercial load profile behaves differently when compared to the residential load profile. Most of the energy consumption takes place during the day, i.e. during working hours. The commercial load power curve was entered into the HOMER software to create a daily load profile, as shown in Fig. 3.4. To yield the daily energy consumption of 60 kWh, the commercial load power curve resulted in a peak power consumption of 5.43 kW, at a small base load of 0.29 kW.

37

After entering a 10% hourly and daily random variability, a more sensible variable load profile was created, as shown in Figs. 3.5 and 3.6. Similar to the residential load demand, it is observed that HOMER allowed the load to peak more during high demand season months (June to August).
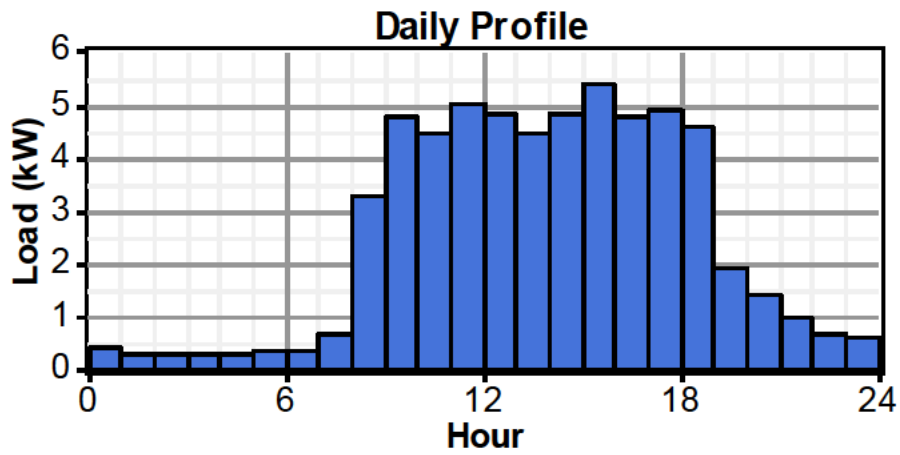
Figure 3.4: 60kWh average daily load profile (commercial)
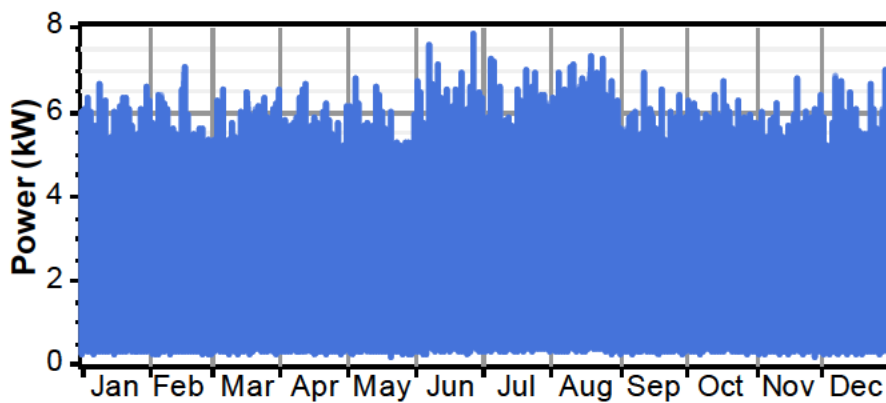
Figure 3.5: Annual load profile with random variability (commercial)

38
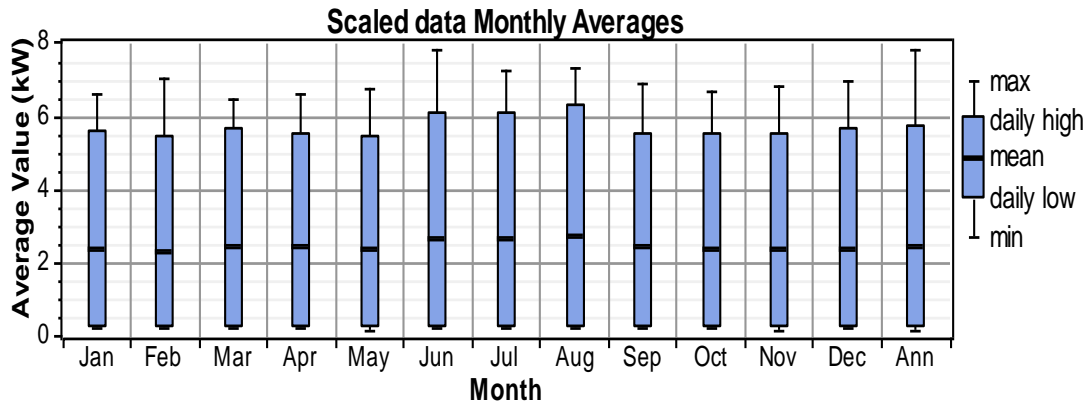
Figure 3.6: Monthly average scaled data (commercial)

3.2.3 Industrial load profile

A typical industrial load curve for low voltage consumers is used in this study to estimate the industrial load behaviour (Jardini et al., 2000). It can be seen that the industrial load profile behaves differently, when compared to both residential and commercial load profiles. Most of the energy consumption takes place during the day, even though the highest peak demand is achieved during morning working hours. Unlike the commercial businesses, most industrial businesses allow their employees a lunch break simultaneously, instead of allowing for various break shifts/sessions to take place. Hence, this lowers the production rate of the industry during lunch break.

For this study, the aforementioned industrial load profile/curve was standardised to have a daily average energy consumption of 60 kWh. The load profile was entered into the HOMER software to create a daily load profile, as shown in Fig. 3.7. To yield the daily energy consumption of 60 kWh, the residential load power curve resulted in a peak power consumption of 7.32 kW at a small base load of 0.14 kW.

After entering a 10% hourly and daily random variability, a preferred variable load profile was created, as shown in Fig. 3.8 and Fig. 3.9. Similar to the residential and commercial load

39

demands, it is observed that HOMER allowed the load to peak more during high demand season months (June to August).
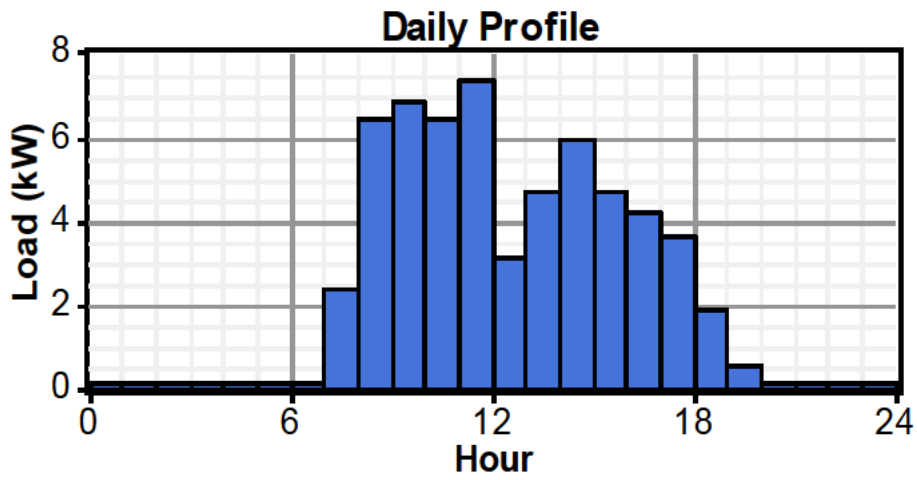
Figure 3.7: 60kWh average daily load profile (industrial)
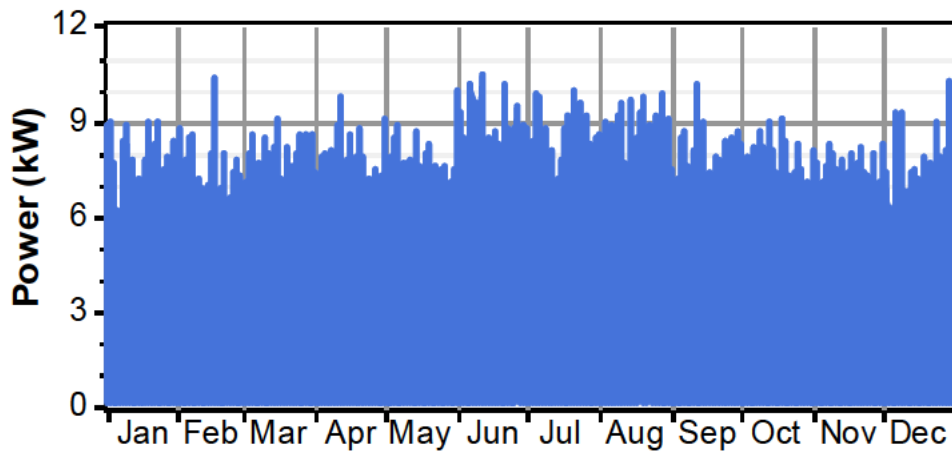
Figure 3.8: Annual load profile with random variability (industrial)
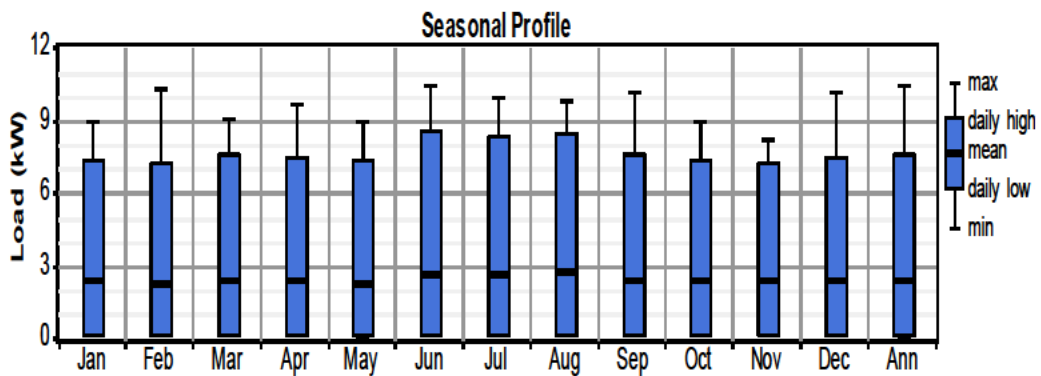
Figure 3.9: Monthly average scaled data (industrial)

40

3.3 Simulation Components Parameters and Costs

The proposed MHK-PHS system consists of the hydrokinetic river system to generate electricity, an inverter to convert DC (direct current) power to AC (alternating current) and a PHS system to store energy. The performance and costs for each component are critical for optimum design configuration. The cost of each component is broken down into capital, replacement, and operation and maintenance (O&M) costs. In this study, all components are assumed to have the replacement costs, equal to the capital costs. During the study, 1 US$ was equivalent to ZAR13.51. Hence, the currency of ZAR will be applied throughout.

3.3.1 Hydrokinetic system (turbine and an inverter)

River-based hydrokinetic turbines are available in a range of 1–10 kW (Vermaak et al. 2014). In this study, a generic 1.5 kW direct current (DC) Darrieus hydrokinetic turbine (DHK), with the swept area of 1.56m^2 is selected (Koko et al., 2014). It will also be used to determine the generated output power. It generates a rated output power of 1.5 kW at water-flow speed of 2 m/s or above. One unit requires a capital cost of US$15,000, with operation and maintenance (O&M) costs considered to be US$300 per year. Similar to wind turbines, the life span is estimated to be 25 years (Hiendro et al., 2013). The output power curve of the turbine is shown in Fig. 3.10.

In this study, an 8 kW, 50 Hz, 230 Vac Victron inverter has been considered to convert DC output power of a hydrokinetic generator into AC power. The cost price of this converter is US$5,509, with the O&M cost assumed to be US$55.09 (Koko et al. 2014). When modelling a PHS system, a battery is the sole component to be connected to a DC bus (Canales & Beluco, 2014).

41
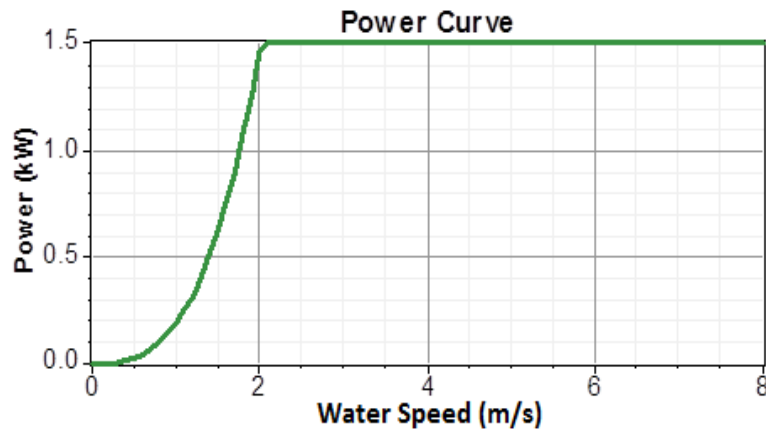
Figure 3.10: Power curve of the Darius hydrokinetic (DHK) turbine (Koko et al. 2014)

3.3.2   Pumped-hydro storage system

To model a PHS system with HOMER software, it has been proven that the battery, which is equivalent to the upper reservoir, is usually created and used (Canales et al. 2015; Iqbal, 2009; Kusakana, 2015). The round-trip efficiency and the minimum state of charge (SOC) of the equivalent battery should be set to 100% and 0%, respectively (Canales et al. 2015). Additionally, HOMER suggests that nothing other than the created battery should be connected to the DC bus, in order to allow for improved observation of a PHS performance. To achieve this constraint, a converter with a round-trip efficiency of 100% should be used to link the battery to a DC bus, during modelling (Canales & Beluco, 2014).

In this study, a Trojan T-105 battery was selected and modified to represent a minimum reference volume of the water. The battery settings were approved to be 230V and 26 Ah, respectively, in order to allow each battery to store up to a maximum of 6 kWh. When supplying a 1kW load, it may discharge for a maximum of 6 hours. The power of the battery is directly proportional to the discharge current (Canales & Beluco, 2014). Therefore, a maximum discharge current was set to 4.35 A, which is equivalent to 0.0926 m^3/s volumetric

42

discharge rate for a maximum volume of 200 m^3 at an assumed water head and round-trip of 18.35 m and 60%, respectively.

The cost of the PHS system has been entered into the battery model, with a lifespan assumed to be 30 years. The installation cost/kWh varies between US$2000 and US$4000 (Kusakana, 2015). In this study, an installation cost/kWh is assumed to be US$3000. The O&M cost is assumed to be 6% of the initial capital cost (Canales et al., 2015). After determining the optimal quantity of the needed batteries, the total storage capacity of the upper reservoir is determined by the product of the nominal capacity of each battery and the battery quantity.

3.3.3   Hydrokinetic resource data

Hydrokinetic resource data is necessary to define the flowing water speeds that a hydrokinetic turbine would experience in a typical river. The monthly average water velocity of a typical river situated in Kwazulu Natal Province (South Africa) has been used as input to the hydrokinetic module, as illustrated in Fig. 3.11. Although there are some months with insufficient water speeds (below 2 m/s), the proposed MHK_PHS system should be designed to meet the load demand throughout the year, without any deficiency.
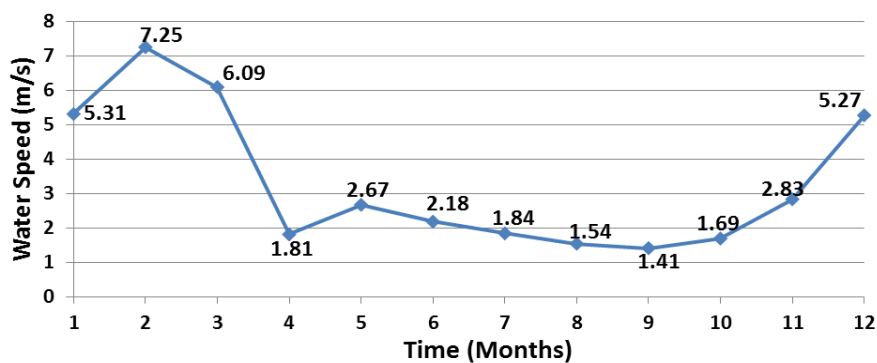
Figure 3.11: Monthly average water velocity (Kusakana, 2015)

3.4 Simulation Results and Discussions

As mentioned previously, the optimal sizing results are computed through the use of the HOMER software, with the aim of analysing the impact of various load classes on sizing and operation of the proposed MHK-PHS system. HOMER legacy version results are compared to the HOMER Pro Version 3.6.1 results, in order to validate the desired approach. Optimal size is computed when the system is operated as a stand-alone and connected to the grid under TOU tariff scheme.

3.4.1   Optimal configuration of a stand-alone MHK-PHS system

The optimal size of the stand-alone MHK-PHS system is determined through the use of the old HOMER Legacy Version and HOMER Pro Version 3.6.1. When using the Legacy Version, the methodology of allowing an anemometer height to be equal to the turbine hub height is applied. The reason is that the old Legacy Version is not equipped with hydrokinetic turbine module in its library. As a result, HOMER is disabled from scaling the wind-speed data. When computing, using the Pro Version 3.6.1, the actual built-in hydrokinetic module is used. For both cases, the residential, commercial and industrial load classes are supplied separately as primary loads, at a 0% capacity shortage. Each load class has been standardised to have a daily energy consumption of 60 kWh for an improved comparison purposes and sensitivity analysis. Additionally, the load random variability of 0% has been used, since the aim is to investigate which methodology is preferably appropriate.

The optical configuration results obtained using the two methods, are as shown in Table 3.1, below. The results show that both methodologies yielded the same hydrokinetic turbine size of 7.5 kW to meet the demand of each load profile, as shown in Fig. 3.12. It is observed

44

that when the monthly average water speed is 2 m/s or above, the maximum power production of 7.5 kW is achieved. This occurs during the months of January, February, March, May, June, November and December. During the other months, the generated power is below 7.5 kW.

However, the discrepancy is that the HOMER Legacy Version methodology oversized the storage system by an additional 11.96 kWh (52Ah) storage capacity for each load profile, leading to higher storage autonomy. Despite the higher storage capacity computed by the HOMER Legacy Version methodology, HOMER Pro Version 3.6.1 proved that the proposed system may offer higher excess energy at lower storage capacity. This is a huge saving that will result in lower capital costs. Henceforth, the oversizing of the storage system, as computed using HOMER Legacy Version methodology, resulted in higher capital cost, NPC, COE and operating cost, when compared to the use of HOMER Pro Version 3.6.1. HOMER Pro Version 3.6.1 proved to be the preferred approach to consider for optimal sizing of the proposed system. Hence, the optimal configuration results used in HOMER Pro Version 3.6.1 will be used to analyse the potential impact of each load profile on sizing and operation of the proposed MHK-PHS system. Moreover, it has a built-in hydrokinetic module. The impacts will be discussed below.
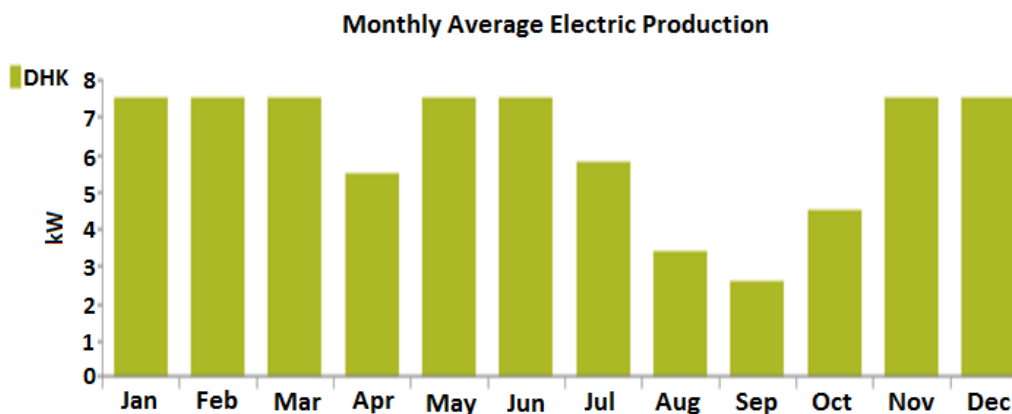
Figure 3.12: Monthly generated output power by a MHK river system (for each load profile)

Table 3.1: HOMER optimal configuration results for the off-grid system

	Residential Load		Commercial Load		Industrial Load	
	* HOMER Legacy Version	HOMER Pro Version 3.6.1	* HOMER Legacy Version	HOMER Pro Version 3.6.1	* HOMER Legacy Version	HOMER Pro Version 3.6.1
Optimal sizing results	7.5 kW hydrokinetic turbine system + 29.9 kWh upper reservoir (5 batteries: 130 Ah)	7.5 kW hydrokinetic turbine system + 17.94 kWh upper reservoir (3 batteries: 78 Ah)	7.5kW hydrokinetic turbine system + 35.88 kWh upper reservoir (6 batteries: 156 Ah)	7.5 kW hydrokinetic turbine system + 23.92 kWh upper reservoir (4 batteries: 104 Ah)	7.5 kW hydrokinetic turbine system + 41.86 kWh upper reservoir (7 batteries: 182 Ah)	7.5 kW hydrokinetic turbine system + 29.9 kWh upper reservoir (5 batteries: 130 Ah)
Capital cost ($)	117,545	111,545	120,545	114,545	123,545	117,545
Operating cost ($/y)	2,635	2,292	2,808	2,464	2,980	2,636
Net present cost ($)	148,258	138,252	153,263	143,257	158,269	148,263
Levelized COE ($/y)	0.581	0.542	0.601	0.562	0.621	0.581
Total Energy Production (kWh/y)	53,767	54,152	53,767	54,152	53,767	54,152
Storage autonomy (h)	11.97	7.18	14.36	9.58	16.76	11.97
Excess electricity (kWh/y)	31,882	32,268	31,885	32,271	31,882	32,267
Turbine-generator hours of operation (h/y)	430	519	613	919	838	1,101
Peak turbine-generator POUT (kW)	2.39	2.55	4	2.83	4.51	4.72
Motor-pump hours of operation (h/y)	2,526	1,693	1,104	1,299	2,532	2,588
Peak motor-pump POUT (kW)	2.73	3	4.3	4.15	5.1	4.33
Storage throughput (kWh/y)	369.03	536.81	908.1	1,219.7	1,057.8	2,055.4

* Using wind turbine module as a substitute for hydrokinetic turbine.

46

3.4.1.1   Impact of the residential load profile

To supply the residential load profile, the optimal configuration of the MHK-PHS system consists of the 7.5 kW hydrokinetic turbine size and a 17.94 kWh storage capacity, as calculated by HOMER Pro Version 3.6.1. The aim is to ensure a 0% unmet residential load demand. Hence, the needed volume of the upper reservoir at a water-head of 18.35m is $600m^3$, when considering the round-trip efficiency of 60%.

Fig. 3.13 and 3.14 present the output power of the turbine-generator unit and motor-pump unit, respectively. The turbine-generator output power indicates that the upper reservoir discharges to generate electrical power to be supplied to the unmet load demand. The motor-pump output power indicates that the upper reservoir is recharged (refilled) to store water, using the excess energy from the hydrokinetic system. Based on Fig. 3.13 and 3.15, it is observed that the upper reservoir discharges to supply the unmet load demand solely through August, September and October, due to the insufficient water speed. The longest discharge hours take place in September, between 19h00 and 00h00. This reveals increased operational hours for the upper reservoir. As a result, the upper reservoir reaches the lowest SOC of almost 40% of the volume capacity, as shown in Fig. 3.15 and begins recharging after 00h00, as shown in Fig. 3.14 (b). During the month of September, up to a maximum of 2.55 kW output power is demanded by the unmet load from the upper reservoir, as shown in Fig. 3.13 (a). This maximum output power is generally used to determine the required hydro-turbine size, for the selected flow rate of 0.0926 m^3/ sec (Iqbal, 2009). On the last day of September, the power required to refill the upper reservoir reaches a maximum value of 3 kW, as shown in Fig. 3.14 (a).

In Table 3.1, the excess energy of 32,268 kWh per annum is generated. Fig. 3.16 shows that most of the excess energy takes place during the months of the sufficient water speed of

47

2 m/s, or above. The excess energy is due to the load demand that has to be met at no

shortage during the months with insufficient water speed too.

Figure 3.13: PHS turbine-generator output power: residential load case (a) maximum

power (b) hourly power
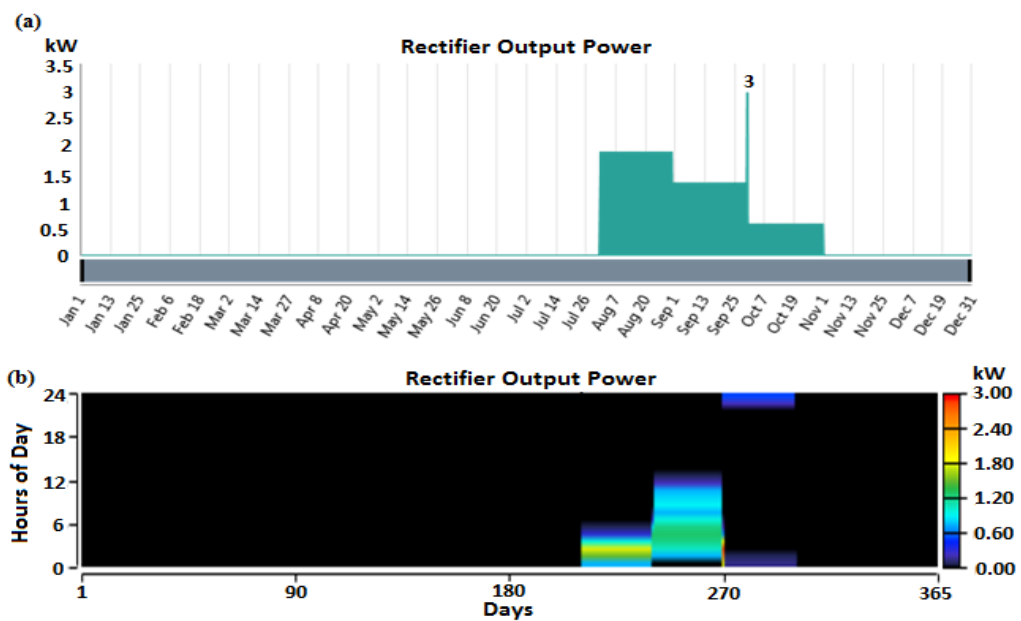
Figure 3.14: PHS motor-pump output power: residential load case (a) maximum power (b)
hourly power

48
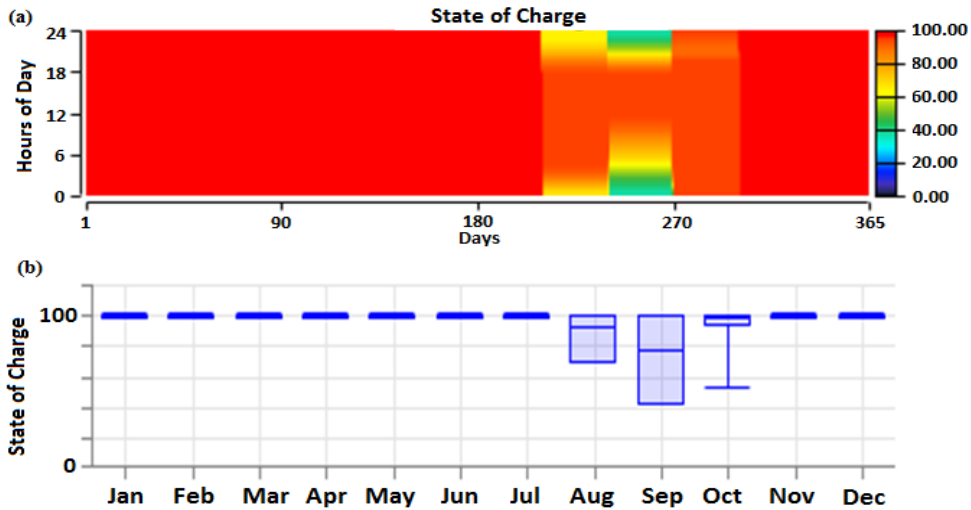
Figure 3.15: Upper reservoir state of charge: residential load case (a) hourly statistic (b) monthly statistic
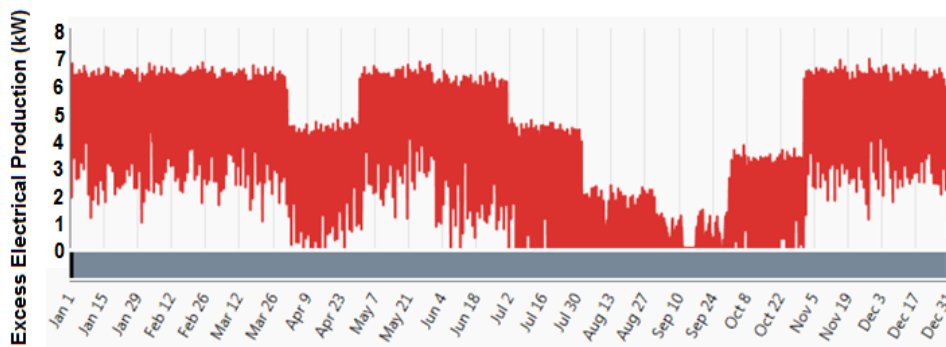
Figure 3.16: Excess electrical production under residential load case

3.4.1.2   Impact of the commercial load profile

Similar to the residential load, the optimal configuration of the MHK-PHS system for the commercial load profile consists of a 7.5 kW hydrokinetic turbine. However, the difference being that the commercial load profile requires a higher storage capacity of 23.92 kWh, instead of 17.94 kWh required by the residential load. Therefore, the proposed MHK-PHS system will require a higher capital cost to satisfy the commercial load demand at no capacity shortage. This resulted in higher NPC, COE and operating costs. Hence, the needed volume

49

of the upper reservoir at the same water-head of 18.35 m and the same round-trip efficiency of 60% is 800 m^3.

Fig. 3.17 and 3.18 show the output power of the turbine-generator unit and motor-pump unit, respectively. Similar to the residential load type, the upper reservoir discharges solely in August, September and October, due to the insufficient water speed, as shown in Fig. 3.17 and 3.19. The longest discharge duration takes place in September as well. However, the difference being that the longest discharge duration takes place between 09h00 – 19h00. This leads to higher operational hours of the upper reservoir, as compared to the residential load case. As a result, the upper reservoir approaches the lowest SOC of 4.18 % of the volume capacity, as shown in Fig. 3.19 and begins recharging after 19h00, as shown in Fig. 3.18 (b). During this month, up to a maximum of 2.88 kW output power is demanded by the unmet load from the upper reservoir, as shown in Fig. 3.15. Hence, a larger hydro-turbine size is required in the PHS system. Fig. 3.18 (a) shows that on the last day of September, the power required to refill the upper reservoir reaches a maximum value of 4.15 kW, which is greater than the residential load power.

In Table 3.1, it can be observed that the excess energy of 32,271 kWh per annum is generated by the MHK-PHS system for the commercial load. Similar to the residential load case, Fig. 3.20 shows that most of the excess energy takes place during the months with sufficient water speed of 2 m/s or above. The excess energy is due to the result of permitting the load demand to be met, even during the months with insufficient water speed.
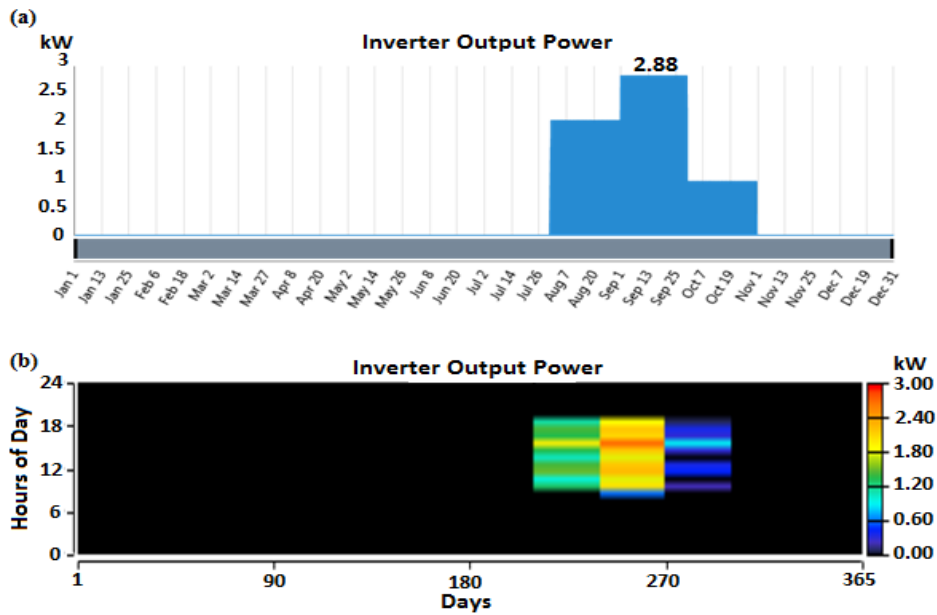
Figure 3.17: PHS turbine-generator output power: commercial load case (a) maximum power (b) hourly power
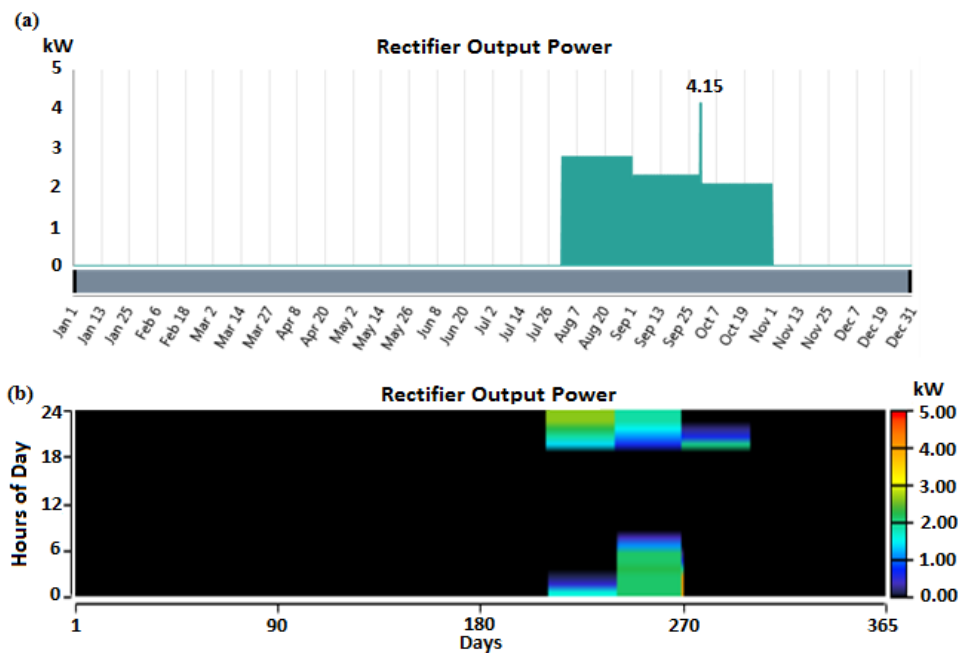
Figure 3.18: PHS motor-pump output power: commercial load case (a) maximum power (b) hourly power
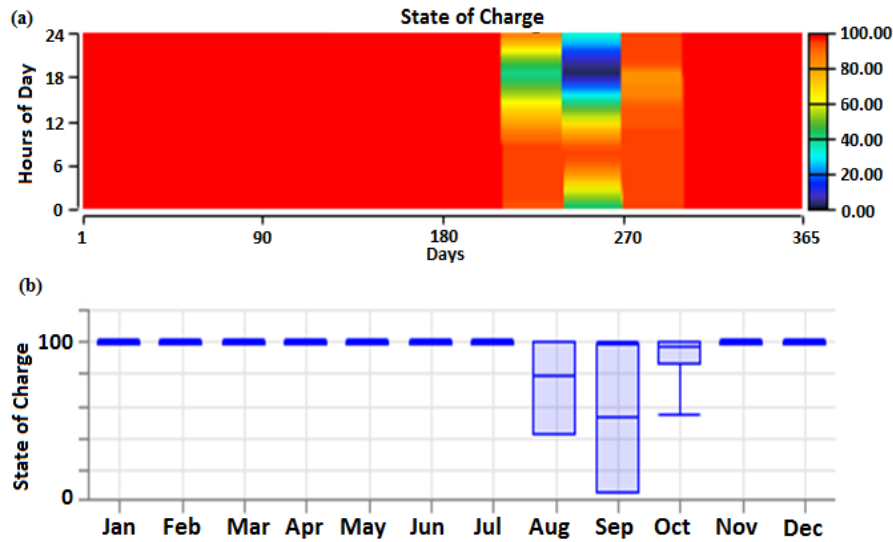
Figure 3.19: Upper reservoir state of charge: commercial load case (a) hourly statistic (b) monthly statistic
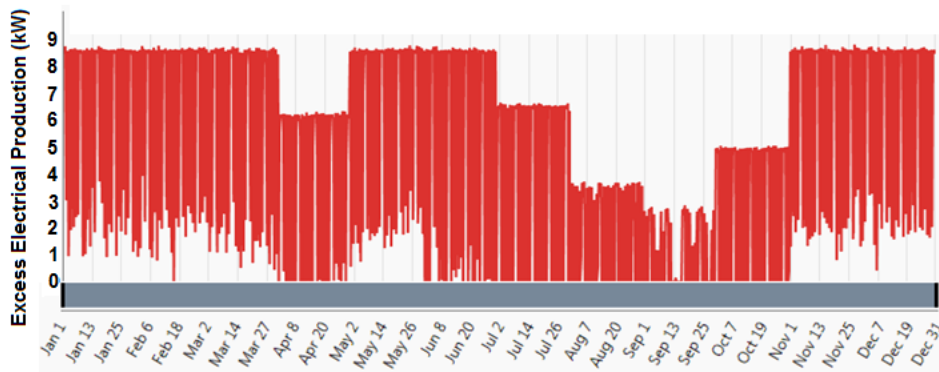
Figure 3.20: Excess electrical production under commercial load case

3.4.1.3   Impact of the industrial load profile

Similar to the residential and commercial load profiles, the optimal configuration of the MHK-PHS system for the industrial load profile further consists of a 7.5 kW hydrokinetic turbine. However, the difference is that the largest storage capacity of 29.9 kWh is required, as compared to the other two load profile cases. Therefore, the proposed MHK-PHS system will require the highest capital cost to satisfy the industrial load demand, at no capacity

52

shortage. This resulted in the highest NPC, COE and operating costs. Hence, the needed volume of the upper reservoir at the same water-head and round-trip efficiency, is 1000 m^3.

Fig. 3.21 and 3.22 show the output power of the turbine-generator unit and motor-pump unit, respectively. Unlike the residential and commercial load profiles, the upper reservoir discharges in April, July, August, September and October, as shown in Figs. 3.21 and 3.23. Therefore, this leads to the highest operational hours of the upper reservoir, as compared to both residential and commercial load cases. The upper reservoir approaches the lowest SOC of 7.84% of the volume capacity during September, particularly between 18h00 and 18h59 as shown by the turbine-generator output power in Fig. 3.23. During this month, the unmet industrial load demands up to a maximum of 4.72 kW output power from the upper reservoir, as shown in Fig. 3.21. Therefore, this leads to the requirement of the largest hydro-turbine size, as compared to the one required for the residential and commercial load profiles. The industrial load profile allows the motor-pump unit to operate for the longest duration when compared to the other load cases. It refills the upper reservoir from 18h00 till 08h00 in the morning, as shown in Fig. 3.22. On the last day of September, the power required to refill the upper reservoir reaches a maximum value of 4.33 kW, which is greater than in the case of residential and commercial loads. Similarly, Fig. 3.24 shows that most of the excess energy takes place during the months of the sufficient water speed.
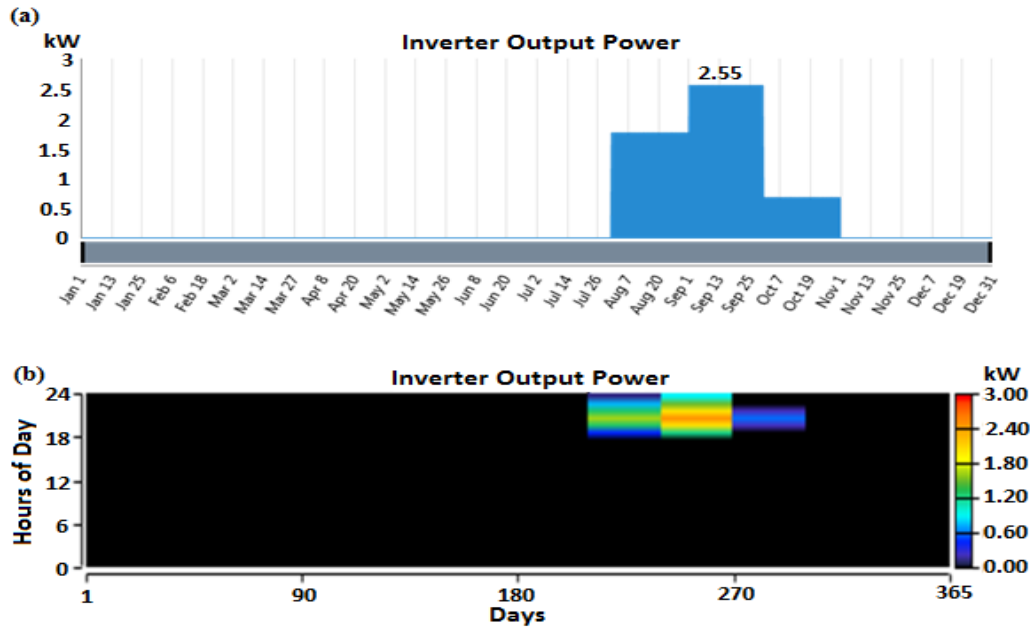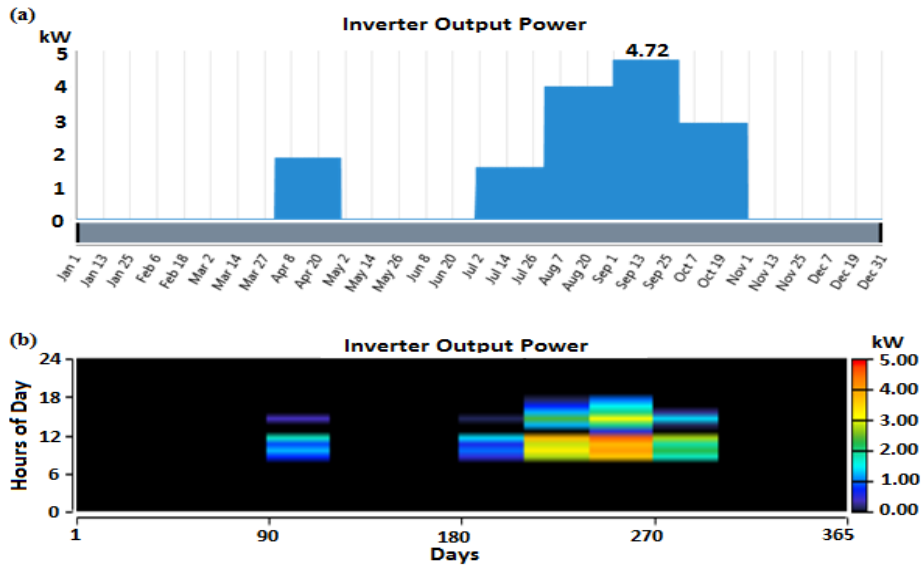
Figure 3.21: PHS turbine-generator output power: industrial load case (a) maximum power (b) hourly power
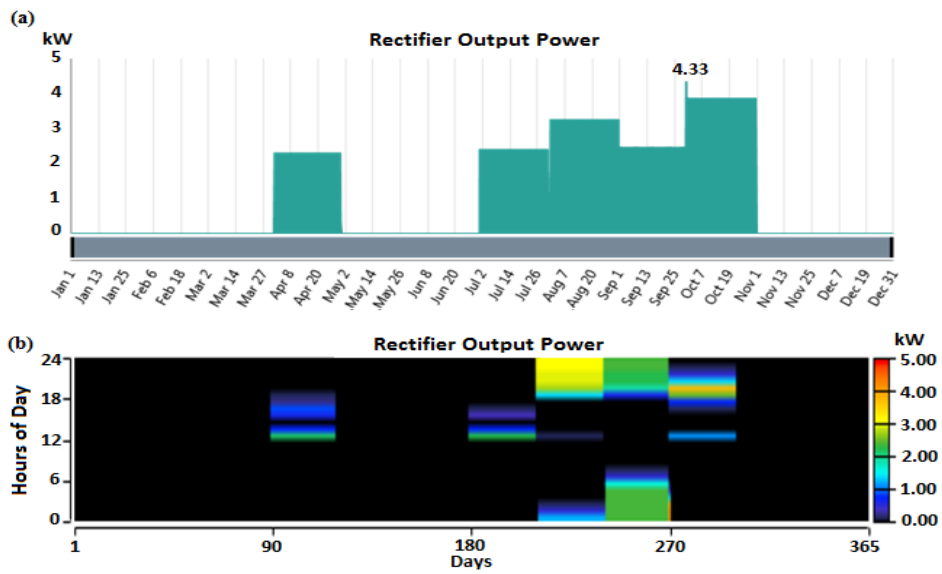
Figure 3.22: PHS motor-pump output power: industrial load case (a) maximum power (b) hourly power

54
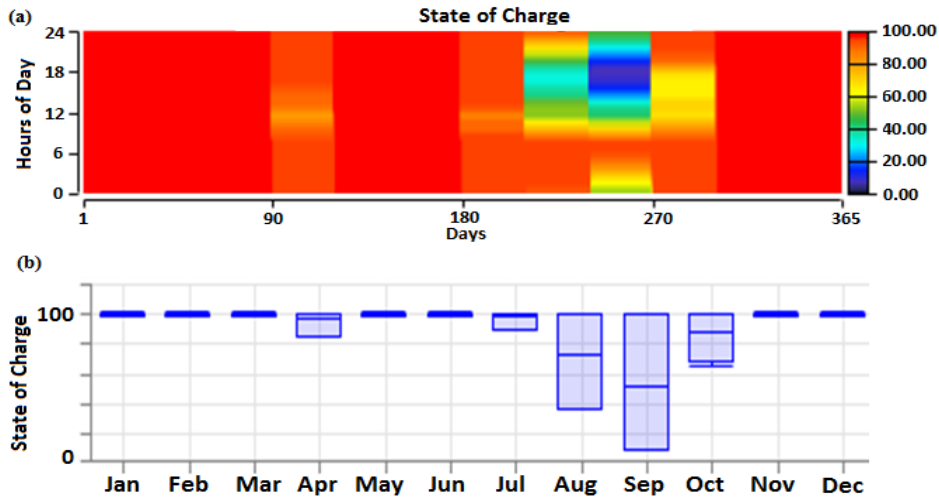
Figure 3.23: Upper reservoir state of charge: industrial load case (a) hourly statistic (b) monthly statistic
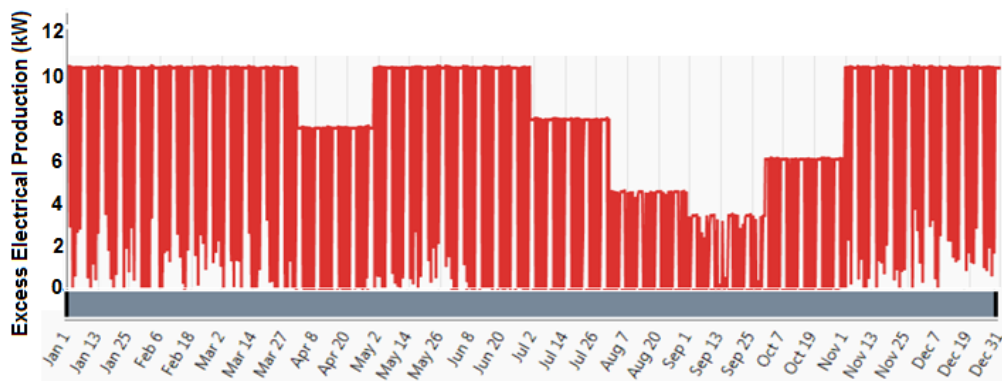
Figure 3.24: Excess electrical production under industrial load case

3.4.2 Optimal configuration results of a grid-connected MHK-PHS system

In section 3.4.1, the HOMER Pro Version 3.6.1 proved to be the preferred approach to use for the sizing of the proposed MHK-PHS system, as compared to the Legacy Version. Hence, in this section, HOMER Pro Version 3.6.1 is used to determine the optimal configuration of a grid-connected MHK-PHS system. The Ruraflex Gen TOU tariff rates, as applied by Eskom are entered into the HOMER software during simulations of the grid-

55

connected MHK-PHS system (Eskom, 2017/2018). Both low demand and high demand seasons' TOU tariffs are entered as shown in Table 3.2, below.

The variable load profile explained in section 3.2, were entered and simulated to yield a 0% capacity shortage. Table 3.3 illustrates the optimal configuration results obtained for each load profile. It is observed that the industrial load profile requires the largest hydrokinetic turbine size, when compared to the residential and commercial load profiles. This resulted in the highest capital and operating costs. The annual energy sales and generated revenue for each load profile are as shown in Table 3.4. The impacts of each load profile on a grid-interactive MHK-PHS system will be discussed below.

Table 3.2: Eskom Ruraflex Gen TOU tariffs and seasonal period (Eskom, 2017/2018)

	High Demand Season (June – August)		Low Demand Season (September – May)	
	TOU tariffs	TOU periods	TOU tariffs	TOU periods
Peak periods	ZAR3.29/kWh	06:00-09:00, 17:00-19:00	ZAR1.07/kWh	07:00-10:00, 18:00-20:00
Standard periods	ZAR0.99/kWh	09:00-17:00, 19:00-22:00	ZAR0.74/kWh	06:00-07:00, 10:00-18:00, 20:00-22:00
Off-peak periods	ZAR0.54/kWh	22:00-06:00	ZAR0.47/kWh	22:00-06:00

56

Table 3.3: HOMER optimal configuration results for the grid-interactive system

	Residential load	Commercial load	Industrial load
Optimization Results	19.5 kW hydrokinetic turbine system + 5.98 kWh (26 Ah) Upper reservoir	28.5 kW hydrokinetic turbine system + 5.98 kWh (26 Ah) Upper reservoir	39 kW hydrokinetic turbine system + 5.98 kWh (26 Ah) Upper reservoir
Capital Cost (US$)	269,617	392,332	532,348
Operating Cost (US$/y)	360.67	-29.07	-333.43
Net Present Cost (US$)	273,820	392,671	532,348
Cost of Energy (US$/y)	0.167	0.164	0.162
Total Energy Production (kWh/y)	140,793	205,789	281,586
Grid Energy Sales (kWh/y)	118,904	183,887	259,702
Energy Purchased from the Grid (kWh/y)	0	0	0

Table 3.4: Energy sales and generated revenue results

Months	Residential Load		Commercial Load		Industrial Load	
	Energy sold (kWh)	Revenue (US$)	Energy sold (kWh)	Revenue (US$)	Energy sold (kWh)	Revenue (US$)
January	12,741	419.95	19,486	641.73	27,295	897.03
February	11,534	377.74	17,563	574.09	24,639	803.82
March	12,698	415.67	19,304	630.31	27,065	881.57
April	8,569	278.73	13,398	435.38	19,061	618.07
May	12,765	421.02	19,385	637.85	27,153	891.36
June	11,928	645.76	18,382	1,024.80	25,921	1,423.80
July	9,033	485.45	14,325	802.05	20,239	1,109.40
August	4,547	238.98	7,508	426.63	10,980	602.21
September	3,137	99.51	5,363	163.34	8,067	253.75
October	6,874	225.34	10,880	356.16	15,536	506.66
November	12,347	406.19	18,780	616.80	26,317	862.39
December	12,731	413.24	19,513	632.72	27,428	887.89
Total	118,904	4,427.60	183,887	6,947.90	259,702	9,737.90

3.4.2.1   Impact of the residential load profile

To be able to meet the residential load demand at no capacity shortage, the optimal configuration of the MHK-PHS hybrid system consists of a 19.5 kW hydrokinetic turbine system and a minimal storage capacity of 5.98 kWh, as calculated by HOMER Pro Version 3.6.1. The hydrokinetic turbines system may generate the maximum output power of 19.5 kW, when the water speed is 2 m/s or above, as shown in Fig. 3.25. Hence, the turbines generate a total annual energy of 140,793 kWh, as shown in Table 3.3. However, solely 15.5% of the annual generated energy is used to supply the load, while 84.5% is sold into the grid.

The optimal configuration of the residential load profile proved to incur the highest operating cost and highest levelized COE, when compared to the commercial and industrial load cases. The large amount of energy sales into the grid takes place during off-peak periods (22h01-05h59) on each month of the year, as shown in Fig. 3.26(a). The bulk amount of energy is sold into the grid during the months whereby the water speed ranges from 2 m/s or above. During both morning and evening peak hours, the energy sales drop. The reason being that the load demands more energy during peak hours.

By considering the TOU peak periods, shown in Table 3.2, it is observed that HOMER does not permit the large amount of energy sales to take place during expensive peak periods. Hence, the chances of yielding the maximum income/revenue are minimal. HOMER does not permit the storage reservoir to be functional, as to allow energy storage process to take place during inexpensive off-peak periods. Upper reservoir was allowed to discharge solely during the beginning of the simulations as shown in Fig. 3.26(c). Afterwards, it was not recharged for the entire year. Additionally, no energy is purchased from the grid throughout the year as shown in both Table 3.3 and Fig. 3.26(b). When considering the ratio between the total

58

annual energy sales and the total generated revenue, shown in Table 3.4, it was concluded that the energy was sold at an average selling price of US$0.037/kWh.
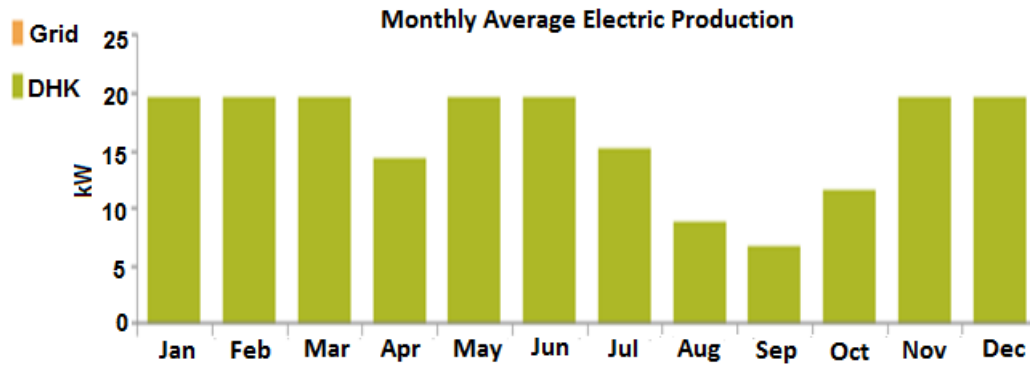
Figure 3.25: Monthly generated renewable output power for residential load
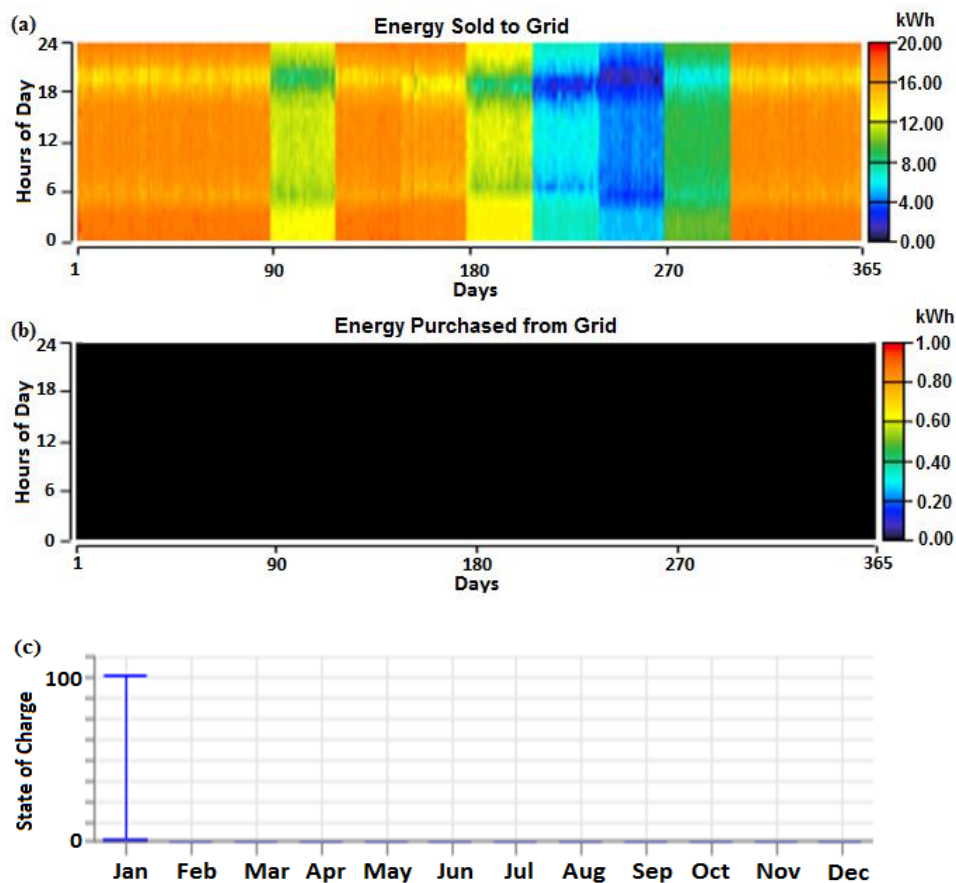
Figure 3.26: Residential load case (a) energy sales into the grid, (b) energy purchased from the grid and (c) PHS state of charge

3.4.2.2   Impact of the commercial load profile

To meet the commercial load demand at no capacity shortage, the optimal configuration of the MHK-PHS hybrid system consists of a 28.5 kW hydrokinetic turbine system and a minimal storage capacity of 5.98 kWh, as calculated by HOMER Pro Version 3.6.1. The hydrokinetic turbines system may generate a maximum output power of 28.5 kW when the water speed is 2 m/s or above, as shown in Fig. 3.27. Hence, the turbines generate a total annual energy of 205,789 kWh, as shown in Table 3.3. However, only 10.6% of the annual generated energy is used to supply the load, while 89.4% is sold into the grid. Similar to the residential load case, an average energy selling price of US$0.037/kWh is achieved.

Similar to the residential load case, the large amount of energy was sold into the grid during the months with water speed of 2 m/s or above, as shown in Fig. 3.28(a). Therefore, based on the TOU tariff periods, only 2 hours (06h00-08h00) of the costly peak periods have been used to sell large amount of energy. This is better compared to the residential load case. However, an improvement is further required to optimally utilize most of the TOU peak periods for energy sales into the grid, in order to generate high revenue.

During the worst month of September, up to a maximum of 8.1 kWh may be sold into the grid between 20h00-08h00. Similar to the residential load case, it may be seen that no energy was purchased from the grid throughout the year and the storage reservoir is discharged during the start of January, without being recharged throughout the year. Hence, no energy storage takes place throughout the year.

Monthly Average Electric Production
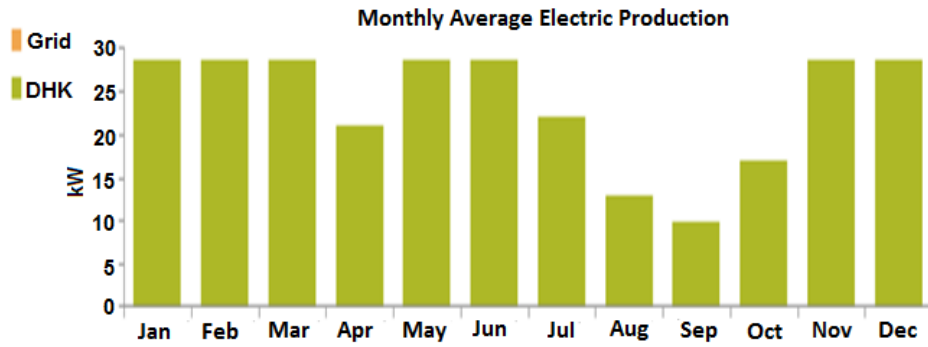
Figure 3.27: Monthly generated renewable output power for commercial load
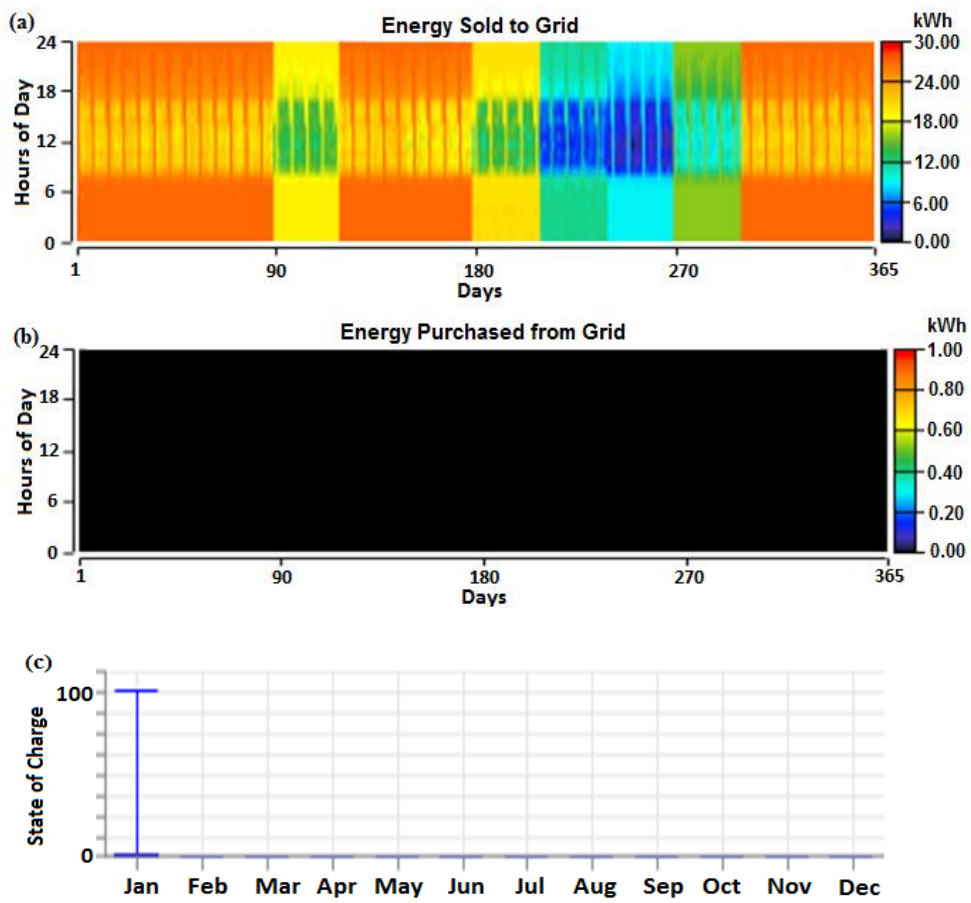
Figure 3.28: Commercial load case (a) energy sales into the grid, (b) energy purchased from the grid and (c) PHS state of charge

61

3.4.2.3 Impact of the industrial load profile

The optimum configuration results for the industrial load type requires a 39 kW hydrokinetic turbine size, to ensure a 0% of the unmet load demand, as shown in Fig. 3.29. This results in the highest capital and net present costs, as compared to both the residential and commercial load cases. However, the industrial load offers the lowest operating and levelized energy costs. The total annual energy of 281,586 kWh is generated, of which solely 7.8% is used to supply the load, while 92.2% is sold to the grid. Similar to both the residential and commercial load cases, an average energy selling price of US$0.037/kWh is achieved.

Similar to the other two cases, it may be seen that more energy was sold into the grid during the months with water speed ranging from 2 m/s and above, as shown in Fig. 3.30(a). The large amount of energy sales is achieved between 19h00 and 08h00, while the minimum energy sales are achieved during business hours. Therefore, based on the TOU periods, only 2 hours of the costly peak periods have been used to sell the large amount of energy. This is similar to the commercial load case and needs further improvement. As with the other two cases, no energy was purchased from the grid throughout the year and no energy storage process took place after discharging the reservoir, as shown in Figs. 3.30(b) and 3.30(c), respectively.
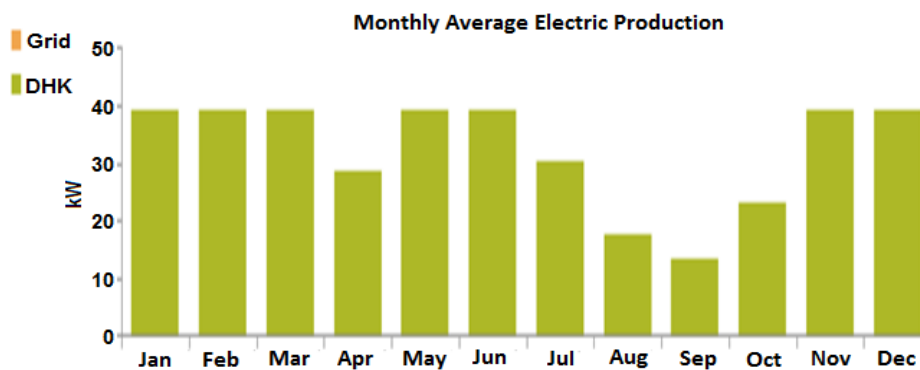
Figure 3.29: Monthly generated renewable output power for residential load

62
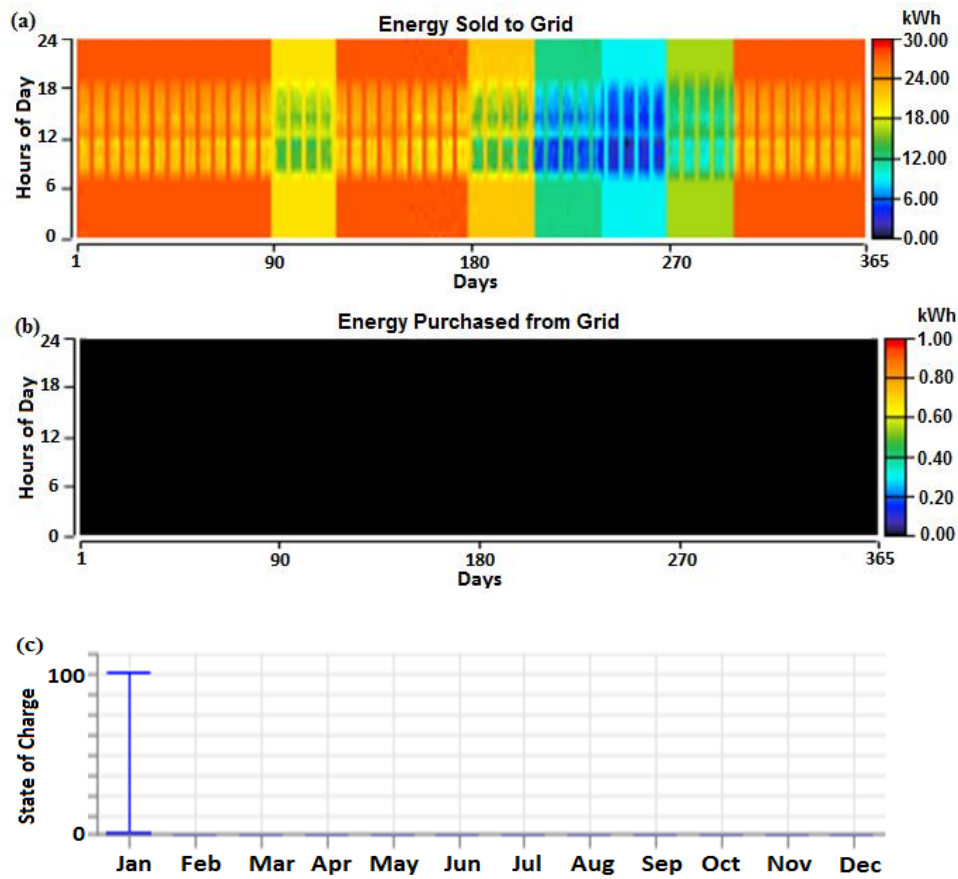
Figure 3.30: Industrial load case (a) energy sales into the grid, (b) energy purchased from the grid and (c) PHS state of charge

3.5 Conclusion

This Chapter determined the optimal configuration of the proposed MHK-PHS system, using HOMER software as the prominently used simulation tool. The HOMER Legacy Version results were compared to the results obtained from using the HOMER Pro Version. The residential, commercial and industrial load curves, having the same daily energy consumption of 60 kWh, were respectively simulated and permitted to be supplied at no capacity shortage. The aim was to analyse the impact brought by each load type on the optimal sizing and performance of the proposed system. The results have revealed that the methodology applying to the Legacy Version, led to the oversizing of the PHS storage

63

capacity by an additional 11.96 kWh for each load type. This oversizing problem resulted in higher system costs.

When analysing the economic impact of each load type, it was observed that the proposed MHK-PHS system is superior when supplying the residential load profiles. The residential load profile requires the lowest capital cost, while leading to the lowest COE and NPC. This is due to the least amount of the storage reservoir capacity, required by the residential load. The optimal configuration results have additionally revealed that, for the same daily energy consumption, the type of a load profile does not affect the size of a hydrokinetic turbine as well as the amount of annual excess energy. It affects the required storage size leading to various operational hours of charging and discharging of the upper reservoir.

The output power results of the turbine-generator unit and motor-pump unit were further investigated. It was observed that for the equivalent daily energy consumption, the industrial load profile requires the largest size of both the turbine-generator and motor-pump units, as compared to the residential and commercial load profiles. Lastly, the commercial load profile led to the lowest operational hours of the pumping unit per year. Hence, the upper reservoir reached the lowest SOC, as compared to the residential and industrial load cases. However, the disadvantage brought by the optimal configuration results, is that the large amount of excess energy is generated and wasted in the presence of the storage system.

When the proposed MHK-PHS system is connected to the grid, the industrial load resulted in a lowest COE. In spite of that, the system proved to be more superior under the residential load case, due to the lowest NPC and capital cost incurred. HOMER results further indicated that the excess energy was sold into the grid for the entire 24 hours, without reserving for later use during peak hours. The PHS system was not permitted to recharge using either MHK or grid power, to store excess energy for later use. This resulted in an oversizing problem for both the MHK and PHS systems. The large amount of energy sales

into the grid took place during off-peak periods. If large amount of energy could take place during expensive peak-periods, increased energy sales revenue could be generated.

Hence, the conclusion is that a need exists to develop an optimal energy management model for the proposed MHK-PHS system. This may lead to a reduced system size. The model should be able to maximize the energy sales into the grid, when the energy retail price is costly and further enables the purchasing from the grid when the energy retail price is affordable. The model should enable the PHS system to store excess energy during inexpensive off-peak period and utilize it during costly peak periods.

CHAPTER 4: OPTIMAL POWER CONTROL FOR A NON-INTERACTIVE GRID-CONNECTED MHK-PHS SYSTEM

4.1 Introduction

This Chapter proposes an optimal energy management model for the proposed non-interactive grid-connected MHK-PHS system, using an open-loop approach. The non-interactive grid-connected MHK-PHS system is defined for consumers who purchase the energy from the grid, when it is economical to do so, or when experiencing energy deficit from the proposed system. Therefore, the consumer is not legalized to sell the excess or stored energy into the grid.

The aim of the model is to ensure an economically feasible system operation, under TOU tariff scheme, while satisfying the demand of residential, commercial and industrial load sectors, respectively. The system is said to be non-interactive with utility grid, since the consumer may not interchange energy with the grid. The load demand is met by the three power sources, namely, MHK system, PHS system and/or the grid. Hence, the main objective of the model is to ensure minimal grid costs under TOU tariff scheme.

In this study, the recent Ruraflex TOU tariffs as applied by Eskom will be used (Eskom, 2017/2018), since they apply to rural customers who purchase and sell energy to and from the grid, respectively. The developed models will be applied into the MATLAB software, in order to perceive the energy cost savings and operation. The results are discussed in Section 4.4. The *linprog* solver is used to solve the optimization problem, since the problem consists of linear constraints.

66

4.2 Model Development

4.2.1   Description of a non-interactive grid-connected MHK-PHS system

System configuration/power flow for the non-interactive grid-connected MHK-PHS system is as shown in Fig. 4.1. The system consists of four sub-models: the power utility grid, MHK, PHS and the primary load. The MHK system is used to generate clean energy and a PHS system is used to store excess energy. The selected PHS system consists of the two separate penstocks used for pumping the water up and for generating electricity, respectively. Therefore, both charging and discharging processes may occur simultaneously. The double-penstock offers a considerably easier way of power-frequency regulation, as required by the grid, although this may lead to a higher system cost (Jamal et al., 2014; Beires et al., 2018).

The motor-pump unit is used to elevate the water from the lower-reservoir (river) to the upper-reservoir (dam), during energy storage process. The turbine-generator unit generates electricity through the use of the falling water from the upper reservoir. The pumping power demand will be met by the on-site MHK generated power and the utility grid power. The excess energy from the MHK system is used to supply the motor-pump unit, to refill the upper reservoir. This might take place when the primary load demands less than the generated MHK output power. In cases whereby the excess energy from the MHK system is not sufficient to meet the pumping demand, the grid energy may be purchased to offset the deficit, particularly during off-peak hours. The objective function and constraints will be formulated through the use of the following variables associated with the system power-flow diagram shown in Fig. 4.1:

$P_{1(t)}$: the electrical power flow (kW) from the MHK river system to the load at time t;

$P_{2(t)}$: the electrical power flow (kW) from the turbine-generator unit to the load at time t;

$P_{3(t)}$: the electrical power flow (kW) from the utility grid to the load at time t;

$P_{4(t)}$: the electrical power flow (kW) from the MHK river system to the motor-pump unit at time t;

$P_{5(t)}$: the electrical power flow (kW) from the utility grid to the motor-pump unit at time t.
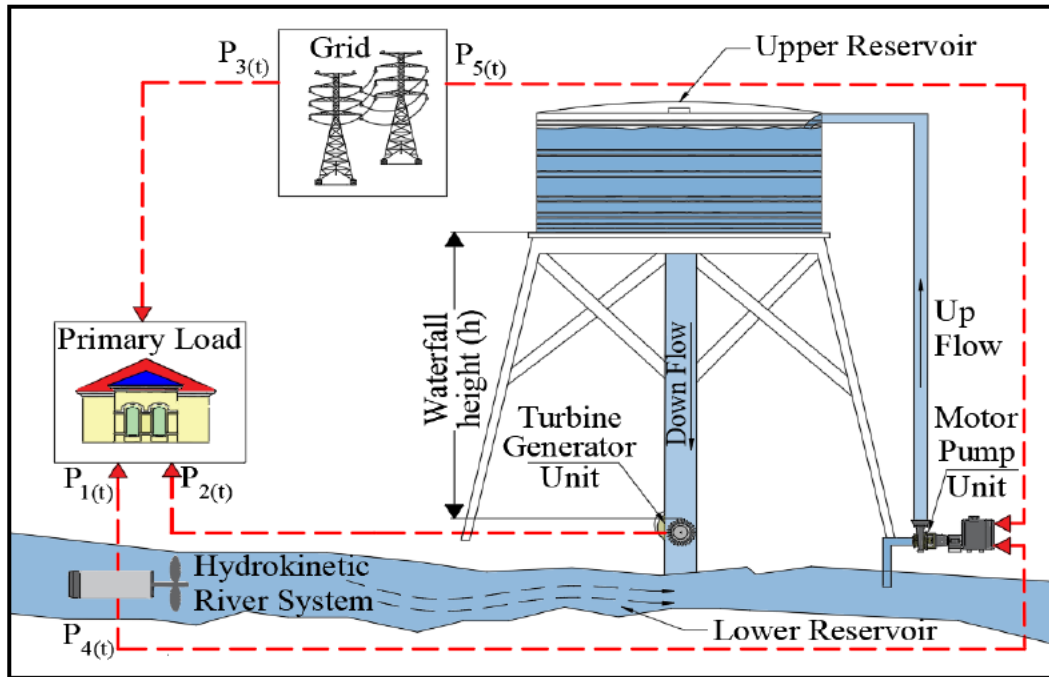
Figure 4.1: Layout of a non-interactive grid-connected MHK-PHS system

4.2.2 Problem formulation

The energy management, in the proposed non-interactive grid-connected MHK-PHS system, may be defined as an optimization challenge for determining the optimal generation and consumption points. In this study, the optimization challenge will be solved under TOU tariff scheme to satisfy the residential, commercial and industrial load demand sectors, respectively. Each demand sector is modelled to have an average energy consumption of 60 kWh/day. In this study, the simulations will be carried out for 216 hours in order to analyse the performance of the proposed model for nine consecutive days, with the aim of

68

including weekend days as well. The sampling time (Δt) is presumed to be 30 minutes, during the simulations. This leads to 432 sampling intervals. The simulation will be analysed under both low demand and high demand seasons. Both the generation and the consumption points should satisfy certain constraints, based on the objective function to be discussed below.

4.2.2.1   Objective function

As mentioned earlier, the objective of the proposed optimal control model for the non-interactive grid-connected MHK-PHS system, is to minimize the COE purchased from the grid at any time of the day. This is subjected to the constraints to be discussed in 4.2.2.2 below. It is therefore of importance to determine the optimum schedule for consuming the grid energy, meeting the primary load demand and/or for the pumping demand. Furthermore, it is important to optimally harvest/utilize the power generated by the MHK system, to meet the primary load demand and/or the pumping demand. The customer will benefit, due to the reduced electricity costs and the power utility will further benefit, due to a reduced peak demand, especially during peak hours. The reduced peak demand may guarantee an improved reliability of the grid network. The objective of minimizing the grid energy cost is presented as follows:

$$\text{Min (energy cost)} = \min \int C_t (P_{3(t)} + P_{5(t)}) dt \qquad (4.1)$$

Where: C_t = TOU electricity price at time, t (R/kWh).

Hence, in the problem formulation, the discrete cost objective function (F), at any sampling interval (j), is presented as follows:

69

$$F = \sum_{j=1}^{N} C_j \cdot (P_{3(j)} + P_{5(j)}) \cdot \Delta t \qquad (1 \le j \le N) \tag{4.2}$$

Where: Δt = the sampling time (i.e. the time between the sampling points);

$j = j^{th}$ sampling interval;

C_j = TOU electricity price at the jth sampling time (R/kWh);

$P_{3(j)}$ = power flow from the utility grid to the primary load (kW);

$P_{5(j)}$ = power flow from the utility grid to the motor-pump unit (kW).

4.2.2.2   Constraints

In the optimization problem, there is an existence of both equality and inequality constraints. The equality constraints will be used to enforce the power balance between the load demand (primary and pumping load) and supply. The inequality constraint is applied for the generation and storage limits. Hence, the objective function will be solved under the following equality and inequality constraints:

(a) Equality constraint for power balancing

The load power balance constraint is critical to ensure that the primary load demand is satisfied at all times. Hence, the sum of the power supplied by the grid, MHK system and PHS turbine-generator unit should be equal to the load power consumption. This is mathematically expressed as follows:

$$P_{Load(t)} = P_{1(t)} + P_{2(t)} + P_{3(t)} \tag{4.3}$$

70

Where: $P_{Load(t)}$ = primary load power demand at time t.

Hence, the load power balancing at any sampling interval (j) may be discretized as follows:

$$P_{Load(j)} = P_{1(j)} + P_{2(j)} + P_{3(j)} \quad (1 \leq j \leq N) \tag{4.4}$$

Where: $P_{1(j)}$ = power flow from the grid to the primary load at j^{th} sampling interval (kW);

$P_{2(j)}$ = power flow from the grid to the primary load at j^{th} sampling interval (kW).

(b) Equality constraint for fixed-final state condition

Another equality constraint is a fixed-final state condition. This aims at permitting the repeated implementation of the optimal energy control (Numbi & Malinga, 2017). Therefore, the water level state at the start of the control horizon is permitted to be same at the end of the control horizon. This is expressed using Equation 4.5.

$$\sum_{j=1}^{N}(P_{4(j)} + P_{5(j)}) - \sum_{j=1}^{N}P_{2(j)} = 0 \quad (1 \leq j \leq N) \tag{4.5}$$

Where: $P_{4(j)}$ = power flow from the MHK system to the motor-pump unit at j^{th} sampling interval (kW).

71

(c) Control variables limits constraints

For the safety purposes of the generation and storage equipment, as well as the stable operation of the system, the control variable boundaries for various power sources are critical. In most instances, control variable limits are due to the physical constraints, such as design/rated specifications. This will enable the generating units to be firmly limited to operate within their minimum and maximum electrical power capacities, at any time. As previously discussed, $P_{1(j)}$, $P_{2(j),}$ … $P_{5(j)}$ are used as control variables of the proposed non-interactive grid-connected MHK-PHS system. They are controllable from the minimum limits of zero to the maximum limits of their rated power or available power, at that point in time. Therefore, the control variables limits (kW) for each jth sampling interval are expressed as follows:

$$0 \leq P_{1(j)} \leq P_{1(j)}^{\mathrm{max}} \quad (1 \leq j \leq N) \tag{4.6}$$

$$0 \leq P_{2(j)} \leq P_2^{rated} \quad (1 \leq j \leq N) \tag{4.7}$$

$$0 \leq P_{3(j)} \leq P_3^{rated} \quad (1 \leq j \leq N) \tag{4.8}$$

$$0 \leq P_{4(j)} \leq P_{4(j)}^{\mathrm{max}} \quad (1 \leq j \leq N) \tag{4.9}$$

$$0 \leq P_{5(j)} \leq P_5^{rated} \quad (1 \leq j \leq N) \tag{4.10}$$

72

Where: $P_{i(j)}^{\max}$ = the maximum power generated by the RE source at j^{th} sampling interval (kW);

P_i^{rated} = the rated power of the component (kW).

(d) Inequality constraints

The inequality constraints are critical for power generation limits of the system. For instance, the MHK river system is used to supply power to the load (P_1) and/or to the motor-pump unit (P_4), as shown in Fig. 4.1. Hence, at any given sampling interval, the sum of the above mentioned powers should not exceed the maximum generated output power of the MHK system. This inequality constraint is then expressed as follows:

$$P_{1(j)} + P_{4(j)} \leq P_{MHK(j)}^{\max} \quad (1 \leq j \leq N) \tag{4.11}$$

Where: $P_{MHK(j)}^{\max}$ = the maximum power generated by the MHK system for each jth sampling interval (kW).

Additionally, the turbine-generator unit should supply up to its rated output power, when supplementing the unmet load demand. This inequality constraint is expressed as follows:

$$P_{2(j)} \leq P_{T:G}^{rated} \quad (1 \leq j \leq N) \tag{4.12}$$

Where: $P_{T:G}^{rated}$ = the rated output power of a turbine-generator unit of a PHS system (kW).

73

In order to refill the upper reservoir as a means of storing energy, the pumping demand is met by the MHK system and/or the grid. This inequality constraint is expressed as follows:

$$P_{4(j)} + P_{5(j)} \le P_{M:P}^{rated} \ (1 \le j \le N) \tag{4.13}$$

Where: $P_{M:P}^{rated}$ = the rated input power of a motor-pump unit (kW).

(e) Upper reservoir's state variable limit constraints

The excess energy from the MHK system may be stored into the upper-reservoir. The grid power may further be used to refill the upper reservoir. The stored potential energy is used during peak demand or when it is uneconomical to use the grid-power for supplementing unmet primary load demand. The storage level is restricted to be within the design storage limits, based on the size of the upper reservoir. The upper reservoir water level state ($Cap_{(j)}$) will be used as a decision variable, to prevent overcharging. In cases whereby the upper reservoir is entirely full, the maximum capacity is represented as 1. Therefore, the constraint for the storage limit level has been imposed on the upper reservoir as follows:

$$Cap^{min} \le Cap_{(j)} \le Cap^{max} \ (1 \le j \le N) \tag{4.14}$$

Where: Cap^{min} = minimum allowable capacity of the upper reservoir;

Cap^{max} = maximum allowable capacity of the upper reservoir.

The state of the water level changes whenever the water is pumped into the upper reservoir or the turbine-generator unit generates electricity. When the motor-pump unit is supplied with electricity (using P_4 and/or P_5), this allows the storage level to increase. Hence, the sum of P_4 and P_5, at any instant time, is made positive to reveal the charging process. Whenever the turbine-generator unit generates electricity to supply the unmet load demand (using P_2), this allows the storage water level to decrease. Hence, P_2 is made negative to imply the discharging process. The water level dynamic state in the upper reservoir can then be expressed as follows:

$$Cap_{(t)} = Cap_{(t-1)} + (P_{4(t)} + P_{5(t)}) \cdot \frac{\eta_p}{E_{pot}} - P_{2(t)} \cdot \frac{1}{\eta_g \cdot E_{pot}} \qquad (4.15)$$

Where: $Cap_{(t)}$ = water level in the upper reservoir at the end of time t;

$Cap_{(t-1)}$ = water level in the upper reservoir at the end of the next time period t-1;

η_p = overall pumping efficiency;

η_g = overall efficiency of the turbine generator unit;

E_{pot} = nominal potential energy in the upper reservoir (kWh).

Hence, the discrete water level dynamic state at any sampling interval (j) is then expressed as follows:

$$Cap_{(j)} = Cap_{(0)} + \sum_{j=1}^{N} [(P_{4(j)} + P_{5(j)}) \cdot \frac{\eta_p}{E_{pot}} \cdot \Delta t] - \sum_{j=1}^{N} P_{2(j)} \cdot \frac{\Delta t}{\eta_g \cdot E_{pot}} \qquad (4.16)$$

Where: $Cap_{(0)}$ = initial water level state.

Equation (4.16) may further be substituted in (4.14) to yield the following boundary limit equation:

$$Cap^{min} \leq Cap_{(0)} + \sum_{j=1}^{N}[(P_{4(j)} + P_{5(j)}) \cdot \frac{\eta_p}{E_{pot}} \cdot \Delta t] - \sum_{j=1}^{N}(P_{2(j)})\frac{\Delta t}{\eta_g \cdot E_{pot}} \leq Cap^{max} \qquad (4.17)$$

By letting: $Y = \dfrac{\eta_p \cdot \Delta t}{E_{pot}}$ and $Z = \dfrac{\Delta t}{\eta_g \cdot E_{pot}}$, Equation 4.17 may be rewritten as follows:

$$Cap^{min} \leq Cap_{(0)} + \sum_{j=1}^{N}[(P_{4(j)} + P_{5(j)}) \cdot Y] - \sum_{j=1}^{N}P_{2(j)} \cdot Z \leq Cap^{max} \qquad (4.18)$$

It may be noted that from Equation 4.18, two linear inequality constraints may be extracted and expressed as shown below:

$$\sum_{j=1}^{N}(P_{4(j)} + P_{5(j)}) \cdot Y - \sum_{j=1}^{N}P_{2(j)} \cdot Z \leq Cap^{max} - Cap_{(0)} \qquad (4.19)$$

$$\sum_{j=1}^{N}P_{2(j)} \cdot Z - \sum_{j=1}^{N}(P_{4(j)} + P_{5(j)}) \cdot Y \leq Cap_{(0)} - Cap^{min} \qquad (4.20)$$

4.2.3 Algorithm formulation and implementation in MATLAB

Optimization approaches are critical in investigating smart operational management, for both grid and off-grid RE systems (Bordin et al., 2017). In this way, it is possible to determine the values for the variables that may maximize or minimize the objective function, through boundaries settings (Tezer et al., 2017). Several optimization methods, such as a trial and error method, vector method, simplex method and linear programming method, may be used to solve a problem consisting of more than two decision variables. The linear programming optimization method has been selected, since the objective functions and the constraints of this Chapter appear to be linear functions of the decision variables. This method is exposed to minimizing or maximizing a linear objective function, subject to linear equality and inequality constraints, as well as to boundary constraints. The general *linprog* solver is formulated in its conical form, as follows:

$$\min_{x}\left\{f^{T}x\right\} \tag{4.21}$$

Subject to the following constraints:

$$Ax \leq b \quad \textit{(Linear inequality constraint);}$$

$$A_{eq}x = b_{eq} \quad \textit{(Linear equality constraint);} \tag{4.22}$$

$$lb \leq x \leq ub \textit{ (Lower and upper bounds).}$$

Based on the *linprog* syntax of the MATLAB Optimization Toolbox, the linear programming solver is expressed as follows:

© Central University of Technology, Free State

$$x = linprog(f, A, b, A_{eq}, b_{eq}, lb, ub) \tag{4.23}$$

4.2.4 Constraints definition in *linprog* syntax

The combination of the objective function and the entire constraints functions consists of five power variables for the proposed non-interactive grid-connected MHK-PHS system. For the modelling purpose, the expressions of the inequality and equality constraints, as well as the lower and upper bounds limits as developed above, will be rewritten and expressed in terms of variable (x). The number of sampling interval will be limited to "$N=2$" and the expression of the various system's constraints, together with the objective function, will be compacted into linear programming canonical form. As $N=2$, the power variables may be developed for two sampling intervals ($j=1$ and $j=2$) and expressed in terms of variable (x) as shown by Equation (4.24 to 4.28). The matrix transformation for the five control variables as contained in both the constraints and objective function, will then be expressed as follows:

$$P_1 = x(1:N) = [x_1, x_2] \tag{4.24}$$

$$P_2 = x(N+1:2N) = [x_3, x_4] \tag{4.25}$$

$$P_3 = x(2N+1:3N) = [x_5, x_6] \tag{4.26}$$

$$P_4 = x(3N+1:4N) = [x_7, x_8] \tag{4.27}$$

$$P_5 = x(4N+1:5N) = [x_9, x_{10}] \tag{4.28}$$

78

4.2.4.1   Inequality constraints

As discussed previously, the optimization challenge for the proposed non-interactive grid-connected system consists of five linear inequality constraints (Equation 4.11, 4.12, 4.13, 4.19 and 4.20). These linear inequalities are to be integrated into constraint matrix A and vector b of the *linprog* arrangement, as to be shown below.

- MHK system (using Equation 4.11)

$$x_1 + x_7 \leq P_{MHK(1)}^{max} \quad (\text{For } j = 1) \tag{4.29}$$

$$x_2 + x_8 \leq P_{MHK(2)}^{max} \quad (\text{For } j = 2) \tag{4.30}$$

- Turbine-generator unit (using Equation 4.12)

$$x_3 \leq P_{T:G}^{rated} \quad (\text{For } j = 1) \tag{4.31}$$

$$x_4 \leq P_{T:G}^{rated} \quad (\text{For } j = 2) \tag{4.32}$$

- Motor-pump unit (using Equation 4.13)

$$x_7 + x_9 \leq P_{M:P}^{rated} \quad (\text{For } j = 1) \tag{4.33}$$

79

$$x_8 + x_{10} \leq P_{M:P}{}^{rated} \quad (\text{For } j = 2) \tag{4.34}$$

- Upper reservoir maximum state (using Equation 4.19)

$$(x_7 + x_9) \cdot Y - (x_3) \cdot Z \leq Cap^{max} - Cap_{(0)} \quad (\text{For } j = 1) \tag{4.35}$$

$$(x_7 + x_9 + x_8 + x_{10}) \cdot Y - (x_3 + x_4) \cdot Z \leq Cap^{max} - Cap_{(0)} \quad (\text{For } j = 2) \tag{4.36}$$

- Upper reservoir minimum state (using Equation 4.20)

$$(x_3) \cdot Z - (x_7 + x_9) \cdot Y \leq Cap_{(0)} - Cap^{min} \quad (\text{For } j = 1) \tag{4.37}$$

$$(x_3 + x_4) \cdot Z - (x_7 + x_9 + x_8 + x_{10}) \cdot Y \leq Cap_{(0)} - Cap^{min} \quad (\text{For } j = 2) \tag{4.38}$$

Hence, using Equation 4.29-4.38, the inequality matrix may be presented as follows:

$$
\begin{bmatrix}
1 & 0 & 0 & 0 & 0 & 0 & 1 & 0 & 0 & 0 \\
0 & 1 & 0 & 0 & 0 & 0 & 0 & 1 & 0 & 0 \\
0 & 0 & 1 & 0 & 0 & 0 & 0 & 0 & 0 & 0 \\
0 & 0 & 0 & 1 & 0 & 0 & 0 & 0 & 0 & 0 \\
0 & 0 & 0 & 0 & 0 & 0 & 1 & 0 & 1 & 0 \\
0 & 0 & 0 & 0 & 0 & 0 & 0 & 1 & 0 & 1 \\
0 & 0 & -Z & 0 & 0 & 0 & Y & 0 & Y & 0 \\
0 & 0 & -Z & -Z & 0 & 0 & Y & Y & Y & Y \\
0 & 0 & Z & 0 & 0 & 0 & -Y & 0 & -Y & 0 \\
0 & 0 & Z & Z & 0 & 0 & -Y & -Y & -Y & -Y
\end{bmatrix}
\cdot
\begin{bmatrix}
x_1 \\ x_2 \\ x_3 \\ x_4 \\ x_5 \\ x_6 \\ x_7 \\ x_8 \\ x_9 \\ x_{10}
\end{bmatrix}
\leq
\begin{bmatrix}
P_{MHK}^{max} \\
P_{MHK}^{max} \\
P_{T:G}^{rated} \\
P_{T:G}^{rated} \\
P_{M:P}{}^{rated} \\
P_{M:P}{}^{rated} \\
Cap^{max} - Cap_{(0)} \\
Cap^{max} - Cap_{(0)} \\
Cap_{(0)} - Cap^{min} \\
Cap_{(0)} - Cap^{min}
\end{bmatrix}
\tag{4.39}
$$

80

Using the canonical formulation, the above-mentioned linear inequality constraints are further expressed as follows:

$$A_1 = \left[eye(N,N), zeros(N,N), zeros(N,N), eye(N,N), zeros(N,N) \right] \tag{4.40}$$

$$A_2 = \left[zeros(N,N), eye(N,N), zeros(N,N), zero(N,N), zeros(N,N) \right] \tag{4.41}$$

$$A_3 = \left[zeros(N,N), zeros(N,N), zeros(N,N), eye(N,N), eye(N,N) \right] \tag{4.42}$$

$$A_4 = \left[zeros(N,N), -Z * tril(ones(N,N)), zeros(N,N), Y * tril(ones(N,N)), Y * tril(ones(N,N)) \right]$$

$$\tag{4.43}$$

$$A_5 = -A_4 \tag{4.44}$$

$$A = [A_1; A_2; A_3; A_4; A_5] \tag{4.45}$$

$$b_1 = P_{MHK}^{\max}(1:N) \tag{4.46}$$

$$b_2 = P_{T:G}^{rated} * ones(N,1) \tag{4.47}$$

$$b_3 = P_{M:P}^{rated} * ones(N,1) \tag{4.48}$$

$$b_4 = (Cap^{\max} - Cap_{(0)}) * ones(N,1) \tag{4.49}$$

$$b_5 = (Cap_{(0)} - Cap^{\min}) * ones(N,1) \tag{4.50}$$

81

$$b = [b_1; b_2; b_3; b_4; b_5] \tag{4.51}$$

4.2.4.2   Equality constraints

The optimization problem consists of two linear equality constraints; namely load demand power balance (Equation 4.4) and fixed-final state condition (Equation 4.5). These linear equalities are to be integrated into constraint matrix A_{eq} and vector b_{eq} of the linprog solver.

- Load demand power balancing (using Equation 4.4)

$$x_1 + x_3 + x_5 = P_{Load(1)} \quad \text{(For } j = 1) \tag{4.52}$$

$$x_2 + x_4 + x_6 = P_{Load(2)} \quad \text{(For } j = 2) \tag{4.53}$$

- Fixed-final state condition (using Equation 4.5)

$$-x_3 - x_4 + x_7 + x_8 + x_9 + x_{10} = 0 \tag{4.54}$$

Hence, using Equation 4.52 - 4.54, the equality matrix may be presented as follows:

82

$$\begin{bmatrix} 1 & 0 & 1 & 0 & 1 & 0 & 0 & 0 & 0 & 0 \\ 0 & 1 & 0 & 1 & 0 & 1 & 0 & 0 & 0 & 0 \\ 0 & 0 & -1 & -1 & 0 & 0 & 1 & 1 & 1 & 1 \end{bmatrix} \cdot \begin{bmatrix} x_1 \\ x_2 \\ x_3 \\ x_4 \\ x_5 \\ x_6 \\ x_7 \\ x_8 \\ x_9 \\ x_{10} \end{bmatrix} = \begin{bmatrix} P_{Load(1)} \\ P_{Load(2)} \\ 0 \end{bmatrix} \tag{4.55}$$

Using the canonical formulation, the above linear inequality constraints are then expressed as follows:

$$A_{eq1} = [eye(N,N), eye(N,N), eye(N,N), zeros(N,N), zeros(N,N)] \tag{4.56}$$

$$A_{eq2} = [zeros(1,N), -ones(1,N), zeros(1,N), ones(1,N), ones(1,N)] \tag{4.57}$$

$$A_{eq} = [A_{eq1}; A_{eq2}] \tag{4.58}$$

$$b_{eq1} = P_{Load}(1:N) \tag{4.59}$$

$$b_{eq2} = zeros(1,1) \tag{4.60}$$

$$b_{eq} = [b_{eq1}; b_{eq2}] \tag{4.61}$$

83

4.2.4.3   Lower and upper bounds

The optimization problem consists of five linear boundaries for various power sources (Equation 4.6 to 4.10). These linear boundaries are to be integrated into lower (l_b) and upper (u_b) boundaries of the *linprog* solver.

- Lower boundaries

$$lb_1 = 0 * ones(N,1)$$

$$lb_2 = 0 * ones(N,1)$$

$$lb_3 = 0 * ones(N,1) \qquad\qquad (4.62)$$

$$lb_4 = 0 * ones(N,1)$$

$$lb_5 = 0 * ones(N,1)$$

Therefore, the lower boundaries are the expressed as follows:

$$lb = [lb_1, lb_2, lb_3, lb_4, lb_5] \qquad\qquad (4.63)$$

84

- Upper boundaries

$$ub_1 = P_1^{\text{max}}(1:N)$$

$$ub_2 = P_2^{rated} * ones(N,1)$$

$$ub_3 = P_3^{rated} * ones(N,1) \qquad (4.64)$$

$$ub_4 = P_4^{\text{max}}(1:N)$$

$$ub_5 = P_5^{rated} * ones(N,1)$$

Therefore, the upper boundaries are then expressed as follows:

$$ub = [ub_1, ub_2, ub_3, ub_4, ub_5] \qquad (4.65)$$

4.2.4.4 Objective function

As mentioned earlier, the main objective is to minimize the COE purchased from the grid. Hence, the linear objective function (Equation 4.2), is used to locate a minimum solution of the specified problem, in the linprog solver syntax.

$$F_1 = C_1 \cdot (x_5 + x_9) \cdot \Delta t \quad (\text{For } j = 1) \qquad (4.66)$$

$$F_2 = C_2 \cdot (x_6 + x_{10}) \cdot \Delta t \quad (\text{For } j = 2) \qquad (4.67)$$

Hence, using Equation 4.66 and 4.67, the matrix may be presented as follows:

85

$$F = \Delta t \cdot \begin{bmatrix} 0 & 0 & 0 & 0 & C_1 & 0 & 0 & 0 & C_1 & 0 \\ 0 & 0 & 0 & 0 & 0 & C_2 & 0 & 0 & 0 & C_2 \end{bmatrix} \cdot \begin{bmatrix} x_1 \\ x_2 \\ x_3 \\ x_4 \\ x_5 \\ x_6 \\ x_7 \\ x_8 \\ x_9 \\ x_{10} \end{bmatrix} \qquad (4.68)$$

$$F = \Delta t \big[zeros\,(N,N), zeros\,(N,N), C*eye(N,N), zeros\,(N,N), C*eye(N,N) \big] \qquad (4.69)$$

4.2.4.5   Time-of-use (TOU) tariffs and periods

The dynamic TOU pricing scheme used by Eskom will be applied during simulations. The 2017/2018 Eskom (Ruraflex) electricity cost price, *C(t)* for both low demand and high demand seasons, will be used as shown by Equation 4.70 and 4.71, respectively (Eskom, 2017/2018).

$$C(t) = \begin{cases} C_p = ZAR1.07\,/\,kWh \\ C_s = ZAR0.74\,/\,kWh \\ C_o = ZAR0.47\,/\,kWh \end{cases} \text{Low demand season} \qquad (4.70)$$

$$C(t) = \begin{cases} C_p = ZAR3.29\,/\,kWh \\ C_s = ZAR0.99\,/\,kWh \\ C_o = ZAR0.54\,/\,kWh \end{cases} \text{High demand season} \qquad (4.71)$$

Where:

86

C_p = the electricity cost during peak period;

C_s = the electricity cost during standard period;

C_o = the electricity cost during off-peak period.

As highlighted by Fig. 1.1 of Chapter 1, it is observed that the weekdays and weekend days have various TOU periods, as established by Eskom. Peak charges do not exist during weekends. Hence, in this study, the simulations will be carried out using both weekdays and weekend days TOU tariffs. It may be seen that both Saturday and Sunday TOU periods are the same for both low demand and high demand seasons, as shown by Equation 4.72 and 4.73. For weekdays, the TOU periods differ seasonally, as shown by Equation 4.74 and 4.75, respectively.

$$Saturdays \cdots \begin{cases} offpeak, t \in [0,7) \cup [12,18) \cup [22,24) \\ std; t \in [18,20) \cup [7,12) \end{cases} \text{Low \& high demand seasons}$$

(4.72)

$$Sundays \cdots \{offpeak; t \in [0,24)\} \text{ Low \& high demand seasons} \tag{4.73}$$

$$Weekdays \cdots \begin{cases} offpeak, t \in [0,6) \cup [22,24) \\ std; t \in [6,7) \cup [10,18) \cup [20,22) \\ peak; t \in [7,10) \cup [18,20) \end{cases} \text{Low demand season}$$

(4.74)

$$Weekdays \cdots \begin{cases} offpeak, t \in [0,6) \cup [22,24) \\ std; t \in [9,17) \cup [19,22) \\ peak; t \in [6,9) \cup [17,19) \end{cases} \text{High demand season}$$

(4.75)

87

4.3 Simulation Results and Discussion

The variable load demand data that has been discussed in Chapter 3 (Section 3.2), is used to evaluate the proposed energy management model, when meeting the demand for the residential, commercial and industrial load profiles, respectively. The simulations have been carried out for high and low demand seasons, respectively. The dynamic pricing scheme used by Eskom has been utilized during simulations, as explained in Section 4.2.4.5.

Simulations for 216 hours have been carried out, to analyse the performance of the proposed model throughout the week for nine consecutive days, with the aim of including both weekdays and weekend days. The sampling time (Δt) is presumed to be 30 min, leading to a total of 432 sampling intervals. Nine days load profile data has been selected from the yearly variable load data generated by the HOMER software in Chapter 3. The flowing water resource data from a typical river of Kwazulu Natal has been used, as shown in Fig. 3.12 (Kusakana, 2015; Koko et al., 2015).

The optimal size of the proposed system, when meeting each load type, has been determined through the use of the HOMER software. However, HOMER has led to an over-sizing difficulty, as revealed by the excess energy production discussed in Chapter 3. Hence, to minimize the initial capital cost, the sizes of both the MHK and PHS systems have been reduced for simulations in this Chapter. The efficiency of the PHS plant ranges from 70 to 85% (Díaz-González et al., 2012). In this study, the efficiencies of the motor-pump and turbine-generator units are presumed to be 84%, respectively (Chen et al., 2016). This leads to the overall PHS system's efficiency of 70.5%.

To study the effectiveness of the developed model, the baseline grid energy cost incurred by each studied load type, if solely supplied by the utility grid (without the MHK-PHS system), is compared to the net energy cost achieved during optimal energy control of the

88

proposed system. Additionally, for appropriate comparison purposes, the fixed-final state condition is used, to allow the upper reservoir's water level state at the start of the control horizon to be equal at the end of the control horizon.

4.3.1   Residential load

Figs. 4.2, 4.3 and 4.4 present the results for low demand season, while Figs. 4.5, 4.6 and 4.7 present the results for high demand season. For low demand season, the variable residential load profile data has been obtained from Sunday (1st January 2017) to Monday (9th January 2017), as shown in Fig. 4.2A. For high demand season, the variable load profile data is obtained from Sunday (4th June 2017) to Monday (12th June 2017) as shown in Fig. 4.4A. In all results' figures, the hours range from 0 to 216. From the 0th hour up until the end of the 24th hour, represents Sunday, while after the 24th hour up until the end of the 144th hour, represents five weekdays. After the 144th hour up until the end of the 168th hour, represents Saturday, after the 168th hour up until the end of the 192nd hour, represents another Sunday and after 192nd up until the end of the 216th hour, represents another Monday.

It may be noticed that for the selected days of the high demand month (June), the evening peak demand is above 5.5 kW for the entire week. For the selected days of the low demand month (January), the evening peak demand is below 5.5 kW for most days. The overall simulation parameters of the residential load case are as shown in Table 4.1.

4.3.1.1   Low demand season

The results for the low demand season are as shown in Figs. 4.2 to 4.4. Fig. 4.3A shows that the average water speed for the month of January varies around 5.31 m/s. Therefore, the

selected 2.5 kW MHK system generates a maximum output power of 2.5 kW (as denoted by the red-dotted lines in Fig. 4.2B and 4.3B), since the average water speed is above 2 m/s during January month.

Table 4.1: Simulation parameters for the non-interactive system (residential load)

Item	Value
Sampling time (Δt)	30 minutes
PHS nominal capacity ($P_{T:G}$= 2.5 kW and $P_{M:P}$= 2.5 kW)	1.5 kWh
PHS maximum volume	100%
PHS minimum volume	5%
Initial upper reservoir capacity	50%
Overall efficiency of the PHS ($\eta_{T:G}$= 84% and $\eta_{M:P}$= 84%)	70.6%
MHK system rating	2.5 kW

Fig. 4.2B shows that the model permits most of the generated MHK power to be utilized for supplying the primary load. The remainder of the load demand is met/supplemented by the turbine-generator unit, as shown in Fig. 4.2C. The grid power is utilised during evening peak hours, when both the MHK and PHS systems may not be able to meet the overall demand, as shown in Fig. 4.2D.

The MHK power is mostly utilised for the pumping purpose during off-peak periods, as shown in Fig. 4.3B. Hence, the upper reservoir level increases at the highest rate during off-peak hours, as shown in Fig. 4.3D. The reason is that the load demand is minimal. Hence, the large amount of excess energy is stored into the upper reservoir. The stored energy will be used later during standard and expensive peak periods. It is observed that the initial upper reservoir's water level state of 50% has been achieved at the end of the control horizon as well.

Sundays have proved to lead to a larger number of charging and discharging cycles, as compared to other days. Sundays of the low demand season, proved to completely exclude the utilization of the grid power for supplementing the pumping demand, as shown in Fig. 4.3C. Instead, the grid power is solely used for the purpose of supplementing the load demand, as shown in Fig. 4.2D.

Using Fig. 4.2D and 4.3C, it is observed that the overall grid cost for the simulated nine days (1st January – 9th January), yielded ZAR3.69. If the 9 day load demand (Fig. 4.2A) is solely met by the utility grid (Eskom), it will incur baseline grid cost of ZAR245.05, as calculated from Fig. 4.4. Hence, through the use of both the MHK-PHS system and the optimization model, the residential consumer is expected to settle only 1.5% of the baseline grid cost, during low demand season. This proves that a potential energy cost saving of 98.5% is possible, when the developed energy management model is applied to the non-grid interactive MHK-PHS system, for the selected nine days.

Figure 4.2: Load demand side power flow during low demand season (residential)

91

Figure 4.3: Water speed and PHS side power flow during low demand season (residential)
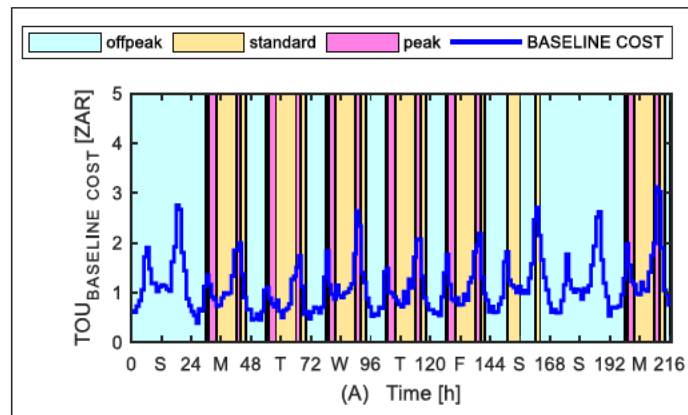
Figure 4.4: Baseline grid cost incurred by the residential load without the MHK-PHS system (low demand season)

4.3.1.2   High demand season

The results for the high demand season are as shown in Figs. 4.5 to 4.7. Fig. 4.6A shows that the average water speed for the June month varies around 2.18 m/s. Therefore, the MHK

92

system steadily generates a maximum output power of 2.5 kW (as denoted by the red-dotted lines in Figs. 4.5B and 4.6B), since the water speed is nevertheless above 2 m/s.

Similar to a low demand season, Fig. 4.5B shows that the model permits most of the generated MHK power to be utilized for supplying the primary load. The other portion of the load demand is met/supplemented by the turbine-generator unit, as shown in Fig. 4.5C. The grid power is utilised during evening peak hours, when both the MHK and PHS systems cannot meet the overall demand, as shown in Fig. 4.5D. The dissimilarity, when compared to low demand season, is that the grid power is further used throughout the entire off-peak hours of the week. Additionally, the grid power is utilised to meet the pumping demand during inexpensive off-peak hours throughout the week. The main aim is to store the cheap-to-buy off-peak energy, for use during standard and costly peak periods of the next day.

Most of the excess energy from the MHK power is stored during off-peak periods, as shown in Fig. 4.6B. Hence, the upper reservoir level increases at the highest rate during off-peak hours, as shown in Fig. 4.6D. Similar to the low demand season case, Sundays have proved to lead to a larger number of charging and discharging cycles, as compared to other days. Additionally, Sunday leads to the utilization of the grid power for the entire 24 hours, for the purpose of supplementing both the motor-pump unit and the load demand, as shown in Figs. 4.5D and 4.6C, respectively.

Using Fig. 4.5D and 4.6C, the overall grid cost for the simulated nine days (4rd June – 12th June), yielded ZAR26.16. The 9 day load demand (Fig. 4.5A) yielded a baseline grid cost of ZAR317.77, if solely met by the utility grid as shown in Fig. 4.6. Hence, through the use of the optimally controlled MHK-PHS system, the residential consumer only settles 8.2% of the baseline grid cost during high demand season. This proves that a potential of 91.8% energy cost saving is possible, for the selected 9 days.
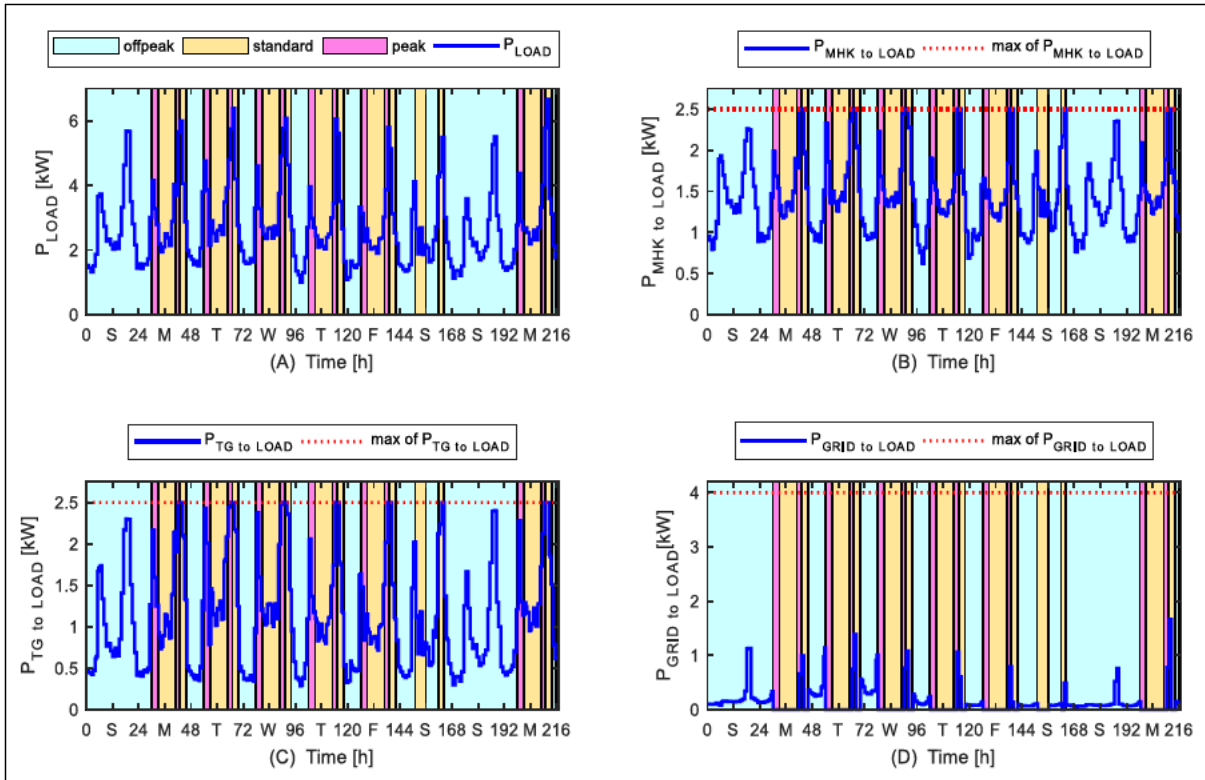
Figure 4.5: Load demand side power flow during high demand season (residential)
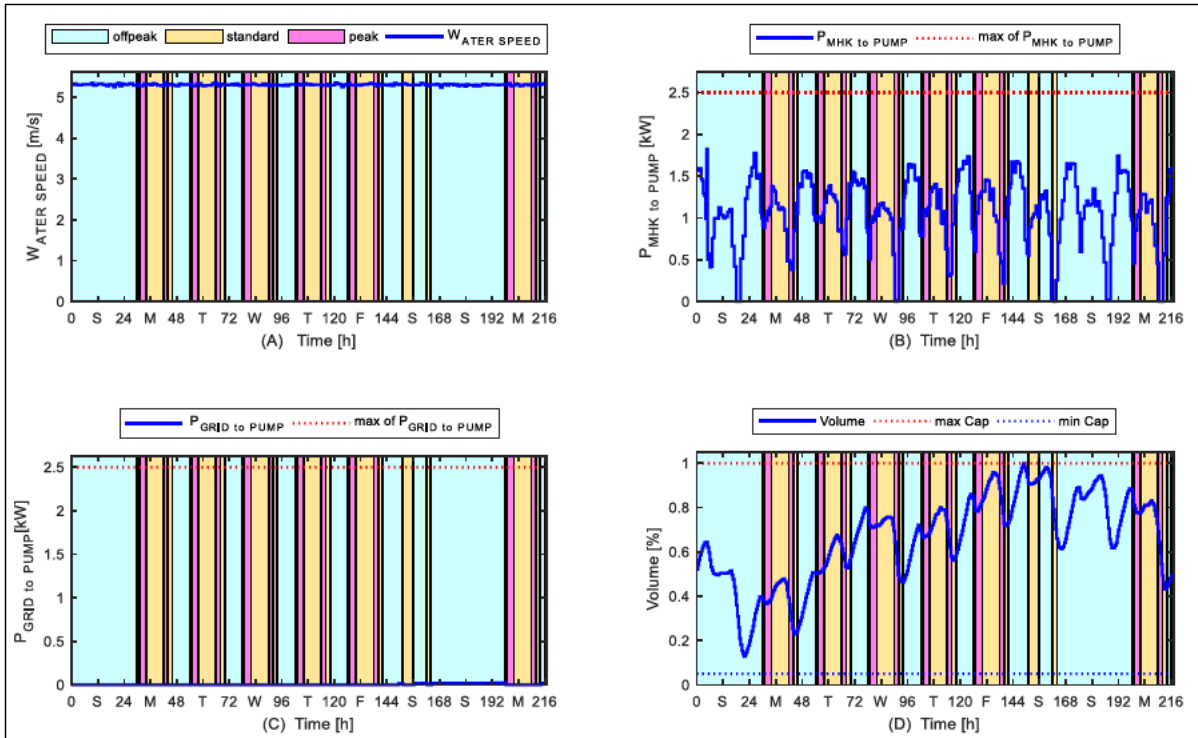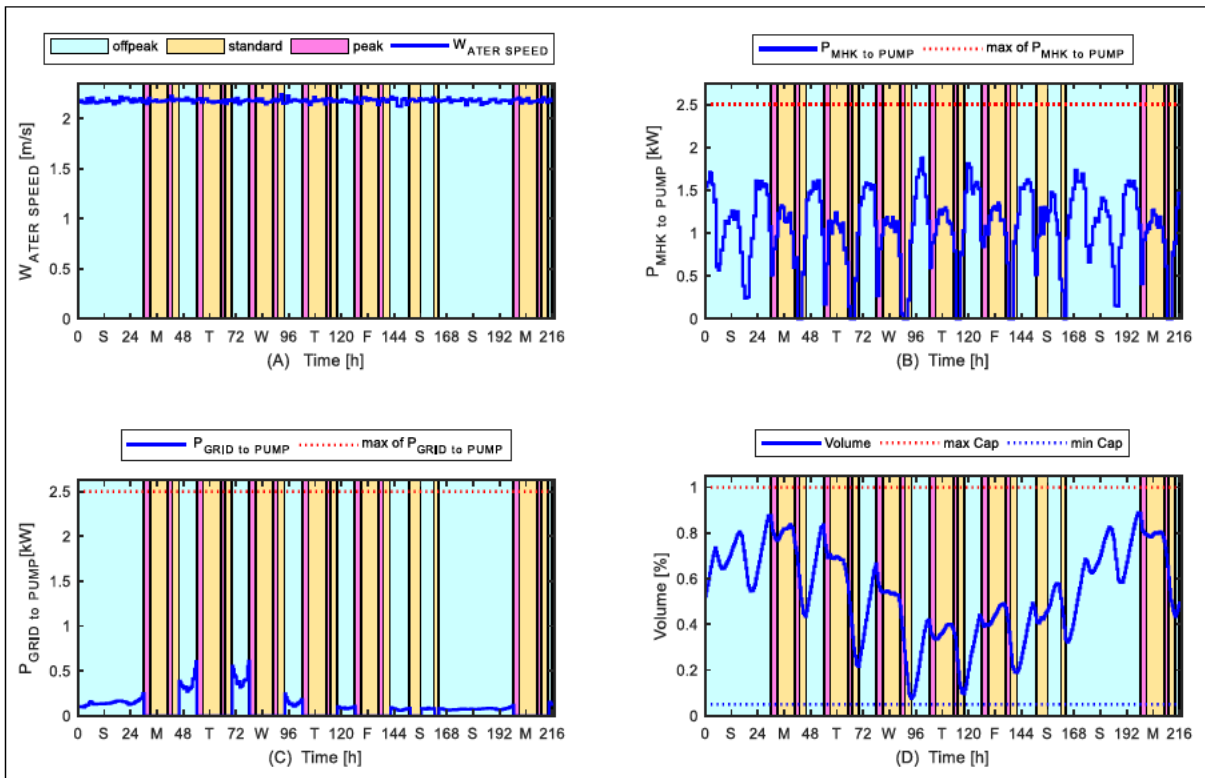

Figure 4.6: Water speed and PHS side power flow during high demand season (residential)
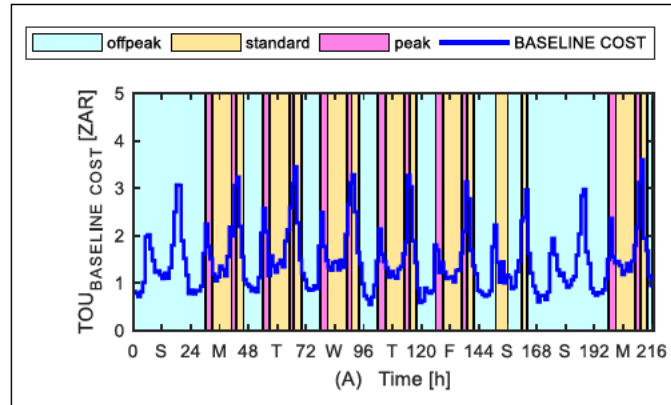
Figure 4.7: Baseline grid cost incurred by the residential load without the MHK-PHS system (high demand season)

4.3.2 Commercial load

The optimal control results for the commercial load are shown in Figs. 4.8 to 4.10 (for low demand season) and Figs. 4.11 to 4.13 (for high demand season). Similar to the residential load case, the variable commercial load profile data has been extracted from Sunday (1st January 2017) to Monday (9th January 2017), as shown in Fig. 4.6A. For high demand season, the variable load profile data has been extracted from Sunday (4th June 2017) to Monday (12th June 2017), as shown in Fig. 4.8A.

It is noted that for the selected days of the June month, the peak demand is above 6 kW for most of the days, while for the low demand season month (January) it is below 6 kW for most of the days. The overall simulation parameters of the commercial load case are shown in Table 4.2. The HOMER simulation results proved that the commercial load requires larger storage unit size, when compared to residential load. Hence, larger storage components' sizes have been selected, as shown in Table 4.2.

Table 4.2: Simulation parameters for the non-interactive system (commercial load)

Item	Value
Sampling time (Δt)	30 minutes
PHS nominal capacity ($P_{T:G}$= 2.6 kW and $P_{M:P}$= 2.6 kW)	2 kWh
PHS maximum volume	100%
PHS minimum volume	5%
Initial upper reservoir capacity	50%
Overall efficiency of the PHS ($\eta_{T:G}$= 84% and $\eta_{M:P}$= 84%)	70.6%
MHK system rating	2.5 kW

4.3.2.1   Low demand season

The results for the low demand season are shown in Figs. 4.8 to 4.10. Similar to the residential case, the selected MHK system generates its rated output power of 2.5 kW as shown in Figs. 4.8B and 4.9B. The results show that the model still allows most of the generated RE power (from MHK and PHS systems) to be utilized, for supplying the primary commercial load, as shown in Figs. 4.8B and 4.8C, respectively. The remainder of the load demand is supplemented by the utility grid, as shown in Fig. 4.8D. The grid supplement takes place during business operation hours, especially during the course of the daylight standard TOU periods. The reason is because the electricity costs are cheaper during these standard periods, as compared to peak periods.

Most of the MHK system's power is stored into the upper reservoir during off-peak periods, as shown in Fig. 4.9B. The reason is that the primary load demand is minimal. Hence, the large amount of excess energy is stored in the upper reservoir, as shown in Fig. 4.9D. The refilling process starts from the evening peak period and ends during the morning peak period. The stored energy is further utilized during business operation hours of the next

96

day (i.e. during morning peak periods and daylight standard periods). Even though Sundays have led to the grid power consumption solely for supplementing the load demand, the grid-to-load operational hours are higher than in the case of the residential load.

Using Figs. 4.8D and 4.9C, the overall grid cost for the simulated nine days (1st January – 9th January) yielded ZAR7.84. If the 9 day load demand, shown in Fig. 4.8A, is to be solely met by the utility grid (Eskom), it will incur baseline grid cost of ZAR243.25, as shown in Fig. 4.10. Hence, through the use of the optimally controlled MHK-PHS system, the commercial consumer only settles 3.2% of the baseline grid cost during low demand season. This proves that during low demand season, a potential energy cost saving of 96.8% is possible for the selected nine days.

Figure 4.8: Load demand side power flow during low demand season (commercial)

97

Figure 4.9: Water speed and PHS side power flow during low demand season (commercial)

Figure 4.10: Baseline grid cost incurred by the commercial load without the MHK-PHS system (low demand season)

4.3.2.2 High demand season

The simulation results for the high demand season are shown in Figs. 4.11 to 4.13. The rated output power of 2.5 kW is generated by the MHK system, as revealed by the red-dotted

98

lines in Figs. 4.11B and 4.12B. To minimize the grid costs, the model still allows most of the generated RE power to be utilized for supplying the primary commercial load, as shown in Figs. 4.11B and 4.11C. The utility grid is further used during business hours, as a last option for supplementing the unmet demand, as shown in Fig. 4.11D. The high demand season leads to a higher grid cost of ZAR24.42, for supplementing the unmet load demand, when compared to low demand season.

In contrary to the low demand season, the high demand season leads to the higher grid cost (ZAR4.44), for supplementing the pumping demand during off-peak periods, as shown in Fig. 12C. When the demand is low during off-peak TOU periods, most of the MHK system power is stored into the upper reservoir, to be utilized during the next business day, as shown in Figs. 4.12B and 4.12D. Similar to the low demand season, the refilling process begins during the evening TOU peak period and ends during the morning TOU peak period. Sunday has proved to lead to the utilization of the grid power for the entire 24 hours, for the purpose of supplementing both the motor-pump unit and the load demand, as shown in Figs. 4.11D and 4.12C.

The grid consumption cost for the simulated nine days, yielded a total cost of ZAR28.86. The baseline utility grid cost of ZAR313.88 is possible if the load demand is solely met by the utility grid company for the entire nine days period, as shown by Fig. 4.13. Hence, through the use of the optimally controlled MHK-PHS system, the commercial consumer only settles 9.2% of the baseline grid cost, during the high demand season. This proves that a potential of 90.8% energy cost saving is possible for the selected nine days.
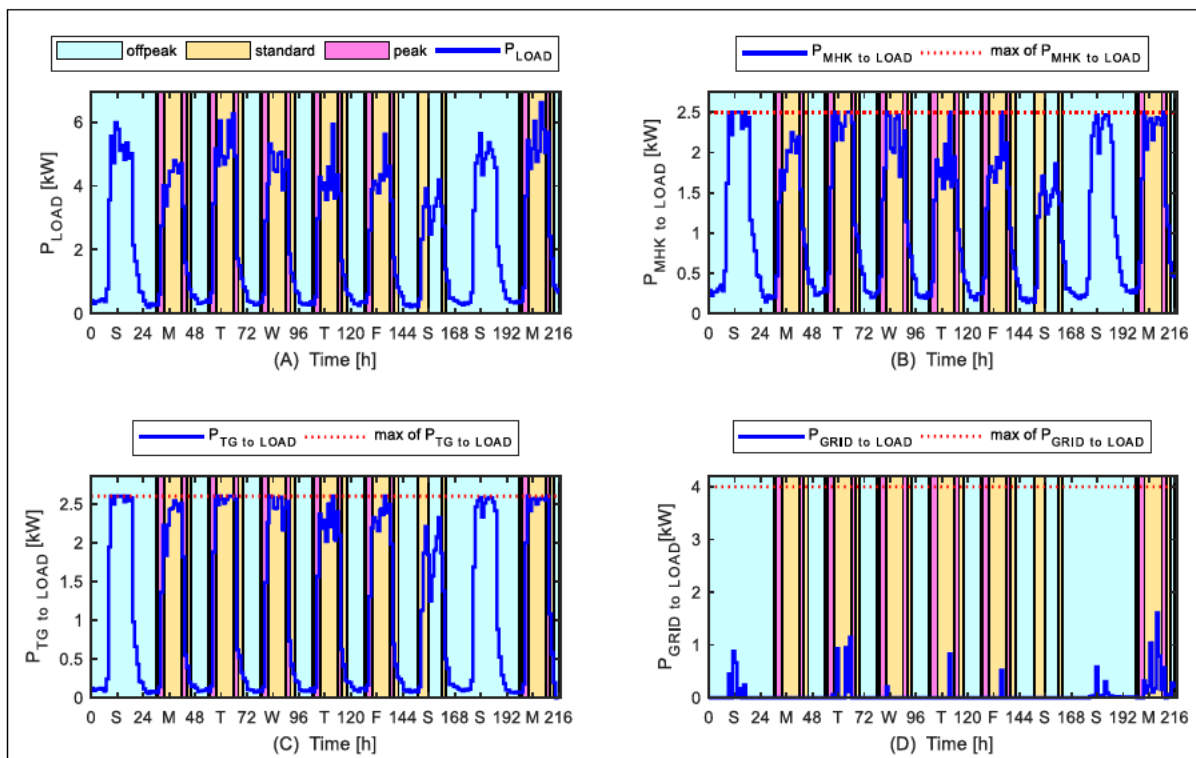
Figure 4.11: Load demand side power flow during high demand season (commercial)
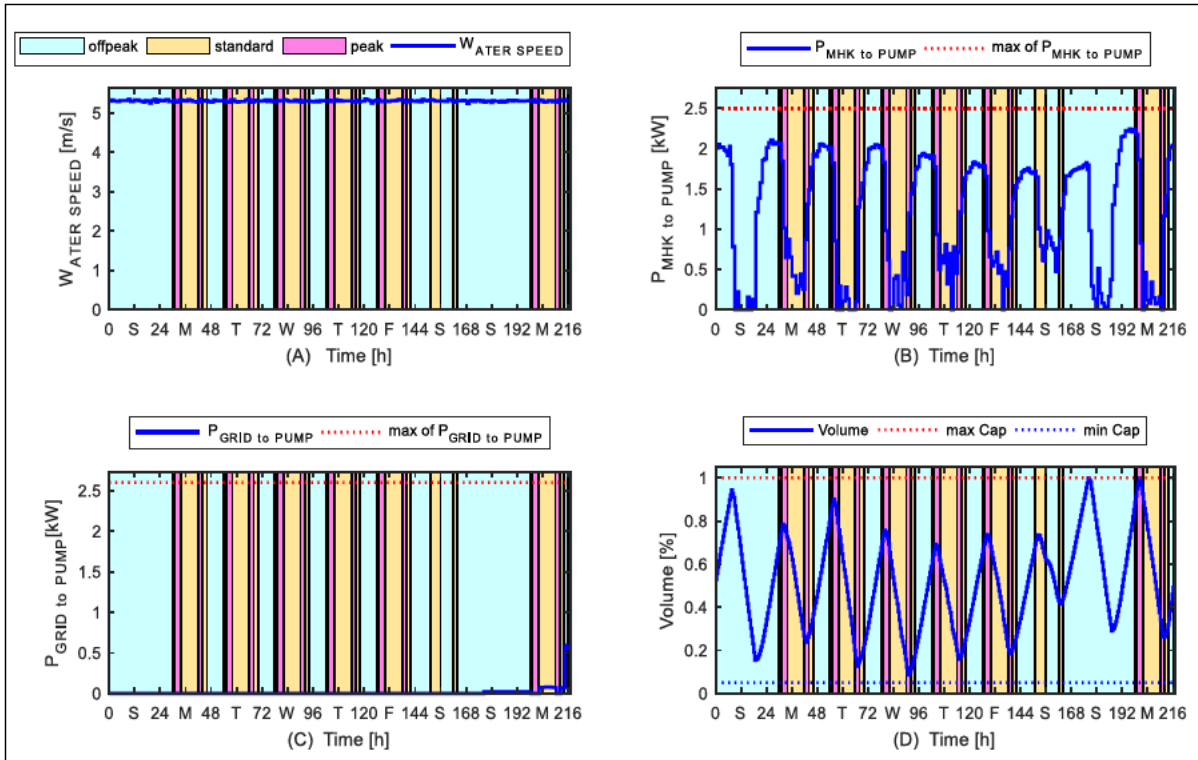

Figure 4.12: Water speed and PHS side power flow during high demand season (commercial)
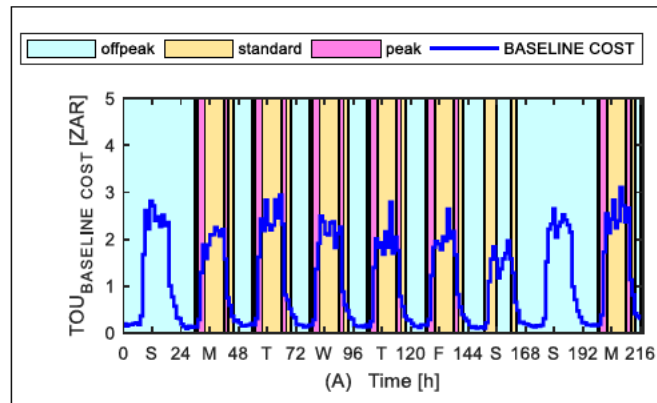
Figure 4.13: Baseline grid cost incurred by the commercial load without the MHK-PHS system (high demand season)

4.3.3 Industrial load

The optimal control results for the industrial load are shown in Figs. 4.14, 4.15 and 4.16 (for low demand season) and Figs. 4.17, 4.18 and 4.19 (for high demand season). The variable industrial load profile data, for the low demand season is from Sunday (1st January 2017) to Monday (9th January 2017), as shown in Fig. 4.14A. For high demand season, the variable load profile data has been obtained from Sunday (4th June 2017) to Monday (12th June 2017), as shown in Fig. 4.17A.

It is noted that for the selected days of the June month, the peak load demand approaches a value above 10 kW and for most of the days the peak demand is above 8 kW. For the selected days of January, a peak load demand of 8.8 kW is approached and for most of the days, the peak demand is below 8 kW. The overall simulation parameters for the industrial load case are shown in Table 4.3. Contrary to both the residential and commercial cases, it is observed that the storage system's simulation parameters for the industrial load case are the highest. The reason is that the MATLAB *linprog* toolbox could not find the optimization solution that satisfies the constraints. Hence, the size of the PHS system had to be increased.

101

Additionally, HOMER simulation results further proved that the industrial load requires a largest storage unit size, when compared to other load types.

Table 4.3: Simulation parameters for the non-interactive system (industrial load)

Item	Value
Sampling time (Δt)	30 minutes
PHS nominal capacity ($P_{T:G}$= 4 kW and $P_{M\,P}$= 3 kW)	2.5 kWh
PHS maximum volume	100%
PHS minimum volume	5%
Initial upper reservoir capacity	50%
Overall efficiency of the PHS ($\eta_{T:G}$= 84% and $\eta_{M:P}$= 84%)	70.6%
MHK system rating	2.5 kW

4.3.3.1   Low demand season

The simulation results for the low demand season are as shown in Figs. 4.14 to 4.16. Similar to the other two cases, the selected MHK system generates its rated output power of 2.5 kW, as shown in Figs. 4.14B and 4.15B. The model allows most of the generated RE power to be utilized for supplying the industrial load, as shown in Figs. 4.14B and 4.14C, respectively. The unmet load demand is supplemented by the utility grid during business operational hours, as shown in Fig. 4.14D, as this is similar for the commercial load case. This resulted in a grid cost of ZAR7.60.

Most of the MHK system power is stored into the upper reservoir during low power demand off-peak periods, as shown in Fig. 4.15B. Hence, the upper reservoir volume increases, as shown in Fig. 4.15D. Similar to the commercial load case, the refilling process

102

starts in the evening peak period and ends during the morning peak period. The stored energy is further utilized during the business operational hours of the next day.

Sundays led to the highest power consumption from the MHK system, for meeting the pumping demand, when compared to other days. The grid power consumption is not utilised to supplement the pumping demand for the entire simulated nine days. It is only utilized to supplement the load demand. The industrial load allows less grid-to-load operational hours when compared to the commercial load case.

Using Fig. 4.14D and 4.15C, the overall grid cost for the simulated nine days yielded a total of ZAR7.60. If the 9 day load demand shown Fig. 4.14A, is to be solely met by the utility grid (Eskom), it will incur baseline grid cost of ZAR242.74 as shown by Fig. 4.16. Hence, through the use of the optimally controlled MHK-PHS system, the industrial consumer settles merely 3.1% of the baseline grid cost during low demand season. This proves that a potential of 96.9% energy cost saving is possible for the selected nine days.

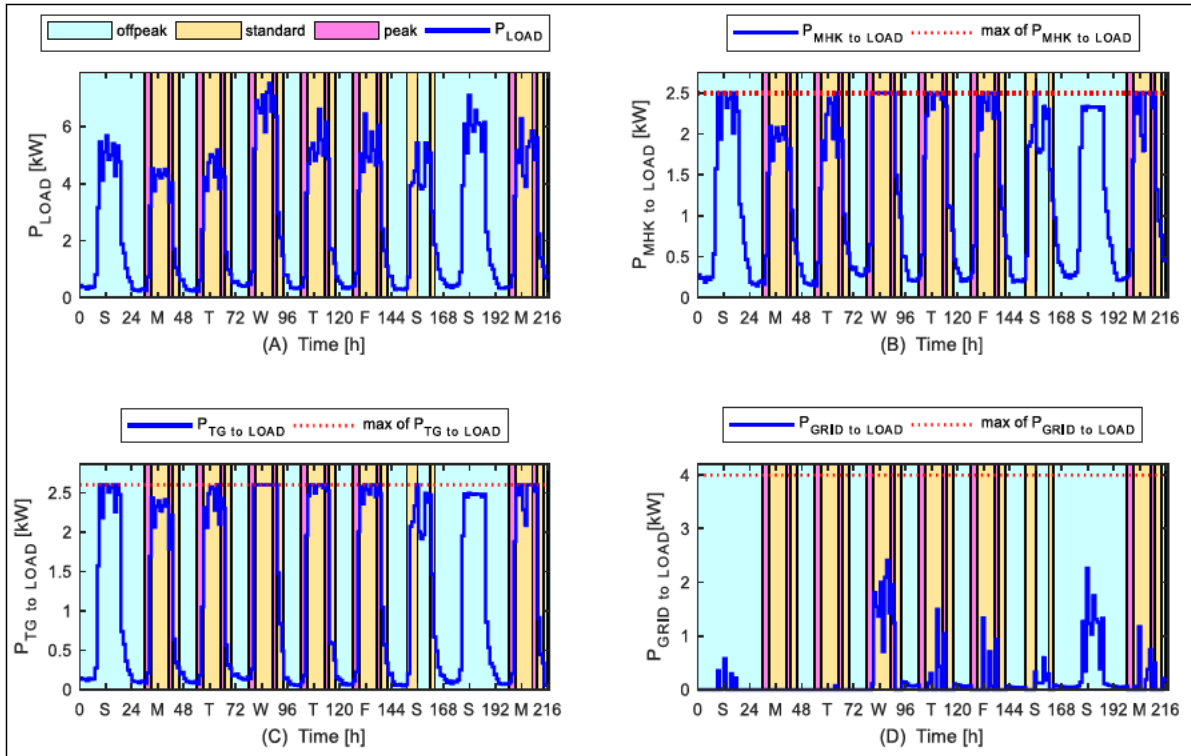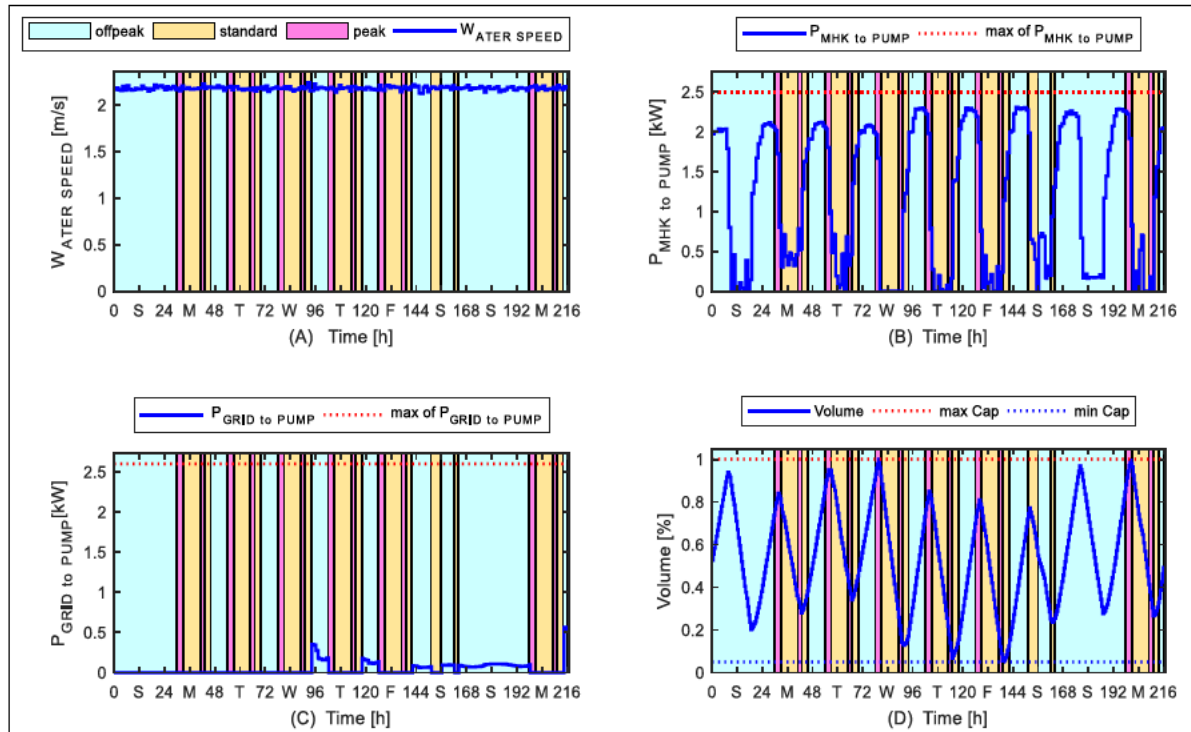Figure 4.14: Load demand side power flow during low demand season (industrial)

103

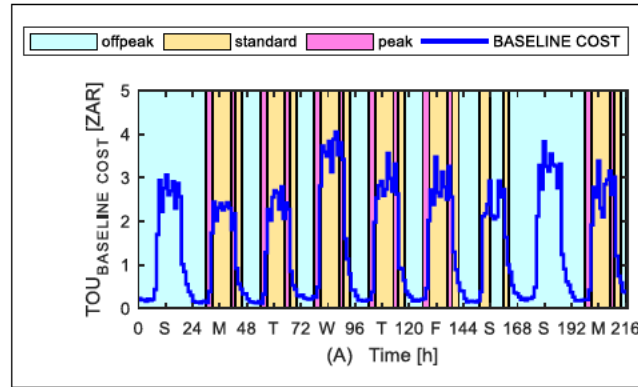Figure 4.15: Water speed and PHS side power flow during low demand season (industrial)

Figure 4.16: Baseline grid cost incurred by the industrial load without the MHK-PHS system (low demand season)

This proves that for the non-interactive grid-connected MHK-PHS system, the cost savings benefits for the industrial load consumer are equals to those of the commercial load consumer. However, since the industrial load requires a larger storage system size, as compared to the commercial load, this will results in a longer payback period.

104

4.3.3.2   High demand season

The simulation results for the high demand season are shown in Figs. 4.17 to 4.19. The rated output power of 2.5 kW is generated by the MHK system, as revealed in Fig. 4.17B and 4.18B. To minimize the grid costs, the model still permits most of the generated RE power to be utilized in supplying the primary industrial load, as shown in Fig. 4.17B and 4.17C, respectively. The utility grid is used during business hours as a last option for supplementing the unmet load demand, as shown in Fig. 4.17D. The high demand season leads to a higher grid cost of ZAR26.11 for supplementing the unmet load demand, when compared to the low demand season.

Unlike the low demand season, the high demand season leads to an additional grid cost of ZAR2.90, by supplementing the pumping demand during off-peak periods, as shown in Fig. 18C. During off-peak TOU periods, most of the MHK system power is stored into the upper reservoir, to be utilized during the next business day, as shown in Figs. 4.18B and 4.18D. Similar to the commercial case, the refilling process starts from the evening TOU peak period and ends during the morning TOU peak period.

Sunday has proved to lead to the utilization of the grid power for the entire 24 hours for the purpose of supplementing both the motor-pump unit and the load demand, as shown in Figs. 4.17D and 4.18C. Both Sundays proved to lead to the large number of charging and discharging cycles, when compared to the other week days.

The grid consumption cost yielded a total cost of ZAR29.01 for the simulated nine days. The baseline utility grid cost of ZAR315.52 is possible, if the load demand is solely met by the utility grid company for the entire nine day period, as shown by Fig. 4.19. Hence, through the use of the optimally controlled MHK-PHS system, the industrial consumer settles merely 9.2% of the baseline grid cost, during high demand season.
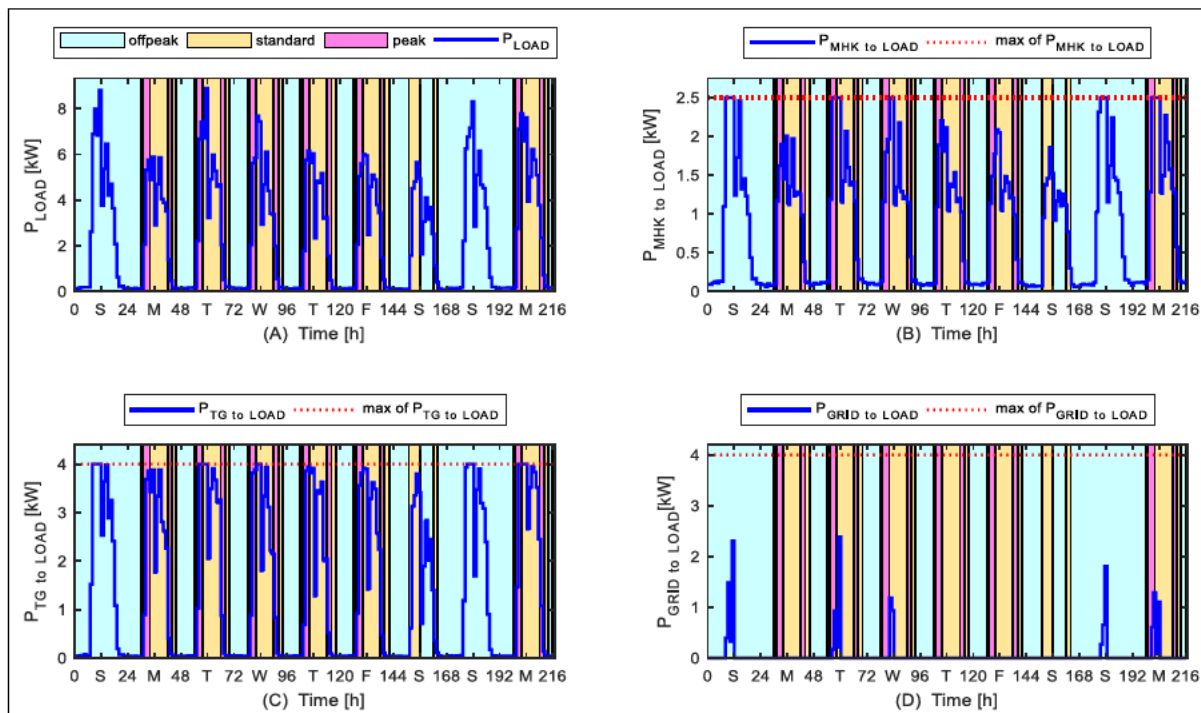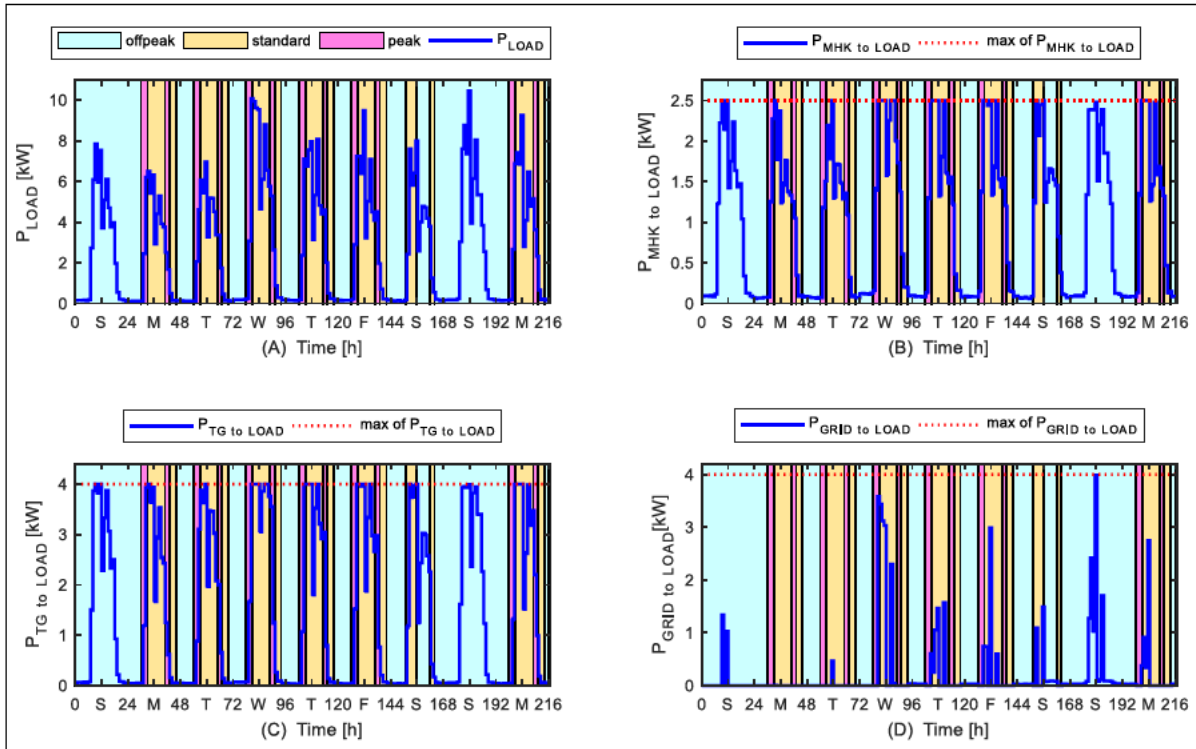
Figure 4.17: Load demand side power flow during high demand season (industrial)
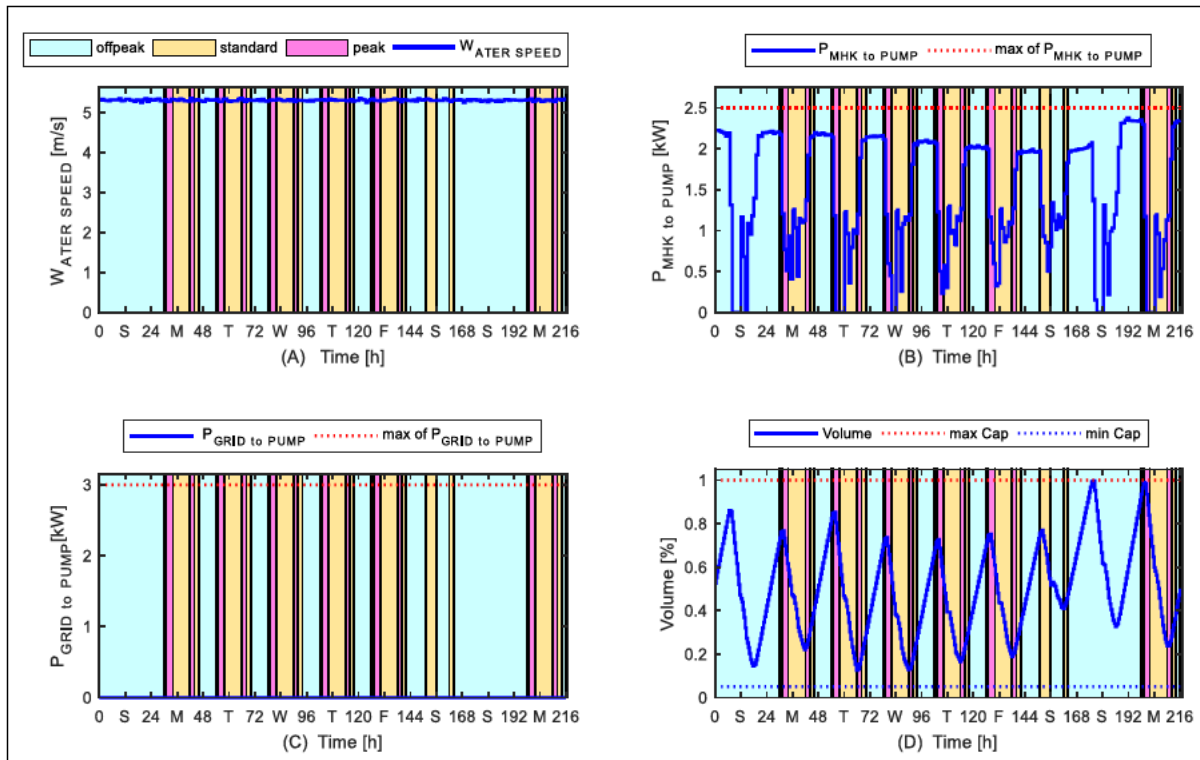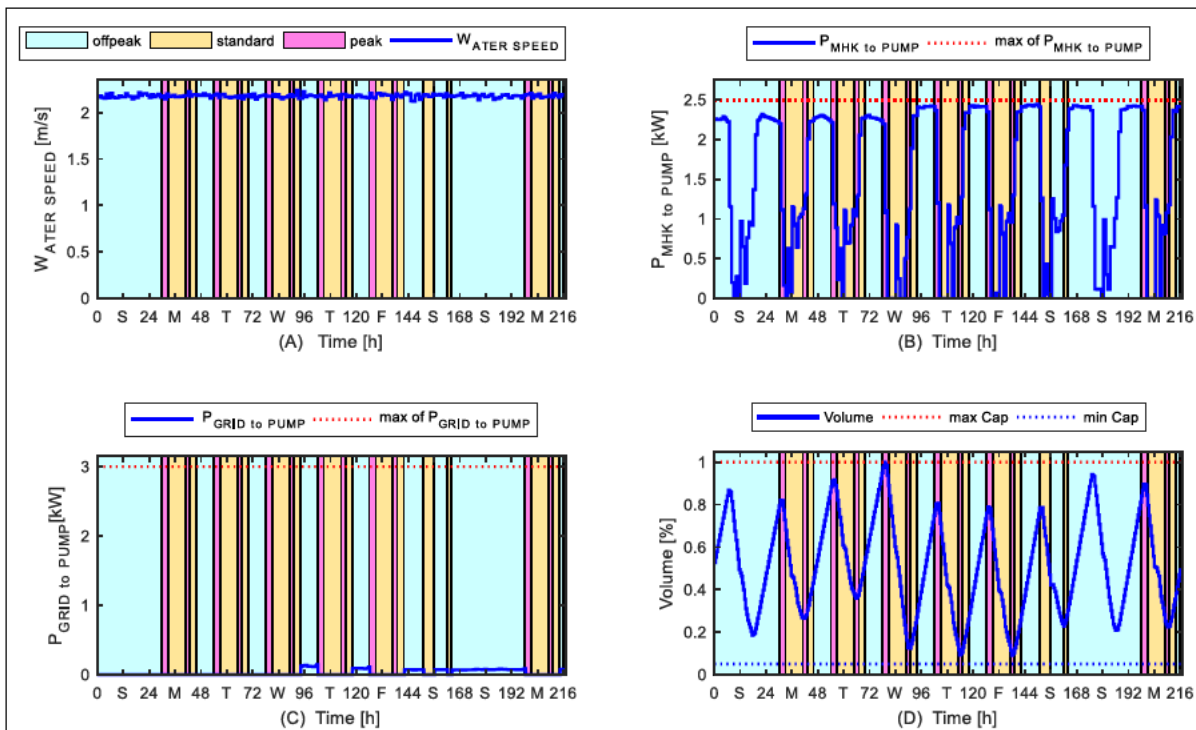

Figure 4.18: Water speed and PHS side power flow during high demand season (industrial)
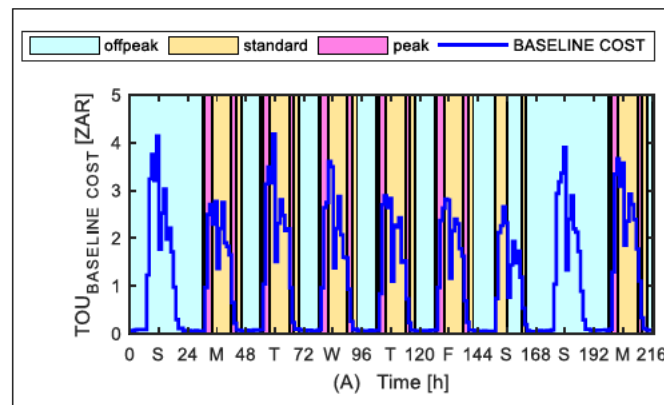
106
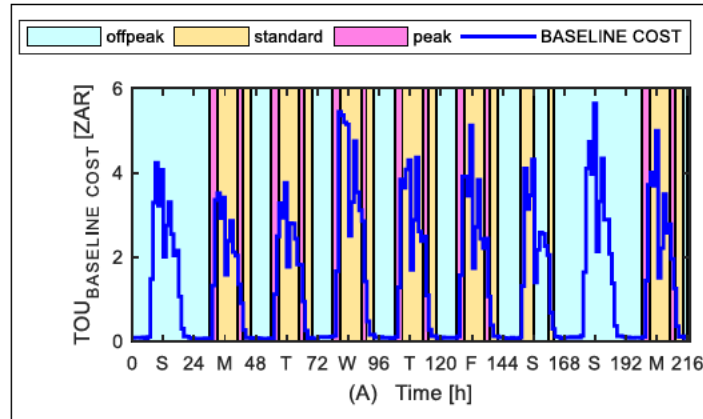
Figure 4.19: Baseline grid cost incurred by the industrial load without the MHK-PHS (high demand season)

This proves that during high demand season, a potential cost savings of 90.8% is possible for the selected nine days. This is the same cost saving benefit as for the commercial load case.

Table 4.4: Summary of the cost savings benefits for the non-interactive grid-connected systems

	Residential Load		Commercial Load		Industrial Load	
	Low Demand Season	High Demand Season	Low Demand Season	High Demand Season	Low Demand Season	High Demand Season
Baseline grid cost (ZAR)	245.05	317.77	243.25	313.88	242.74	315.52
Optimal control grid cost (ZAR)	3.69	26.16	7.84	28.86	7.60	29.01
Cost saving (%)	98.5%	91.8%	96.8%	90.8%	96.9%	90.8%

4.4 Conclusion

This Chapter presented an optimal energy management algorithm for the non-interactive grid-connected MHK-PHS system, which permits consumers to buy electricity from the

107

utility grid, when it is economically viable. The electricity purchasing price was based on Ruraflex TOU tariffs (during low and high demand seasons), as applied by Eskom. The model aimed at ensuring the optimal power purchasing strategy, through minimized grid consumption cost. The *linprog* solver has been applied to solve the optimization problem, since the nature of the problem consists of linear constraints.

The performance of the model has been studied through the use of the variable residential, commercial and industrial load types, respectively. Each load type has been studied during low demand season and high demand season, respectively. The simulations have been carried for nine consecutive days (216 hours), in order to analyse the behaviour of the model during both week and weekend days. For appropriate comparison purpose, the optimal control simulations have been undertaken with the assurance that the initial water level at the start of the control horizon is retained at the end of the control horizon. To study the effectiveness of the developed model, the baseline grid energy cost incurred by each studied load type, is compared to the incurred optimal grid cost.

The simulation results have revealed the effectiveness of the proposed model, to optimally control the power flow of the proposed non-interactive grid connected MHK-PHS system. The model allowed the effective use of the power generated by the RE system (MHK and PHS) as first priorities when meeting each load type (residential, commercial and industrial, respectively). It has been noted that for all three load types, the model allowed the grid power to be utilized as a last resort for supplementing the unmet load demand. Additionally, the model allowed the grid power to be stored within the upper reservoir, during inexpensive TOU off-peak periods, for all the three various load demand cases, during high demand season only. Hence, the objective of minimizing the grid consumption cost has been achieved.

The model proved to perform precisely the same way for all the three load types, under both high demand and low demand seasons. When comparing the baseline grid cost of the three various loads types, it is observed that they are more or less the same for each season as shown in Table 4.4. The reason is that the HOMER software generated the three load types to have the same daily average energy consumption. The baseline grid cost for the residential load profile is slightly higher than one of the other two load types. The reason being that the residential load commonly demands peak power during the costly TOU peak periods (both in the morning and evening). In contrary, the commercial and industrial load types demand peak power mostly during standard TOU periods.

The optimal control technique proved to bring cost saving benefits for all the three load types, during both seasons. The higher costs saving benefits are achieved during low demand season, since the grid power is solely used to supplement the unmet load demand, instead of supplying the motor-pump unit. However, even though the residential load had the highest baseline grid cost, highest cost saving benefits have been achieved by the residential load type, when compare to the other two load types for both seasons. This was due to the resulted least optimal grid cost. Hence, the model proves that the residential load type will have the shortest payback period (due to the highest cost saving benefit at the smallest storage size), as compared to both the commercial and industrial load types. Hence, this proves that the non-interactive grid-connected MHK-PHS system favours the residential load more than the other load types. The residential load profile proved to permit the largest amount grid power to be stored within the upper reservoir, when compared to the commercial and industrial cases. This led to largest number of charging and discharging cycles, particularly on Sundays.

CHAPTER 5: OPTIMAL POWER CONTROL FOR A GRID INTERACTIVE MHK-PHS SYSTEM

5.1 Introduction

This Chapter presents an optimal energy management algorithm for a grid-interactive MHK-PHS system. The selected grid-interactive MHK-PHS system is defined for customers who purchase the energy from the grid and further sell the stored energy and/or excess energy into the grid. Therefore, the proposed energy management model to be developed, aims to ensure optimal power dispatching performance. The model should be able to minimize the COE purchased from the grid, while maximizing the energy sales revenue, based on the TOU tariffs. The developed models will be applied in MATLAB software, in order to perceive the cost saving benefit and operation. The *fmincon* solver is used to solve the optimization challenge, since the problem consists of non-linear and linear constraints to be discussed below.

5.2 Model Development

5.2.1 Description of a grid-interactive MHK-PHS system

The configuration/power flow layout of the proposed grid-interactive MHK-PHS system is as shown in Fig. 5.1. Similar to the non-interactive MHK-PHS system shown in Fig. 4.1, the system also consists of the same components. The main difference is that, in addition to the purchasing of energy from the utility grid, the consumer may additionally sell energy into

the grid network, as a means of generating revenue. This simply implies that the excess energy from the MHK system may be sold into the utility grid, after satisfying the primary load demand as a first priority. This will further depends on the TOU tariff schedule/rates. Moreover, the energy generated by the PHS system may be used to supplement the unmet load demand and/or be sold into the grid, depending on the TOU tariff rates. Similar, to the non-interactive system, the energy from the utility grid may be used to supply the primary load and/or the motor-pump unit, in order to store energy for later use. The objective function and constraints will be formulated through the use of the following variables associated with the system power-flow diagram:

$P_{1(t)}$: the electrical power flow (kW) from the MHK river system to the load at time t;

$P_{2(t)}$: the electrical power flow (kW) from the turbine-generator unit to the load at time t;

$P_{3(t)}$: the electrical power flow (kW) from the utility grid to the load at time t;

$P_{4(t)}$: the electrical power flow (kW) from the MHK river system to the motor-pump unit at time t;

$P_{5(t)}$: the electrical power flow (kW) from the utility grid to the motor-pump unit at time t;

$P_{6(t)}$: the electrical power (kW) from the MHK river system to the utility grid at time t; and

$P_{7(t)}$: the electrical power (kW) from the turbine-generator unit to the utility grid at time t.

5.2.2   Problem formulation

The energy operation management in the proposed grid-interactive MHK-PHS system, is defined as an optimization problem for determining the optimal generation, consumption and selling points. The optimization challenge will be solved through the consideration of TOU tariff scheme. The residential, commercial and industrial load demand sectors should be

111

satisfied at all times, respectively. The generation, consumption and retailing points must satisfy certain constraints, to ensure optimal energy management subject to the constraints discussed below.
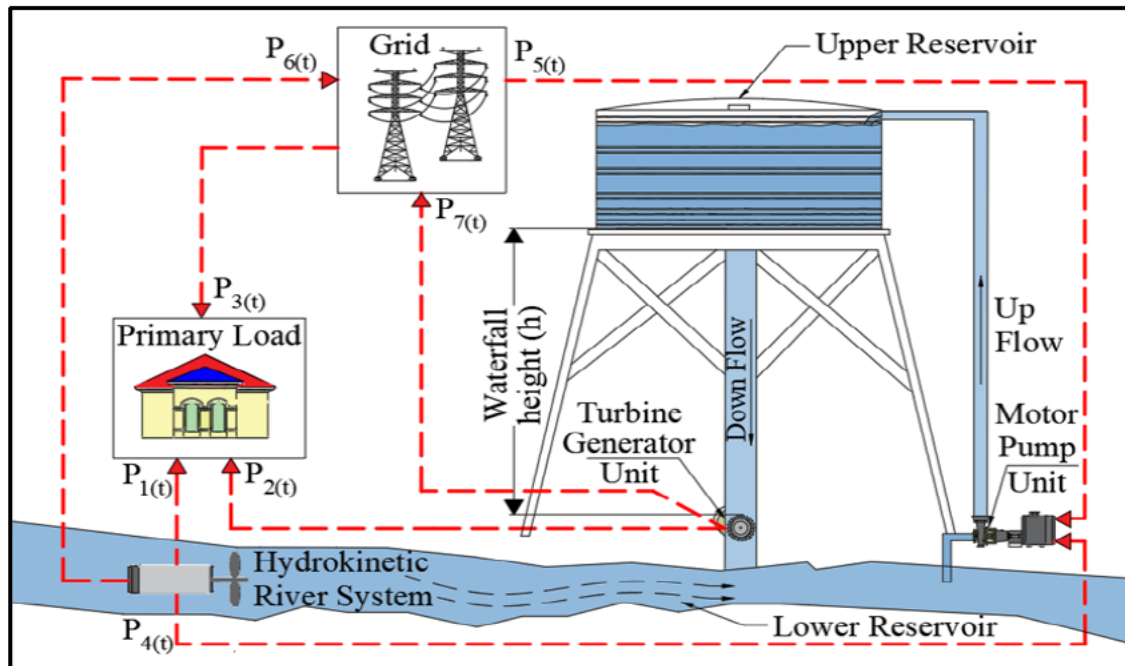
Figure 5.1: Layout of the grid-interactive MHK-PHS system

5.2.2.1 Objective function

As mentioned earlier, the objective of the proposed optimal control model for the grid-interactive MHK-PHS system will serve two functions; to minimize the COE purchased from the grid, as well as maximizing the energy sales revenue. However, the economic dispatch is a challenge to solve such a multi-objective function. Therefore, it is of great importance to determine the optimum schedule for consuming grid energy and for selling energy into the grid. Furthermore, it is important to optimally harvest/utilize the power generated by the MHK and PHS systems as much as possible.

Consumers are usually allowed to sell the onsite generated RE at a pre-set price per kWh. This pre-set price is based on the long-term feed-in purchase agreement reached between the utility company and the consumer. Some FIT policies allow market-dependent FIT design models, while others allow market-independent models at a fixed price, for the entire contract period (Ramli & Twaha, 2015). In this study, a market-dependent FIT design model that applies a fixed percentage (without additional bonus), will be considered. This simply implies that the compensation paid to the customer (who sells RE), is a fixed percentage of the utility retail market price at that point in time. This fixed percentage is customarily selected to allow the selling price to be less than the utility retail price (Ramli & Twaha, 2015). Hence, in this study, a fixed percentage is assumed to be 65% of the utility retail price (Kusakana, 2016).

Since the proposed model aims at minimizing the grid cost, while maximizing the energy sales revenue, then the overall discrete multi-objective function (F) is expressed as follows:

$$F = \sum_{j=1}^{N} C_j \cdot (P_{3(j)} + P_{5(j)}) \cdot \Delta t - C_j \cdot R_a \sum_{j=1}^{N} (P_{6(j)} + P_{7(j)}) \cdot \Delta t \qquad (1 \le j \le N) \qquad (5.1)$$

Where: $P_{3(j)}$ = power flow from the utility grid to the primary load at j^{th} sampling time (kW);

$P_{5(j)}$ = power flow from the utility grid to the motor-pump unit at j^{th} sampling time (kW);

$P_{6(j)}$ = power flow from the MHK system to the utility grid at j^{th} sampling time (kW);

$P_{7(j)}$ = power flow from the turbine-generator unit to the utility grid at j^{th} sampling time (kW);

C_j = TOU electricity price at the jth sampling time (ZAR/kWh);

R_a = contracted/agreement percentage ratio during FIT (65%).

113

5.2.2.2   Constraints

The objective function stated above will be solved under the following equality and inequality constraints:

(a) Equality constraint for power balancing

Similar to the first case, the load demand should be met at all times, through the use of the three sources, depending on the availability and TOU periods. This equality constraint is mathematically discretized as follows:

$$P_{Load(j)} = P_{1(j)} + P_{2(j)} + P_{3(j)} \quad (1 \le j \le N) \tag{5.2}$$

Where: $P_{1(j)} =$ power flow from the MHK system to the primary load at j^{th} sampling interval (kW);

$P_{2(j)} =$ power flow from the PHS system to the primary load at j^{th} sampling interval (kW).

(b) Equality constraint for fixed-final state condition

For a repeated implementation of the optimal energy control, the water level state at the start of the control horizon is permitted to be equal at the end of the control horizon. This constraint is then expressed as follows:

114

$$\sum_{j=1}^{N}(P_{4(j)} + P_{5(j)}) - \sum_{j=1}^{N}(P_{2(j)} + P_{7(j)}) = 0 \qquad (1 \le j \le N) \qquad (5.3)$$

Where: $P_{4(j)}$ = power flow from the MHK system to the motor-pump unit at j^{th} sampling interval (kW).

(c) Non-linear equality constraint for the exclusion of power flow

It is important to note that a consumer should purchase electricity from the grid when there is a deficit from the RE systems (MHK and PHS). Therefore, the customer should not purchase and sell the energy at the same time (Numbi & Malinga, 2017). Simultaneous buying and selling is economically infeasible based on the agreement FIT ratio. Therefore, the product of both the purchased and sold power should be equals to 0, as denoted by Equation (5.4). This results in a non-linear equality constraint.

$$(P_{3(j)} + P_{5(j)}) * (P_{6(j)} + P_{7(j)}) = 0 \qquad (1 \le j \le N) \qquad (5.4)$$

(d) Control variables limits constraints

The optimization problem consists of seven control variables that should be firmly limited to operate within their minimum limits (zero) and maximum operating levels. These power constraints limits (kW) are expressed into a discrete form, as follows:

$$0 \le P_{1(j)} \le P_{1(j)}^{\max} \qquad (1 \le j \le N) \qquad (5.5)$$

115

$$0 \le P_{2(j)} \le P_{2(j)}^{rated} \qquad (1 \le j \le N) \qquad\qquad (5.6)$$

$$0 \le P_{3(j)} \le P_{3(j)}^{rated} \qquad (1 \le j \le N) \qquad\qquad (5.7)$$

$$0 \le P_{4(j)} \le P_{4(j)}^{\max} \qquad (1 \le j \le N) \qquad\qquad (5.8)$$

$$0 \le P_{5(j)} \le P_{5(j)}^{rated} \qquad (1 \le j \le N) \qquad\qquad (5.9)$$

$$0 \le P_{6(j)} \le P_{6(j)}^{\max} \qquad (1 \le j \le N) \qquad\qquad (5.10)$$

$$0 \le P_{7(j)} \le P_{7(j)}^{rated} \qquad (1 \le j \le N) \qquad\qquad (5.11)$$

Where: $P_{i(j)}^{\max}$ = the maximum generated power at j^{th} sampling interval (kW);

P_i^{rated} = the rated power of the component (kW).

(e) Inequality constraints

The MHK river system is used to supply power to the load (P_1) and/or to the motor-pump unit (P_4), as well as to sell power to the utility grid (P_6). Hence, at any given sampling interval, the sum of the above mentioned powers should not exceed the maximum generated output power of the MHK system. This inequality constraint is expressed as follows:

$$P_{1(j)} + P_{4(j)} + P_{6(j)} \le P_{MHK(j)}^{\max} \quad (1 \le j \le N) \qquad\qquad (5.12)$$

116

Similarly, the turbine-generator unit should supply up to a maximum of its rated output power, when supplementing the unmet load demand and/or selling energy to the grid. This inequality constraint may be discretized as follows:

$$P_{2(j)} + P_{7(j)} \leq P_{T:G}^{rated} \quad (1 \leq j \leq N) \tag{5.13}$$

Similar to the non-interactive system, the pumping demand for refilling the upper reservoir is met by the MHK system and/or the grid. This constraint is achieved as follows:

$$P_{4(j)} + P_{5(j)} \leq P_{M:P}^{rated} \quad (1 \leq j \leq N) \tag{5.14}$$

(f) Upper reservoir's state variable limit constraints

Similar to the first case of non-interactive system, the upper reservoir boundaries are expressed using Equation (4.14). When refilling the upper reservoir, the motor-pump unit can be supplied by the MHK system and/or the utility grid, as done in the first case. However, the main dissimilarity is that the turbine-generator unit generates electricity for two reasons, namely to supplement the unmet load demand and/or for sale. Hence, at any sampling interval, the discrete dynamic state of the water level in the upper reservoir is further expressed as follows:

$$Cap_{(j)} = Cap_{(0)} + \sum_{j=1}^{N} [(P_{4(j)} + P_{5(j)}) \cdot \frac{\eta_p}{E_{pot}} \cdot \Delta t] - \sum_{j=1}^{N} [(P_{2(j)} + P_{7(j)}) \cdot \frac{\Delta t}{\eta_g \cdot E_{pot}}] \tag{5.15}$$

117

Since $Y = \dfrac{\eta_p \cdot \Delta t}{E_{pot}}$ and $Z = \dfrac{\Delta t}{\eta_g \cdot E_{pot}}$, by substituting Equation (5.15) into (4.14)

results into the following limit equation:

$$Cap^{\min} \le Cap_{(0)} + \sum_{j=1}^{N} [(P_{4(j)} + P_{5(j)}) \cdot Y] - \sum_{j=1}^{N} (P_{2(j)} + P_{7(j)}) \cdot Z \le Cap^{\max} \tag{5.16}$$

Therefore, it may be noted that Equation 5.16 consists of two linear inequality constraints that may be expressed as follows:

$$\sum_{j=1}^{N} (P_{4(j)} + P_{5(j)}) \cdot Y - \sum_{j=1}^{N} (P_{2(j)} + P_{7(j)}) \cdot Z \le Cap^{\max} - Cap_{(0)} \tag{5.17}$$

$$\sum_{j=1}^{N} (P_{2(j)} + P_{7(j)}) \cdot Z - \sum_{j=1}^{N} (P_{4(j)} + P_{5(j)}) \cdot Y \le Cap_{(0)} - Cap^{\min} \tag{5.18}$$

5.2.3 Algorithm formulation and implementation in MATLAB

Unlike for the non-interactive system, the objective function for the grid-interactive system is subjected to a non-linear equality constraint, in addition to the linear inequality and equality constraints. Hence, instead of using the *linprog* solver, an *fmincon* solver is used to solve the optimization problem in MATLAB. This solver is expressed in its canonical form as follows:

118

$$\min_x \{f(x)\} \text{ subject to } \begin{cases} c(x) \le 0 \\ c_{eq}(x) = 0 \\ A \cdot x \le b \\ A_{eq} \cdot x = b_{eq} \\ lb \le x \le ub \end{cases} \tag{5.19}$$

Where: A and b are the coefficients associated with inequality constraints, A_{eq} and b_{eq} are the coefficients associated with equality constraints, lb and ub are the lower and upper bounds of the variables, respectively; $c(x)$ and $c_{eq}(x)$ are functions that return vectors; $f(x)$ is the function that returns scalar vectors. Functions $c(x)$, $c_{eq}(x)$ and $f(x)$ may be non-linear.

5.2.4 Constraints definition in *fmincon* syntax

Similar to the first case, the number of sampling intervals will still be limited to *N=2*. The matrix transformation for the seven control variables as contained in the constraints and objective function will be presented as follows:

$$P_1 = x(1:N) = [x_1, x_2] \tag{5.20}$$

$$P_2 = x(N+1:2N) = [x_3, x_4] \tag{5.21}$$

$$P_3 = x(2N+1:3N) = [x_5, x_6] \tag{5.22}$$

$$P_4 = x(3N+1:4N) = [x_7, x_8] \tag{5.23}$$

$$P_5 = x(4N+1:5N) = [x_9, x_{10}] \tag{5.24}$$

$$P_6 = x(5N+1:6N) = [x_{11}, x_{12}] \tag{5.25}$$

$$P_7 = x(6N+1:7N) = [x_{13}, x_{14}] \tag{5.26}$$

5.2.4.1 Inequality matrix

The optimization challenge for the proposed grid-interactive MHK-PHS system, consists of 5 linear inequality constraints (Equation 5.12, 5.13, 5.14, 5.17, 5.18). This incorporates 7 control variables that should be integrated into constraint matrix A and vector b, of the *fmincon* solver.

- MHK river system (using Equation 5.12)

$$x_1 + x_7 + x_{11} \leq P_{HK(1)}^{\max} \quad \text{(For } j = 1) \tag{5.27}$$

$$x_2 + x_8 + x_{12} \leq P_{HK(2)}^{\max} \quad \text{(For } j = 2) \tag{5.28}$$

- Turbine-generator unit (using Equation 5.13)

$$x_3 + x_{13} \leq P_{T:G}^{rated} \quad \text{(For } j = 1) \tag{5.29}$$

$$x_4 + x_{14} \leq P_{T:G}^{rated} \quad \text{(For } j = 2) \tag{5.30}$$

120

- Motor-pump unit (using Equation 5.14)

$$x_7 + x_9 \leq P^{rated}_{M:P(1)} \quad \text{(For } j = 1\text{)} \tag{5.31}$$

$$x_8 + x_{10} \leq P^{rated}_{M:P(2)} \quad \text{(For } j = 2\text{)} \tag{5.32}$$

- Upper reservoir maximum state (using Equation 5.17)

$$(x_7 + x_9) \cdot Y - (x_3 + x_{13}) \cdot Z \leq Cap^{max} - Cap_{(0)} \quad \text{(For } j = 1\text{)} \tag{5.33}$$

$$(x_7 + x_9 + x_8 + x_{10}) \cdot Y - (x_3 + x_{13} + x_4 + x_{14}) \cdot Z \leq Cap^{max} - Cap_{(0)} \quad \text{(For } j = 2\text{)} \tag{5.34}$$

- Upper reservoir minimum state (using Equation 5.18)

$$(x_3 + x_{13}) \cdot Z - (x_7 + x_9) \cdot Y \leq Cap_{(0)} - Cap^{min} \quad \text{(For } j = 1\text{)} \tag{5.35}$$

$$(x_3 + x_{13} + x_4 + x_{14}) \cdot Z - (x_7 + x_9 + x_8 + x_{10}) \cdot Y \leq Cap_{(0)} - Cap^{min} \quad \text{(For } j = 2\text{)} \tag{5.36}$$

Hence, using Equation 5.27-5.36, the inequality matrix may be presented as follows:

121

$$
\begin{bmatrix}
1 & 0 & 0 & 0 & 0 & 0 & 1 & 0 & 0 & 0 & 1 & 0 & 0 & 0 \\
0 & 1 & 0 & 0 & 0 & 0 & 0 & 1 & 0 & 0 & 0 & 1 & 0 & 0 \\
0 & 0 & 1 & 0 & 0 & 0 & 0 & 0 & 0 & 0 & 0 & 0 & 1 & 0 \\
0 & 0 & 0 & 1 & 0 & 0 & 0 & 0 & 0 & 0 & 0 & 0 & 0 & 1 \\
0 & 0 & 0 & 0 & 0 & 0 & 1 & 0 & 1 & 0 & 0 & 0 & 0 & 0 \\
0 & 0 & 0 & 0 & 0 & 0 & 0 & 1 & 0 & 1 & 0 & 0 & 0 & 0 \\
0 & 0 & -Z & 0 & 0 & 0 & Y & 0 & Y & 0 & 0 & 0 & -Z & 0 \\
0 & 0 & -Z & -Z & 0 & 0 & Y & Y & Y & Y & 0 & 0 & -Z & -Z \\
0 & 0 & Z & 0 & 0 & 0 & -Y & 0 & -Y & 0 & 0 & 0 & Z & 0 \\
0 & 0 & Z & Z & 0 & 0 & -Y & -Y & -Y & -Y & 0 & 0 & Z & Z
\end{bmatrix}
\cdot
\begin{bmatrix} x_1 \\ x_2 \\ x_3 \\ x_4 \\ x_5 \\ x_6 \\ x_7 \\ x_8 \\ x_9 \\ x_{10} \\ x_{11} \\ x_{12} \\ x_{13} \\ x_{14} \end{bmatrix}
\leq
\begin{bmatrix}
P_{MHK}^{max} \\
P_{MHK}^{max} \\
P_{TG}^{rated} \\
P_{TG}^{rated} \\
P_{M:P}^{rated} \\
P_{M:P}^{rated} \\
Cap^{max} - Cap_{(0)} \\
Cap^{max} - Cap_{(0)} \\
Cap_{(0)} - Cap^{min} \\
Cap_{(0)} - Cap^{min}
\end{bmatrix}
\tag{5.37}
$$

Using the canonical formulation, the above linear inequality constraints are further expressed as follows:

$$
A_1 = \begin{bmatrix} eye(N,N), zeros(N,N), zeros(N,N), eye(N,N), zeros(N,N), \\ eye(N,N), zeros(N,N) \end{bmatrix}
\tag{5.38}
$$

$$
A_2 = \begin{bmatrix} zeros(N,N), eye(N,N), zeros(N,N), zeros(N,N), zeros(N,N), \\ zero(N,N), eye(N,N) \end{bmatrix}
\tag{5.39}
$$

$$
A_3 = \begin{bmatrix} zeros(N,N), zeros(N,N), zeros(N,N), eye(N,N), \\ eye(N,N), zero(N,N), zeros(N,N) \end{bmatrix}
\tag{5.40}
$$

$$
A_4 = \begin{bmatrix} zeros(N,N), -Z*tril(ones(N,N)), zeros(N,N), Y*tril(ones(N,N)), \\ Y*tril(ones(N,N)), zeros(N,N), -Z*tril(ones(N,N)), \end{bmatrix}
\tag{5.41}
$$

$$
A_5 = -A_4
\tag{5.42}
$$

$$A = [A_1; A_2; A_3; A_4; A_5] \tag{5.43}$$

$$b_1 = P_{HK}^{\max}(1:N) \tag{5.44}$$

$$b_2 = P_{T:G}^{rated} * ones(N,1) \tag{5.45}$$

$$b_3 = P_{M:P}^{rated} * ones(N,1) \tag{5.46}$$

$$b_4 = (Cap^{\max} - Cap_{(0)}) * ones(N,1) \tag{5.47}$$

$$b_5 = (Cap_{(0)} - Cap^{\min}) * ones(N,1) \tag{5.48}$$

$$b = [b_1; b_2; b_3; b_4; b_5] \tag{5.49}$$

5.2.4.2   Linear equality constraints

Using Equation 5.2 and 5.3, these linear equalities are to be integrated into constraint matrix A_{eq} and vector b_{eq} of the *fmincon* solver, as shown below.

- Load demand power balancing (using Equation 5.2)

$$x_1 + x_3 + x_5 = P_{Load(1)} \quad \text{(For } j = 1) \tag{5.50}$$

123

$$x_2 + x_4 + x_6 = P_{Load(2)} \quad \text{(For } j = 2)\tag{5.51}$$

- Fixed-final state condition (using Equation 5.3)

$$-x_3 - x_4 + x_7 + x_8 + x_9 + x_{10} - x_{13} - x_{14} = 0 \tag{5.52}$$

Hence, using Equation 5.50 - 5.52, the equality matrix may be presented as follows:

$$\begin{bmatrix} 1 & 0 & 1 & 0 & 1 & 0 & 0 & 0 & 0 & 0 & 0 & 0 & 0 & 0 \\ 0 & 1 & 0 & 1 & 0 & 1 & 0 & 0 & 0 & 0 & 0 & 0 & 0 & 0 \\ 0 & 0 & -1 & -1 & 0 & 0 & 1 & 1 & 1 & 1 & 0 & 0 & -1 & -1 \end{bmatrix} \cdot \begin{bmatrix} x_1 \\ x_2 \\ x_3 \\ x_4 \\ x_5 \\ x_6 \\ x_7 \\ x_8 \\ x_9 \\ x_{10} \\ x_{11} \\ x_{12} \\ x_{13} \\ x_{14} \end{bmatrix} = \begin{bmatrix} P_{Load(1)} \\ P_{Load(2)} \\ 0 \end{bmatrix} \tag{5.53}$$

Using the canonical formulation, the above linear equality constraints are further expressed as follows:

$$A_{eq1} = \begin{bmatrix} eye(N,N), eye(N,N), eye(N,N), zeros(N,N), zeros(N,N), \\ zeros(N,N), zeros(N,N) \end{bmatrix} \tag{5.54}$$

124

$$A_{eq2} = \begin{bmatrix} zeros(1,N), -ones(1,N), zeros(1,N), ones(1,N), ones(1,N), \\ zeros(1,N), -ones(1,N) \end{bmatrix} \tag{5.55}$$

$$A_{eq} = [A_{eq1}; A_{eq2}] \tag{5.56}$$

$$b_{eq1} = P_{Load}(1:N) \tag{5.57}$$

$$b_{eq2} = zeros(1,1) \tag{5.58}$$

$$b_{eq} = [b_{eq1}; b_{eq2}] \tag{5.59}$$

5.2.4.3   Lower and upper bounds

The optimization challenge consists of seven linear boundaries for various power variables (Equation 5.5 to 5.11). These linear boundaries are to be integrated into lower (l_b) and upper (u_b) boundaries of the *fmincon* solver.

- Lower boundaries

$$lb_1 = 0 * ones(N,1)$$

$$lb_2 = 0 * ones(N,1)$$

$$lb_2 = 0 * ones(N,1)$$

$$lb_3 = 0 * ones(N,1) \qquad (5.60)$$

$$lb_4 = 0 * ones(N,1)$$

$$lb_6 = 0 * ones(N,1)$$

$$lb_7 = 0 * ones(N,1)$$

$$lb = [lb_1, lb_2, lb_3, \ldots, lb_7] \qquad (5.61)$$

- Upper boundaries

$$ub_1 = P_1^{max}(1:N)$$

$$ub_2 = P_2^{rated} * ones(N,1)$$

$$ub_3 = P_3^{rated} * ones(N,1)$$

$$ub_4 = P_4^{max}(1:N) \qquad (5.62)$$

$$ub_5 = P_5^{rated} * ones(N,1)$$

$$ub_6 = P_6^{max}(1:N)$$

$$ub_7 = P_7^{rated} * ones(N,1)$$

$$ub = [ub_1, ub_2, ub_3, \ldots, ub_7] \qquad (5.63)$$

5.2.4.4 Non-linear equality constraint

The non-linear equality constraint, presented in Equation (5.4) will be integrated into (C_{eq}) of the *fmincon* solver, as shown below:

$$C_{eq} = (x(2 \cdot N + 1 : 3 \cdot N) + x(4 \cdot N + 1 : 5 \cdot N))(x(5 \cdot N + 1 : 6 \cdot N) + x(6 \cdot N + 1 : 7 \cdot N)) \qquad (5.64)$$

$$C_{eq} = zeros(N, 1) \qquad (5.65)$$

5.2.4.5 Objective function

As mentioned before that for the grid-interactive system, the main objective of the developed optimal control model is to minimize the COE purchased from the grid as well as maximizing the energy sales revenue. Hence, the multi-objective function (Equation 5.1) is further expressed as follows:

$$F_1 = C \cdot (x_5 + x_9) \cdot \Delta t - C \cdot R_a (x_{11} + x_{13}) \cdot \Delta t \qquad \text{(For } j = 1\text{)} \qquad (5.66)$$

$$F_2 = C \cdot (x_6 + x_{10}) \cdot \Delta t - C \cdot R_a (x_{12} + x_{14}) \cdot \Delta t \qquad \text{(For } j = 2\text{)} \qquad (5.67)$$

127

$$F = \Delta t \cdot \begin{bmatrix} 0 & 0 & 0 & 0 & C & 0 & 0 & 0 & C & 0 & -C*R_a & 0 & -C*R_a & 0 \\ 0 & 0 & 0 & 0 & 0 & C & 0 & 0 & 0 & C & 0 & -C*R_a & 0 & -C*R_a \end{bmatrix} \cdot \begin{bmatrix} x_1 \\ x_2 \\ x_3 \\ x_4 \\ x_5 \\ x_6 \\ x_7 \\ x_8 \\ x_9 \\ x_{10} \\ x_{11} \\ x_{12} \\ x_{13} \\ x_{14} \end{bmatrix} \quad (5.68)$$

$$F = \Delta t \begin{bmatrix} zeros\,(N,N), zero\,(N,N), C*eye\,(N,N), zeros\,(N,N), C*eye\,(N,N), \\ -C*R_a*eye\,(N,N), -C*R_a*eye\,(N,N) \end{bmatrix} \quad (5.69)$$

5.2.4.6   Time-of-use (TOU) tariffs and periods

The same Ruraflex electricity cost prices and TOU periods revealed in Section 4.2.4.5, are used during the simulations of the grid-interactive system.

5.3 Simulation Results and Discussion

The optimal control simulation results of the proposed grid-interactive MHK-PHS system model, supplying the residential, commercial and industrial load demands, respectively, will be discussed below. During energy sales, negative signs are used to represents the accumulated revenue.

5.3.1 Residential load

The optimal control results for the residential load type are shown in Figs. 5.2, 5.3 and 5.4 for low demand season, while for high demand season are shown in Figs. 5.5, 5.6 and 5.7. The same variable residential load data used in Chapter 4 during low demand and high demand season, are further used for the grid-interactive simulations, as shown in Fig. 5.2A and 5.5A, respectively. Therefore, the same baseline grid costs will be considered when evaluating the cost saving benefits under each load profile, respectively. The main dissimilarity is the size of the system's parameters, since larger system sizes are required by the solver to determine the feasible points that satisfy the constraints. The reason is because the energy sales have been considered. The parameter of the MHK-PHS system for meeting the residential load demand, are as revealed in Table 5.1.

Table 5.1: Simulation parameters for the grid-interactive system (residential load)

Item	Value
Sampling time (Δt)	30 minutes
PHS nominal capacity ($P_{T:G}$= 2.55 kW and $P_{M\,P}$= 2.55 kW)	3 kWh
PHS maximum volume	100%
PHS minimum volume	5%
Initial upper reservoir capacity	50%
Overall efficiency of the PHS ($\eta_{T:G}$= 84% and $\eta_{M\,P}$= 84%)	70.6%
MHK system rating	3 kW

129

5.3.1.1   Low demand season

The results for the residential load demand, during low demand season, are as shown in Figs. 5.2 to 5.4. Fig. 5.3A shows that the average water speed for the month of January varies around 5.31 m/s. Therefore the MHK system generates a maximum output power of 3 kW (as denoted by the red-dotted lines in Fig. 5.2B). The reason is because the water speed is above 2 m/s.

Fig. 5.2B shows that the model allows most of the generated MHK power to be used for supplying the load throughout 24 hours. The turbine-generator unit is further used to supplement the unmet load demand, mostly during standard and peak periods, as shown in Fig. 5.2C. During weekdays' off-peak periods, the unmet load demand is supplemented using the grid power, instead of being supplemented by the turbine-generator unit, as shown in Figs. 5.2C and 5.2D. Additionally, the model allows the energy storage process to take place, mostly during the off-peak period, as shown in Fig. 5.3B and 5.3C. The energy from both the grid and the MHK system is therefore stored. The reason is to recharge the upper reservoir for later use, during both standard and costly peak periods of the following day, as shown in Fig. 5.3D.

Sundays have proved to lead to the utilization of the grid power for the entire 24 hours, for the purpose of supplementing both the motor-pump unit and the residential load demand, as shown in Figs. 5.2D and 5.3C, respectively. Therefore the upper-reservoir's volume increases at the highest rate to approach 100% state of charge, when compared to other days, as shown in Fig. 5.3D. During peak periods, the model is intolerant of allowing the MHK system to recharge the upper reservoir, since the primary load demand is high, as shown Fig. 5.3B. Instead, it is used to supply the primary load and sold into the grid as a means of maximizing the energy sales, during costly peak periods. The energy sale is not permitted to

130

take place during the off-peak period, since this will lead to minimal revenue, as shown in Figs. 5.4A and 5.4B. Hence, the majority of the energy sales take place during peak periods and followed by the standard periods.

Fig. 5.4C shows that the model prevents the residential consumer from simultaneously selling and purchasing the energy, due to the exclusive power flow constraint, explained in Equation (5.4). The overall energy sales and grid consumption for the simulated nine days are as shown in Fig. 5.4C. The overall grid cost and the generated energy sales revenue yielded ZAR40.34 and ZAR-64.90, respectively. The overall grid cost is a result of a grid-to-load consumption cost of ZAR18.92 and grid-to-pump consumption cost of ZAR21.42. Hence, the difference between the overall energy sales revenue and the grid cost is ZAR-24.56, for the simulated nine days. Based on the baseline grid cost of ZAR245.05 (Fig. 4.4), the energy cost saving potential of 110% has been achieved. This implies that the consumer is not expected to settle any energy cost.

Figure 5.2: Load side power flow during low demand season (grid-interactive: residential)
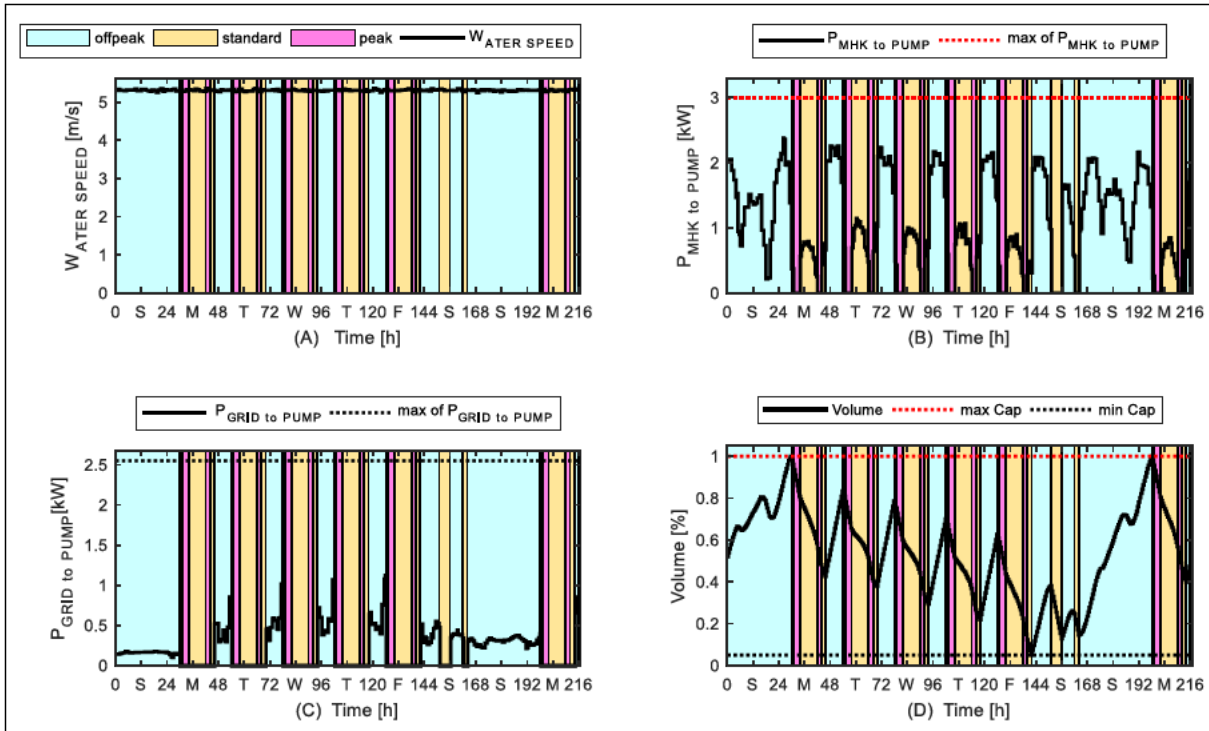
131

Figure 5.3: Water speed and PHS side power flow during low demand season (grid-interactive: residential)
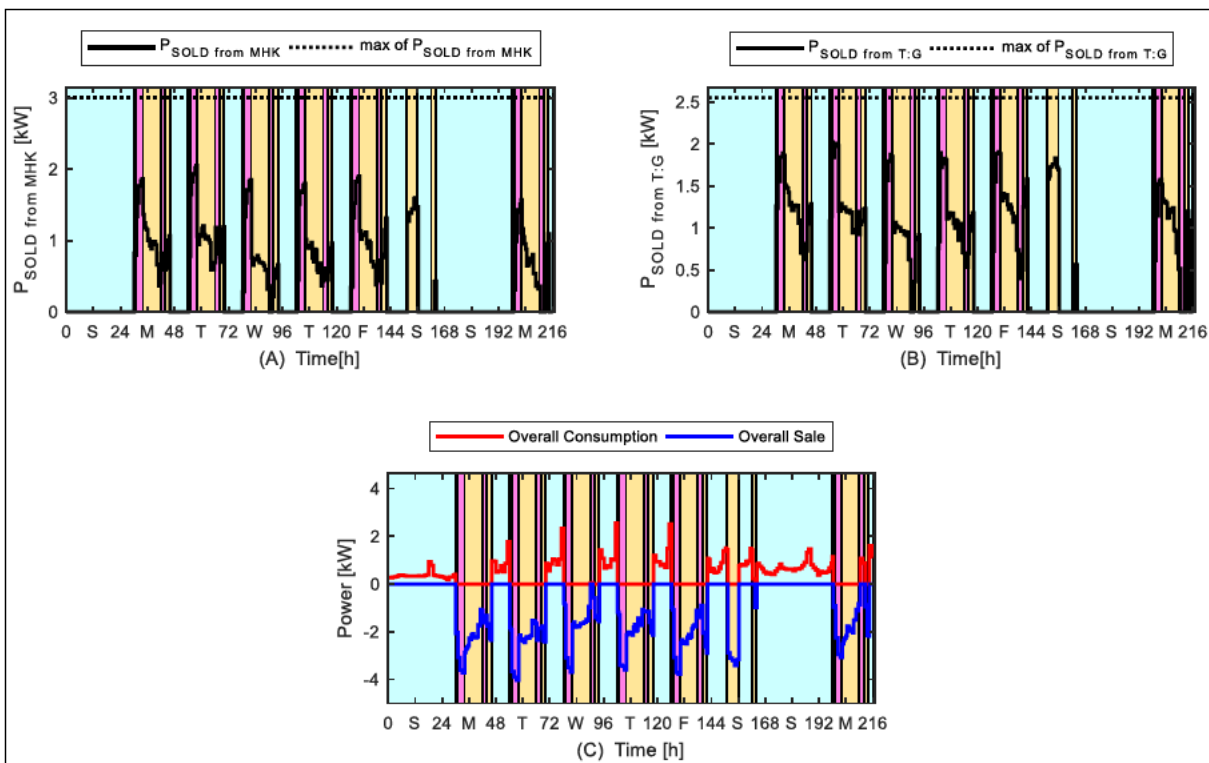

Figure 5.4: Overall power consumption and sales during low demand season (residential)

132

5.3.1.2   High demand season

The optimal control results for the residential load demand, during high demand season, are as shown in Figs. 5.5 to 5.7. It is observed that the model performs precisely the same way for both high demand and low demand seasonal results. The difference being that the high demand season leads to the consumption of grid energy during other weekdays' standard and peak periods, due to the unmet load demand, as shown Fig. 5.5D. This leads to the dissimilarity in economic figures, due to various power flow levels to be discussed below.

In order to maximize the selling revenue, majority of the energy sales continue to takes place during the costly peak periods and followed by the standard periods. The overall energy sales and grid consumption for the simulated nine days are shown in Fig. 5.7C. The high demand season led to the overall grid cost and the generated energy sales revenue of ZAR50.11and ZAR-53.47, respectively. The difference between the overall energy sales revenue and the grid cost yielded ZAR-3.36, for the simulated nine days. The baseline grid cost incurred by the 9 day residential load demand, proved to be ZAR317.77 for high demand season, as revealed in Fig. 4.7. Hence, a potential of 101.1% energy cost saving is possible, meaning that the consumer is not expected to settle any energy costs.

Irrespective of the high priced TOU energy tariffs during high demand season, the high demand season proved to generate less energy sales revenue, as compared to the low demand season.
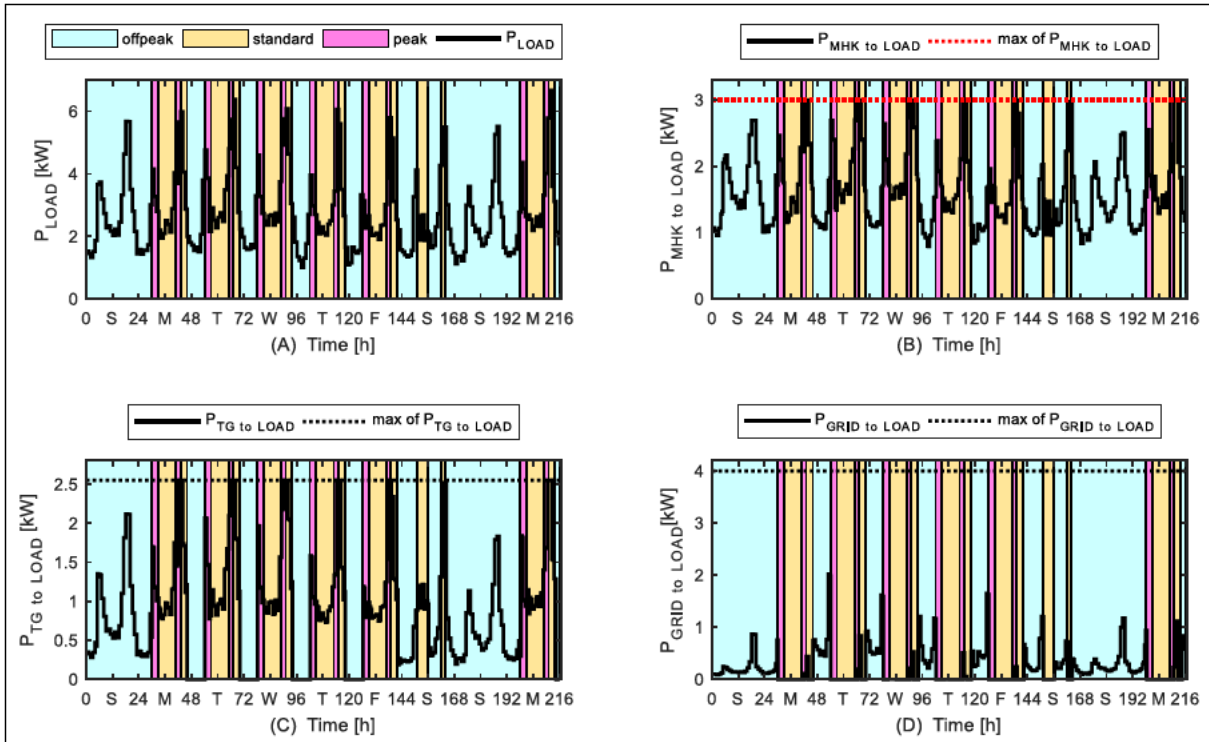
133

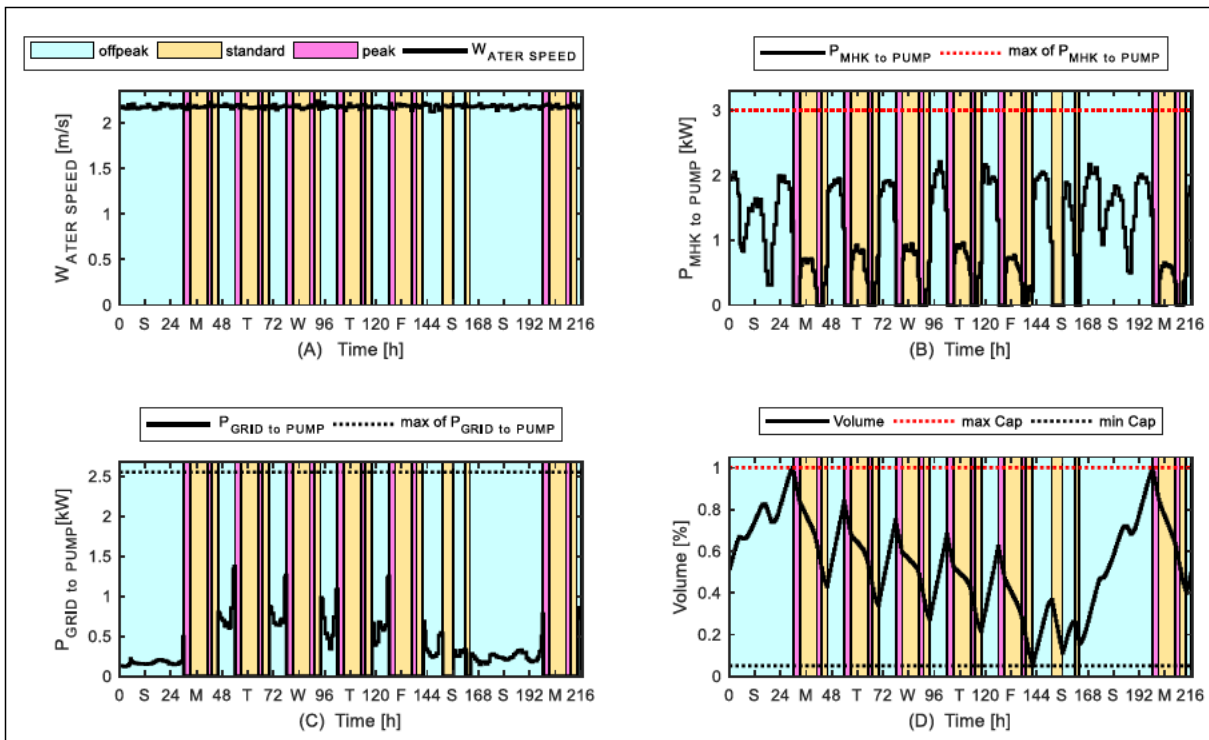Figure 5.5: Load side power flow during high demand season (grid-interactive: residential)

Figure 5.6: Water speed and PHS side power flow for high demand season (grid-interactive: residential)
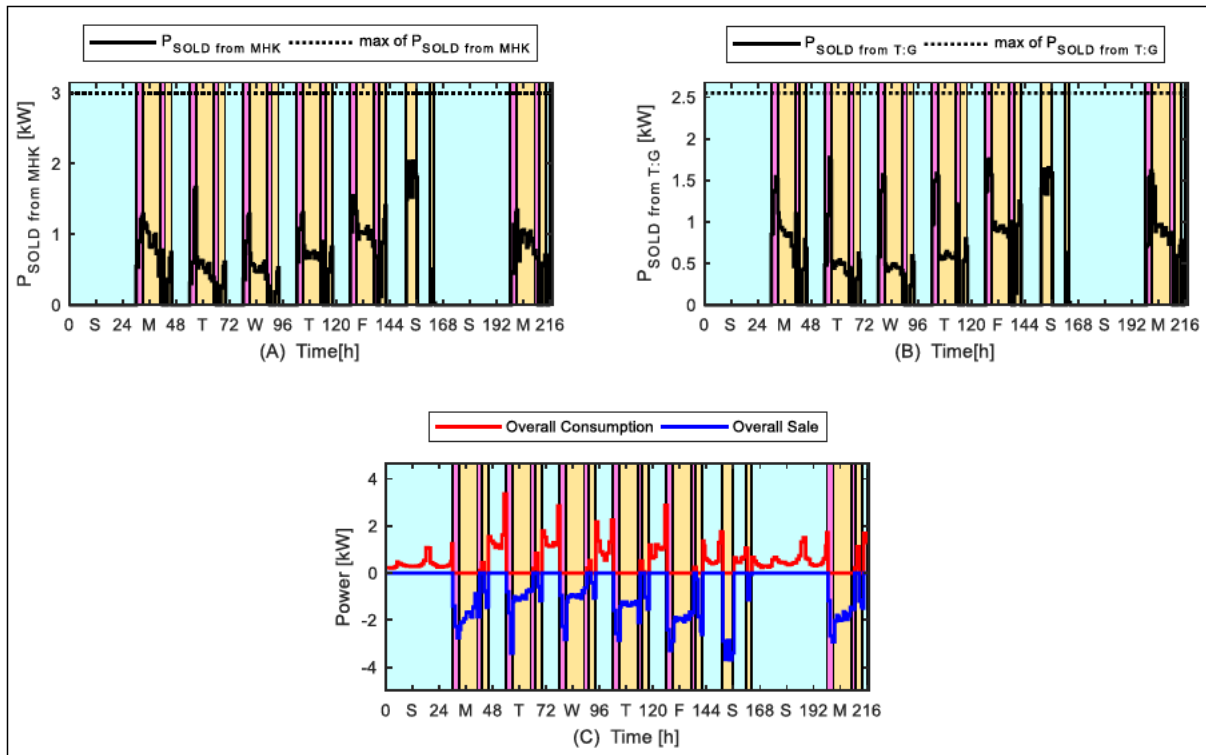
134

Figure 5.7: Overall power consumption and sales during high demand season (residential)

5.3.2 Commercial load

The optimal control results for the commercial load, throughout the low demand season, are as shown in Figs. 5.8 to 5.10, while for high demand season are shown in Figs. 5.11 to 5.13. The same variable commercial load profile data used in Chapter 4, have been used for the grid-interactive simulations, as shown in Figs. 5.8A and 5.11A. The solver requires larger storage capacity to be able to determine the feasible points that satisfy the constraints, when compared to the residential load case. The parameters of the MHK-PHS system, for meeting the commercial load demand, are as revealed in Table 5.2.

Table 5.2: Simulation parameters for the grid-interactive system (commercial load)

Item	Value
Sampling time (Δt)	30 minutes
PHS nominal capacity ($P_{T:G}$= 2.83 kW and $P_{M:P}$= 2.83 kW)	4 kWh
PHS maximum volume	100%
PHS minimum volume	5%
Initial upper reservoir capacity	50%
Overall efficiency of the PHS ($\eta_{T:G}$= 84% and $\eta_{M:P}$= 84%)	70.6%
MHK system rating	3 kW

5.3.2.1   Low demand season

The results for the commercial load during low demand season are shown in Figs. 5.8 to 5.10. Fig. 5.8B reveals that the MHK system generates a maximum of its rated output power (3 kW), since the water speed is above 2 m/s.

It may be observed that most of the generated MHK power is used to supply the commercial load during business hours, as shown in Fig. 5.8B. During the off-peak period, it is further stored into the upper reservoir, as shown in Fig. 5.9B. The turbine-generator unit is further utilized to supplement the unmet load demand during business hours, as shown in Fig. 5.8C. The grid power is mostly used to supplement the primary load during the off-peak hours, in order to allow most of the MHK power to be stored within the upper reservoir, as shown in Fig. 5.8D.

During the weekdays' off-peak periods, the unmet load demand is supplemented using the grid power, as shown in Fig. 5.8D. Both the grid power and most of the MHK power are allowed to be stored during the off-peak periods, as shown in Figs. 5.9B and 5.9C. The

136

reason is to recharge the upper reservoir for later use, during the standard and expensive peak periods of the next business day, as shown in Fig. 5.9D.

Sundays lead to considerably high grid energy consumption level, when compared to other days, due to the affordable grid energy price. Similar to the residential case, the grid power is utilized for the entire 24 hour period with the intention of supplementing both the motor-pump unit and the load demand, as shown in Figs. 5.8D and 5.9C, respectively. Furthermore, Sundays further leads to the 100% state of charge in order to prepare for the beginning of the Monday to Friday business undertaking, as shown in Fig. 5.9D. During weekdays' TOU peak periods, the MHK power is not utilised for recharging the upper reservoir. Instead, it is utilized for energy sales into the grid, as a means of maximizing the revenue. During standard periods, it performs two functions of simultaneous selling and recharging of the upper reservoir.

Simultaneous selling and purchasing of energy does not take place, as shown by Fig. 5.10C. In order to maximize the selling revenue, most of the energy sales into the grid take place during the costly peak periods and seconded by the standard periods. Hence, the model finds it absolutely uneconomical to sell energy during off-peak periods. Low demand season led to the overall grid cost and the generated energy sales revenue of ZAR22.06 and ZAR-54.19, respectively. Hence, the difference between the overall energy sales revenue and the grid cost yielded ZAR-32.13 for the simulated nine days. In comparison with baseline grid cost of ZAR243.25 (Fig. 4.10), the energy cost saving potential of 113% has been achieved. Therefore, the commercial consumer is not expected to settle any energy costs.
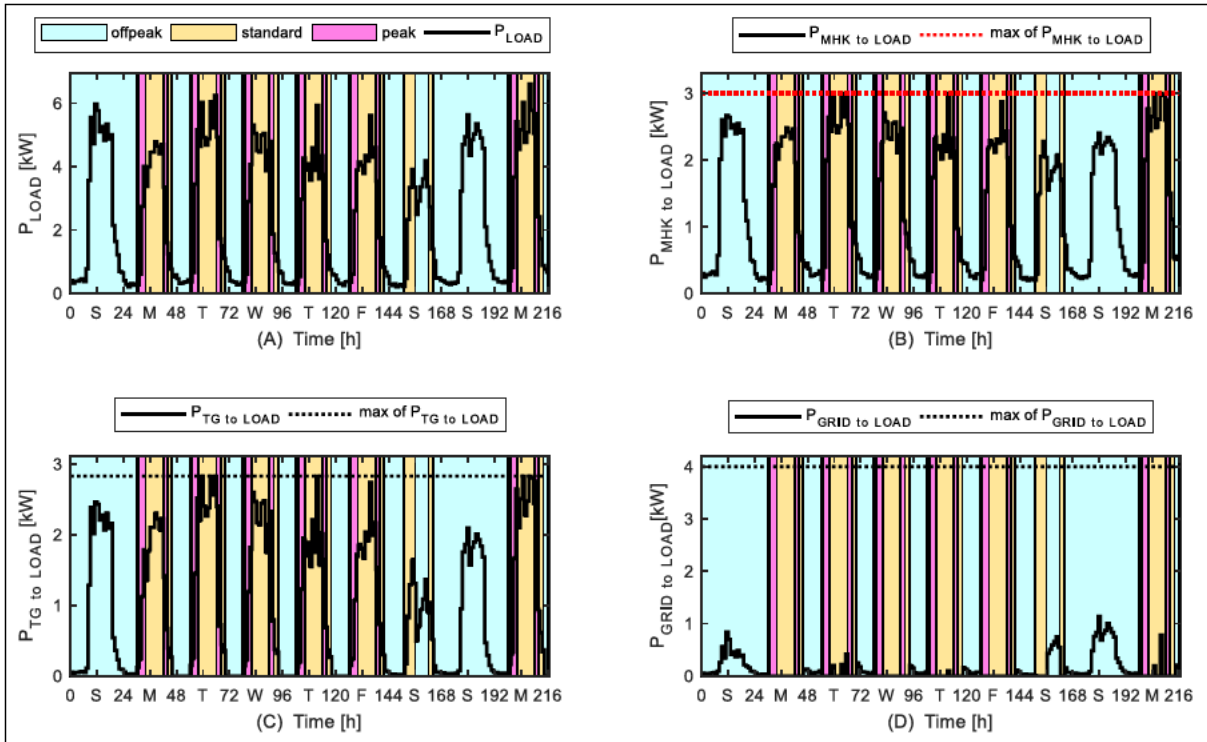
137

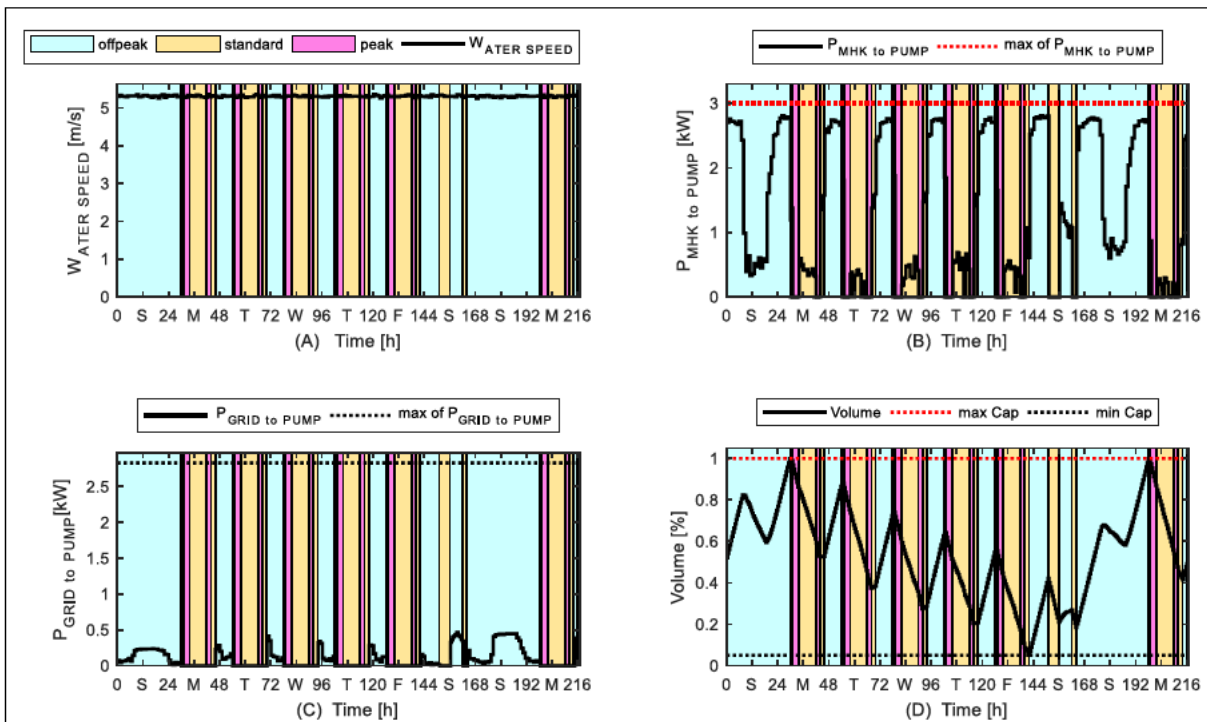Figure 5.8: Load side power flow during low demand season (grid-interactive: commercial)

Figure 5.9: Water speed and PHS side power flow during low demand season (grid-interactive: commercial)
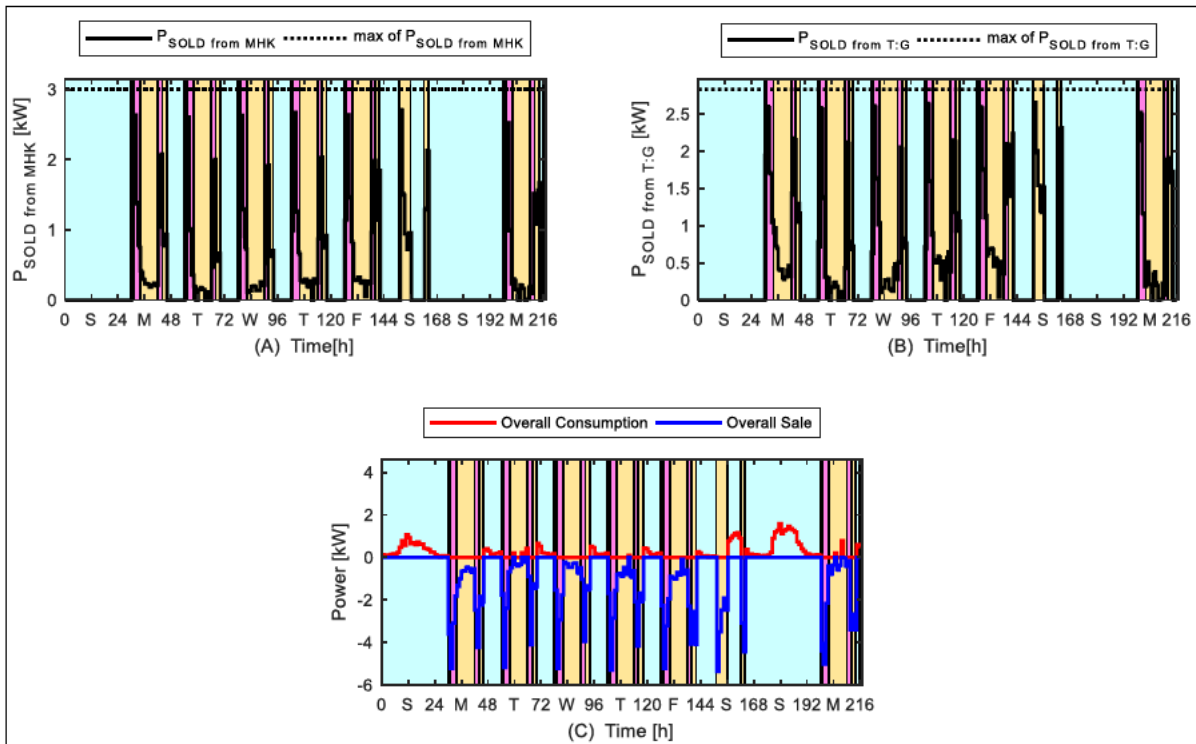
138

Figure 5.10: Overall power consumption and sales during low demand season (commercial)

5.3.2.2   High demand season

The optimal control results for the commercial load, during high demand season, are shown in Figs. 5.11 to 5.13. It is observed that the model performs exactly the same ways under both high demand and low demand seasons. The difference is that the high demand season leads to higher grid power consumption during weekday business hours, in order to supplement the unmet load demand, as shown in Fig. 5.11D.

Similarly, most of the energy sales into the grid still take place during the costly peak periods and seconded by the standard periods. The overall energy sales and grid consumption for the simulated nine days are as shown in Fig. 5.13C. The high demand season led to the overall grid cost and the generated energy sales revenue of ZAR41.21 and ZAR-50.21, respectively. The difference between the overall energy sales revenue and the grid cost yielded a gain of ZAR-9.00, for the simulated nine days. Irrespective of the high priced TOU

energy tariffs, the high demand season proved to generate less energy sales revenue, as compared to the low demand season. Based on the baseline grid cost of ZAR313.88 (Fig. 4.13), therefore the energy cost saving potential of 102.9% has been achieved.
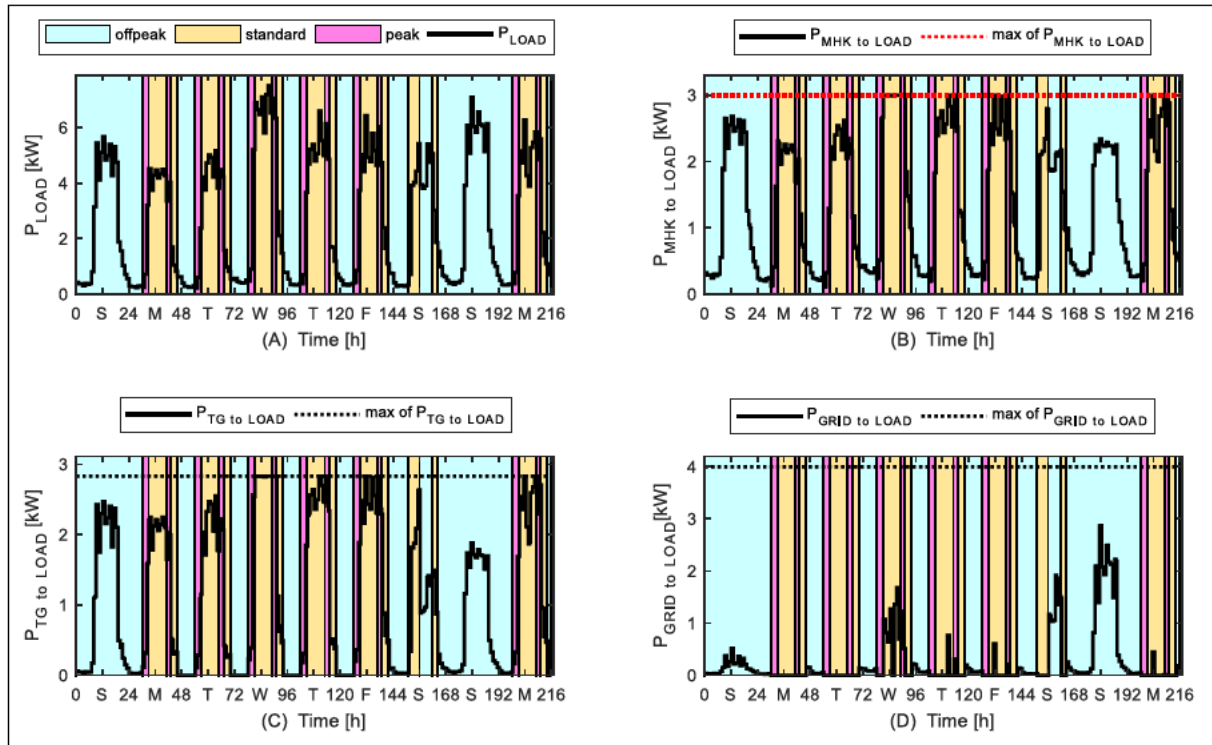

Figure 5.11: Load side power flow during high demand season (grid-interactive: commercial)
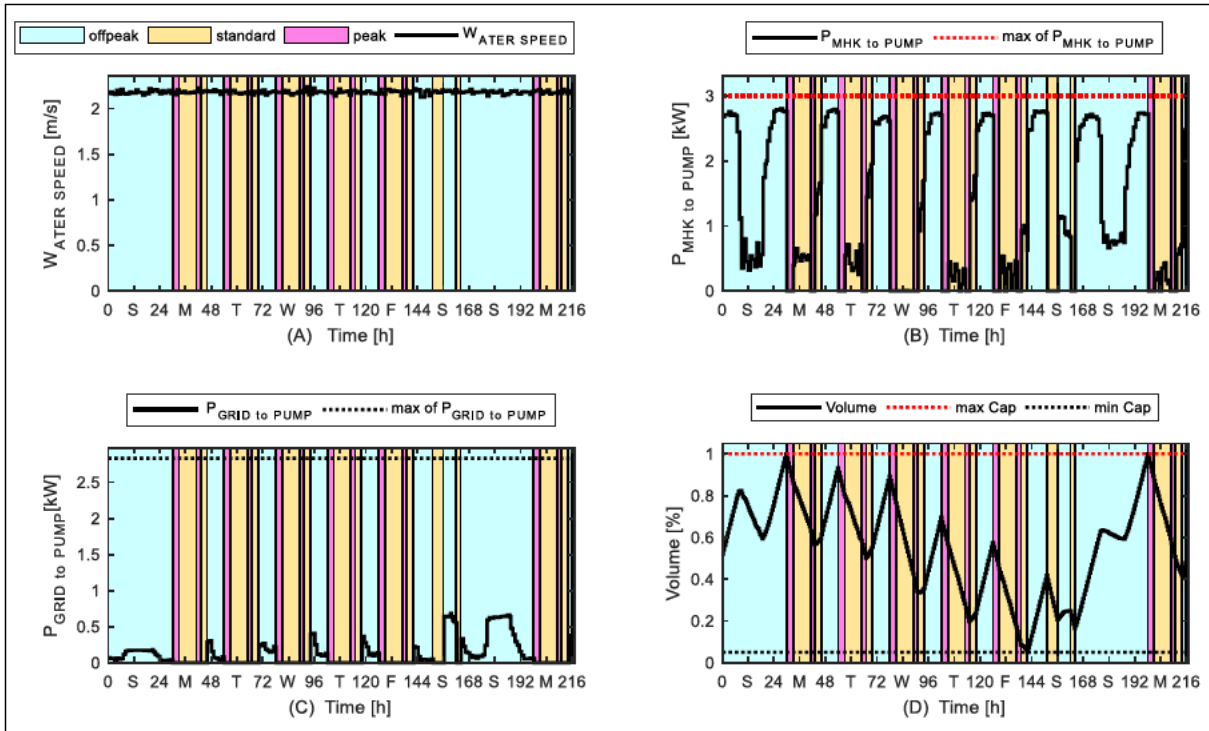
Figure 5.12: Water speed and PHS side power flow during high demand season (grid-interactive: commercial)
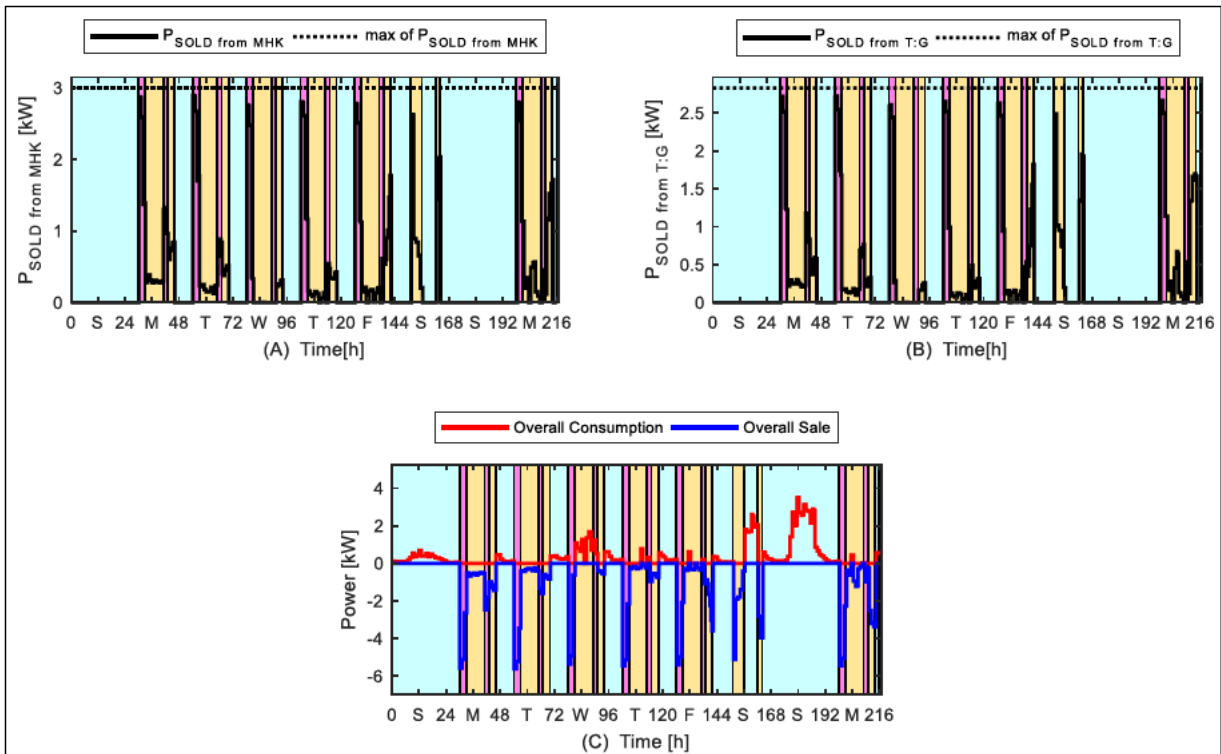

Figure 5.13: Overall power consumption and sales during high demand season (commercial)

141

5.3.3 Industrial load

The optimal control results for the industrial load during low demand season, are shown in Figs. 5.14 to 5.16, while for high demand season are shown in Figs. 5.17 to 5.19. The same variable industrial load data as used in Chapter 4, have been used to carry out the grid-interactive simulations, as shown in Fig. 5.14A and 5.17A, respectively. The solver proved to require the largest storage size, to be able to determine the feasible points that satisfy the constraints, when compared to the residential and commercial load cases. Hence, the parameters of the MHK-PHS system for meeting the industrial load demand are as revealed in Table 5.3.

Table 5.3: Simulation parameters for the non-interactive system (industrial load)

Item	Value
Sampling time (Δt)	30 minutes
PHS nominal capacity (P$_{T:G}$= 4.3 kW and P$_{M:P}$= 4.3 kW)	5 kWh
PHS maximum volume	100%
PHS minimum volume	5%
Initial upper reservoir capacity	50%
Overall efficiency of the PHS ($\eta_{T:G}$= 84% and $\eta_{M:P}$= 84%)	70.6%
MHK system rating	3 kW

5.3.3.1   Low demand season

The results for the industrial load during low demand season are as shown in Figs. 5.14 to 5.16. Fig. 5.14B shows that the MHK system generates a maximum of its rated output power (3 kW), since the water speed is above 2 m/s.

Similar to the commercial case, it can be noted that most of the generated MHK power continues to supply the primary load during business hours, as shown in Fig. 5.14B. During the off-peak TOU periods, most of the MHK power is then stored into the upper reservoir, as shown in Fig. 5.15B. In addition to the MHK power, the turbine-generator unit is further used to supplement the unmet load demand during business hours, as shown in Fig. 5.14C. The grid power is mostly used to supply the industrial load during off-peak hours as well as on Sundays, in order to permit most of the MHK power to be stored into the upper reservoir, as shown in Fig. 5.14D.

Similar to the other two cases, the unmet load demand is supplemented by the grid during off-peak TOU periods for the entire nine days. Most of the MHK power and the grid power is stored within the upper reservoir during off-peak TOU periods, as shown in Figs. 5.15B and 5.15C. Therefore, the upper reservoir is recharged, in order to store energy for later use during both standard and costly peak periods of the next business day, as shown in Fig. 5.15D.

Sundays lead to considerably high grid energy consumption level, as compared to other days, due to the affordable grid energy price. This leads to a 24 hour grid utilization period. Hence, this leads the upper reservoir to approach 100% state of charge, as to prepare for the beginning of Monday to Friday business venture, as shown in Fig 5.15D. During weekday TOU peak periods, the MHK power is not utilised for recharging the upper reservoir. Instead, it is used to sell the energy into the grid, as a means of maximizing the energy sales revenue. During standard periods, the MHK power is used to recharge the upper reservoir, while simultaneously selling the remaining energy into the grid. Therefore, the energy sale is not permitted during the off-peak TOU periods. Similar to the other two cases, Saturday and Sundays proved to lead to larger number of charging and discharging cycles, when compared to other days.

Similar to other cases, the simultaneous selling and purchasing of energy does not take place, as shown by Fig. 5.16C. The low demand season led to the overall grid cost and the generated energy sales revenue of ZAR54.06 and ZAR-75.64, respectively. The difference between the overall energy sales revenue and the grid cost yielded ZAR-21.26 for the simulated nine days. By considering, the previously determine baseline grid cost of ZAR242.74 (Fig. 4.16), the energy cost saving potential of 108.8% has been achieved.
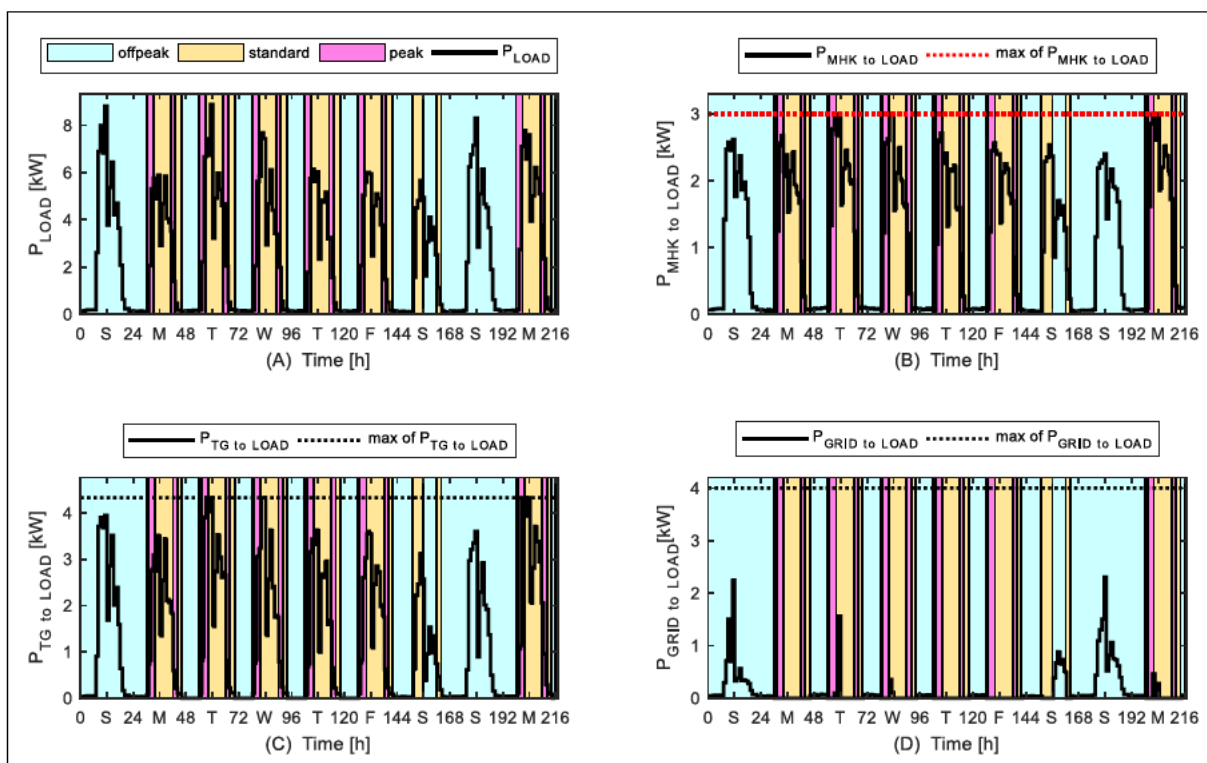

Figure 5.14: Load side power flow during low demand season (grid-interactive: industrial)
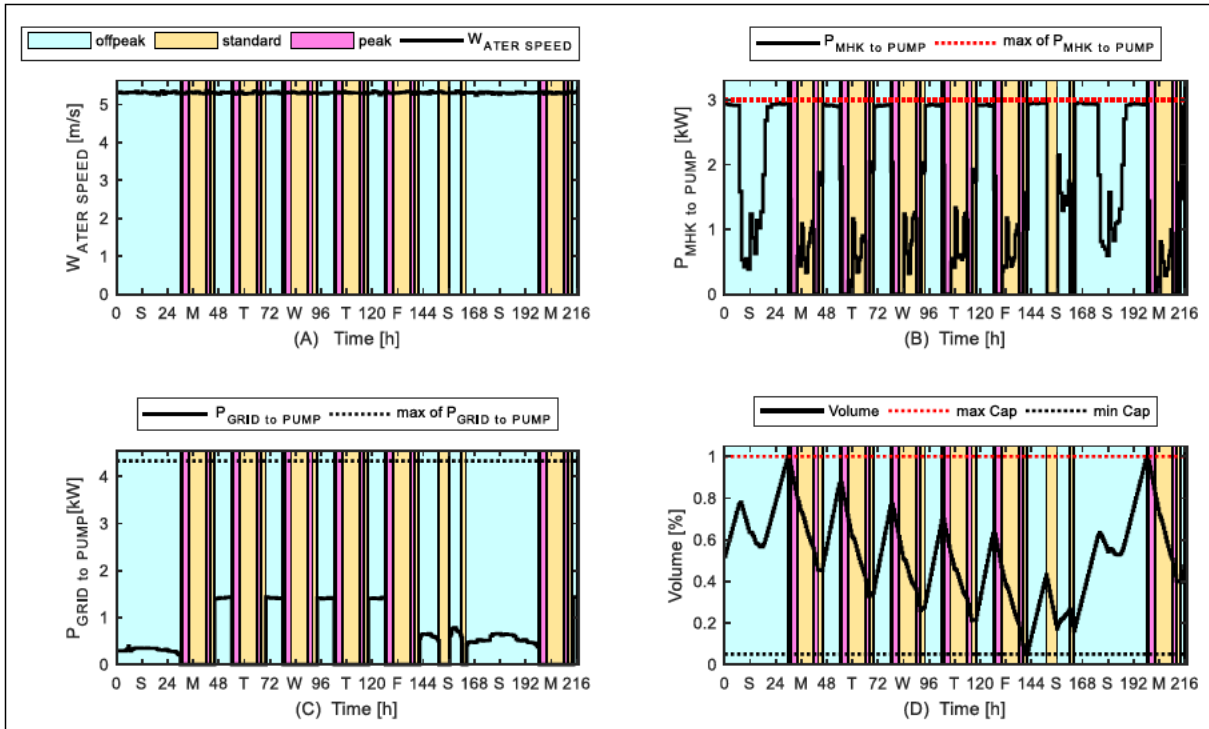
144

Figure 5.15: Water speed and PHS side power flow during low demand season (grid-interactive: industrial)
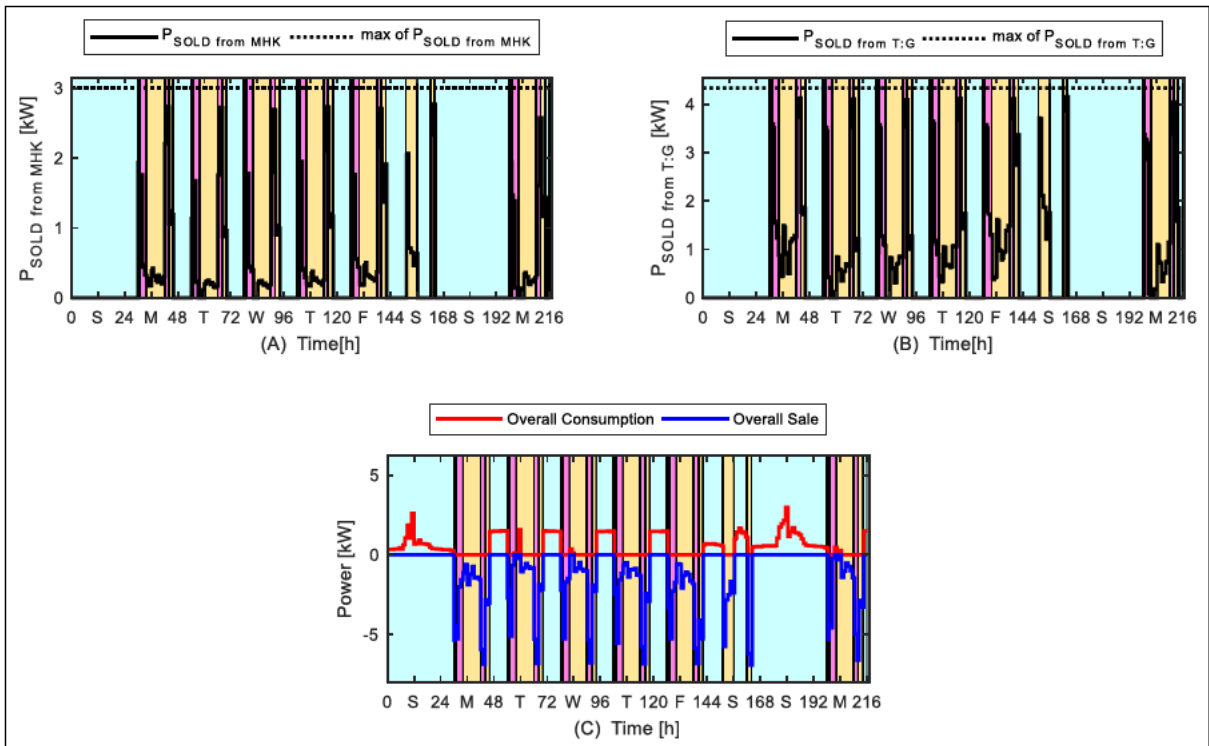

Figure 5.16: Overall power consumption and sales during low demand season (industrial)

145

5.3.3.2   High demand season

The optimal control results for the industrial load during high demand season are shown in Figs. 5.17 to 5.19. It may be observed that the model performs precisely the same way for both high demand and low demand seasonal results. The difference being that the high demand season leads to a higher grid power consumption cost, during weekday business hours, in order to supplement the unmet load demand, as shown in Fig. 5.17D.

Similarly, most of the energy sales into the grid continues to take place during the costly peak periods and seconded by the standard periods, in order to maximize the sales revenue. The overall energy sales as well as the grid consumption, for the simulated nine days are shown in Fig. 5.19C. The high demand season led to the overall grid cost and the generated energy sales revenue of ZAR79.50 and ZAR-74.04, respectively. The difference between the overall energy sales revenue and the grid cost yielded a grid cost of ZAR5.46 for the simulated nine days. This is the cost to be settled by the consumer for the simulated nine days. The selected nine days load proved to incur a baseline grid cost of ZAR315.52, if solely supplied by the utility grid during the high demand season (Fig. 4.19). Hence, the energy cost saving potential of 98.27% is achieved, since the industrial consumer is expected to pay 1.73% of the baseline cost.

Irrespective of the high priced TOU energy tariffs, the high demand season proved to generate less energy sales revenue, when compared to the low demand season, for the industrial load.
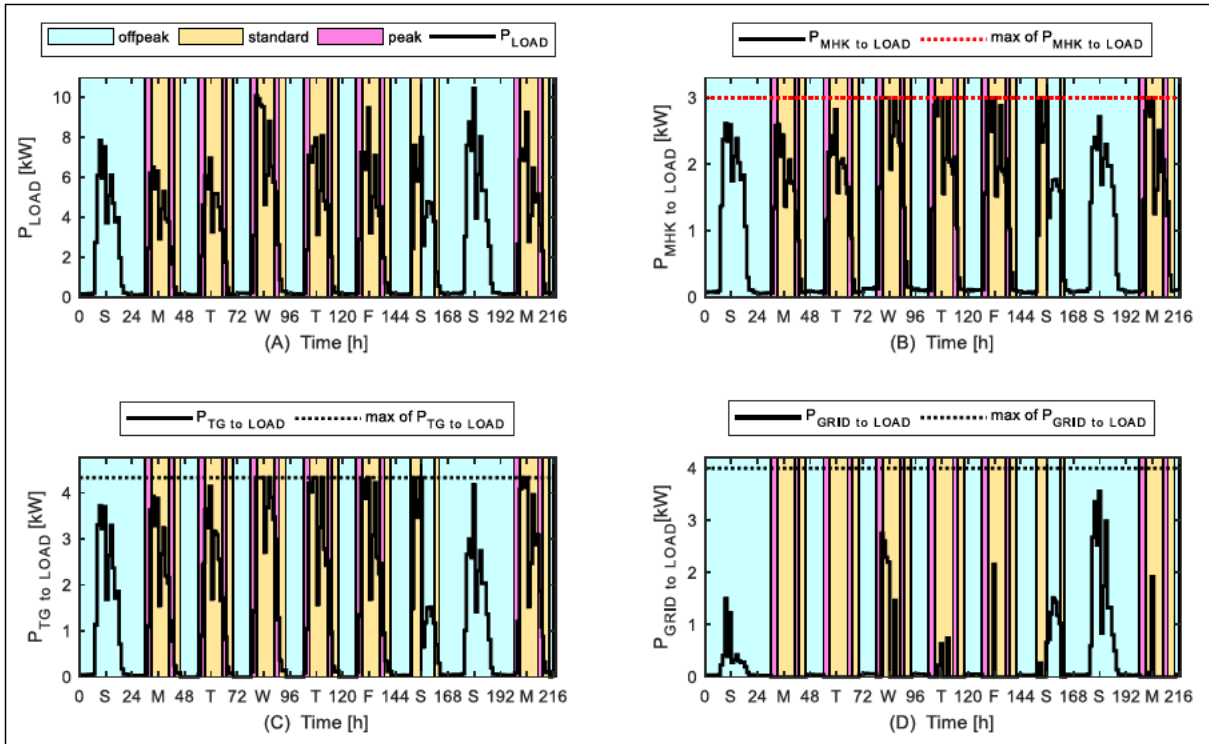
146

Figure 5.17: Load side power flow during high demand season (grid-interactive: industrial)
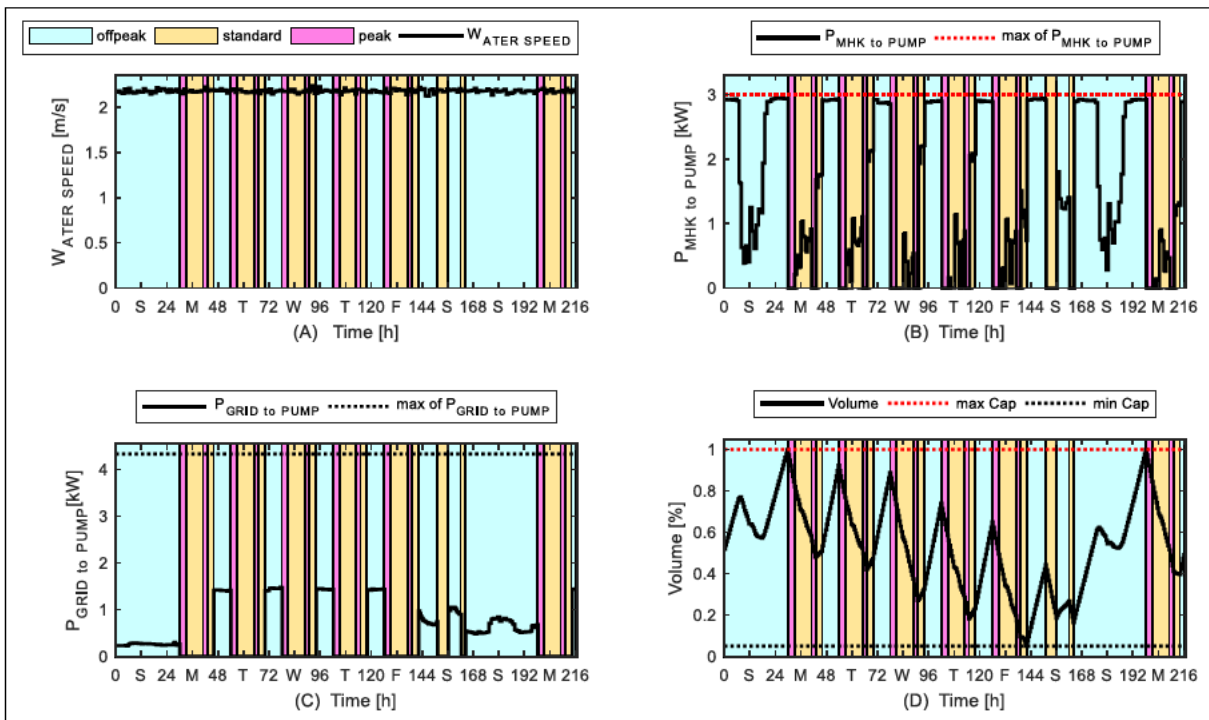

Figure 5.18: Water speed and PHS side power flow during high demand season (grid-interactive: industrial)

147
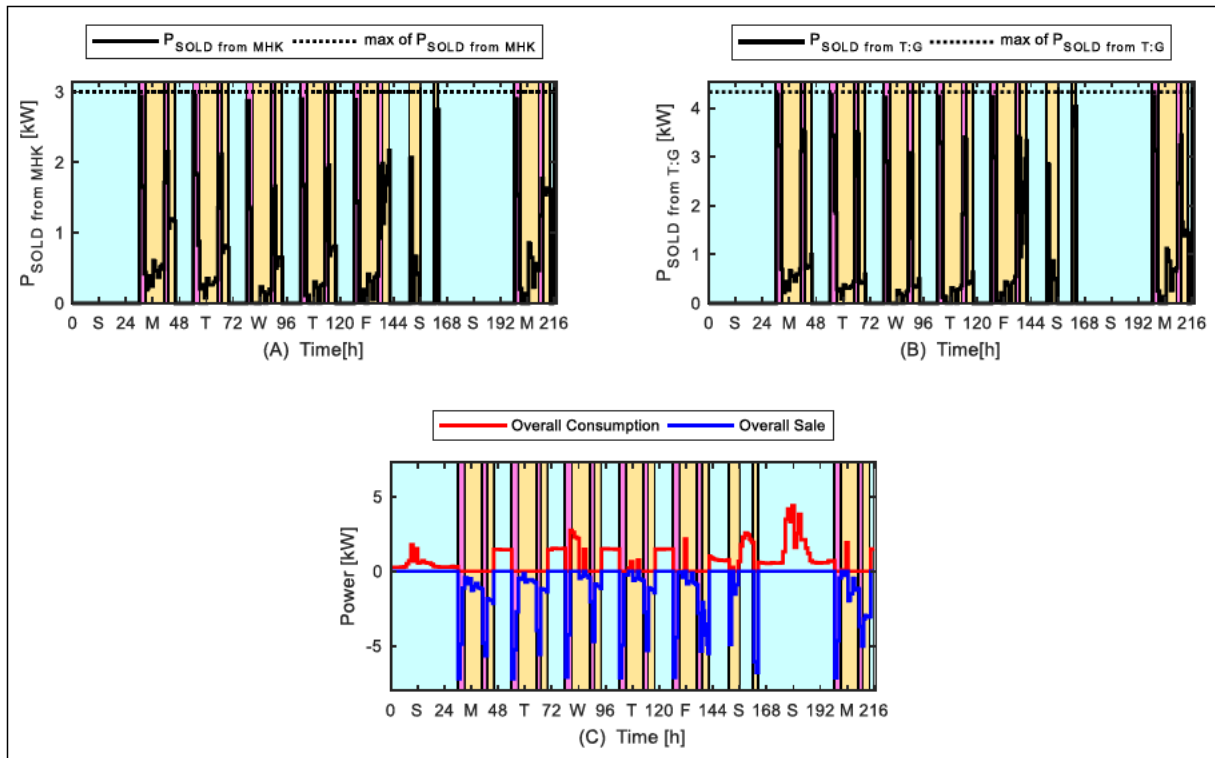
Figure 5.19: Overall power consumption and sales during high demand season (industrial)

Table 5.4: Summary of the cost savings benefits for the grid-interactive systems

	Residential Load		Commercial Load		Industrial Load	
	Low Demand Season	High Demand Season	Low Demand Season	High Demand Season	Low Demand Season	High Demand Season
Baseline grid cost (ZAR)	245.05	317.77	243.25	313.88	242.74	315.52
Optimal control grid cost (ZAR)	40.34	50.11	22.06	41.21	54.06	79.50
Optimal control grid sales (ZAR)	-64.90	-53.47	-54.19	-50.21	-75.32	-74.04
Net energy income/cost (ZAR)	-24.56	-3.36	-32.13	-9.00	-21.26	5.46
Cost saving (%)	110%	101.1%	113%	102.9%	108.8%	98.27%

148

5.4 Conclusion

This Chapter presented an optimal energy management algorithm for the grid-interactive MHK-PHS system, allowing consumers to purchase energy from the utility grid, under Ruraflex TOU tariffs and to sell excess/stored energy to the utility grid, through a market-dependent FIT model that applies a fixed percentage of 65% (without additional bonus). The model aimed at ensuring an optimal power dispatch by minimizing the grid consumption cost and maximizing the energy sales revenue. The *fmincon* solver has been used to solve the optimization problem, since the nature of the problem consists of the non-linear and linear constraints.

The performance of the model has been studied through the use of the variable residential, commercial and industrial load types. Each load type has been studied during low demand season and high demand season, respectively. The simulations have been carried out for nine consecutive days (216 hours), in order to analyse the behaviour of the model during week and weekend days. For an appropriate comparison, the optimal control simulations have been undertaken to ensure that the initial water level, at the start of the control horizon, is retained at the end of the control horizon. To study the effectiveness of the developed model, the baseline energy cost, incurred by each studied load type without the inclusion of MHK-PHS system, is compared to the net energy cost achieved through the optimal energy control of the proposed system.

The simulation results have revealed the effectiveness of the proposed model, to optimally control the power flow of the grid-interactive MHK-PHS system. The model allowed the effective use of the RE power (MHK and PHS), as the first priority for meeting each load demand (residential, commercial and industrial), respectively. For all three load types, the grid power has been used as a last resort for supplementing the unmet demand.

149

Additionally, the model allowed the grid power to be stored into the upper reservoir, during inexpensive TOU off-peak periods, for all three load demand cases and both seasons. Hence, the objective of minimizing the grid consumption cost has been achieved.

Under all TOU periods (off-peak, standard and peak), the model did not permit the customer to import and export power simultaneously to and from the utility grid system, in order to avoid a loss in revenue. As soon as there is a power deficit (from both the MHK and PHS systems) due to high load demand, the model immediately discontinues the energy sales. Additionally, the developed model allowed most of the energy sales into the grid to take place during costly TOU peak periods and followed by standard periods. When there is excess RE during off-peak periods, it is then stored together with the grid energy. Hence, the energy sale is allowed to take place later, during peak and standard periods. This simply implies that the objective of maximizing the energy sales revenue has been achieved.

The model proved to perform precisely in the same way for all three load types under both high demand and low demand season. The baseline grid costs of the three load types proved to be more or less the same and have been used to study the cost saving benefit achieved by each load type. The optimal simulation results revealed that the industrial load type generates more sales revenue, while incurring more grid cost, as compared to the other two cases, for both seasons. Additionally, the industrial load type leads to peak energy sales during the evening TOU peak period, than during the morning TOU peak period, as compared to the other load types. This led to a least net energy income. However, from a cost savings point of view, the commercial load proved to outperform both the residential and industrial loads due to the least optimal grid cost. The least optimal grid cost steered to the highest income for both season.

From the Eskom TOU tariffs structure, it is observed that the energy prices are costly during high demand season, than in low demand season. However, low demand season

150

proved to generate more sales revenue for the three load types' cases. As compared to the other weekdays, Saturday proved to lead to the largest number of charge and discharge cycles, and followed by Sundays. Sundays proved to lead to the highest grid consumption level, as compared to the other days, due to the inexpensive off-peak periods. Hence, the grid power is stored in the upper reservoir and also used to supply certain portion of the load for the entire 24 hours. The foremost aim is to disallow the discharging of the PHS during off-peak hours.

CHAPTER 6: RULE-BASED CONTROL STRATEGY TO CATER FOR LOAD DEMAND UNCERTAINTY

6.1 Introduction

The optimal control of the proposed grid-interactive MHK-PHS system's power flow has been obtained in Chapter 5. An open-loop optimization-based control approach has been applied through the use of the *fmincon* solver in MATLAB. Nevertheless, the open-loop optimization-based approach relies heavily on prediction precision. The prediction itself might be imprecise, when compared to the real-time measurements. Therefore, this could destruct the open-loop optimization performance or even lead to an undesired system operation, by acting against the expressed constraints (Wang, 2013). Hence, the prediction impression may source a disturbance within the operation of a power system.

The exceedingly typical disturbance to be considered in this study is an inconsistence associated with electrical load demand. Load forecasting is very critical to ensure a reliable operation of the power system. However, load forecasting is difficult due to variety of factors such as change in weather conditions and holidays (Luh, 2010). Therefore, the load demand uncertainty provides a considerable challenging task to the open-loop optimization-based control approach. Through the use of approaches such as model predictive control (MPC) strategy, it is difficult to guarantee the accuracy, since MPC heavily depends on the prediction accuracy (Kong et al., 2017). Therefore, this necessitates the development of a supplementary control model in addition to the developed open-loop optimization-based model of the grid-interaction MHK-PHS system. The model should be capable of allowing the optimization-based approach, to handle load demand uncertainties. Therefore, this would

152

allow an open-loop optimization-based approach to be able to ensure self-correction capability, in real-time.

For this purpose, this chapter deals with the implementation of a control strategy, that is capable of assisting the developed open-loop optimization-based control model, to be able to deal with load demand uncertainties. The aim is to ensure that the actual load demand is sufficiently and economically met at all times, in order to achieve a reliable system operation. This should be achieved without compromising the power balance constraints, rated components' capacities, as well as the storage boundaries.

In this study, a rule-based control strategy has been considered to deal with the load demand uncertainty problem. A rule-based strategy does not require forecasting, since the real-time measurement may be used (Kanwar et al., 2015). Few modes of operations are to be implemented as real-time supervisory control, in order to manage the power flow of the proposed grid-interactive MHK-PHS system. The load demand should be met during peak, standard and off-peak periods, while maintaining the PHS levels within the desired limits.

6.2 Load Demand Uncertainties

The simulation results, under open-loop optimization-based approach, usually rely on prediction precision, whereby the predicted load demand being equivalent to the actual one. The uncertainties associated with load demand may take place in real-time. Therefore, the predicted load demand may be greater or less than the actual one. Hence, an open-loop optimization-based control approach may not be able to cater for such disturbance. In this Chapter, a rule-based control algorithm is developed to assist the developed open-loop optimization-based control approach, to handle the load demand uncertainties. The aim is to ensure that the load demand is reliably and economically met, even in the presence of the

153

demand uncertainties. In this Chapter, the predicted power variables are presented using the subscript P, while the actual ones are presented without the subscript P. Letter r is used to represent the sampling interval during rule-based control algorithm. It ranges between 1 and N. The rule-based control algorithm will be tested using low demand season data.

6.2.1 Proposed algorithm when the actual load demand is more than predicted

The first case is based on time steps, whereby the actual load demand (P_{Load}) is more than the predicted load demand (P_{PLoad}). Such occurrences may lead to unmet load demand, if an open-loop optimization-based approach is solely applied. Hence, a rule-based controller should be implemented to solve such problem. The three sources which are used to meet the load demand in the proposed MHK-PHS system, need to be given priority orders when applying a rule-based criterion. Starting with the most affordable option and concluding with the most costly one.

6.2.1.1   Adjustment of predicted MHK output power to supply the unmet load demand

To efficiently solve the unmet load demand challenge, both the predicted grid-to-load power (P_{P3}) and turbine-generator-to-load power (P_{P2}) are permitted to be constant, as shown in Equation (6.1) and (6.2). The reason is to permit the adjustment of the predicted MHK-to-load power (P_{P1}) as a first priority. Hence, it should be adjusted to a new/actual value, (P_1). Therefore, the predicted energy sale from the PHS into the grid (P_{P7}) is also maintained constant, since P_{P2} has not been adjusted.

$$P_{2(r)} = P_{P2(r)} \ (1 \leq r \leq N) \tag{6.1}$$

154

$$P_{3(r)} = P_{P3(r)} \quad (1 \le r \le N) \tag{6.2}$$

$$P_{7(r)} = P_{P7(r)} \quad (1 \le r \le N) \tag{6.3}$$

Where: $P_{2(r)} =$ actual PHS-to-load power at r^{th} sampling interval (kW);

$P_{3(r)} =$ actual grid-to-load power at r^{th} sampling interval (kW);

Therefore, to meet the actual load demand (P_{Load}) while maintaining the power balance constraint, the actual load demand is then expressed as follows:

$$P_{Load(r)} = P_{1(r)} + P_{P2(r)} + P_{P3(r)} \quad (1 \le r \le N) \tag{6.4}$$

Therefore, the new or actual MHK-to-load power is expressed as follows:

$$P_{1(r)} = P_{Load(r)} - P_{P2(r)} - P_{P3(r)} \quad (1 \le r \le N) \tag{6.5}$$

In addition to supplying the primary load, the MHK system is further used to supply electricity to the motor-pump unit and sell excess to the grid, as shown in the grid-interactive MHK-PHS system layout (Fig. 5.1). Therefore, the adjusted MHK-to-load power may further be expressed as follows:

$$P_{1(r)} = P_{P1(r)} + P_{P4(r)} + P_{P6(r)} \quad (1 \le r \le N) \tag{6.6}$$

Where: $P_{P4(r)} =$ predicted MHK-to-motor-pump power at r^{th} sampling interval (kW);

155

$P_{P6(r)}$ = predicted MHK-to-grid power at r^{th} sampling interval (kW);

However, when it comes to a possibility that the actual load demand is too high to be satisfied by Equation (6.4), the adjusted P_1 may exceed the rated output power of the MHK system. To prevent such likelihood, the actual MHK-to-load power is then expressed as follows:

$$P_{1(r)} = \min((P_{Load(r)} - P_{P2(r)} - P_{P3(r)}),(P_{P1(r)} + P_{P4(r)} + P_{P6(r)})) \qquad (1 \leq r \leq N) \qquad (6.7)$$

An increase of P_{P1} to the new P_1 value, is permitted to initially affect the predicted MHK's energy sales before the storage reservoir. Hence, P_{P6} is adjusted to a new/actual P_6. Therefore, it has been reduced by (P_1 - P_{P1}) and should lie between zero and (P_{P6} – (P_1 – P_{P1})), to avoid negative value. The newly adjusted/actual value is then expressed as follows:

$$P_{6(r)} = \max(0,(P_{P6(r)} - (P_{1(r)} - P_{P1(r)}))) \qquad (1 \leq r \leq N) \qquad (6.8)$$

After the reduction of P_{P6} to a new value (especially 0 kW), it may happen that there is still a power deficit for meeting the actual load demand (P_{Load}). Hence, an additional shortage will be extracted from P_{P4} in order to supply the load with up to the maximum of the MHK system's rated power. Therefore, the actual value, P_4 is then expressed as follows:

$$P_{4(r)} = P_{P4(r)} + \min(0,(P_{P6(r)} - (P_{1(r)} - P_{P1(r)}))) \qquad (1 \leq r \leq N) \qquad (6.9)$$

156

To maintain the storage level pattern of the PHS system, the predicted grid-to-pump power (P_{P5}) should be increased by the value equivalent to the adjustment of ($P_{P4} - P_4$). Hence, the actual/adjusted value is then expressed as follows:

$$P_{5(r)} = P_{P5(r)} + (P_{P4(r)} - P_{4(r)}) \quad (1 \leq r \leq N)$$ (6.10)

Since P_{P5} represents the predicted grid-to-pump power, therefore, the energy sales from the PHS system (P_{P7}) should not take place. The aim is to disallow concurrent purchasing and selling of energy. Therefore, the actual value of the PHS-to-grid power is then expressed as follows:

$$P_{7(r)} = zeros(1,1) \quad (1 \leq r \leq N)$$ (6.11)

6.2.1.2 Adjustment of the predicted PHS output power to supply the unmet load demand

When it comes to a point, whereby the adjusted P_1 is not sufficient to satisfy Equation (6.4), the predicted PHS-to-load (P_{P2}) power should be adjusted/increased to the actual value named P_2. It is worth noticing that the turbine-generator unit has been used to sell the predicted power to the grid (P_{P7}) and to supply the predicted power to load (P_{P2}), during the optimization-based control. Therefore, it should be ensured that the actual P_2 does not exceed the rated capacity of the turbine-generator unit. The adjusted P_2 is then expressed as follow:

$$P_{2(r)} = \min((P_{Load(r)} - P_{1(r)} - P_{P3(r)}), (P_{P2(r)} + P_{P7(r)})) \quad (1 \leq r \leq N)$$ (6.12)

157

6.2.1.3   Adjustment of the predicted grid power to supply the unmet load demand

It may happen that the adjustment/increase of P_1 and P_2 is still not sufficient to meet the actual load demand. The last option is therefore to supplement the unmet load demand through the use of the utility grid. The actual/adjusted grid-to-load power will be expressed as follows:

$$P_{3(r)} = P_{Load(r)} - P_{1(r)} - P_{2(r)} \qquad (1 \leq r \leq N)$$
(6.13)

6.2.2   Proposed algorithm when the actual load demand is less than predicted

The second case is based on time steps, whereby the actual load demand is less than the predicted load demand. During such occurrences, the optimization-based control model is capable of meeting the load demand, without any deficit. However, the optimization-based control approach may supply more than what is needed by the load. Hence, a rule-based algorithm should be prepared to disable the excessive supply of power. The power from the three sources should be reduced, by starting with the costly one (grid-to-load) and concluding with the affordable RE options.

6.2.2.1   Adjustment of the predicted grid-to-load power

P_{P1} and P_{P2} are kept constant, since the main objective is to minimize the predicted grid-to-load power (P_{P3}). To avoid negative values, the new/actual grid-to-load power is then expressed, as shown in Equation (6.14). Therefore, as soon as the sum of P_{P1} and P_{P2} is

158

greater than the actual load demand, the grid-to-load power is discontinued. Therefore, all the other predicted power variables will be constant as shown by Equation (6.15).

$$P_{3(r)} = \max(0, (P_{Load(r)} - P_{P1(r)} - P_{P2(r)})) \qquad (1 \le r \le N) \tag{6.14}$$

$$P_{i(r)} = P_{Pi(r)} \quad (i = 1, 2, 4, 5, 6, 7) \qquad (1 \le r \le N) \tag{6.15}$$

6.2.2.2   Adjustment of the predicted MHK-to-load power

In some instances, it may occur that after discontinuing the grid-to-load power, the overall RE power supplied to the actual load is nevertheless more than the demanded P_{Load}. Hence, the next simplest step is to reduce the predicted MHK-to-load power (P_{P1}) to a new P_1. Starting with the adjustment P_{P1}, before adjusting P_{P2}, facilitates the preservation of the PHS state of charge. Hence, P_1 is expressed as follows:

$$P_{1(r)} = \max(0, P_{Load(r)} - P_{P2(r)}) \qquad (1 \le r \le N) \tag{6.16}$$

After successfully reducing P_{P1} to P_1, the difference should be sold into the grid solely during peak and standard periods (if $C_{(r)} > 0.47$). Therefore, the actual P_6 is then expressed as shown in Equation (6.17). During off-peak period, the difference should be supplied to the motor pump unit as shown in Equation (6.18). As soon as the difference is supplied to the pump unit, the predicted grid-to-pump power (P_{P5}) should be reduced by the same difference ($P_4 - P_{P4}$) as shown by Equation (6.19).

$$P_{6(r)} = \max(0, (P_{P6(r)} - (P_{1(r)} - P_{P1(r)}))) \quad C_{(r)} > 0.47 \quad (1 \le r \le N) \tag{6.17}$$

$$P_{4(r)} = P_{P4(r)} + \max(0, (P_{P1(r)} - P_{1(r)})) \quad C_{(r)} = 0.47 \quad (1 \le r \le N) \tag{6.18}$$

$$P_{5(r)} = \max(0, (P_{P5(r)} - (P_{4(r)} - P_{P4(r)}))) \quad (1 \le r \le N) \tag{6.19}$$

6.2.2.3   Adjustment of the predicted PHS-to-load power

In some instances, it may happen that the actual P_{Load} is however less than the sum of the predicted P_{P2} and adjusted P_1. Therefore, MHK can solely meet the actual load demand as shown by Equation (6.20). Hence, the predicted P_{P2} should be discontinued, in order to allow a new P_2 value to be zero as shown by Equation (6.21).

$$P_{1(r)} = P_{Load(r)} \quad (1 \le r \le N) \tag{6.20}$$

$$P_{2(r)} = zeros(1,1) \quad (1 \le r \le N) \tag{6.21}$$

6.2.3   Proposed algorithm when the actual load demand is the same as predicted

The third case is based on time steps, whereby the actual load demand is equal to the predicted load demand. Therefore, if $P_{Load} = P_{PLoad}$, the optimization-based control algorithm will neither lead to excessive power supply, nor power shortage. Hence, all the predicted power variables are permitted to be equal to the actual power variables, as shown in Equation (6.22).

160

$$P_{i(r)} = P_{Pi(r)} \qquad (1 \leq i \leq 7) \qquad (1 \leq r \leq N) \tag{6.22}$$

6.3 Simulation Results and Discussion

The rule-based control model has been developed to supplement the open-loop optimization-based control model, developed in Chapter 5. The control strategy has been tested under residential, commercial and industrial load demands, respectively. The main aim is to allow the actual load demand to be met at all times, under demand uncertainty conditions caused by forecasting error, while maintaining the predicted upper-reservoir's state of charge. A nine day January load demand data (Sunday 1st January to Monday 9th January) has been selected and used to represent the predicted load demand, since it has been used in Chapter 5. The actual load demand is assumed to be equal to the nine day February load demand data (Sunday 5th February to Monday 13th February). Since the two data sets are different, this will simplify the observation of the rule-based model's behaviour under load demand uncertainty. The results for the commercial and industrial loads are shown in Appendix A, for supplementary purpose.

6.3.1   Residential load

The simulation results for the residential load during optimization-based approach and after applying the rule-based approach are shown in Figs. 6.1 to 6.10. The same simulation parameters found in Table 5.1 have been used during the simulations. The same TOU tariffs for low demand season have been applied. The predicted and the actual residential load demands are shown Fig. 6.1. When comparing the two load demand graphs, it may be noted that they are not the same during each time step. If the two load demands are solely met by

161

the grid power during low demand season, the predicted load demand incurs a baseline cost of ZAR245.05, while the actual load demand incurs ZAR247.49. Therefore, the overall energy consumption of the actual load demand is slightly higher than the one of the predicted load demand. However, it does not imply that the actual load demand is greater than the predicted load demand for all hours or days of the control horizon.

6.3.1.1 Before load demand uncertainties

Fig. 6.2 shows how the predicted load demand (P_{PLoad}) has been met, before the involvement of the actual load demand (P_{Load}), through the application of the open-loop optimization-based method. Hence, it means that P_{PLoad} is assumed to be equal to P_{Load}. Therefore, it observed that the predicted load demand (black solid line) is adequately met by the combination of the three power sources (green-dotted marks), without any shortage or excessive energy supply.
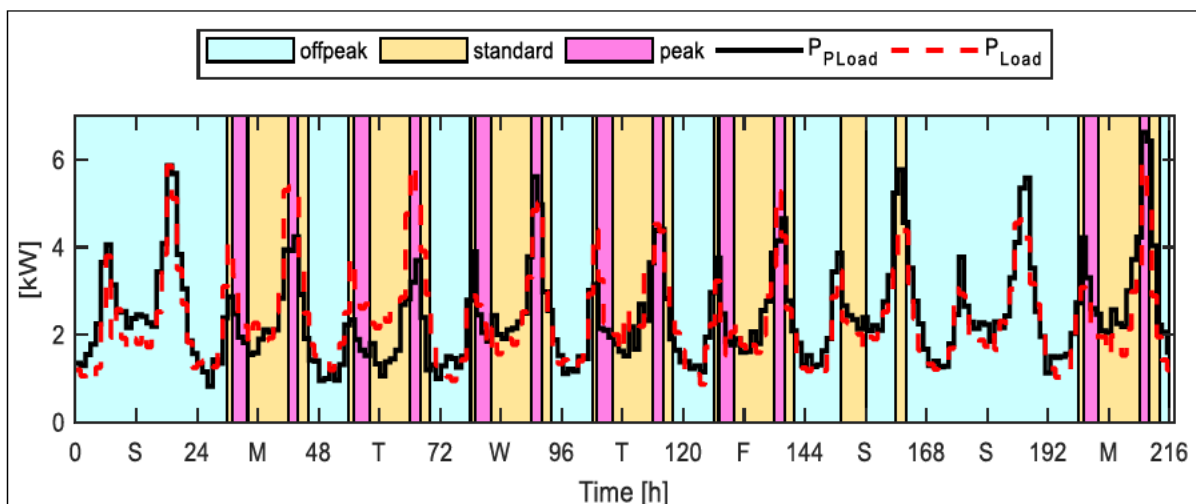
Figure 6.1: Predicted and actual residential load demand
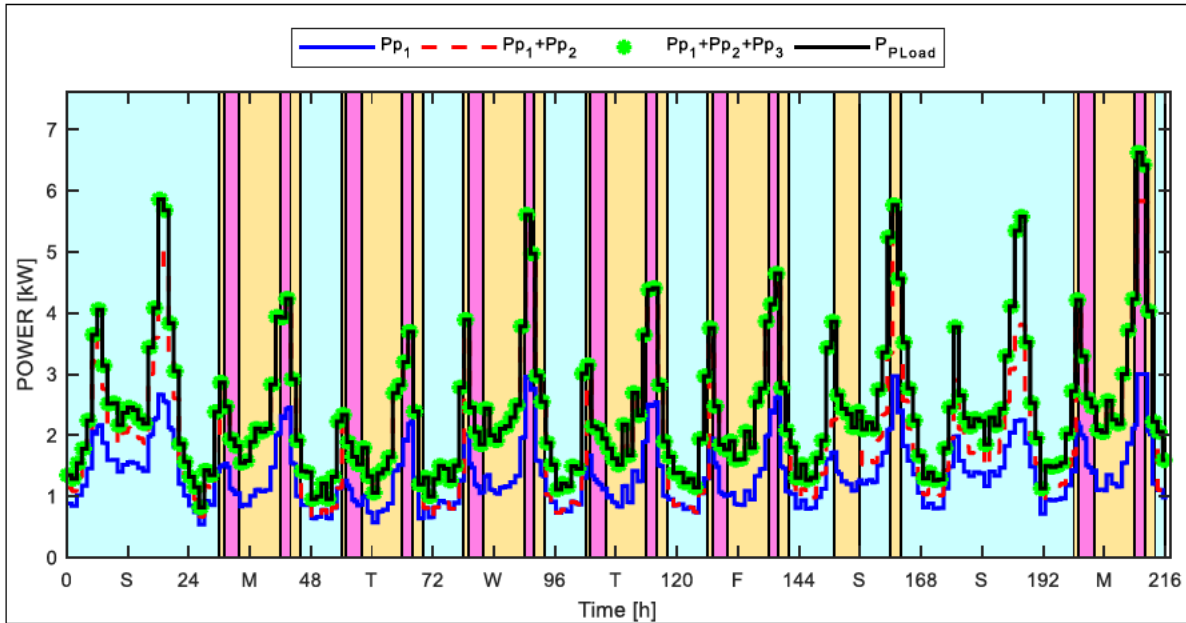
Figure 6.2: Optimization-based power flow before load demand uncertainty (residential)

6.3.1.2   During load demand uncertainties

The next step is to introduce the actual load demand shown in Fig. 6.1 (red-dotted line), into the open-loop optimization-based model. The aim is to represent a load demand uncertainty disturbance. After introducing the actual load demand, the open-loop optimization-based model is unable to permit the three power sources to adequately meet the actual load demand, as shown in Fig. 6.3. This has resulted in an unmet demand, particularly during morning and/or evening peak-periods of weekdays. In addition to the unmet load demand, other days such as Wednesday, Saturday and Sundays, have resulted in an excessive supplied energy. Therefore, the three power sources supply more than the demanded load power, instead of just supplying the unmet load demand and then store the excess energy for later use.

Through the application of the developed rule-based control algorithm, the open-loop optimization-based model is therefore capable of allowing the three-power sources to

163

adequately meet the actual load demand, as shown in Fig. 6.4. The actual load demand has been met for the entire nine days, without any shortage or excessive supply of power.

Fig. 6.5 shows the grid-to-load power, before and after the introduction of the actual load demand. The black solid line represents the predicted grid-to-load power (P_{P3}) supplied during the open-loop optimization-based method, while the red-dotted line represents the actual grid-to-load power (P_3) as supplied and control by the rule-based control algorithm.

It may be noted that, during the morning peak demand of the first Sunday, the open-loop optimization-based model has led to the excessive supply of power, as revealed in Fig. 6.3. An overall power of 4.06 kW has been supplied to the actual load, while the load demanded merely 3.79 kW of peak power. This has resulted in an excess power of 0.27 kW. Therefore, the developed rule-based control algorithm made permission for the predicted grid-to-load power (P_{P3}) to be reduced from 0.27 kW to 0, in order to diminish that excessive supplied power, as shown in Fig. 6.5 (red-dotted lines). Hence, the predicted RE power from the PHS-to-load and MHK-to-load is kept constant, as shown in 6.6. Therefore, the main mission of reducing the grid cost has been achieved.

Similarly, during the evening peak hours of Wednesday, an excessive supply of power took place. An overall power of 5.61 kW has been supplied to the actual load, while the load demanded merely 4.84 kW of peak power. This has resulted in an excess power of 0.77 kW. Therefore, the developed rule-based control algorithm made permission again for the predicted grid-to-load power (P_{P3}) to be reduced (from 0.059 kW to 0), in order to diminish that excessive supplied power, as shown in Fig. 6.5. After the reduction of P_{P3}, there was still an outstanding excessive power of 0.711 kW. Hence, the predicted hydrokinetic-to-load power (P_{P1}) was reduced by that outstanding difference (from 3 kW to a new value of 2.29 kW), as shown in Fig. 6.6A. Therefore, that difference of 0.711 kW was then transferred to the grid to increase the energy sale, as shown in Fig. 6.9. This is achieved whenever there is

164

an existence of a supplied excessive power, during standard or peak period. During off-peak hours, the difference between P_{P1} and P_1 is stored into the upper reservoir, instead of being sold into the grid.
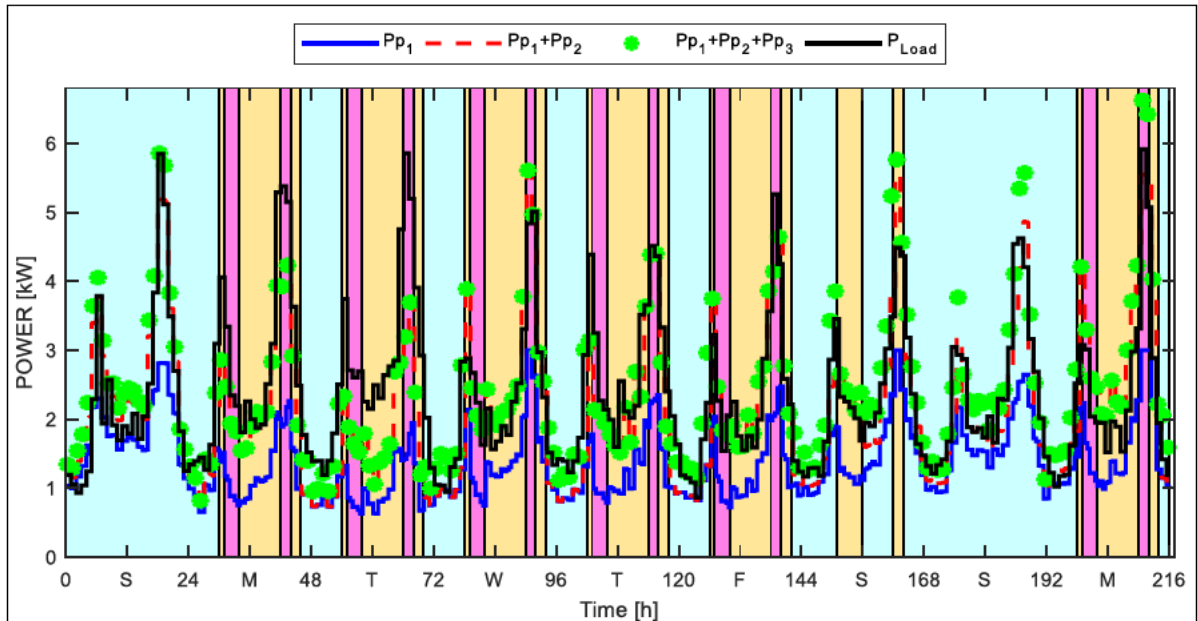

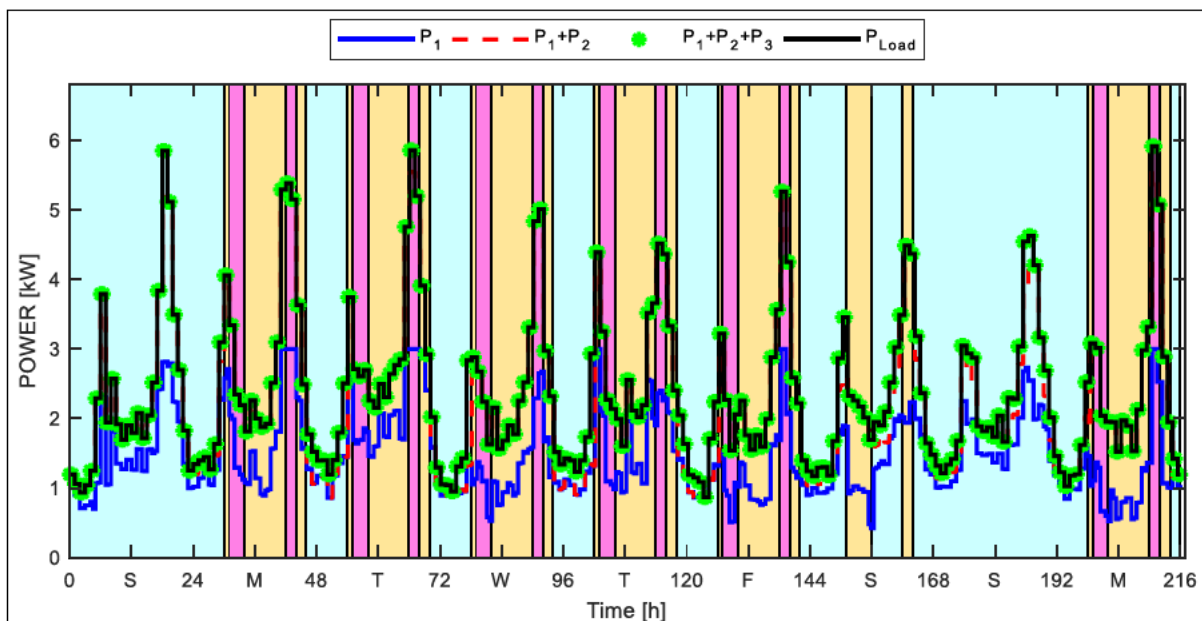Figure 6.3: Optimization-based power flow during load demand uncertainty (residential)

Figure 6.4: Rule-based power flow during load demand uncertainty (residential)

165

During Monday evening TOU peak period, it may be observed that a certain portion of the load demand has not been met, as shown in Fig. 6.3. The open-loop optimization-based model permitted merely 3.96 kW of power to be supplied to the actual load, although the load demands 5.383 kW peak power during the beginning of the evening peak period. Hence, this leads to a 1.42 kW of power shortage. As a result, the rule-based control algorithm permitted the predicted MHK-to-load power (P_{P1}) to increase from 1.93 kW to a new/actual value (P_1) of 3 kW, as shown in Fig. 6.6A. However, a shortage of 0.35 kW still exists. Therefore, the control algorithm allowed the shortage to be supplemented by the PHS. The predicted P_{P2} value is thereof increased from 2.03 kW to become 2.383 kW, as shown in Fig. 6.6B. The predicted P_{P3} is maintained at 0, since both the MHK and PHS systems, are able to meet the overall demand. So, P_{P3} is allowed to increase solely if the RE system cannot meet the entire demand, as shown in Fig. 6.5 (during the evening peak hours of Tuesday). However, in order to maintain the level of the upper reservoir, the predicted grid-to-pump power (P_{P5}) is increased by a difference of 0.353 kW, which results from P_2 - P_{P2}, as shown in Fig. 6.8. Therefore, since there is energy consumption from the grid to the pump, the energy sale was allowed to drop to zero, for the purpose of disallowing simultaneous buying and selling, as shown in Fig. 6.9. Through such operation, the actual upper reservoir state of charge is therefore maintained to be equal to the predicted state of charge, as shown in Fig. 6.10.
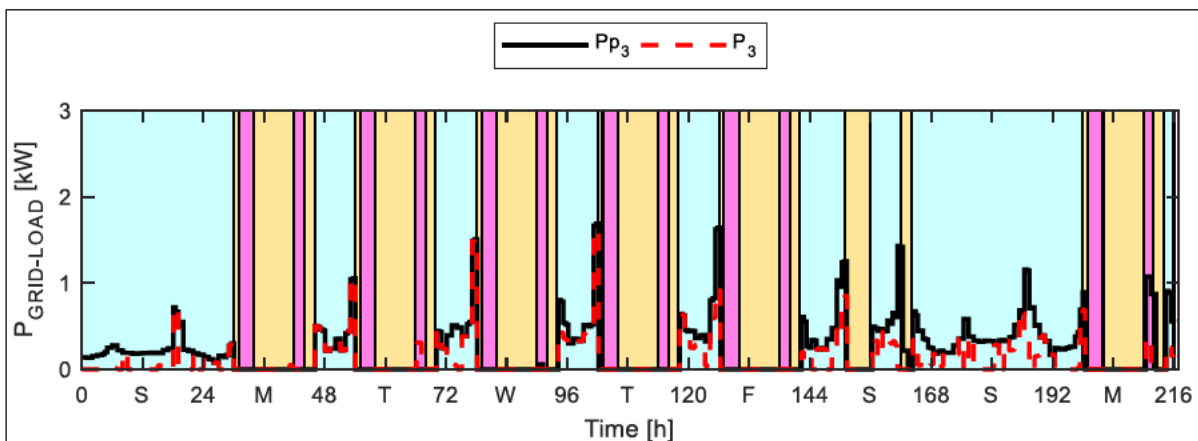

Figure 6.5: Grid-power supplied to the residential load

166

As mentioned earlier that the actual load demand incurs a marginally higher baseline grid cost of ZAR246.49 as compared to the ZAR245.05 incurred by the predicted load demand. In Section 5.3.1.1, it has been noted that the predicted load demand resulted in an overall grid costs and energy sales revenue of ZAR40.34 and ZAR-64.90, respectively. The actual load demand has affected both the overall grid cost and energy sales revenue, as shown in Fig. 6.9. The overall grid costs have decreased to ZAR28.15, while the overall energy sales revenue has decreased to ZAR-59.34. A decrease in energy sale occurs during the hours whereby the P_{Load} is greater than the P_{PLoad}, since buying and selling cannot occur simultaneously. With reference to the baseline grid cost of P_{Load}, the newly acquired energy cost saving is 112%. This has been achieved through the use of rule-based control algorithm. This is slightly higher than 110% that was acquired in Section 5.3.1.1, when the predicted load demand was used. Therefore, the reliable system operation has been accomplished at a higher energy cost saving, through the mitigation of both the unmet load demand and excessive energy supply.
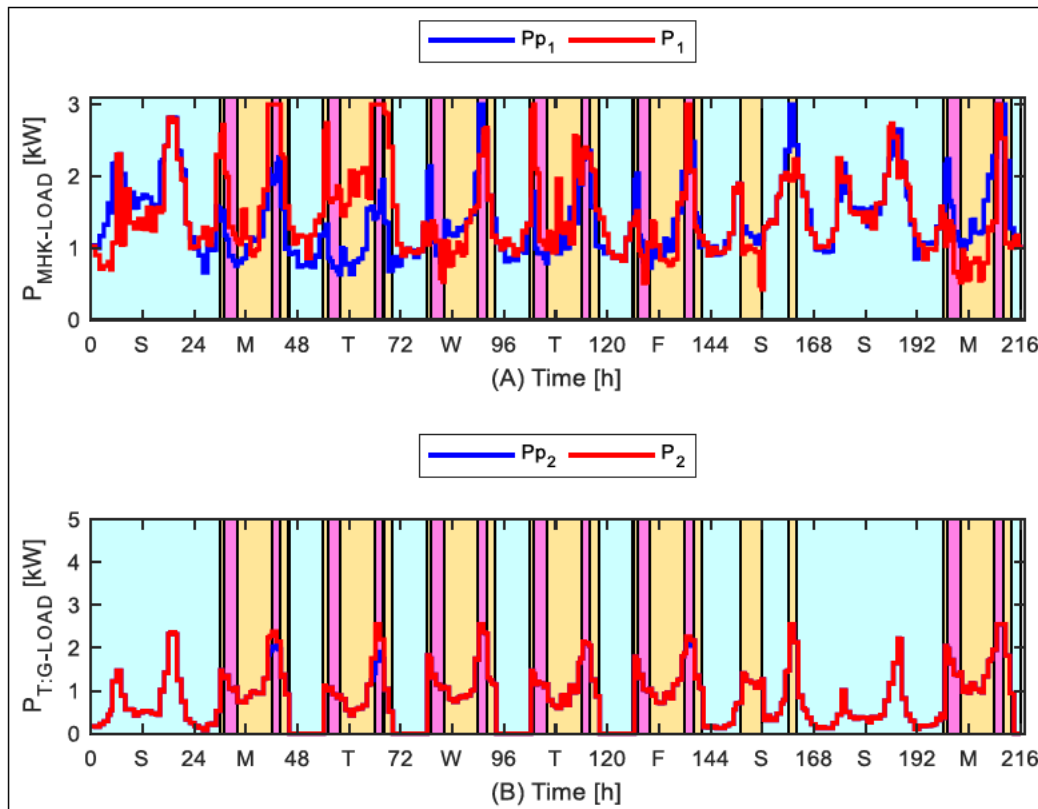

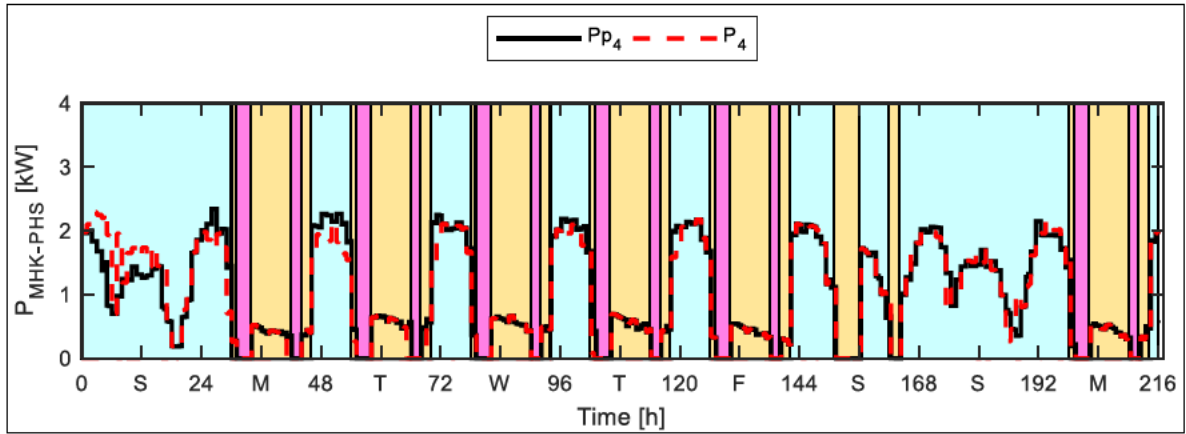Figure 6.6: RE system power supplied to the residential load

167

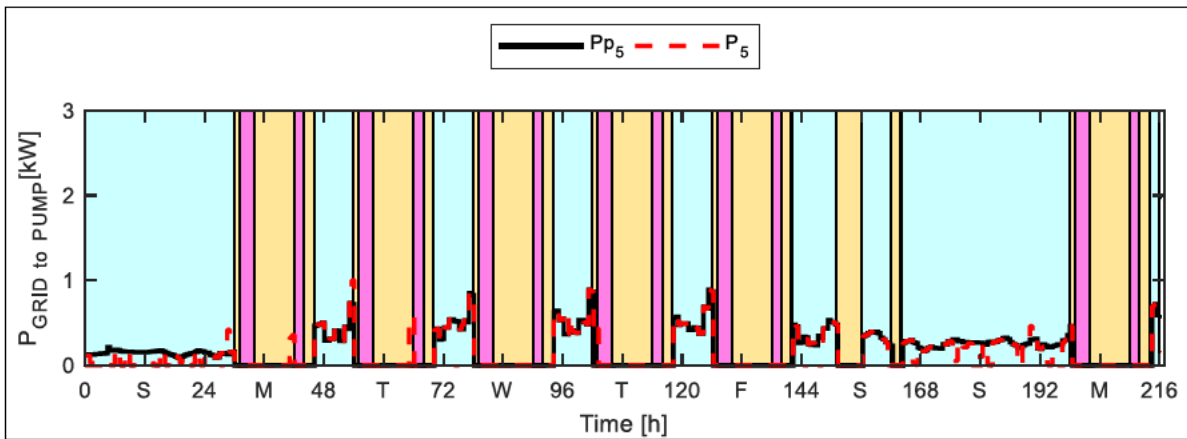Figure 6.7: MHK-power supplied to the pumping unit (residential)

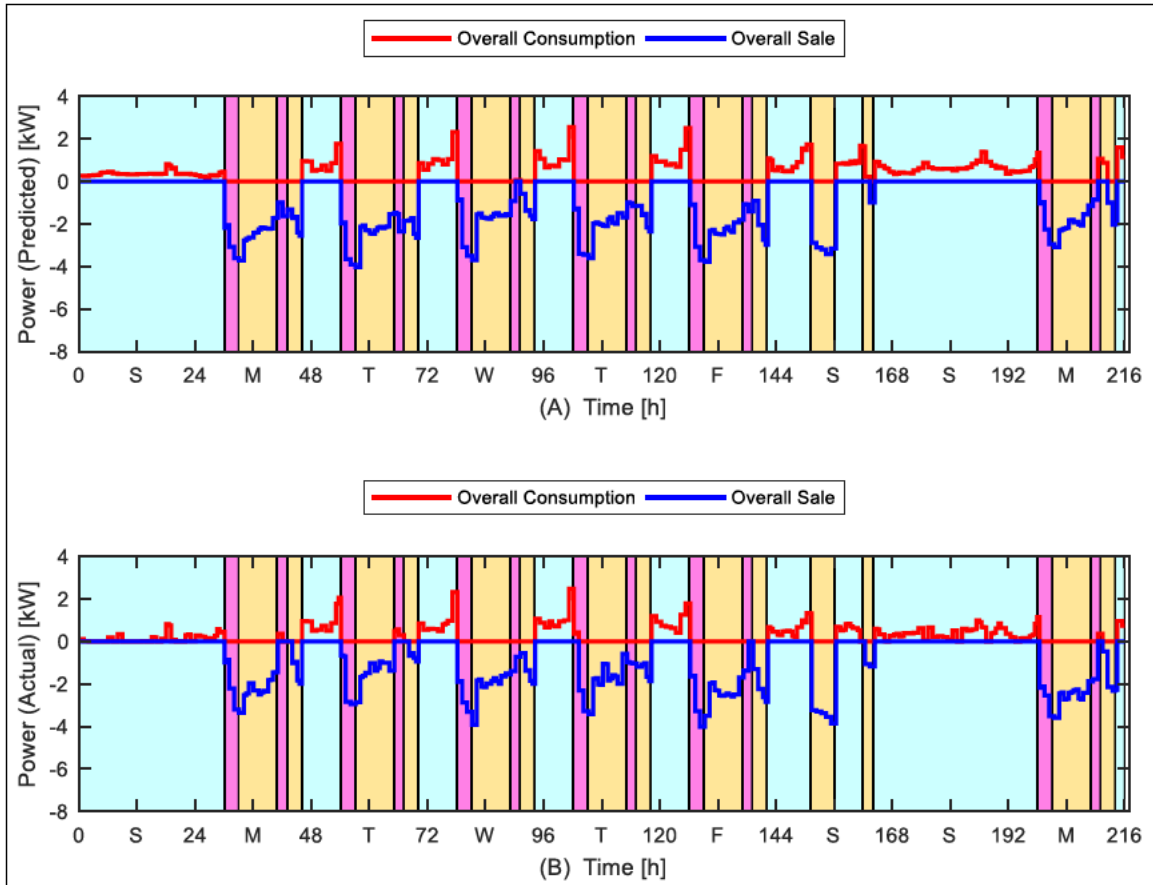Figure 6.8: Grid-power supplied to the pumping unit (residential)

168

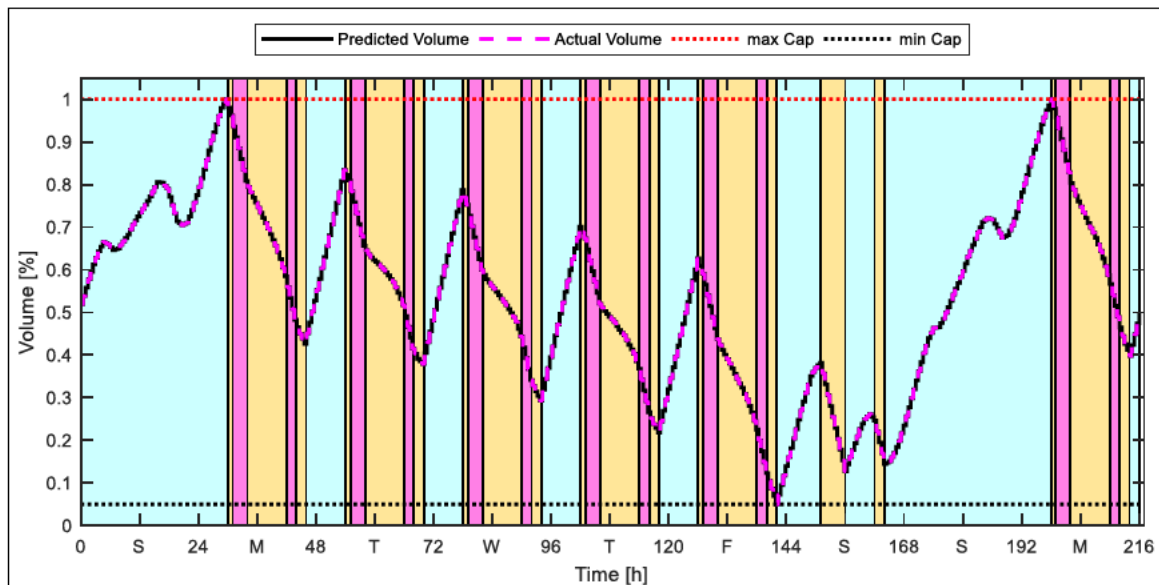Figure 6.9: Overall predicted and actual power consumption and sales (residential)

Figure 6.10: Upper Reservoir state of charge (residential)

169

6.4 Conclusion

This Chapter presented a rule-based control strategy for the grid-interactive MHK-PHS system, as a means of allowing the load demand to be consistently met during load demand uncertainty. The main aim is to assist the developed open-loop optimization-based model, to be able to cater for load demand uncertainties, without affecting the boundaries/limits of the power variables. The control algorithm proved to be able to utilize the three power sources effectively, when supplying the residential, commercial and industrial loads, respectively. Whenever there is a power shortage, the model proved to initially increase the RE power when mitigating the deficit. Therefore, a grid-to-load power consumption is increased as a last option for supplementing the deficit. The developed rule-based algorithm further proved to reduce the excessive supplied power, whenever the actual load demand is less than predicted. This was made possible by initially prioritising to reduce a grid-to-load power before reducing the RE power.

The control algorithm proved to handle the load demand uncertainty, while successfully managing the upper reservoir's state of charge. Whenever the PHS is used to supplement the unmet load demand, grid-to-pump power is increased to maintain the storage level. The excess energy from the MHK system is also utilized for pumping purpose, during off-peak periods.

For the studied residential load, the rule-based control algorithm resulted in a decreased overall grid-power consumption cost and energy sales by 43.3% and 8.6%, respectively, with respect to the predicted load demand. A decrease in grid consumption cost was attained mostly when the estimated load demand is less than the predicted demand and when the generated RE power is sufficient to meet the demand. The overall energy cost saving for the simulated nine days, has increased from 110% (attained during open-loop optimization) to

112% (attained during rule-based control), even though the baseline grid cost of the actual load demand is slightly higher than the one of the predicted load demand. This reveals the effectiveness of the developed rule-based control technique.

CHAPTER 7: CONCLUSION AND FUTURE STUDIES

7.1 Conclusion

This Chapter presents a summary of conclusion and potential future work to be carried out based on the proposed MHK-PHS system.

This research work was stimulated by the ever increasing energy demand leading to the rising electricity price, due to the rising global fossil fuel prices. Hydrokinetic technology is gaining considerable interest around the globe, since it overcomes the intermittent nature of solar PV and WT technologies. This research study aimed to reveal the potential energy savings benefit, to be reaped by electrical consumers, through the use of MHK technology. Hence, an optimal energy management model has been developed, with the objective of minimizing the grid consumption cost, while maximizing the energy sales revenue and reliably meeting the load demand.

Chapter 2 has revealed that most of the grid-connected optimization studies have focused mainly on the common goal of minimizing the grid energy expenditure. Considerably limited studies have concentrated on energy management of a hydrokinetic-based system. Most of the energy management studies have mainly focussed on solar PV and WT technologies. Nevertheless, the research gap is that none of the studies have simultaneously considered factors such as variability of the daily load demand, load demand types and seasonal TOU tariffs, as well as the load demand uncertainties. Such factors may affect the behaviour of the optimization model.

In Chapter 3, the optimal size of the proposed MHK-PHS system was determined through the use of HOMER software, as the most commonly used optimization tool. The optimal configuration results revealed that the type of a load profile does not affect the size of the

172

hydrokinetic system and the amount of the yearly excess energy, under the same daily average consumption. Instead, it affects the size of the storage system components. However, the optimal configuration results led to a large amount of redundant annual excess energy generation. As the system was connected to the grid, the excess energy was sold into the grid for the entire 24 hours without utilizing the available storage system to store excess energy, for later use. This problem has led to a recommendation of designing an optimal energy management model, as to help with the reduction of the MHK-PHS system size. The model should be able to allow the system to store excess energy during the affordable off-peak period and use it later, during the costly peak periods. Additionally, it should be able to minimize the grid consumption costs and maximize the energy sales during costly peak periods.

Chapter 4 demonstrated the behaviour of the developed optimal energy management model for the non-interactive grid-connected MHK-PHS system, supplying the residential, commercial and industrial loads, respectively. Low and high demand TOU tariffs have been considered during the analysis of the model. The model ensured an effective flow of power by utilizing the RE power as a first priority, when meeting the load demand. The grid power was utilized during inexpensive off-peak periods or to supplement the unmet load demand during the costly peak periods. During the high demand season, the grid power was stored during off-peak periods and thereafter, utilized during the standard and peak-periods. Sundays led to the largest number of charging and discharging cycles, when compared to other days. The results have revealed that all the three load types yielded an energy cost saving greater than 90%, when compared to the baseline grid cost for the selected nine days. From a comparison perspective, the non-interactive grid-connected MHK-PHS system proved to favour the residential load type mainly due to the highest energy cost savings at the lowest capital cost.

173

Chapter 5 developed an optimal energy management model for the grid-interactive MHK-PHS system that allows consumers to purchase and sell energy into the grid. The model revealed its effectiveness by optimally controlling the power flow, with the aim of minimizing the grid cost and maximizing the energy sales revenue, while satisfactorily meeting each load demand. The RE power was utilized as a first priority for meeting the load demand and supplying the pumping unit. The grid was mainly utilized during off-peak periods, in order to permit the RE system to store excess energy into the PHS system. To maximize the energy sales revenue, the model did not allow the sales to take place during the off-peak periods. Instead, most of the energy sales took place during costly peak periods and followed by the standard periods. The model did not tolerate both the energy sales and purchasing to take place at the same time, since it is economically infeasible.

Chapter 6 demonstrated the development of a rule-based control strategy, to assist the previously developed open-loop optimization-based model to handle the disturbances due to load demand uncertainty. The open-loop optimization-based model proved to lead to the unmet load demand and excessive supply of power, during load demand uncertainty. The rule-based control proved to effectively mitigate the issue of unmet load demand, by prioritizing the use of RE before utilizing the grid energy, during energy deficit. The grid power has further been used to compensate the pumping demand. Hence, the load demand uncertainty issue was solved, without affecting the predicted upper reservoir SOC. From economic perspective, the grid-power reduction has been prioritised as a first option, when reducing the excessively supplied power. An overall energy savings benefit of 112% has been achieved after satisfactorily meeting the higher demanding actual load.

The results of the study have presented the potential benefit of investing in the proposed system, when it is non-interaction or interactive with the grid. The results have shown that it

174

is of importance to involve an energy management technique, in order to allow for an optimal power flow. The study has additionally been used for the following highlights:

- Analysed the importance of energy management model by reducing the capital cost of the grid-connect MHK-PHS system, as opposed to the optimal size determined by the HOMER simulation tool.

- Analyse the impact of various demand seasons on the overall energy cost saving benefit. It is noted that irrespective of the load type, the low demand season generates higher sales revenue when compared to a higher demand season, even though the electricity TOU rates are lower.

- Analysed the impact of various load profiles on the peak energy sales. In contrary to the residential and commercial load profiles, it noted that an industrial load profile leads to peak energy sales during evening TOU peak period, than during the morning TOU peak period. This leads to the least net energy income, since the number of hours during the evening peak period are less than the morning peak hours.

- Revealed the importance of storing excess RE as well as storing the grid-energy during off-peak TOU periods. Hence, this revealed that an acceptable investment potential exists if the energy is stored during off-peak period and further sold and/or used during costly peak periods.

- Demonstrated the importance of considering a rule-based control method, in addition to the optimization-based model, due to unavoidable load demand uncertainties that may be caused by an inaccurate load forecasting.

175

7.2 Suggestions for Further Studies

The study has revealed that further research work needs to be done as explained below:

- Further work should be carried out on developing optimal scheduling model for the proposed MHK-PHS system, when applying the load shifting mechanism.

- Further work should be carried out to monitor the behaviour of the optimal model for cases of the industrial and commercial businesses which are not operating on Saturdays and/or Sundays.

- Furthermore, it would be of interest to investigate how the developed optimal control model would perform under further dynamic pricing schemes, such as real-time pricing.

- Future work in this area would be necessary to analyse the life cycle cost and payback period for each load demand type, based on the achieved energy savings.

REFERENCES

Akinyele D.O., Rayundu R.K., 2014. *"Review of energy storage technologies for sustainable power networks"*. Sustainable Energy Technologies and Assessments, 8: 74-91.

Al Zohbi G., Hendrick P., Renier C., Bouillard P., 2016. *"The contribution of wind-hydro pumped storage systems in meeting Lebanon's electricity demand"*. International Journal of Hydrogen Energy, 41: 6996-7004.

Alasseri R., Tripathi A., Joji Rao T., Sreekanth K.J., 2017. *"A review on implementation strategies for demand side management (DSM) in Kuwait through incentive-based demand response programs"*. Renewable and Sustainable Energy Reviews, 77: 617-635.

Al-falahi M.D.A., Jayasinghe S.D.G., Enshaei H., 2017. *"A review on recent size optimization methodologies for standalone solar and wind hybrid renewable energy system"*. Energy Conversion and Management, 143: 252-274.

Asif M., Muneer T., 2007. "*Energy supply, its demand and security issues for developed and emerging economies"*. Renewable and Sustainable Energy Reviews, 11(7):1388-1413.

Azofra D., Jimenez E., Martinez E., Blanco J., Saenz-Diez J.C. 2015. *"Economical–environmental impact of subsidised renewable energy sources for electricity (RES-E) in the Spanish system"*. Energy for Sustainable Development, 29: 47-56.

Babu C.A., Ashok S., 2009. *"Optimal utilization of renewable energy-based IPPs for industrial load management"*. Renewable Energy, 34: 2455-2460.

Badwawi R.A, Abusara M., Mallick T., 2015. *"A review of hybrid solar PV and wind energy system"*. Smart Science, 3(3): 127-138.

Bahramara S., Moghaddam M., Haghifam M., 2016. *"Optimal planing of hybrid renewable energy systems using homer: a review"*. Renewable and Sustainable Energy Review, 62: 609-620.

Banshwar A., Sharma N.K., Sood Y.R., Shrivastava R. 2017. *"Renewable enenrgy sources as a new participant in acillary service markets"*. Energy Strategy Reviews, 18: 106-120.

Beires P., Vasconcelos M.H., Moreira C.L., Pecas Lopes J.A., 2018. *"Stability of autonomous power systems with reversible hydro power plants"*. Electric Power Systems Research, 158: 1-14.

Bekker J.C., 2012. "Efficient Modelling of a Wind Turbine System for Parameter Estimation Applications", Master's Thesis, University of Stellenbosch.

Bokhari A., Alkan A., Dogan R., Diaz-Aguilo M., Leon F., Czarkowski D., Zabar Z., Birenbaum L., Noel A. and Uosef R.E., 2014. "*Experimental Determination of the ZIP Coefficients for Modern Residential, Commercial, and Industrial Loads*," IEEE Transcript, Power Delivery, 29 (3): 1372-1381.

Bordin C., Anuta H.O., Crossland A., Gutierrez I.L., Dent C.J., Vigo D. 2017 *"A linear programming approach for battery degradation analysis and optimization in offgrid power systems with solar energy integration"*, Renewable Energy, 101, 417-430.

Bryans AG., 2006. "*Impacts of tidal stream devices on electrical power systems*", Ph.D. thesis, Faculty of Engineering and Physical Science, The Queen's University of Belfast.

Cai Q., Adjiman C.A., Brandon N.P., 2014. "*Optimal control strategies for hydrogen production when coupling solid oxide electrolysers with intermittent renewable energies*". Journal of Power Sources, 268: 212-224.

Canales F.A., Beluco A., 2014. "*Modelling pumped hydro storage with the micropower optimization model (HOMER)*". Journal of Renewable and Sustainable Energy, 6: 043131.

Canales F.A., Beluco A., Mendes C.B., 2015. "*A comparative study of a wind hydro hybrid system with water storage capacity: Conventional reservoir or pumped storage plant*?". Journal of Energy Storage, 4: 96-105.

178

Capellán-Pérez I., Mediavilla M., de Casto C., Carpintero Ó., Miguel L.J., 2014. *"Fossil fuel depletion and socio-economic scenarios: An integrated approach"*. Energy, 77: 641-666.

Chauhan A., Saini R.P., 2014. *"A review on Integrated Renewable Energy System based power generation for stand-alone applications: Configurations, storage options, sizing methodologies and control"*. Renewable and Sustainable Energy Reviews, 38: 99-120.

Chen C.L., Chen H.C., Lee J.Y., 2016. "*Application of a generic superstructure-based formulation to the design of wind-pumped-storage hybrid systems on remote islands"*. Energy Conversion and Management, 111: 339-351.

Cheng J., Chu F., Liu M., Wu P., Xia W., 2017. *"Bi-criteria single-machine batch scheduling with machine on/off switching under time-of-use tariffs"*. Computer and Industrial Engineering, 112: 721-734.

Cosmo V.D., O'Hora D., 2017. *"Nudging electricity consumption using TOU pricing and feedback: evidence from Irish households"*. Journal of Economic Psychology, 61: 1-14.

Di Santo K.G., Di Santo S.G., Monaro R.M., Saidel M.A., 2018. "*Active demand side management for households in smart grids using optimization and artificial intelligence*", Measurement, 115: 152-161.

Díaz-González F., Sumper A., Gomis-Bellmunt O., 2016. *"Energy storage in power systems"*. Wiley, Barcelona (Spain), 1st edition.

Díaz-González F., Sumper A., Gomis-Bellmunt O., Villafáfila-Robles R., 2012. "*A review of energy storage technologies for wind power applications"*. Renewable and Sustainable Energy Review, 16: 2154-2171.

Eskom "Schedule of standard prices for Eskom tariffs (2017-2018)", (Accessed 22 May 2017), Available at:

Foley A.M., Leahy P.G., Li K., McKeogh E.J., Morrison A.P., 2015. "*A long-term analysis of pumped hydro storage to firm wind power*". Applied Energy, 137: 638-648.

179

Geem Z.W., Yoon Y., 2017. *"Harmony search optimization of renewable energy charging with energy storage system"*. Electric Power and Energy Systems, 86: 120-126.

Goswami D.Y., Kreith F., 2008. *"Energy conversion"*. Taylor & Francis Group, United State of America.

Grabbe M., Yuen K., Goude A., Lalander E., Leijon M., 2009. *"Design of an Experimental Setup for Hydro-Kinetic Energy Conversion"*, The International Journal on Hydropower & Dams, 16(5), 112-116.

Güney M.S., Kaygusuz K., 2010. "*Hydrokinetic Energy Conversion Systems: a technology status review*", Renewable and Sustainable Energy Reviews, 14(9): 2996-3004.

Hemmati R., 2017. "*Technical and economic analysis of home energy management system incorporating small-scale wind turbine and battery energy storage system*". Journal of Cleaner Production, 58: 106-118.

Hiendro A., Kurnianto R., Rajagukguk M., Simanjuntak Y.M., Junaidi, 2013. "*Techno-economic Analysis of Photovoltaic/wind Hybrid System for Onshore/remote area in Indonesia*", Energy, 59:652-657.

Hil Baky Md. A., Rahman Md. M., Sadrul Islam A.K.M., 2017. "*Development of renewable energy sector in Bangladesh: Current status and future potentials"*. Renewable and Sustainable Energy Reviews, 73: 1184-1197.

HOMER Energy Support, 2016. "Modeling a hydrokinetic turbine", (Accessed August 18, 2016), Available at:

http://usersupport.homerenergy.com/customer/en/portal/articles/2188862-modeling-a-hydrokinetic-turbine

http://www.eskom.co.za/CustomerCare/TariffsAndCharges/Documents/Eskom%20schedule%20of%20standard%20prices%202017_18%2015_02_2017%20%2800%29.pdf

Iqbal T., 2009. *"Feasibility study of pumped hydro energy storage for Ramea wind-diesel hybrid power system"*. Faculty of Engineering and Applied Science, Memorial University.

Ishigaki Y., Kimura Y., Matsusue I., Miyoshi H., Yamagishi K., 2014. *"Optimal energy management system for isolated micro grids"*. Environment and Energy, 78: 73-78.

Jamal G.F., Ghandour M., Ibrahim H., Assi A.H., 2014. "Technical feasibility study of solar-pumped hydro storage in Lebanon". Renewable Energy for Developing Countries (REDEC): 23-28.

Jardini J.A., Tahan C.M.V., Gouvea M.R., Ahn S.E., Figueiredo F.M., 2000. "*Daily load profiles for residential, commercial and industrial low voltage consumers*". IEEE Transactions on Power Delivery, 15: 375-380.

Kanwar A., Rodríguez D.I.H., Appen J.V., Braun M., 2015. "*A Comparative Study of Optimization-and Rule-Based Control for Microgrid Operation*". In Proceedings of the Power and Energy Student Summit, Dortmund, Germany, 13–14 January 2015; pp. 1–6.

Koko S.P., 2014. *"Techno-economic analysis of an off-grid hydrokinetic river system as a remote rural electrification option"*. Master thesis, Central University of Technology, Bloemfontein.

Koko S.P., Kusakana K., Vermaak H.J., 2014. "*Hydrokinetic for Remote Rural Electrification*". International Journal of Electrical, Computer, Electronics and Communication Engineering, 8: 1659-1663.

Koko S.P., Kusakana K., Vermaak H.J., 2015. "*Micro-hydrokinetic river system modelling and analysis as compared to wind system for remote rural electrification*". Electric Power Systems Research, 126: 38-44.

Kong, Z., Zou, Y. and Liu, T., 2017. "*Implementation of real-time energy management strategy based on reinforcement learning for hybrid electric vehicles and simulation validation*". PloS one, 12 (7): p.e0180491.

181

Kumar A. and Saini R.P., 2016. "Performance parameters of Savonius type hydrokinetic turbine–A Review". Renewable and Sustainable Energy Reviews, 64, pp.289-310.

Kusakana K., 2014. *"Techno-economic analysis of off-grid hydrokinetic-based hybrid energy systems for onshore/remote area in South Africa".* Energy, 68: 947-957.

Kusakana K., 2015. *"Feasibility analysis of river off-grid hydrokinetic systems with pumped hydro storage in rural applications".* Energy Conversion and Management, 96: 352-362.

Kusakana K., 2016. *"Optimal operation control of a grid-connected photovoltaic-battery hybrid system".* PowerAfrica 2016 IEEE PES, 239-244.

Kusakana K., 2017a. *"Energy management of a grid-connected hydrokinetic system under Time of Use tariff".* Renewable Energy, 101: 1325-1333.

Kusakana K., 2017b. "*Optimal power flow of a battery/wind/PV/grid hybrid system: case of South Africa*". Smart Energy Grid Design for Island Countries, Green Energy and Technology, Springer, Cham, 2017: 447-465.

Kusakana K., 2018. "*Impact of different South African demand sector on grid-connected PV systems' optimal energy dispatch under time of use tariff*". Sustainable Cloud and Energy Services, Springer, Cham 2018: 243-260.

Kusakana K., Vermaak H.J., 2014. *"Cost and performance evaluation of hydrokinetic-diesel hybrid systems".* Energy Procedia 2014, the 6th International Conference on Applied Energy (ICAE2014), 61: 2439–2442.

Kusakana K., Vermaak HJ., 2013. "*Hydrokinetic power generation for rural electricity supply: case of South Africa*". Renewable Energy, 55: 467–473.

Kuschke M., Strunz K., 2011. "*Modeling of Tidal Energy Conversion Systems for Smart Grid Operation*", IEEE Power and Energy Society General Meeting, San Diego, 1-3.

Li R., Wang Z., Gu C., Li F., Wu H., 2016. *"A novel time-of-use tariff design based on Gaussian Mixture Model".* Applied Energy, 162: 1530-1536.

Lu X., Zhou K., Yang S. *"Multi-objective optimal dispatch of microgrid containing electric vehicles"*. Journal of Cleaner Production, 165: 1572-1581.

Luh P.B., Michel L.D., Friedland P., Guan C., Wang Y. *"Load forecasting and demand response"*. In Proc. IEEE Power and Engineering Society General Meeting, July 2010.

Ma T., Yang H., Lu L., Peng J., 2014. "*Technical feasibility study on a standalone hybrid solar-wind system with pumped hydro storage for a remote island in Hong Kong*". Renewable Energy, 69: 7-15.

Meyabadi A.F., Deihimi M.H., 2017. *"A review of demand-side management: Reconsidering theoretical framework"*. Renewable and Sustainable Energy Reviews, 128: 367-379.

Mollahosseinia A., Hosseinib S.A., Jabbaric M., Figolid A., Rahimpoura A., 2017. "*Renewable energy management and market in Iran: A holistic review on current state and future demands"*. Renewable and Sustainable Energy Reviews, 80: 774-788.

Ngoko B.O., Sugihara H., Funaki T., 2018. "*Optimal power flow considering line-conductor temperature limits under high penetration of intermittent renewable energy sources*", Electrical Power and Energy Systems, 101: 255-267.

Numbi B.P., Malinga S.J., 2017. "*Optimal energy cost and economic analysis of a residential grid-interactive solar PV system- case of eThekwini municipality in South Africa*", Applied Energy, 186: 28-45.

Obi M., Bass R., 2016. *"Trends and challenges of grid-connected photovoltaic systems – A review"*. Renewable and Sustainable Energy Review, 58: 1082-1094.

Pallonetto F., Oxizidis S., Milano F., Finn D., 2016. *"The effect of time-of-use tariffs on the demand response flexibility of an all-electric smart-grid-ready dwelling"*. Energy and Buildings, 128: 56-67.

Phiri S.F., Kusakana K., 2017. *"Demand side management of a grid-connected PV-WT-battery hybrid system"*. Industrial and Commercial Use of Energy (ICUE) 2016 international conference, 45-51.

Ramli M.A. and Twaha S., 2015. "*Analysis of renewable energy feed-in tariffs in selected regions of the globe: Lessons for Saudi Arabia*". Renewable and Sustainable Energy Reviews, 45: 649-661.

Saad M.M., Asmuin N., 2014. *"Comparison of horizontal axis wind turbines and vertical axis wind turbines"*, IOSR Journal of Engineering, 4(8), 27-30.

Setlhogo L.K., Figlan T. and van Rensburg J.F., 2017. "*Review of the residential customer load modelling in Eskom* ", 2017 International Conference on the Domestic Use of Energy (DUE), Cape Town, April 2017, IEEE, 135-143.

Sichilalu S.M., Mathaba T., Xia X., 2017. *"Optimal control of a wind-PV-hybrid powered heat pump water heater"*. Applied Energy, 185: 1173-1184.

Sichilalu S.M., Tazvinga H., Xia X., 2016a. *"Integrated energy management of grid-tied-PV-fuel cell hybrid system"*. Energy Procedia, 103: 111-116.

Sichilalu S.M., Tazvinga H., Xia X., 2016b. *"Optimal control of a fuel cell/wind/PV/grid hybrid system with thermal heat pump load"*. Solar Energy, 135: 59-69.

Sichilalu S.M., Xia X., 2015b. *"Optimal energy control of grid tied PV-diesel-battery hybrid system powering heat pump water heater"*, Solar Energy, 115: 243-254.

Sichilalu S.M., Xia X., 2015a. *"Optimal power dispatch of a grid tied-battery-photovoltaic system supplying heat pump water heaters"*. Energy Conversion and Management, 102: 81-91.

Sinha S., Chandel S.S., 2014. *"Review of software tools for hybrid renewable energy systems"*. Renewable and Sustainable Energy Review, 32: 192-205.

Siti M.W., Tiako R., Bansal R.C., 2016. "*A model predictive control strategy for grid-connected solar-wind with pumped hydro storage*". 5th IET International Conference on Renewable Power Generation (RPG); 1-6.

Soudmand B.M., Esfetanaj N.N., Mehdipour S., Rezaeipour R., 2017. "*Heating hub and power hub models for optimal performance of an industrial consumer*". Energy Conversion and Management, 150: 425-432.

Ter-Gazarian A., 1994. *"Energy storage for power systems"*. Peter Peregrinus Ltd, London (UK), Vol. 6: pp. 87.

Tezer T., Yaman R., Yaman G. 2017 *"Evaluation of approaches used for optimization of stand-alone hybrid renewable energy systems"*, Renewable and Sustainable Energy Reviews, 73, 840-853.

Vermaak H. J., Koko S. P. and Kusakana K., 2014. "*Status of micro-hydrokinetic river technology in rural applications: A review of literatures*". Renewable and Sustainable Energy Review, 29: 625-633.

Wang B., 2013. *"Intelligent control and power flow optimization of microgrid: energy management strategies"*. Doctoral thesis, University of Technology of Compiegne, France.

Wang X., El-Farra N.H., Palazoglu A., 2017. *"Optimal scheduling of demand responsive industrial production with hybrid renewable energy systems"*. Renewable Energy, 100: 53-64.

Wanjiru E.M, Sichilalu S.M., Xia X., 2016. *"Optimal integrated diesel grid-renewable energy system for hot water devices"*. Energy Procedia, 103: 117-122.

Wanjiru E.M, Sichilalu S.M., Xia X., 2017a. "*Model predictive control of heat pump water heater-instantaneous shower powered with integrated renewable-grid energy systems*". Applied Energy, 204: 1333-1346.

Wanjiru E.M, Sichilalu S.M., Xia X., 2017b. *"Optimal operation of integrated heat pump-instant water heaters with renewable energy"*. Energy Procedia, 105: 2151-2156.

Wanjiru E.M, Sichilalu S.M., Xia X., 2017c. *"Optimal control of heat pump water heater-instantaneous shower using integrated renewable-grid energy systems"*. Applied Energy, 201: 332-342.

Wu Z., Xia X., 2015. *"Optimal switching renewable energy system for demand side management"*. Solar Energy, 114: 278-288.

Yakub U., Nayeem S.M., GolamMostafa S.M., Samrat N., 2014. "*An investigation on hydro kinetic energy and analyzing its potentiality in Bangladesh*". 2nd International Conference on Green Energy and Technology (ICGET), IEEE, 45–49.

Yang L., Dong C., Johnny Wan C.L., To Ng C., 2013. *"Electricity time-of-use tariff with consumer behavior consideration"*. Int. J. Production Economics, 402-410.

Yang P., Tang G. and Nehorai A., 2013. *"A game-theoretic approach for optimal time-of-use electricity pricing"*. IEEE Transactions on Power Systems, 28(2): 884-892.

Yoon Y., Kim Y., 2014. "*Charge Scheduling of an Energy Storage System under Time-of-Use Pricing and a Demand Charge*", The Scientific World Journal, 2014.

Yuen K., Thomas K., Grabbe M., Deglaire P., Bouquerel M., Österberg D., Leijon M., 2009. *"Matching a permanent magnet synchronous generator to a fixed pitch vertical axis turbine for marine current energy conversion"*, IEEE Journal of Oceanic Engineering, 34(1), 24-31.

Zang H., Cai J., Fang K., Zhao F., Sutherland J.W., 2017. *"Operational optimization of a grid-connected factory with onsite photovoltaic and battery storage systems"*. Applied Energy, 205: 1538-1547.

Zhao H., Wu Q., Hu S., Xu H., Rasmussen C.N., 2015. *"Review of energy storage system for wind power integration support"*. Applied Energy, 137: 545-553.

Zhou H., 2012. "*Maximum Power Point Tracking Control of Hydrokinetic Turbine and Low-Speed High-Thrust Permanent Magnet Generator Design*", MSc Thesis, Missouri University of Science and Technology, 2012.

APPENDICES

APPENDIX A: CHAPTER 6 supplementary simulation results:

commercial and industrial loads

A1: Commercial Load
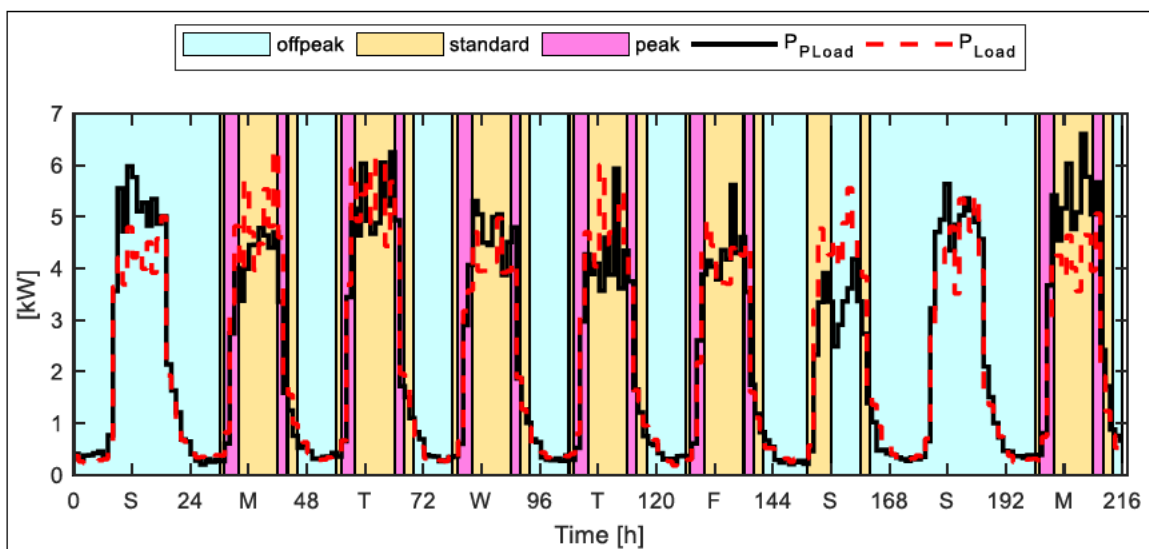
Figure A1.1: Predicted and actual commercial load demand
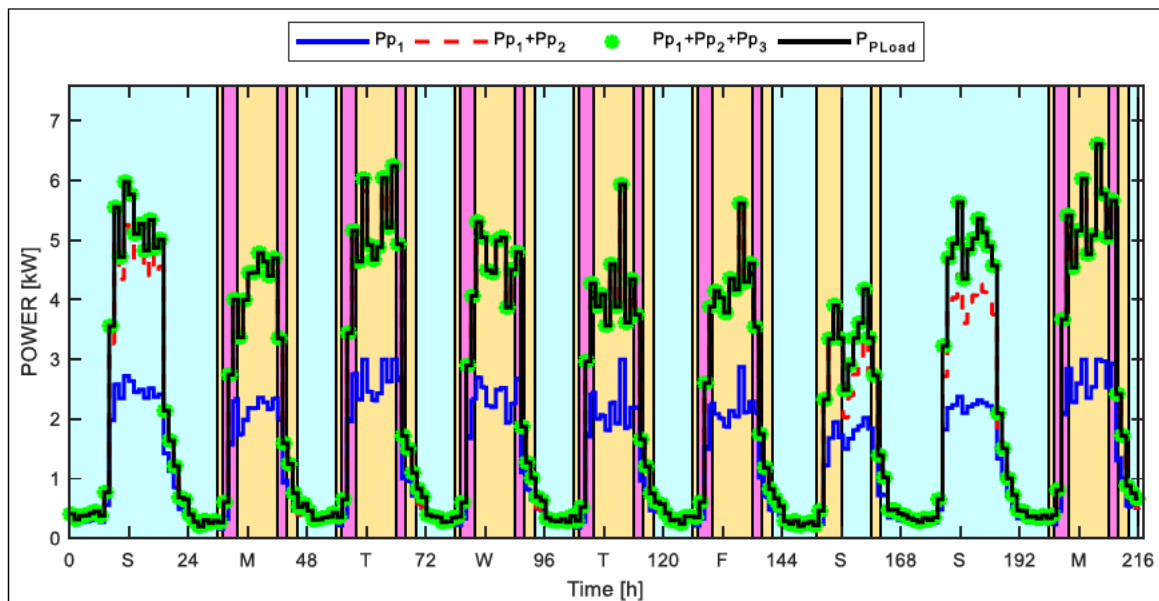
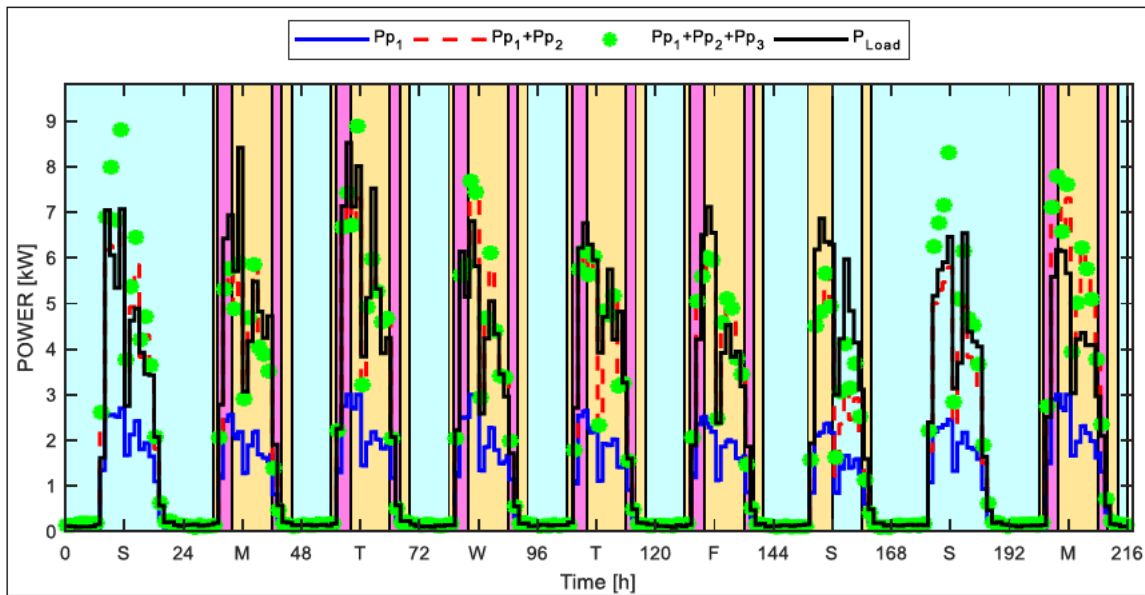Figure A1.2: Optimization-based power flow before load demand uncertainty (commercial)

188
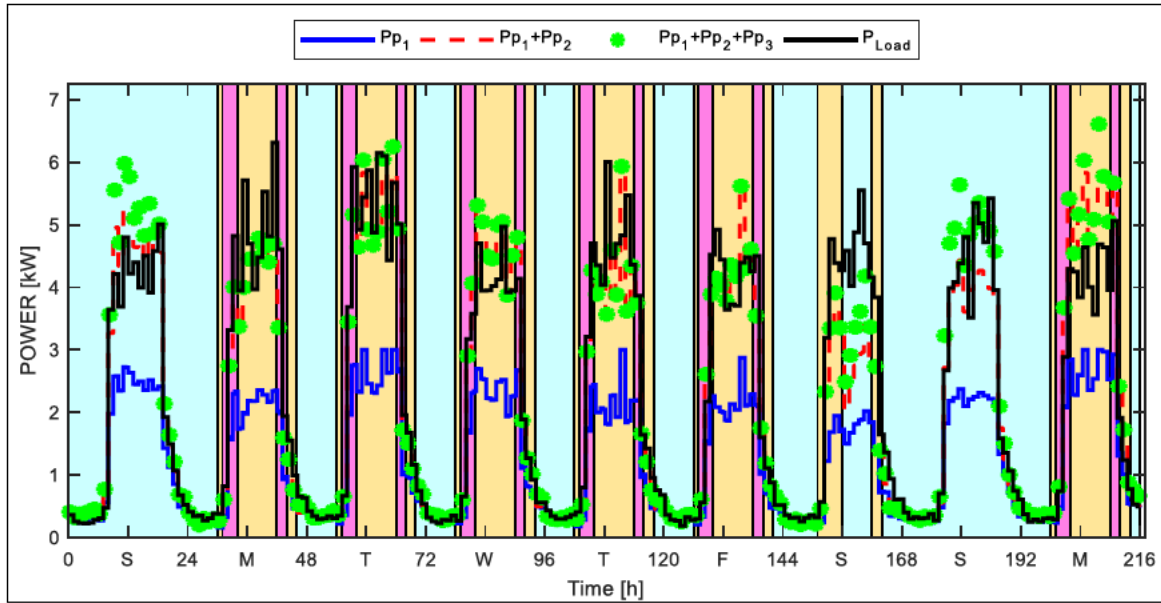
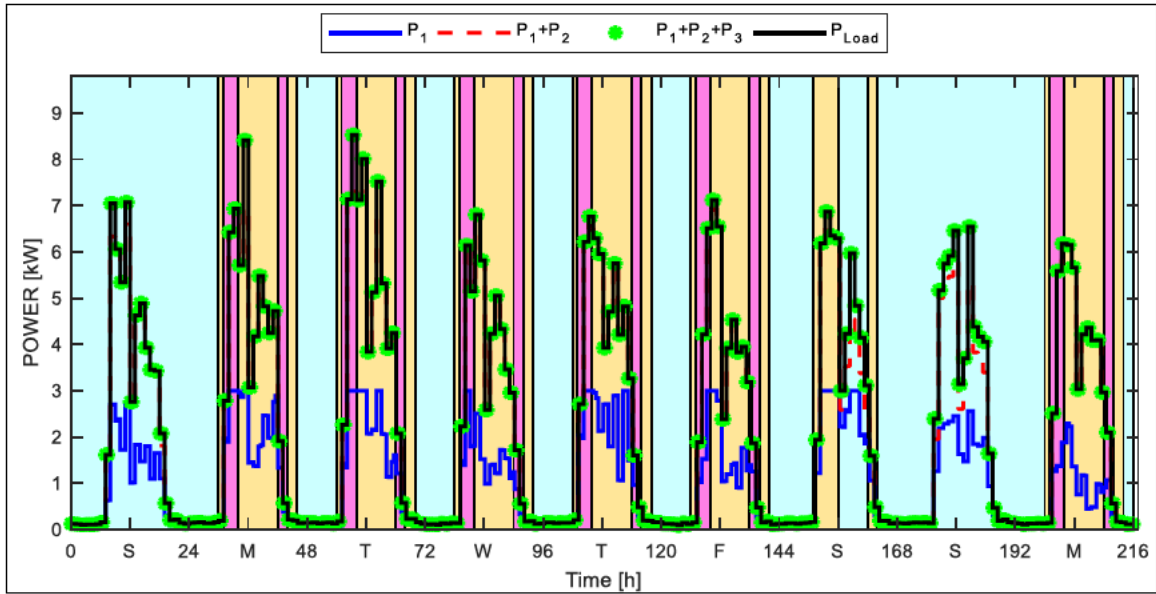Figure A1.3: Optimization-based power flow during load demand uncertainty (commercial)
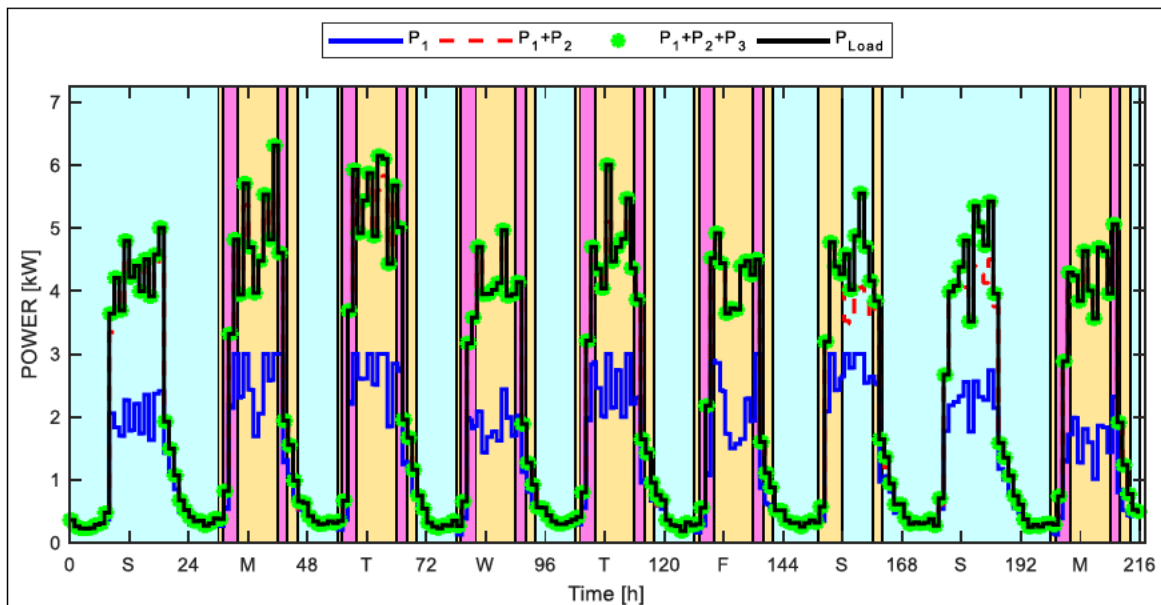
Figure A1.4: Rule-based power flow during load demand uncertainty (commercial)
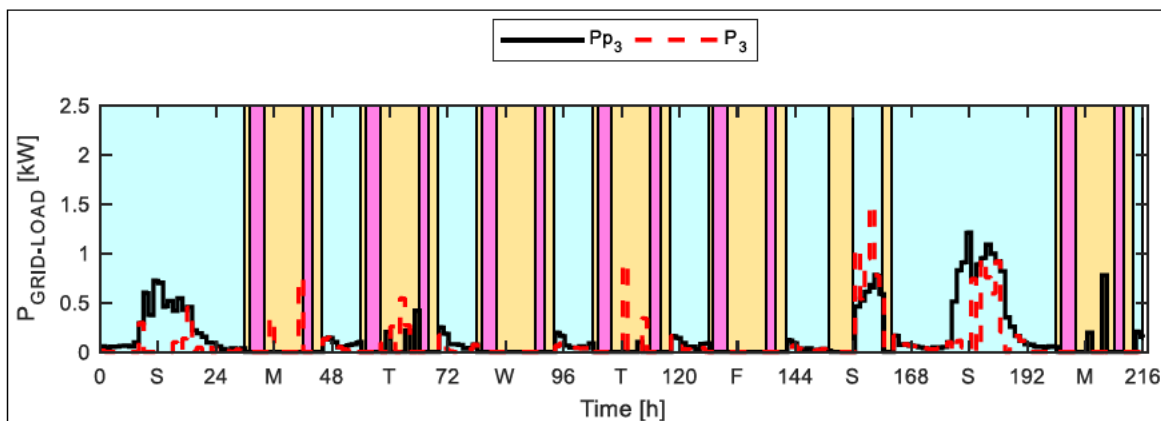
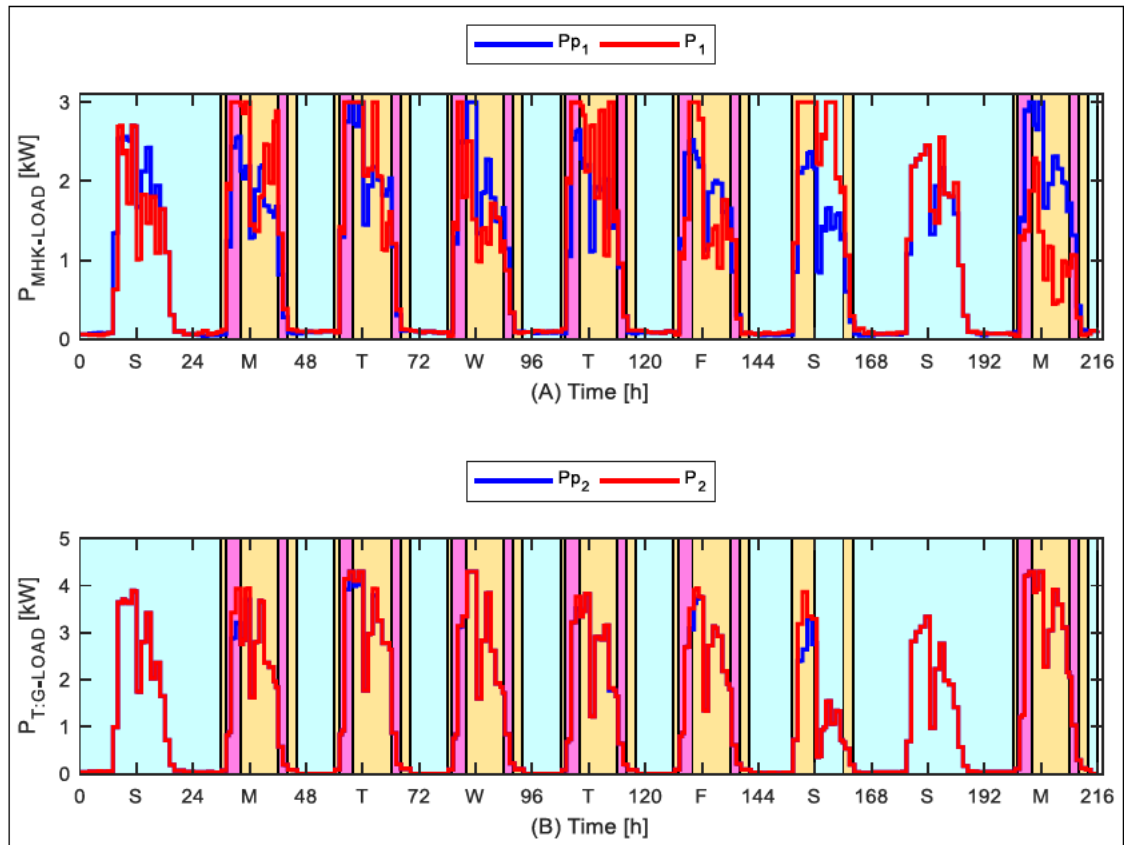Figure A1.5: Grid-power supplied to the commercial load

189
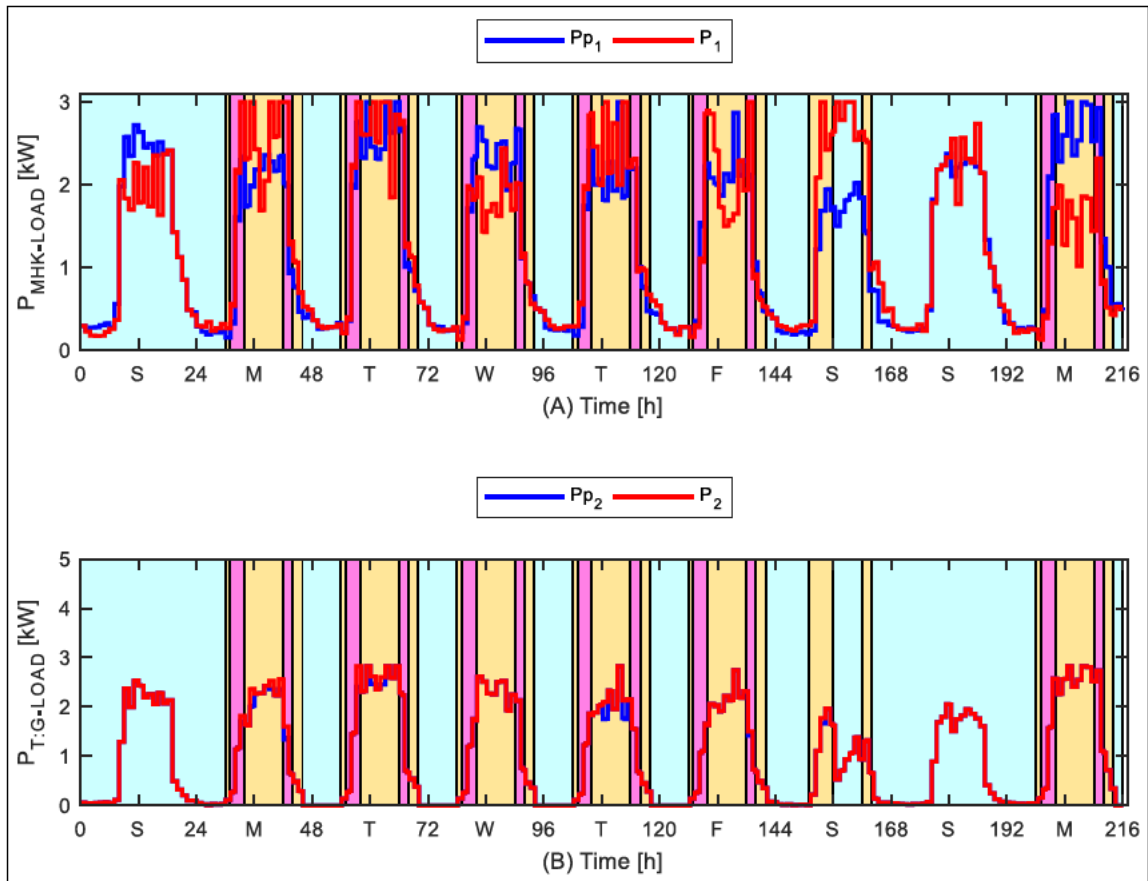
Figure A1.6: RE system power supplied to the commercial load
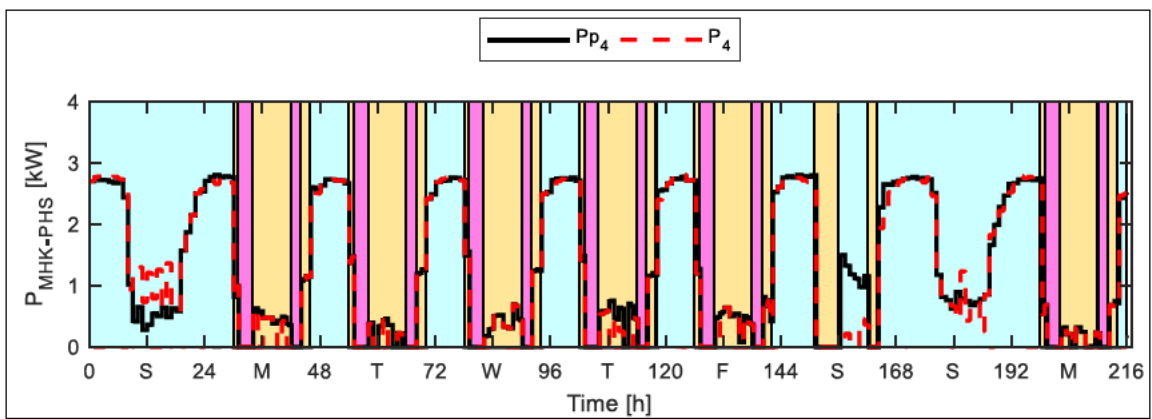
Figure A1.7: MHK-power supplied to the pumping unit (commercial load)

190
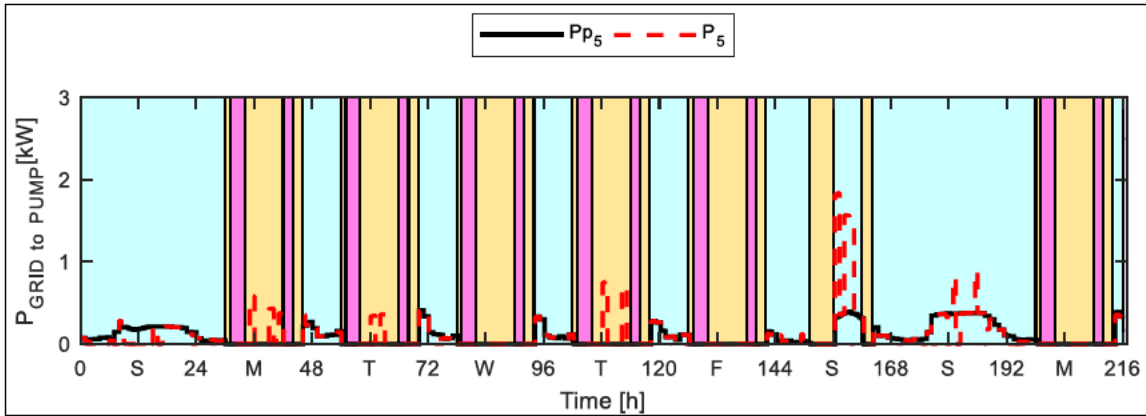
Figure A1.8: Grid-power supplied to the pumping unit (commercial load)
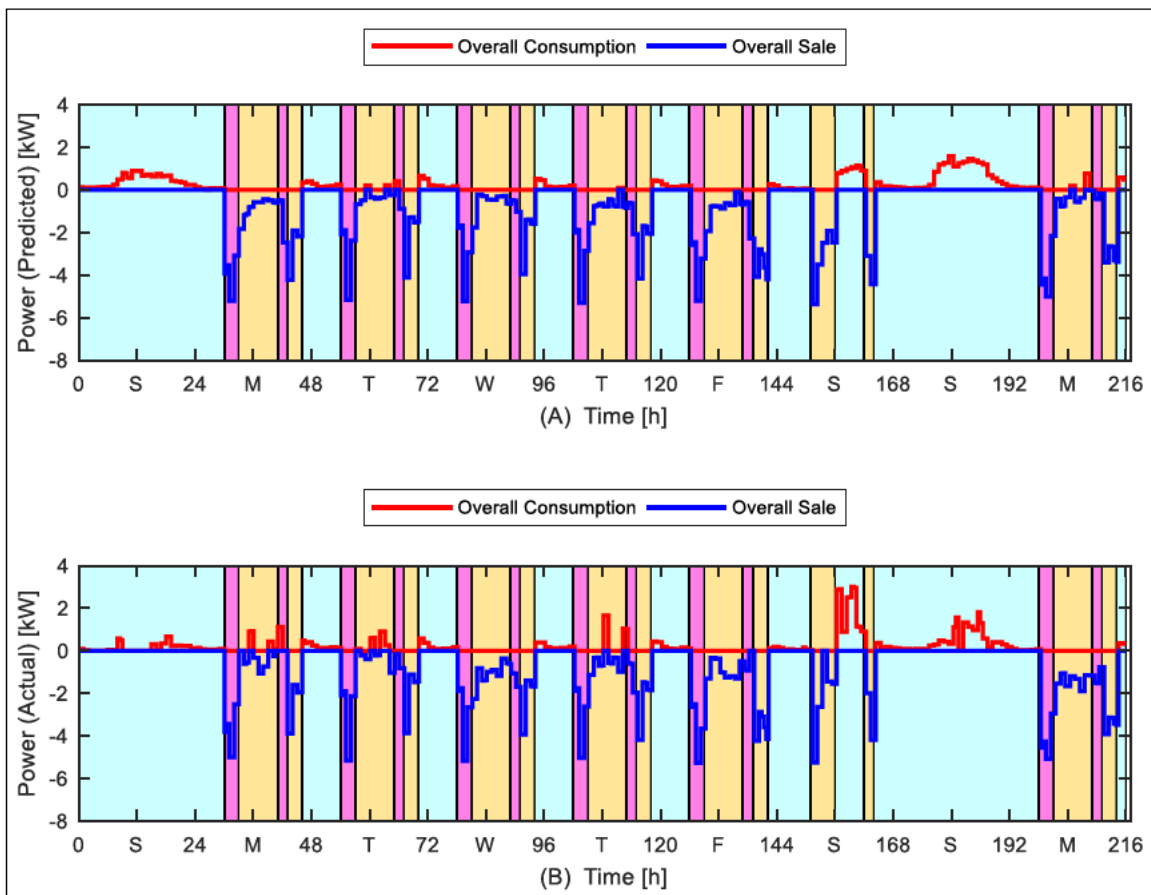
Figure A1.9: Overall predicted and actual power consumption and sales (commercial)

191
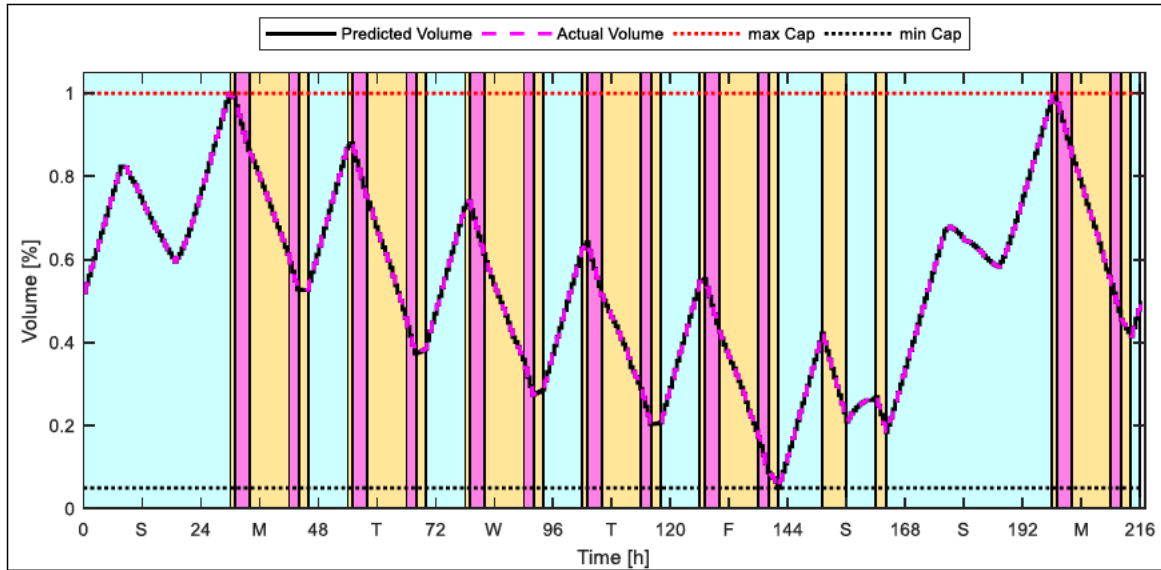
Figure A1.10: Upper reservoir state of charge (commercial load)

A2: Industrial Load
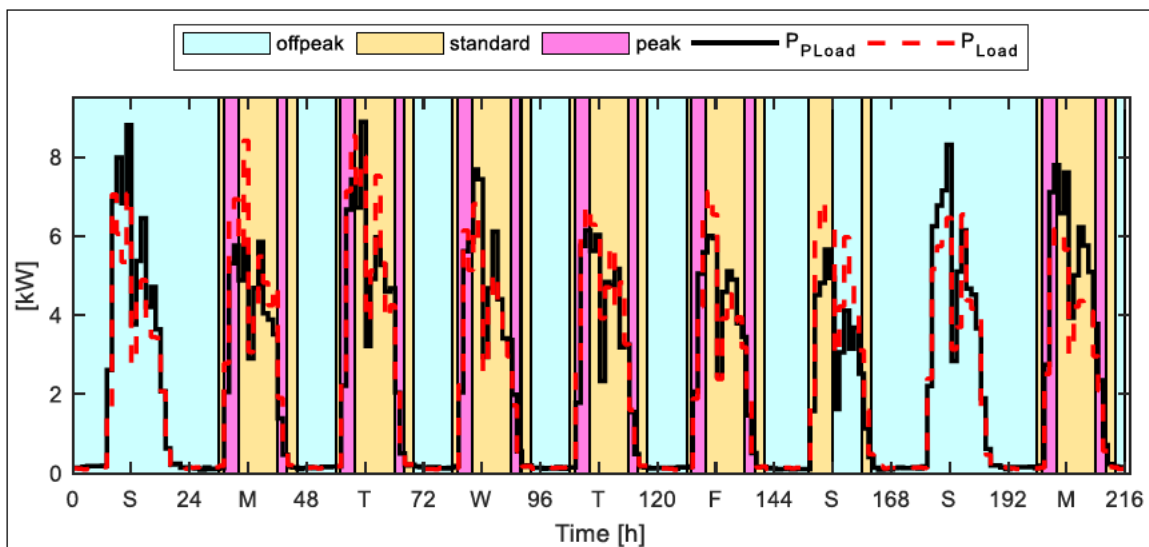
Figure A2.1: Predicted and actual industrial load demand
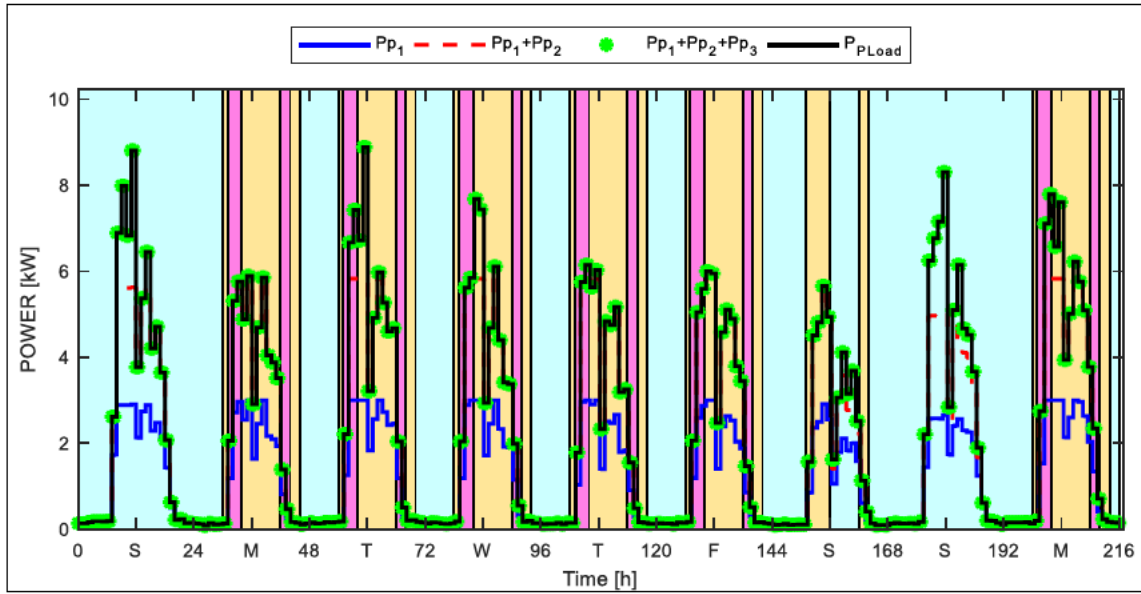
Figure A2.2: Optimization-based power flow before load demand uncertainty (industrial)

Figure A2.3: Optimization-based power flow during load demand uncertainty (industrial)

Figure A2.4: Rule-based power flow during load demand uncertainty (industrial)
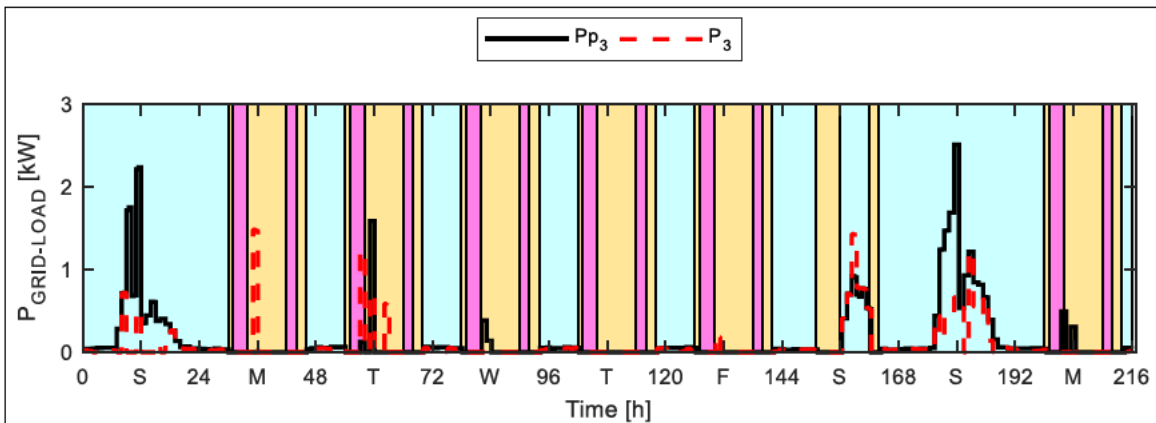
Figure A2.5: Grid-power supplied to the industrial load

194

Figure A2.6: RE system power supplied to the industrial load
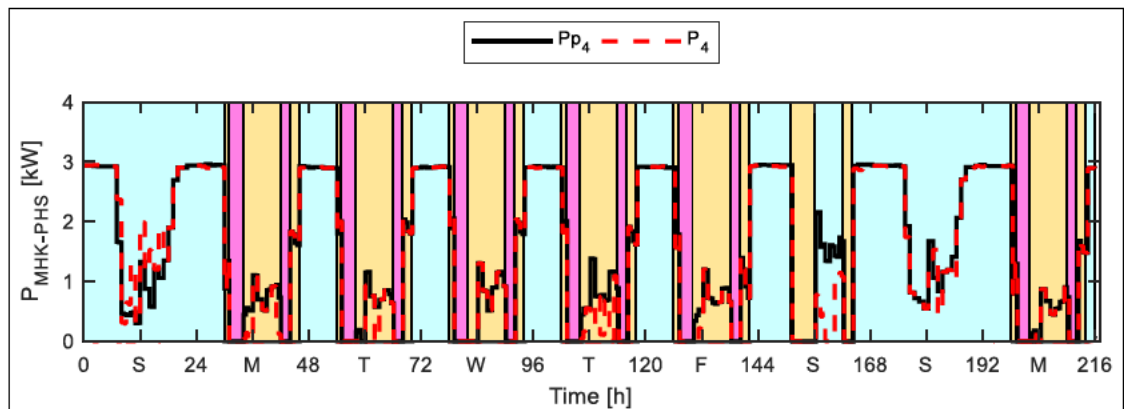
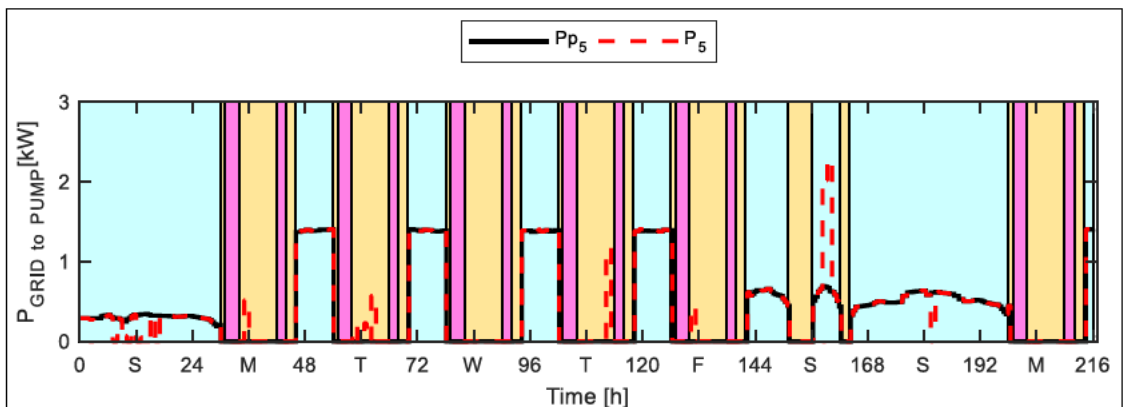Figure A2.7: MHK-power supplied to the pumping unit (industrial load)

Figure A2.8: Grid-power supplied to the pumping unit (industrial load)
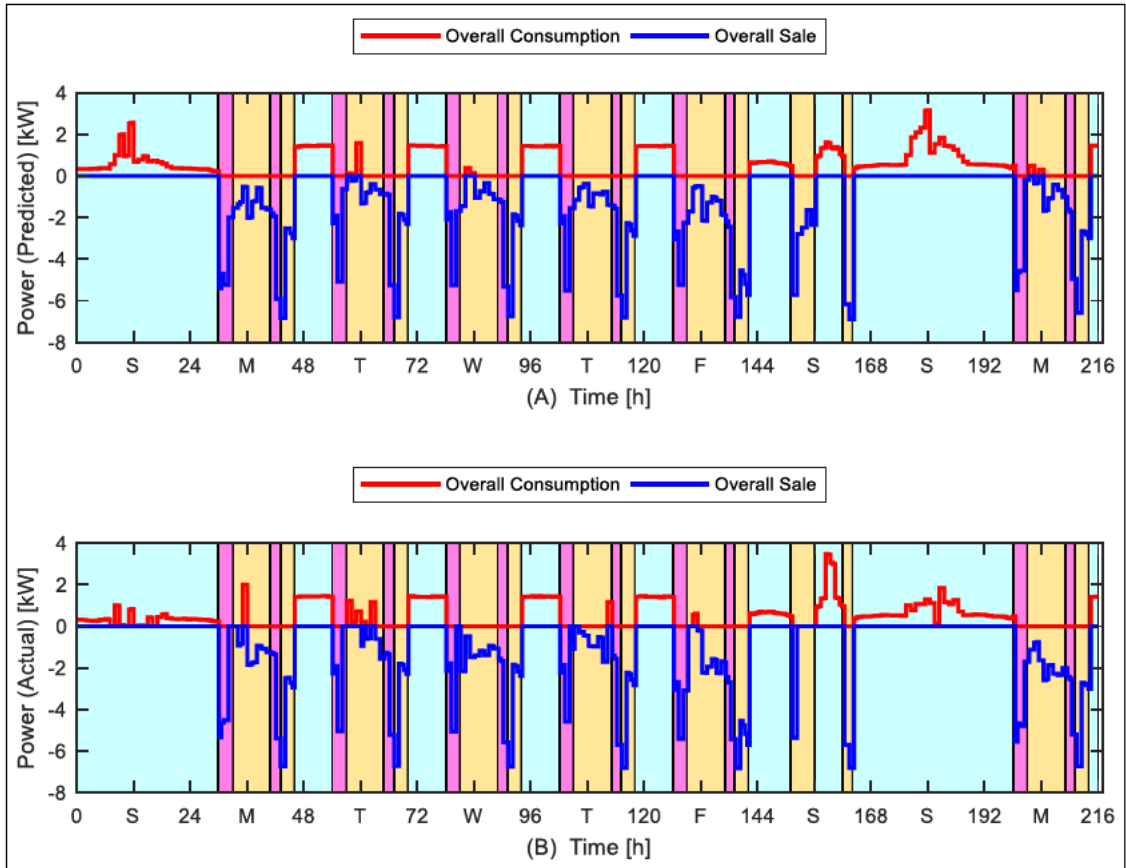
195

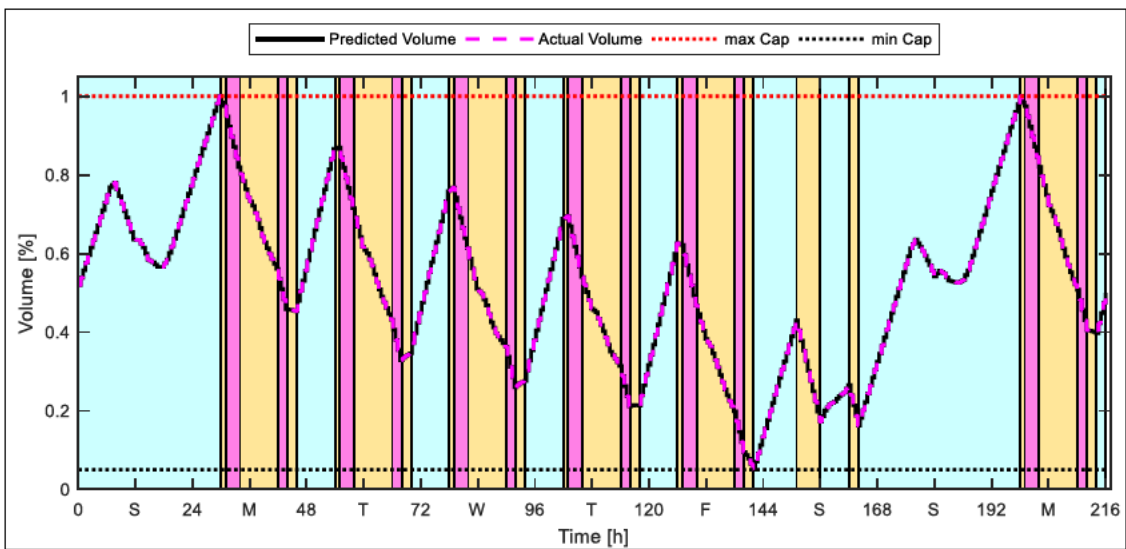Figure A2.9: Overall predicted and actual power consumption and sales (industrial)

Figure A2.10: Upper reservoir state of charge (industrial load)